RESEARCH & DEVELOPMENT

Evaluation of Inverted Pavement for NC Roadways

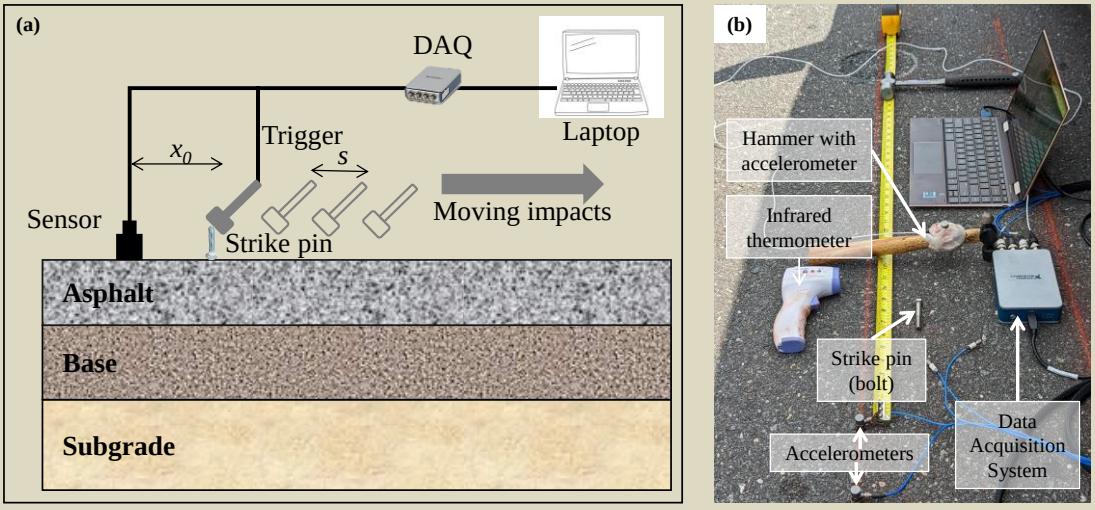

Surface wave testing setup; (a) test schematic and (b) test at field site

B. Shane Underwood, Ph.D.

Murthy Guddati, Ph.D.

Vivek Samu, Ph.D.

Department of Civil, Construction, and Environmental Engineering

North Carolina State University

NCDOT Project 2020-17

December 2022

This page is intentionally blank

TECHNICAL DOCUMENTATION PAGE

1. Report No. **FHWA/NC/2020-017**	2. Government Accession No.	3. Recipient's Catalog No.
4. Title and Subtitle Evaluation of Inverted Pavement for NC Roadways		5. Report Date September 28, 2022 6. Performing Organization Code
7. Author(s) B. Shane Underwood, Ph.D, Murthy Guddati, Ph.D., Vivek Samu, Ph.D., Nathanial Williams		8. Performing Organization Report No.
9. Performing Organization Name and Address Civil, Construction, and Environmental Engineering, North Carolina State University 915 Partners Way Raleigh NC 27606		10. Work Unit No. (TRAIS) 11. Contract or Grant No.
12. Sponsoring Agency Name and Address North Carolina Department of Transportation Research and Development Unit 104 Fayetteville Street Raleigh, North Carolina 27601		13. Type of Report and Period Covered Final Report 08/01/2019 – 07/31/2022 14. Sponsoring Agency Code RP2020-12
Supplementary Notes: None		

16. Abstract

The North Carolina Department of Transportation (NCDOT) currently uses either flexible or rigid pavement designs. The aim of this project was to evaluate the feasibility of a third design, inverted pavements, which derive their structural capacity from a highly confined unbound aggregate base layer. Inverted pavements have proven to be more economical and less environmentally impactful in certain situations than either flexible or rigid pavements due to a thinner asphalt layer and reduced need for high quality/ clean aggregates. Despite their good performance and benefits in comparison to conventional pavements, they are not widely adopted in the US. For this study, an extensive literature review was conducted on the history, design methods, and performance for inverted pavements in South Africa and the United States. The inverted and conventional experimental pavement sections at the Vulcan Materials Pineville Quarry haul road were then chosen to conduct an in-depth study on the long-term performance and to develop and evaluate the in-service material properties of the individual layers using a nondestructive surface wave-based method. A detailed condition survey concluded that the inverted pavement section is performing equally well, if not better than the conventional pavement section. Falling weight and traffic speed deflectometer tests show less deflections in the inverted section and more importantly less variation in the inverted pavement over time compared against an up to 58% increase in the deflection in the conventional section. The experimental program in this project evaluated six field cores from each pavement type using the impact resonance (IR) and AASHTO TP 132 test protocols. To supplement these laboratory tests, an in-situ surface wave testing method was developed and used to test both the conventional and inverted pavement sections. Testing was conducted at multiple locations across the lane width, on multiple days/seasons, and at multiple sites along the road. Surface wave testing resulted in asphalt modulus values that compared well with the IR and TP 132 estimates across a wide range of temperatures and frequencies. The deeper layer modulus estimates were within the typical range of values expected. The modulus of the ABC layer in the inverted section was 2.5 times higher than the conventional section. It is believed that given the magnitude of the surface wave testing load that these differences were associated with a higher degree of compaction and likely not the stress state effects. Given the potential cost savings, performance benefits and benefits to material suppliers it is recommended that the NCDOT work to identify candidate projects where inverted pavements can be deployed and monitored before widespread adoption across the state. Surface wave testing methodology has shown sufficient promise and this study warrants further efforts to develop it into a standard methodology that will benefit NCDOT estimate individual layer properties.

17. Key Words Inverted pavement, condition survey, impact resonance, surface wave testing	18. Distribution Statement		
19. Security Classif. (of this report) Unclassified	20. Security Classif. (of this page) Unclassified	21. No. of Pages 185	22. Price

Form DOT F 1700.7 (8-72) **Reproduction of completed page authorized**

This page is intentionally blank

Disclaimer

The contents of this report reflect the views of the author(s) and not necessarily the views of the University. The author(s) are responsible for the facts and the accuracy of the data presented herein. The contents do not necessarily reflect the official views or policies of either the North Carolina Department of Transportation or the Federal Highway Administration at the time of publication. This report does not constitute a standard, specification, or regulation.

Acknowledgments

The research team would like to express their gratitude and appreciation to the North Carolina Department of Transportation (NCDOT) for the provided funding needed to conclude this research study. The research team also wishes to acknowledge the contributions from other researchers at NCSU who assisted with the field testing, sample preparation and testing of the field cores; Boris Goenaga, Jaehoon Jeong, Deepika Karanam, Kazuo Kuchiishi, Omar Othman, and Zhe 'Alan' Zeng. Vulcan Materials supported this project and the contributions from Kevin Vaughan and Rusty Medlin, who allowed the research team access to the haul road for testing, are especially appreciated. During the course of the project the NCDOT was also instrumental in providing support for coring and access to the FWD and TSD data. The research team acknowledges the contributions and assistance from Clark Morrison (project champion) and Joseph Barbour.

This page is intentionally blank

TABLE OF CONTENTS

LIST OF FIGURES

LIST OF TABLES

EXECUTIVE SUMMARY

The North Carolina Department of Transportation (NCDOT) currently designs pavements using of two primary strategies; 1) those whose structural capacity comes primarily from asphalt concrete (flexible pavements) and 2) those whose structural capacity comes primarily from portland cement concrete (rigid pavements). These designs have been used successfully in many applications throughout the State; however, they utilize a large amount of relatively expensive and difficult to produce materials (asphalt concrete and portland cement concrete). A third technique, inverted pavement design that requires less of these materials and is purported to provide equivalent or superior performance is not a current NCDOT design strategy, but is technically feasible within the current NCDOT specifications. Inverted pavements consist of a 2 - 3.5-inch asphalt concrete surface, supported by a 6 – 10-inch layer of unbound aggregate base and then by 8 - 12 inches of a cement treated aggregate base. Literature and experience have shown that these pavements can be designed and used in many applications at a substantial cost savings. However, there are many unknowns when directly adopting design specifications from elsewhere as local materials, practices, and experience may not be fully accounted for. Thus, there exists a need to gain state specific experience in the engineering and performance of these structure before their adoption can be considered.

With respect to this need, the proposed research plan will achieve four objectives; 1) observe and catalog the long-term performance of the Vulcan Materials', Pineville Quarry road; 2) determine and compare the in-service material properties of the individual layers in both the traditional and inverted pavement section using a non-destructive stress wave method; 3) on the basis of the differences in material properties, estimate the costs and benefits for using inverted pavements on a wider scale; and 3) if found to be a viable technique, develop a guide and roadmap for further use of inverted pavements in North Carolina.

These steps taken to achieve these objectives included the following.

1. The relevant literature on inverted pavement design, NCDOT materials and structural design practices, and experiences and expertise from international experts were reviewed and documented.
2. All available performance, design, and construction data for the Pineville Quarry road was obtained and the overall pavement condition of the Pineville Quarry road was assessed for visible surface distresses. In addition, and with cooperation from the NCDOT, falling weight deflectometer and traffic speed deflectometer test results were obtained and evaluated.
3. A stress wave testing methodology originally developed under the auspices of FHWA/NC/2016-21 was revised, updated, and verified for use with asphalt pavements in order to identify the material properties for individual layers in an asphalt pavement. This method was then used to evaluate the inverted and traditional pavement sections to identify the material properties of individual layers. The research team also intended to perform long-term performance simulations of the site, but given the uncertainty in traffic loading and overall pavement thicknesses and material properties identified through the other steps, this process was not performed.
4. A cost-benefit analysis was carried out to estimate the comparative costs of inverted pavements for different applications throughout the state.
5. The next steps needed for further evaluation and potential implementation of inverted pavements in North Carolina were articulated based on the knowledge gained from the test sites and resultant testing and analysis in the previous tasks.

6. A final report summarizing the methodology, results, and recommendations was prepared.

With respect to the overall performance of the inverted pavement section, it was found that the inverted pavement section is performing equally well, if not better than the conventional pavement section. The FWD and TSD deflection also show less deflections in the inverted section and more importantly less variation in the inverted pavement over time compared against an up to 58% increase in the deflection in the conventional section. This finding confirms the conclusions from the condition survey. Since the initial construction cost of the inverted section was lower than the conventional pavement at the test site, there does appear to be an overall cost benefit of this pavement type. However, the generalizability of the costs from widespread adoption could not be estimated.

From Step 3, the primary findings were that if the thickness of the asphalt layer is known at the surface wave test location, the asphalt layer moduli can be estimated with high confidence and the results compare well with the laboratory dynamic modulus master curve. On the inverted section though, the preliminary results from the back calculation of the ABC and CTB layer properties resulted in a wide range of values. The average ABC modulus from the surface wave testing was higher than the typical range of values for a regular ABC, but the ABC layer in the inverted section is expected to be at a higher modulus due to the better compaction and the estimated values are in line with this. The back calculated modulus of the CTB was approximately 13.4% lower than the modulus estimated from known correlation between compressive strength and elastic modulus. Given the uncertainty in these estimations, the results were deemed reasonable. Results from the back calculation of the ABC and subgrade layer properties resulted in estimates within the range of typical properties.

Based on these conclusions, the research team has made the following recommendations regarding inverted pavements and surface wave testing.

- The NCDOT should work to identify two to three candidate projects where an inverted pavement design can be deployed and monitored. These sites should be at least 1,000 feet in length and preferably long enough to incorporate both a conventional pavement and an inverted one. It is also preferable that the sites be located near contractors who are already regularly producing CTB and can reliably produce a material with a 7-day compressive strength of approximately 500 psi.
- Additional sites are recommended to address issues that could not be addressed or evaluated in this study with respect to long-term performance of inverted pavements in humid environments on high volume roadways, situations where maintenance is not being performed carefully, and situations where construction practices and quality control/assurance are not being carefully followed. If test sites are constructed, the research team recommends that the NCDOT make every effort to carefully catalog the construction process and retain samples of the as constructed materials for mechanical investigation and for use in later performance assessments.
- Further study and development is recommended before adoption of the surface wave testing for routine evaluation. However, it is recommended that NCDOT consider using the surface wave testing method for forensic or research purposes to increase the amount of data collected and further refine the test method. If done, then investigations should include FWD, ground penetrating radar (GPR), and potentially pavement coring.

1. INTRODUCTION

1.1. Overview

The long-term serviceability and performance of roadways in North Carolina is a priority for the North Carolina Department of Transportation (NCDOT). To meet this goal while remaining flexible and adaptable to varying demands placed on these roadways, the NCDOT must have many different tools and techniques at their disposal. There are currently two primary design strategies used by pavement engineers on NCDOT roadways; 1) those whose structural capacity is predominantly from asphalt concrete (flexible pavement) and 2) those whose structural capacity is predominantly from portland cement concrete (rigid pavement). A third design, inverted pavements, derives its structural capacity from a highly confined unbound aggregate base layer, and is not currently permitted in North Carolina. This third design has proven to be more economical and less environmentally impactful in certain situations than either flexible or rigid pavements. These benefits emerge because inverted pavements use a thinner asphalt concrete surface layer and thus require overall less asphalt cement and less high quality/clean aggregate.

The basic inverted pavement design consists of a 2 - 3.5-inch asphalt concrete surface, supported first by 6 - 10 inches of unbound aggregate base and then by 8 - 12 inches of a cement treated aggregate base course (unconfined compressive strength between 100 to 500 psi). There are two known examples where inverted pavement has been used in North Carolina. The first example is the US 421 test road in Chatham County (constructed in 1989 and 1990), which contained two sites where the basics components of inverted pavement existed (sites 5 and 17). These sites performed well, but they used a cement stabilized soil instead of a cement treated aggregate base and one of the sections used a 12-inch aggregate base. Thus, this example is not prototypical of modern inverted pavement design. Besides the slight differences in structural design, this experience is now nearly 30 years old and has limited applicability since the technology has evolved substantially in recent years. The second example is the road into Vulcan Materials' Pineville Quarry that was constructed in 2010. This site has purportedly performed well in comparison to a more traditional design that was also built at the same time.

In both examples, limitations exist that prevent the NCDOT from making general conclusions on the broad applicability of the inverted pavement design in North Carolina. The study described in this report has evaluated the performance and applicability of inverted pavement designs in North Carolina. A study to systematically investigate the performance of the Pineville quarry road was needed because of an overall lack of experience with or usage of inverted pavements in the United States in general and in North Carolina specifically. As a result, there currently does not exist any guidance on this pavement type from AASHTO, NCHRP, or other national bodies. The initial phase of this project envisioned constructing and experimenting on a purpose built project. However, the research team and the NCDOT were unable to identify a suitable site and so the scope of the project adjusted to more deeply examine the Pineville Quarry road and to develop a method to estimate individual asphalt layer moduli using surface wave testing. The specific objectives of this project were as follows.

1. Observe and catalog the long-term performance of the Vulcan Materials', Pineville Quarry Road.
2. Determine and compare the in-service material properties of the individual layers in both the traditional and inverted pavement section using a non-destructive stress wave method.

3. On the basis of the differences in material properties, estimate the costs and benefits for using inverted pavements on a wider scale.
4. If found to be a viable technique, develop a guide and roadmap for further use of inverted pavements in North Carolina.

1.2. Status of the Literature

A comprehensive review of the literature pertaining to this project is presented in Appendix A, while a summary of most relevant components of this review is presented below.

1.2.1. Inverted pavement

A conventional flexible pavement system uses the asphalt layer to carry most of the stress, which is then distributed throughout the pavement system. This redistribution is done by having a thicker asphalt pavement layer that can spread the load to the rest of the pavement system. In a conventional pavement system, if the ABC was subjected to the high stresses at the surface it would fail because its modulus would not be high enough (due to a lack of confinement). The asphalt layer in this system makes up most of the structural capacity while the aggregate layer and other layers are assumed to have a lower structural capacity. Inverted pavement design uses the aggregate base in an entirely different way.

In an inverted pavement, the basic design consists of a 2 – 3.5-inch asphalt concrete surface layer, supported first by 6 – 10 inches of unbound aggregate base and then 8 – 12 inches of a cement treated subbase (CTB) (unconfined, 7-day compressive strength between 100 to 500 psi). The majority of the structural capacity of these pavements comes from the unbound aggregate base, which is derived because the unbound layer is confined between the thin asphalt surface and the cement treated subbase. As the load increases on the surface layer, the unbound layer is confined and compressed between the surface layer and the subbase, increasing the overall bulk stress of the unbound aggregate layer.

Though the specific origin of inverted pavements is not known, it is widely accepted that they were in experimental use in New Mexico as early as the 1950's and by the US Army Corp of Engineers in the 1970's (Ahlvin et al. 1971). Despite these early efforts, there does not exist widespread usage of inverted pavements in the US and examples primarily exist in experimental sections that have been constructed in Georgia, New Mexico, Virginia, and North Carolina. In general, these experimental studies have demonstrated the efficacy of inverted pavements and show performance that are as good if not better than comparable conventional pavement sections (Johnson 1961; Rasoulian et al. 2000; Metcalf et al. 2001; Weingart 2010; Lewis et al. 2012; Chen et al. 2014). From the literature only one state, Louisiana, was identified as having a standard pavement type that closely resembles an inverted pavement. Their design is referred to as a 'Stone Interlayer Pavement' and is widely used on secondary and low volume roadways. The International Center for Aggregates Research (ICAR) has also developed an analytical design method for inverted pavements, but the testing and analysis method requires considerable testing involving variable dynamic confining pressure (Tutumluer et al., 2003). Internationally, South Africa uses inverted pavements regularly and considers them to be the 'gold standard' pavement type for high truck volume roadways (Freeme et al. 1980). Their design method involves a catalog where the final design is a function of the road category, cumulative equivalent single axle loads (ESALs) (calculated according to the South African specific procedure), and subgrade type (DTSA 1996).

While the structural design approach followed by South Africa differs somewhat from the North Carolina DOT method, they share conceptual similarities. In addition, the standard materials (asphalt, aggregate base, and cement treated base) specified in North Carolina are largely the same or highly compatible with those specified in the South African standards. With respect to asphalt concrete surface mixtures, the North Carolina type C or type D mixes are the ones most similar to South African mixtures. The North Carolina aggregate base is similar to South African G1 base, which is specified for use in the highest volume inverted pavements. However, there are some additional tests that are commonly performed on South African materials to evaluate aggregate strength, wear resistance, and sulfate resistance that are not specified for North Carolina bases. These properties have greater significance in inverted pavements because these pavements subject aggregate bases to higher overall stresses than conventional pavements. Finally, CTB compressive strengths are similar between the highest traffic category CTB for South Africa and current North Carolina specifications. However, for low to moderate volume inverted pavements the compressive strength requirement is lower in South African CTB. The South African standard has a lower and upper limit on the compressive strength to balance the need for construction stability with the potential for shrinking cracking.

Finally, the literature review evaluated how construction practices might differ for inverted pavement production. No major differences or hurdles were identified with respect to asphalt, CTB, and subgrade preparation. However, there were differences in the recommended construction practices of the aggregate base course. First, it was noted that generally the density of the aggregate base course achieved when compacting on a CTB layer could increase. South Africa also uses a unique method of increasing density of their aggregate base even further. This method, called slushing, basically floods a compacted aggregate base with water, and then rolls a vibratory compactor over the flooded base layer. This action forces fines to migrate through the aggregate base and further densifies the layer (Lewis et al. 2012; Papadopoulous 2014). A review of the case studies conducted in the U.S. found that some pavements were constructed with the slushing technique (Georgia) and some were not (North Carolina).

1.2.2. Surface Wave Testing of Asphalt Pavements

Surface wave testing is an extensively used method for near surface geophysical imaging and geotechnical site characterization (Foti et al. 2011). The basic idea of surface wave testing is to record the surface acceleration that occurs from an impact on the pavement and in turn use these accelerations to calculate the dispersion properties of the pavement layers. This testing consists of two important steps: (i) characterization of the experimental dispersion curve (phase velocity vs frequency) by measuring the surface response of the layered system to an impact loading and (ii) inversion of layer properties by matching the experimental dispersion curves through a theoretical model of the layered system. Though conceptually similar to the more common falling weight deflectometer (FWD) testing and analysis, surface wave testing is fundamentally different with respect to the impact, frequency content, and the ability to estimate individual layer properties The efficiency of the process is dependent on the experimental measurements and accuracy of the back calculated layer properties is dependent on the forward model and inversion strategy. Due to decreasing velocity with depth for pavement layers the underlying wave propagation mechanisms becomes more complex in comparison to the soil layers. (Heisey et al. 1982) first introduced the Spectral Analysis of Surface Waves (SASW) to nondestructively estimate the moduli of pavement layers by measuring the surface waves generated from an impact at two receiver locations. The back calculation of layer properties from SASW for pavements is challenging as the phase

difference calculated from two receivers cannot resolve multiple modes that are typical for pavement structures. This can be overcome using Multichannel Analysis of Surface Wave (MASW) (Foti et al. 2011) method where the response is recorded at multiple receivers, often between 12 and 24, resulting in a two-dimensional wavefield. MASW has been successfully used in several applications such as geophysical explorations, mapping the top 30 m of soil layers, locating buried objects.

The recorded data from MASW can provide sufficient resolution when computing dispersion curves, but the process of data acquisition is tedious and time consuming. In addition, traditional MASW requires bulky equipment along with multiple accelerometers for pavement applications resulting in high cost and long test durations. To overcome this Multichannel Simulation with One Receiver (MSOR) was developed (Rydén et al. 2001). MSOR uses a single receiver (accelerometer) and the source (hammer impact) is moved along a line to simulate the effect of MASW thus reducing the need for bulky and costly equipment. The key to successful implementation of the MSOR methodology is the use of an accurate trigger in the impact mechanism to synchronize the data acquisition in the sensor with the impact. This technique is simple, but the response can be sensitive to local changes and the reliable frequency range is smaller compared to the MASW method (Lin 2014).

1.2.3. Knowledge Gaps

Overall inverted pavements seem to perform well under many conditions, making them a technology that requires some additional study for North Carolina. The various layers that make up the pavement structure can be constructed using North Carolina DOT specifications in many cases. However, while the literature shows the efficacy of the technology, it also demonstrates some caution should be exercised before fully adopting the technique. In North Carolina, a single case study has been performed, but not within the control of the North Carolina DOT. The literature review supports the overall need for this study by finding that knowledge gaps remain with respect to the long-term performance of inverted pavements in the United States. The use of full-scale studies to fill in knowledge gaps on the use and performance of inverted pavements represents the state of practice and has been used successfully by other states. In conducting the full scale study the research team will need to consider the following aspects; stress dependency of aggregate base and its toughness to withstand the higher stresses that will exist in inverted pavements, the modulus and strength of CTB as this affects the level of confinement that is achieved when compacting the aggregate base, the traffic that will use the roadway, adapting existing material specifications for proper material selection, and careful control during construction to produce a high quality pavement and informative outcomes.

With respect to the surface wave testing, the method has been successfully implemented on conventional pavement in a controlled setting (Rydèn and Park 2006), they have never been implemented on inverted pavements. In addition, a recently developed forward model (Astaneh and Guddati 2016) for efficient computation of effective dispersion curves and inversion for soil layers will be modified to apply for pavement systems. The experimental setup including the key parameters, data acquisition procedure, data analysis to compute the dispersion curves and back calculation of the layer properties for both the conventional and inverted pavements are detailed in Section 3.

1.3. Report Organization

This report is organized into 6 primary sections and 6 appendices. Section 1 (this section) describes the overall project, need, state of the literature, and report organization. Section 2 provides an overview of the Pineville Quarry Road including observed field performance. Section 3 describes the surface wave testing methodology and findings. Section 4 summarizes the conclusions of this project along with some specific recommendations. Section 5 provides an overview of the implementation and technology transfer plan for the project results. Finally, Section 6 lists the references cited in this report. Appendix A includes the detailed literature review, while appendices B-F provide the detailed analysis results related to Sections 2 and 3.

This page is intentionally blank

2. PAVEMENT SECTION AT PINEVILLE QUARRY

2.1. Pineville Pavement Section

Vulcan materials became interested in the prospect of inverted pavement because multiple sizes of aggregate could be used within the structure eliminating waste from aggregate production. New inverted pavements tend to have the same total aggregate demand as a new conventional flexible pavement, but the proportion of base aggregate to clean aggregate is much higher (Buchanan). Such a balance is important to aggregate manufacturers particularly because the majority of current production involves overlays, which use 100% clean stone. Vulcan saw a chance to try out this new pavement structure when a haul road needed to be relocated at their Pineville Quarry near Charlotte, North Carolina. The relocation of the road was a good candidate site to implement the inverted pavement structure because the new road was going to be long enough for an inverted test section and a control section; and also a cement silo and pugmill are on site at the quarry making it easy to construct the cement treated base.

The road was constructed in 2015 and the design closely followed South Africa's catalog method. The hall road consisted of 800 feet of inverted pavement and then the other 800 feet consisted of conventional pavement. The two sections of the haul road can be seen in the road profile shown in Figure 1. The inverted section starts at the left of the figure and extends to the 800-foot mark which is the black line at the top of the figure. Satellite views of the site and a photograph of the division between conventional and inverted pavement are shown in Figure 2. It is noted that according to the current NCDOT AASHTO design standard the inverted pavement has a total pavement structural number of 3.78 and the conventional pavement has a total structural number of 4.04. Schematic cross-sections of the pavements are shown in Figure 3. Both pavements were constructed on top of native compacted subgrade, and Figure 4 shows some images of the road under construction.

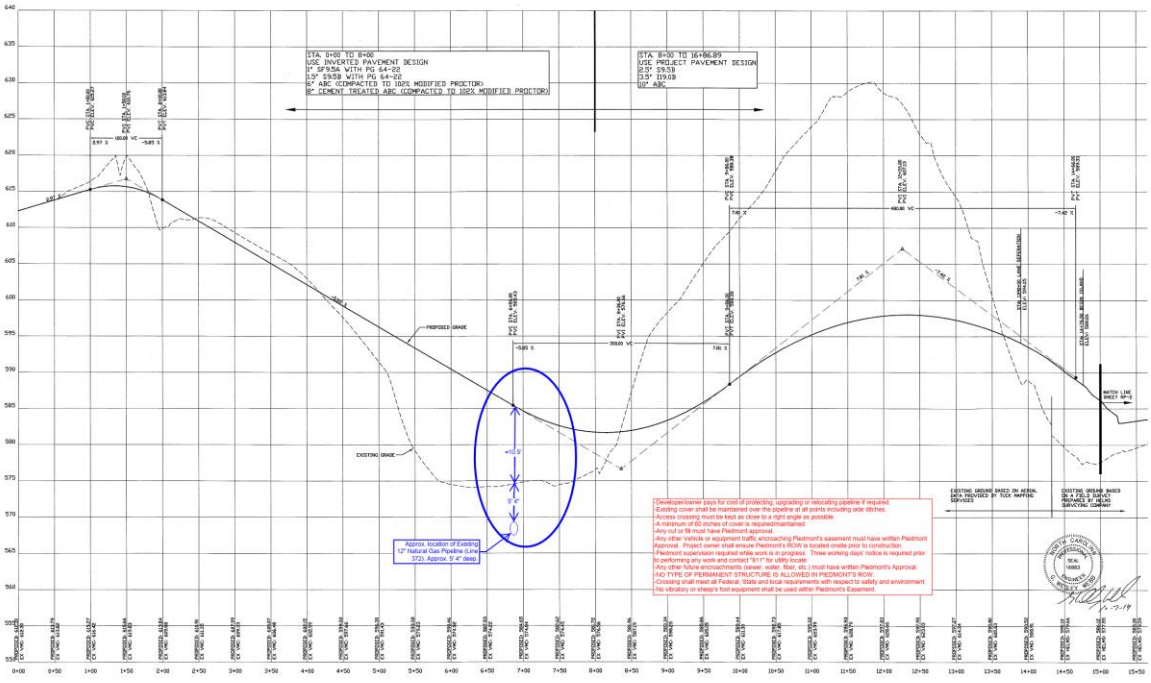

Figure 1. Pineville quarry site road profile [Vaughan 2019].

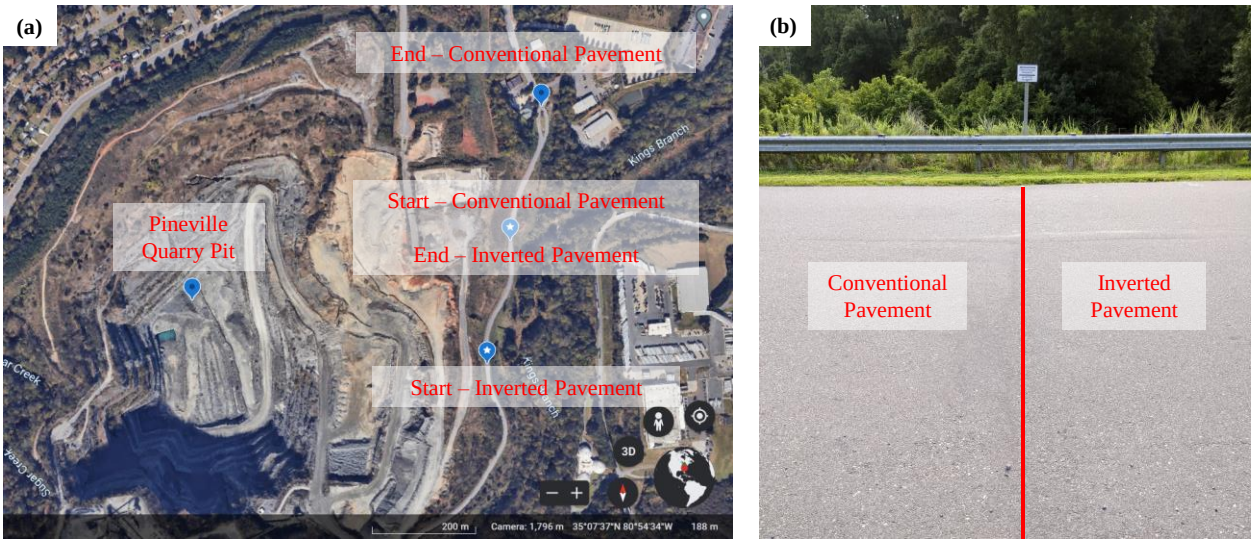

Figure 2. Vulcan materials Pineville quarry site; (a) map view of the pavement segment and (b) conventional and inverted pavement junction at 800 ft.

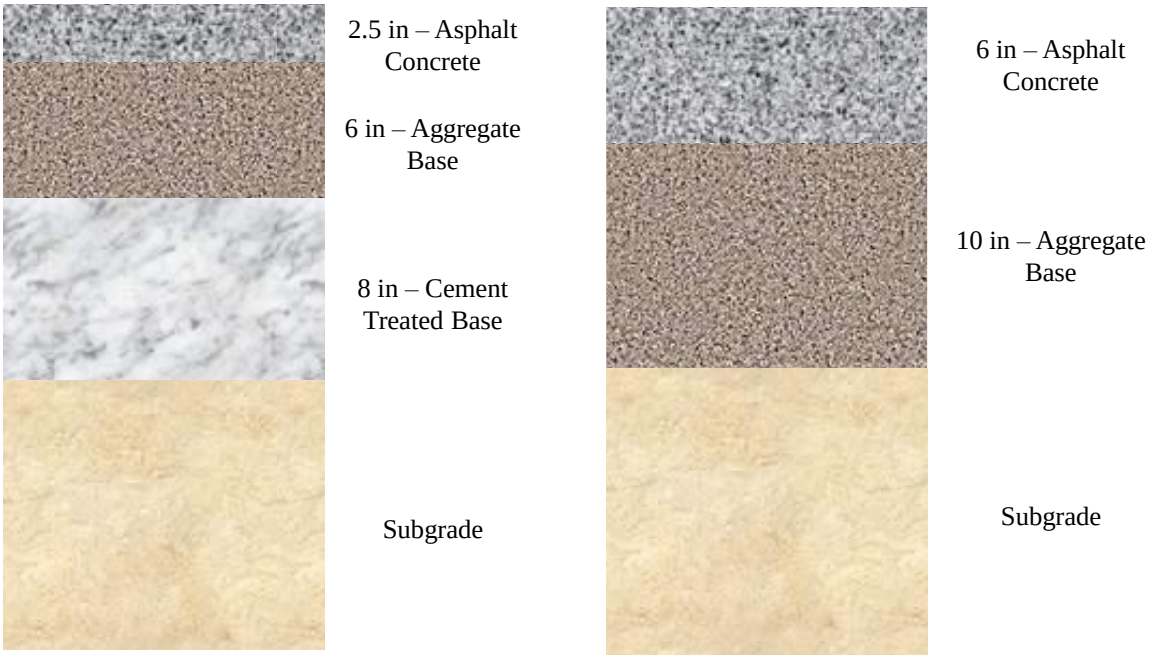

(a) **(b)**

Figure 3. Pavement designs in Pineville quarry site; (a) inverted pavement design and (b) conventional pavement design.

The 2.5 in. asphalt concrete layer in the inverted pavement was built using a 1 in. lift of SF9.5A and 1.5 in. lift of S9.5B mixture. The 6 in. asphalt concrete in the conventional pavement was built using 2.5 in. of S9.5B and 3.5 in. of I19B mixture. The actual layer thicknesses were estimated using cores taken in January of 2022. For both the conventional and inverted pavement sites, a total of six cores, three in the center of the lane and three near the outer edge of the lane, were extracted resulting in a total of 12 field cores as shown in Figure 5 (a) and (b). All cores were taken in the southbound lane. The conventional cores were extracted near station 10+50 while the

inverted cores were extracted near 3+50. The measured core dimensions are shown in Table 1 along with the specimen naming convention. Note that based on the average thickness of the measured cores the as-constructed SN for the two pavements are almost identical (3.644 for conventional and 3.714 for inverted). All the cores in the conventional section had a thickness 15-20% less than the design thickness of 6 in. Additionally, the cores taken from the center of the lane were consistently shorter compared to the ones close to the outer wheel path of the lane as shown in Figure 5 (c) and (d). The thickness of all the cores from the inverted pavement were also less than the design thickness although the overall difference is less (average of 6% difference) and there is no clear trend between the cores from the center and outer path of the lane.

Figure 4. Images of Pineville quarry site during construction; (a) compacted subgrade, (b) placing cement treated base, (c) compacted base, and (d) finished surface.

The cores were also tested using the standard bulk gravity test to calculate the bulk specific gravity (G_{mb}) values for each of the cores and the results are shown in Figure 6. For the conventional site, the overall G_{mb} for the core are presented along with the G_{mb} values for the surface layer (marked as T) and the intermediate layer (marked as B). The research team approximated to their best ability the interface between the surface and intermediate layers and sliced the cores along this line. In the conventional pavement section, the cores from the lane center were at a slightly higher specific gravity compared to the outer path. The maximum specific gravity (G_{mm}) of these mixtures was not measured and the job mix formula for the mixtures used on the site were not available. However, using a typical G_{mm} value (2.6) suggests that the difference in air void between the center and outer locations for the conventional sections is approximately 2%. In addition, a difference in air voids of 2.4% was observed between the surface layers of the center and outer locations. The intermediate layers were at a higher density and the difference between the center and outer was smaller (estimated at 1.5%). Using a similar approach, the difference in air void between the center and outer for the inverted sections is approximately 1%.

The CTB design was estimated to require 2% cement to meet the desired strength of 400 – 500 psi. However, testing during construction found that the CTB had a substantially higher strength than expected (approximately 1560 psi). With respect to the aggregate base, it was constructed on both the inverted and conventional pavements at the same time. The presence of the cement treated

base in the inverted pavement resulted in an aggregate base layer compaction of 103.4% in comparison to 99.8% in case of the conventional pavement.

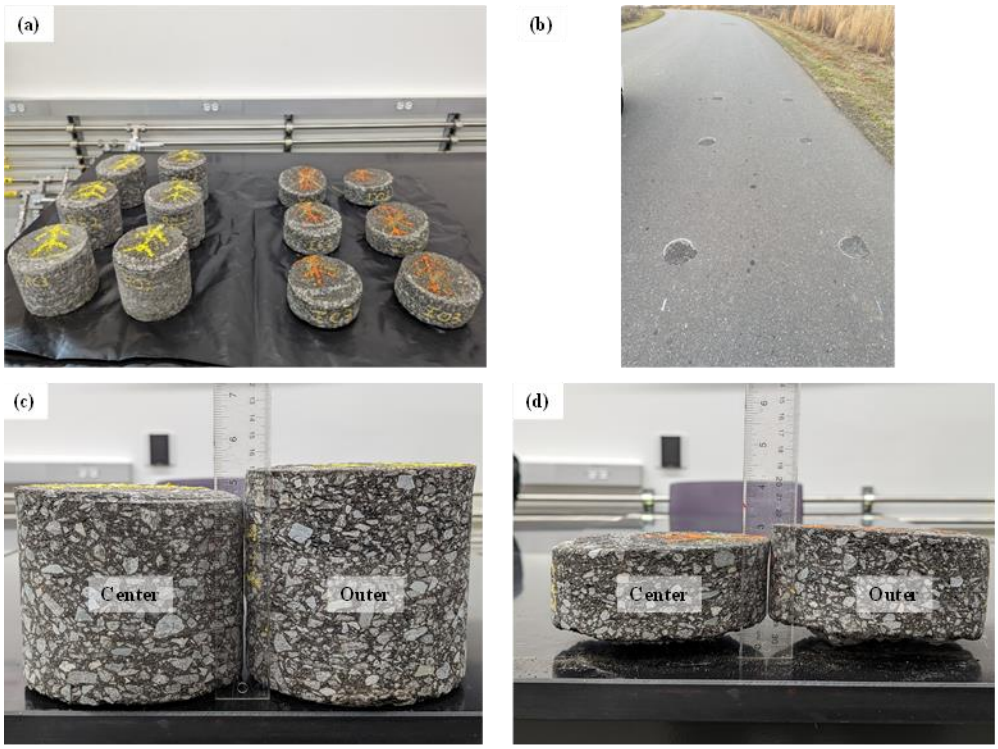

Figure 5. Summary of field cores from Pineville quarry road; (a) field cores, (b) core locations, (c) conventional core depth comparison, and (d) inverted core depth comparison.

Table 1. Field Core Dimensions

Section	Lane Position	Specimen Number	Specimen Code[a]	Depth (in.)	Diameter (in.)
Conventional	Center	1	CC1	4.8	5.9
		2	CC2	5.0	5.9
		3	CC3	5.0	5.9
		Average		***4.9***	***5.9***
	Outer	1	CO1	5.4	5.9
		2	CO2	5.2	5.9
		3	CO3	5.3	5.9
		Average		***5.3***	***5.9***
Inverted	Center	1	IC1	2.4	5.9
		2	IC2	2.5	5.9
		3	IC3	2.1	5.9
		Average		***2.3***	***5.9***
	Outer	1	IO1	2.3	5.9
		2	IO2	2.4	5.9
		3	IO3	2.5	5.9
		Average		***2.4***	***5.9***

[a] Specimen code includes Section ID, Lane Position, and Specimen Number

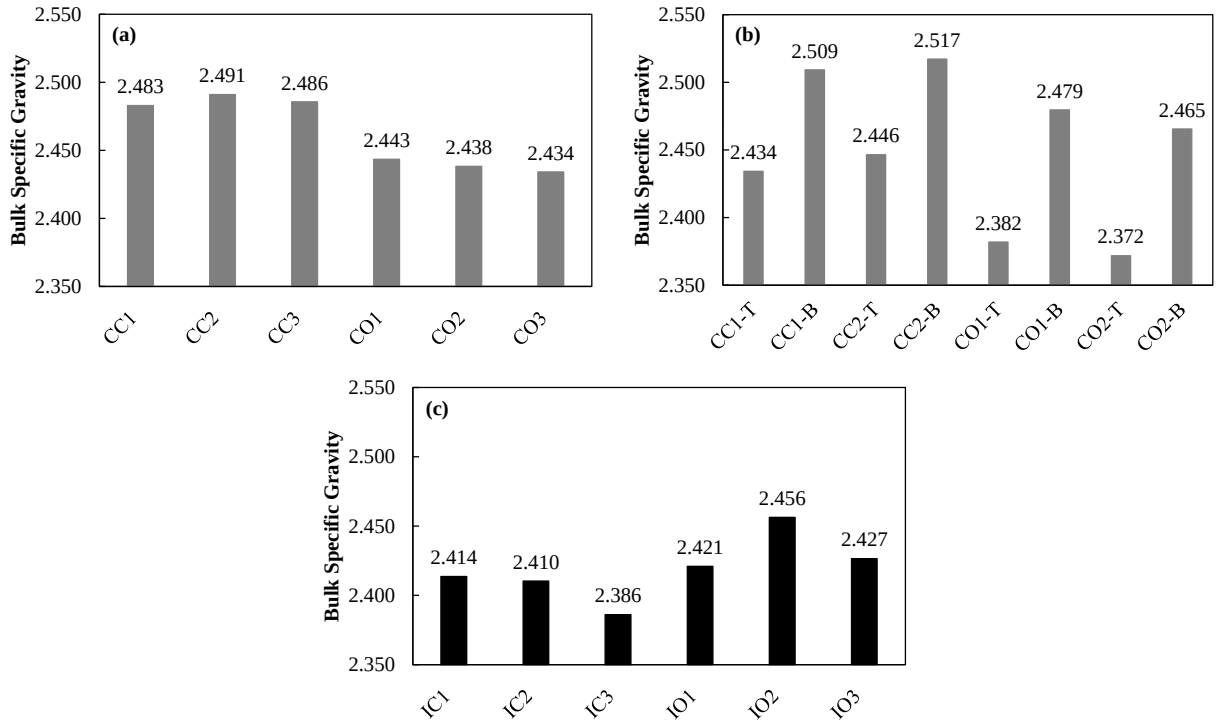

Figure 6. Bulk specific gravity measurements; (a) conventional pavement cores, (b) cut conventional pavement cores to separate surface and intermediate layers, and (c) inverted pavement cores.

2.2. Condition Survey

The research team conducted condition surveys in accordance with the ASTM D6433 − 18 procedure on August 21, 2021, and July 2, 2022. The condition survey was conducted by the project PI to maintain consistency, but the surveys were conducted at different times of the day (August 2021 midday and July 2 in the morning). Table 2 and Table 3 summarizes the observed distresses for both surveys and Figure 7 and Figure 8 show a selection of photographs from the sites. It is noted that the stations listed in these tables were based on the markings at the site (every 0+50 stations) with intermediate stations determined using a rolling wheel meter. It is also noted that in the case of the longitudinal cracking the station listed corresponds to the station where the crack was found to begin. Finally, the condition surveys did not measure rutting in the sites; however, traffic speed deflectometer (TSD) testing carried out in September 2021 found only one measurement that would be categorized as 'Low' severity according to ASTM D6433-18 (0.25 in. limit), see Figure 9. This measurement was taken at station 15+00 near the gate and was thus rutting was ignored when calculating the PCI and PCR.

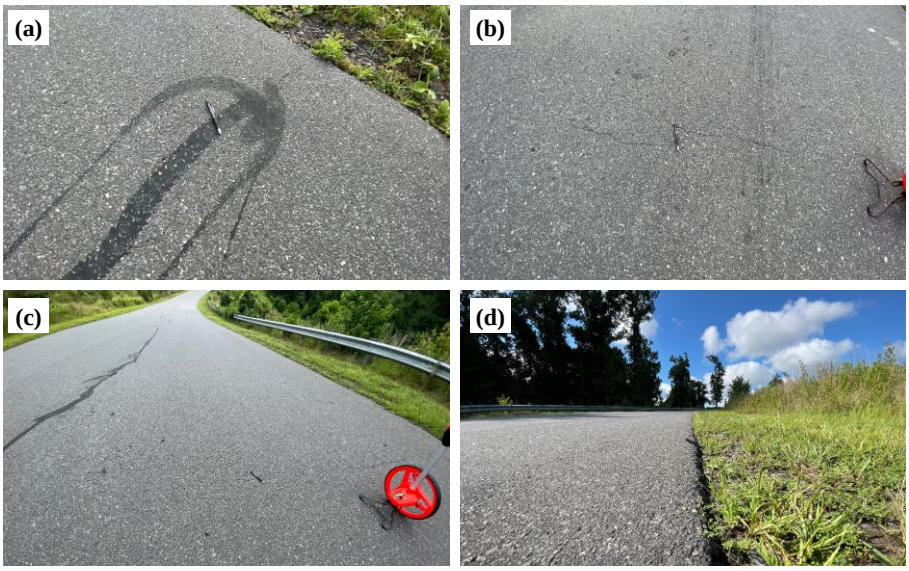

Figure 7. Select photographs from July 2022 condition survey on inverted test site; (a) transverse crack at northbound 02+12, (b) transverse crack at northbound 02+97, (c) transverse crack and longitudinal crack at northbound 06+62, and (d) shoulder deterioration at southbound 06+50.

As seen in Table 2, the most common distresses in the inverted site was longitudinal and transverse cracking. All of this cracking was low severity (see examples in Figure 7) and many were sealed. It is believed (though could not be confirmed) that many of these cracks originated from cracks in the cement treated base, which had reflected through the pavement surface. Recall, that the cement treated base in the study site was ultimately produced with a compressive strength substantially higher than what was desired and also higher than the recommended values in the South African standard (1400 psi versus a target of 200 – 500 psi). Comparing the August 2021 and July 2022 distresses it is found that some of the sealed and unsealed cracks have increased in length. The average increase in these cases was 2.3 ft.

In the case of the conventional section the two main distresses observed on the site were fatigue cracking at the end of the site between stations 14+50 to 16+00 and shoulder deterioration, see Table 3. Examples of the distresses are shown in Figure 8. With respect to the fatigue cracking, these stations are at the end of the site near the exit gate and may be subject to slower speeds and possibly more standing traffic, which may partially explain why they appear. Note that the FWD data also shows a greater deflection in this area so there may also be some slightly lower foundation support as well.

Table 2. Distresses Identified in Inverted Pavement Condition Surveys

Station[a]	Distress[b]	August 21, 2021		July 2, 2022	
		Extent (ft)	Severity	Extent (ft)	Severity
2+68-N	LC-U	0	--	2.5	Low
6+38-S	LC-U	0	--	20	Low
5+50-N	LC-S	250[c]	Low	24	Low
5+62-N	LC-S			51	Low
6+06-N	LC-S			45	Low
6+50-N	LC-S			100	Low
7+70-N	LC-S			30	Low
7+36-N	LS-P			42	Low
0+05-S	TC-U	0	--	4	Low
0+06-N	TC-U	0	--	2	Low
0+35-S	TC-U	0	--	2	Low
0+87-N	TC-U	0	--	2	Low
0+89-S	TC-U	0	--	9	Low
1+13-N	TC-U	0	--	3	Low
1+13-S	TC-U	6	Low	8	Low
1+47-S	TC-U	5	Low	7	Low
2+97-N	TC-U	3	Low	3.5	Low
2+97-S	TC-U	6	Low	9	Low
3+85-N	TC-U	1.5	Low	6	Low
3+87-S	TC-U	6	Low	9	Low
3+98-S	TC-U	0	--	2	Low
4+92-S	TC-U	6	Low	8.5	Low
5+41-S	TC-U	6	Low	6	Low
5+71-S	TC-U	8	Low	9	Low
6+62-N	TC-U	6	Low	12	Low
6+62-S	TC-U	0	--	6	Low
7+00-S	TC-U	6	Low	6	Low
7+22-S	TC-U	0	--	1	Low
7+68-S	TC-U	6	Low	8	Low
7+71-N	TC-U	2	Low	2.5	Low
0+35-N	TC-P	2	Low	3	Low
2+12-N	TC-P	12	Low	12	Low
2+60-S	TC-P	10	Low	12	Low
2+68-N	TC-P	4	Low	4	Low
3+40-N	TC-P	4	Low	5	Low
4+91-N	TC-P	9	Low	11	Low
2+12-S	TC-S	12	Low	11	Low
3+40-S	TC-S	8	Low	12	Low
6+50-S	SD	62[d]	Low	100	Low

[a] End letter designates Northbound direction (N) or Southbound direction (S)

[b] LC = Longitudinal Cracking, SD = Shoulder Deterioration, TC = Transverse Cracking, P = Partial Sealed, S = Sealed, U = Unsealed

[c] Total longitudinal crack was measured and not segregated by individual cracks

[d] Shoulder deterioration was noted as starting at station 6+62 in this survey

Figure 8. Select photographs from July 2022 condition survey on conventional test site; (a) edge cracking at northbound 10+00, (b) shoulder deterioration at northbound 11+00, (c) fatigue cracking at northbound 14+59, and (d) slippage cracking at northbound 14+25.

Table 3. Distresses Identified in Conventional Pavement Condition Surveys

Station[a]	Distress[b]	August 21, 2021		July 2, 2022	
		Extent (ft)	Severity	Extent (ft)	Severity
10+00-N	EC-U	44	Low	71	Low
10+00-S	EC-U	0	--	21	Low
9+87-S	EC-U	2	Low	0	--
14+50-N	FC-U	36	Low	27	Low
14+59-N	FC-U	36	Moderate	63	Moderate
15+00-N	FC-U	81	Low	45	Moderate
15+18-N	FC-U	0	--	16.5	Low
16+00-N	FC-U	12	Low	12	Low
14+87-N	LC-U	0	--	3	Low
15+65-N	LC-U	0	--	1	Low
15+80-N	LC-U	0	--	3	Low
15+85-N	LC-U	0	--	3	Low
8+32-S	RC[c]	36	Low	18	Low
9+75-S	RC[c]	74	Low	37	Low
14+25-N	SC-U	20[d]		31.5	Low
12+46-N	TC-U	6	Low	2	Low
12+50-N	TC-U	0	--	1	Low
11+00-N	SD	225	Low	225	Moderate
12+25-S	SD	97[e]	Low	175	Low
15+00-S	SD	172	Moderate	173	Moderate

[a] End letter designates Northbound direction (N) or Southbound direction (S)

[b] EC = Edge Cracking, FC = Fatigue Cracking, LC = Longitudinal Cracking, RC = Random Cracking, SD = Shoulder Deterioration, TC = Transverse Cracking, P = Partial Sealed, S = Sealed, U = Unsealed

[c] RC was treated as low severity FC for deduct value calculations

[d] Recorded as a longitudinal crack in August 2021 survey

[e] Shoulder deterioration was noted as starting at station 11+47 in this survey

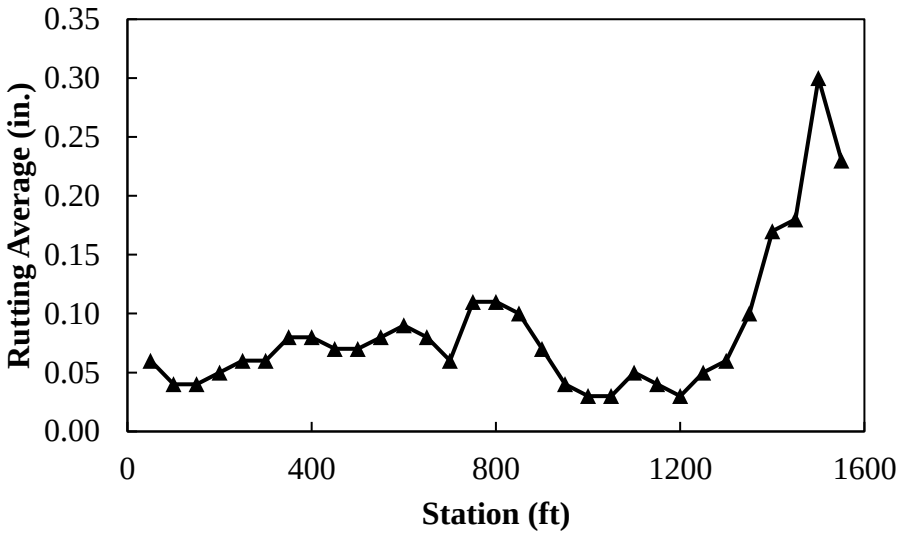

Figure 9. Measured rutting at test site from TSD measurements in September 2021.

As per the ASTM standard, the conditions on the site were assessed according to their severity and extent. The deduct values were first computed using the tables in ASTM D6433-18 and then cumulated according to the methodology provided in the standard. Table 4 below summarizes the results of the condition survey, which suggest an overall lower PCI value for the conventional section than the inverted section (75.7 versus 90.6). However, the PCI value for the conventional pavement ranking was heavily influenced by the aforementioned fatigue cracking that was observed in the northbound side of the conventional section between stations 14+50 to 16+00. If these distresses are ignored, then the ranking for the two sites is very similar (90.3 versus 90.6). The research team also calculated the PCR value for the northbound direction of each site using the standard NCDOT deduction equation. Calculating the deduct values for only a single direction is not standard, but was performed here because the two directions showed somewhat different performance. The results are also summarized in Table 4. It should be noted that for these calculations the fatigue extents (1-10 extent) were rounded to the nearest tenth (single percentage values), which as the research team understands is also non-standard. To approximate the impact of the non-wheel path longitudinal cracking in the inverted section and the presence of sealed transverse cracks at various intervals a 'Light' rating was given to the transverse cracking distress in the case of the inverted pavement.

Table 4. PCI Ratings from ASTM D6433-18

Survey	Site	PCI Values	PCR Values
August 21, 2021	Inverted	92.6	95.0
	Conventional	79.3	96.7
	Conventional without Fatigue	90.3	100
July 2, 2022	Inverted	90.6	95.0
	Conventional	75.7	96.2
	Conventional without Fatigue	90.3	100

The detailed PCI and PCR calculations are provided in Appendix B. Based on these surveys it can be, at the very least, concluded that the inverted section is performing as well, if not better than

the conventional pavement section. This result is despite the potential reflective cracking caused by the overly stiff concrete base.

2.3. Summary of Falling Weight Deflectometer Testing

The North Carolina DOT has conducted falling weight deflectometer (FWD) testing on six different occasions; September 2015, June 2016, December 2016, August 2017, April 2018, August 2020, and October 2022. The tests were conducted at different times of the year and a summary of the test date, corresponding pavement surface temperature and air temperature are shown below in Table 5. Deflections at the loading plate, D0, values from each of the FWD tests at every100 ft are shown in Table 6.

Table 5. FWD Test Details

Test Number	Test Date	Test Time	Surface Temperature (°F)	Air Temperature (°F)
1	9/29/2015	10:30 am	76	76
2	6/7/2016	10:45 am	95	78
3	12/12/2016	7:31 am	49	46
4	8/3/2017	7:51 am	95	76
5	4/17/2018	10:55 am	58	56
6	8/27/2020	9:52 am	87	80
7	10/18/2022	10:34 am	56	58

Table 6. FWD Deflection (D0) Data Summary

Section	Station	Deflection (mils)						
		Test 1	Test 2	Test 3	Test 4	Test 5	Test 6	Test 7
Inverted	1+00	8.28	9.87	5.61	7.43	6.71	7.20	8.28
	2+00	7.91	8.94	5.90	7.21	6.62	7.06	7.91
	3+00	7.67	9.87	6.26	7.69	6.79	7.29	7.67
	4+00	7.87	10.42	6.55	8.14	7.35	7.57	7.87
	5+00	6.47	8.76	5.33	7.02	6.30	7.01	6.47
	6+00	7.45	9.88	6.45	8.46	7.23	7.63	7.45
	7+00	8.56	8.39	5.74	7.42	6.58	7.09	8.56
	8+00	8.53	10.82	6.34	8.40	7.41	7.93	8.53
Conv.	9+00	10.07	17.53	8.71	15.46	11.16	14.33	10.07
	10+00	11.49	19.92	10.83	17.43	14.22	17.47	11.49
	11+00	12.28	21.47	9.88	16.89	12.58	15.81	12.28
	12+00	9.61	20.76	10.27	17.04	12.30	16.22	9.61
	13+00	12.66	33.73	14.45	29.63	21.16	24.62	12.66
	14+00	9.66	23.94	9.67	20.61	13.71	19.24	9.66
	15+00	11.95	31.89	11.76	29.46	15.92	25.05	11.95
	16+00	12.05	25.34	10.53	22.09	14.22	21.29	12.05

Due to this seasonal variation, the deflections values in Table 6 along with their corresponding surface temperatures from Table 5 were corrected to 68°F using the methodology described in the AASHTO 1993 design guide (AASHTO 1993). This method essentially multiples the measured deflection by a correction factor, *CF*, obtained from charts in the design guide, see Equation (1).

$$D0_{corrected} = D0 \times CF \quad (1)$$

The chart for granular base was used to correct the conventional pavement (Figure 5.6 in the design guide), while the chart for cement or pozzolanic treated base was used for correcting the inverted pavement (Figure 5.7 in the design guide). The temperature corrected deflection (D0) below the load at stations every 100 ft is shown in Figure 10. The following observations can be made from the deflection measurements.

1. Despite applying temperature correction, the seasonal variation in the displacement is still evident especially for the conventional pavement.
2. Overall, the average deflection in the inverted section was 7.61 mils and less in comparison to the average deflection of 16.04 mils in the conventional pavement.
3. A clear increasing trend can be observed in the deflection with time for the conventional with an average increase of 58% from 09/29/2015 to 8/27/2020, whereas there is very little variation in the deflection in inverted section over the same time.

Based on the above observations, it can be concluded that the inverted pavement has performed better in comparison to the conventional pavements with age. Generally speaking, this result is in line with the conclusions from the condition survey summarized in the previous section. The most recent measurements on the inverted site (10/18/2022) show a larger increase than other sequential measurement and warrant continued investigation of the site.

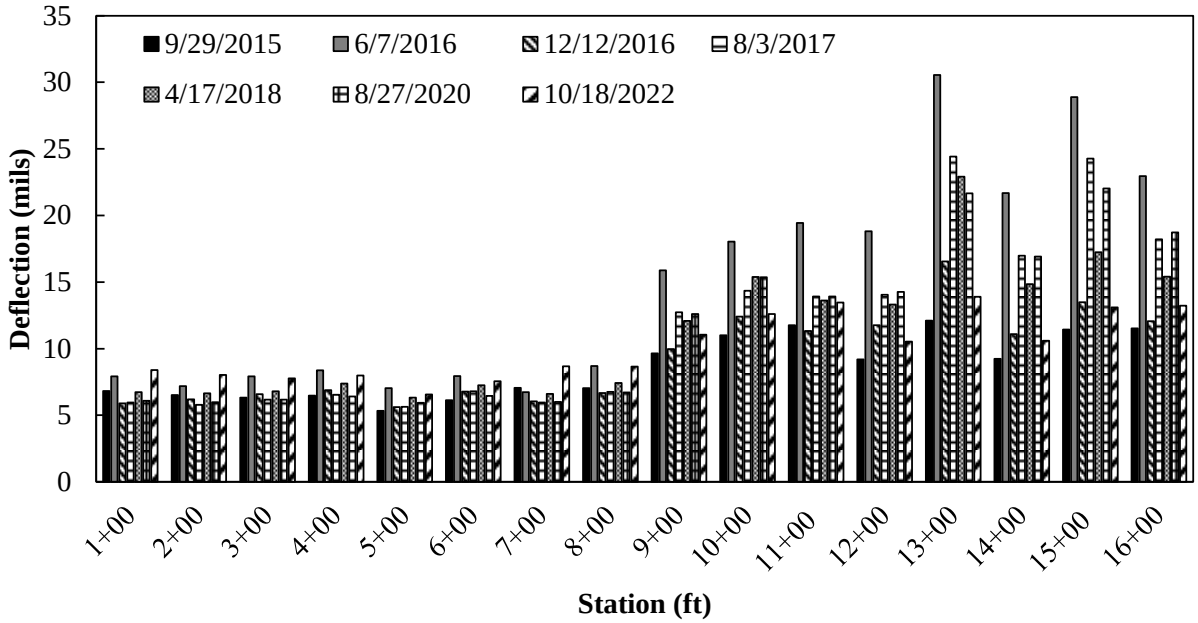

Figure 10. Temperature corrected FWD deflection (D0) across the entire pavement section.

2.4. Summary of TSD testing

In addition to the FWD tests, a TSD test was conducted at the site in September 2021. TSD can measure deflection of the pavement at traffic speed to generate a continuous profile unlike FWD where only discrete measurements are made. Deflections (D0) from the TSD measurements show a similar trend in comparison to FWD measurements from 08/27/2020 and shown in Figure 11. The air temperature at the time of TSD testing was 29.4°C and the surface temperature was 38.7°C. FWD testing on 08/27/2020 was done at an average air temperature of 26.5°C and average surface temperature of 30.4°C. Although the temperatures are different, a direct comparison of the deflections is presented without any corrections. The average defection from TSD is 4.17 mils and 17.04 mils for the inverted and conventional sections respectively. The average defection from FWD is 7.33 mils and 19.85 mils for the inverted and conventional sections respectively. Average TSD deflection in the inverted section is smaller than the FWD deflection by approximately 55%. In the conventional site, the TSD is also higher for stations 9+00 through 12+00 (approximately 19% greater), but very similar for all remaining sections (except station 15+00). TSD deflections are lower than the FWD measurements in spite of the test being conducted at a higher temperature. Further, any temperature correction will only exacerbate the differences between the TSD and FWD measurements. The higher percentage difference between TSD and FWD deflections in the inverted section is interesting, but no definitive explanation was found in the data. Nevertheless, the systematic bias would warrant further investigation should inverted pavements be deployed and if TSD were to be used extensively. Overall TSD measurements paint a picture similar to the condition survey and FWD results, but the exact differences suggested by each method differs slightly.

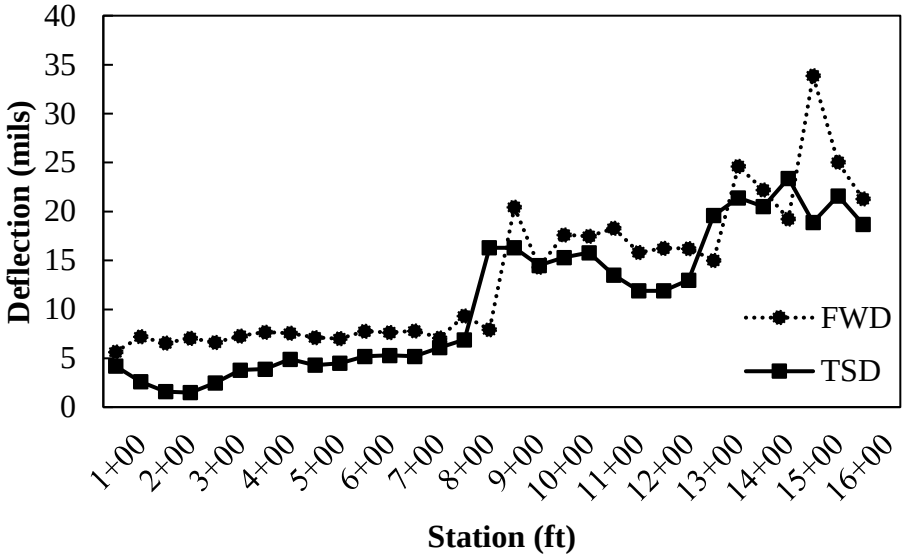

Figure 11. TSD vs FWD deflections at Pineville site.

2.5. Field Cores Testing

After confirming the pavement thickness and density, the field cores were used to estimate the modulus and thus the material integrity of the layers in the inverted and conventional pavement sites. The testing plan involved first measuring modulus using the impact resonance (IR) method on the as-extracted cores and on disks sliced for extracted cores to separate the surface and intermediate layers (conventional pavement only). After IR testing, the extracted cores were then

cored again, this time horizontally, to obtain specimens for mechanical testing of dynamic modulus.

2.5.1. Impact Resonance Testing

IR testing of pavement cores is a well-studied and standardized technique to estimate the dynamic modulus (Ryden 2009; Kim and Kim 2017). The IR method has the advantage of being simpler and more efficient compared to the standard axial compression dynamic modulus tests. ASTM C215-08 and ASTM E1876-02, originally developed for portland cement concrete, have often been adopted to test thin disk pavement cores. Prior to testing, approximately the top and bottom 5 mm were removed using a saw. This process ensured that the surface of the specimen was smooth and flat.

Applying IR testing directly on field cores poses a challenge because their dimensions do not conform to the requirements of the ASTM standards and thus the equations from the standards cannot be used to calculate the modulus from the resonant frequencies. Nevertheless, irrespective of the specimen dimensions, modulus is proportional to the square of the resonant frequency and the constant of proportionality is a complex function of the dimensions, density, and Poisson's ratio. In this study, the cores were modelled using finite elements in ANSYS with their accurate dimensions, calculated density, an assumed Poisson's ratio, and a modulus value of 1 N/m^2. A unit value for the modulus is assumed to facilitate the direct computation of the constant of proportionality from the ANSYS modelling, which can then be used along with the resonant frequency calculated from the IR test to estimate the modulus of the core. Poisson's ratio of asphalt is also dependent on the temperature and frequency. Given the IR tests were conducted in room temperature and frequency range of the resonant frequencies, a Poisson's ratio of 0.3 was deemed appropriate (Momen 2004). Several impact and measurement scenarios were tested, but the most standard method of impacting the center of the top face with a steel ball and measuring the response at the opposite face was adopted. All IR tests were conducted with specimen supported on soft foam layers to excite free-free resonant modes. The test configuration and the corresponding mode of vibration from ANSYS are shown in Figure 12. Further details on the different modes and corresponding modulus back calculation can be found in Appendix (C). The same mode of testing was adopted for both the conventional and inverted pavement cores.

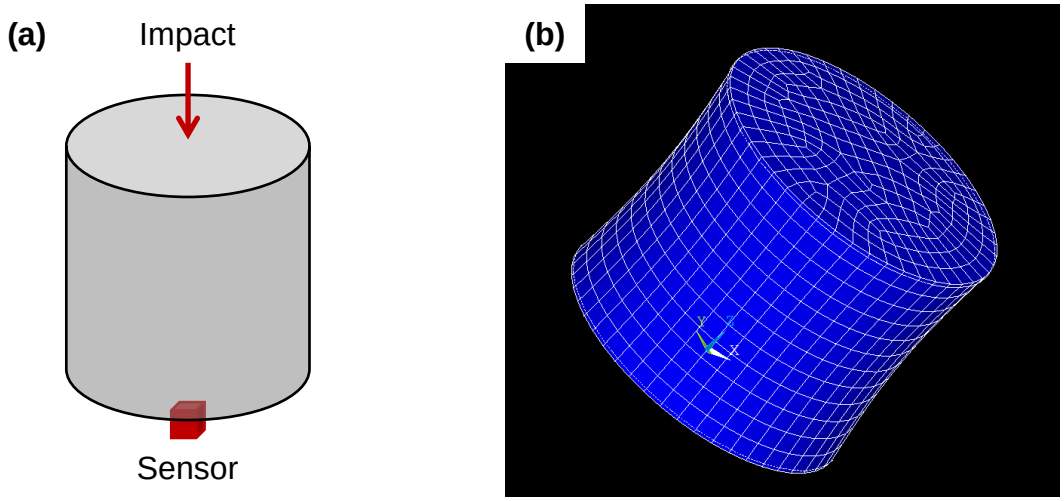

Figure 12. Impact resonance testing; (a) test configuration and (b) mode shape (ANSYS).

The IR modulus values computed using the above procedure for all the cores are summarized below in Figure 13 and Table 7. The Conventional pavement design consisted of 2.5 in. of S9.5B mix on top of 3.5 in. of I19B mix. The inverted pavement design consisted of 1 in. of S9.5A on top of 1.5 in. of S9.5B. It is expected that the IR modulus computed from the entire core is an average of the two layers. After testing the whole conventional pavement cores, they were sliced into two thinner layers to approximately separate the surfaced and intermediate layer materials. The same IR method was then used to measure the modulus of both layers. The computed modulus values for the full core, top section and bottom section are shown in Figure 13. The IR modulus from the bottom section of the cores were higher compared to the top section of the same core indicating that the I19B mix has a higher modulus compared to the S9.5B surface mix. Since the inverted pavement cores were thinner to start with, no further cutting was possible to test the individual layers. The modulus values from the inverted cores were lesser compared to the conventional cores on an average.

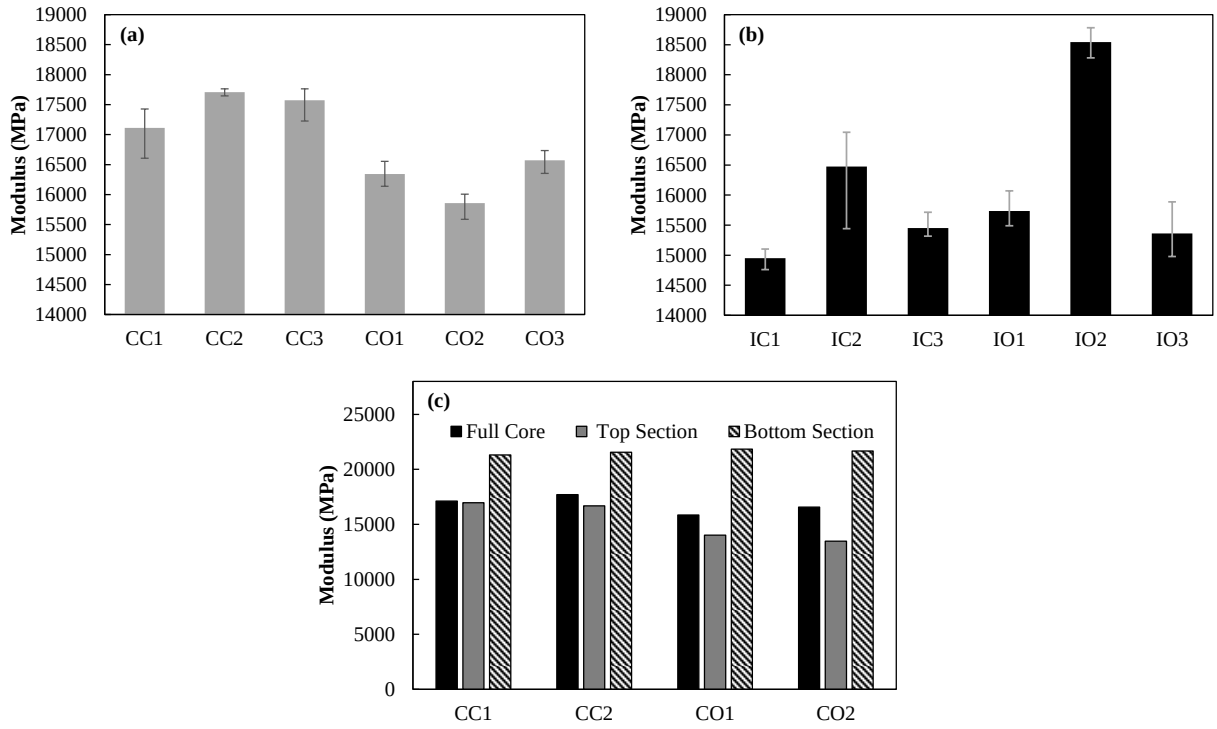

Figure 13. IR modulus estimate; (a) conventional pavement cores, (b) inverted pavement cores, and (c) surface and intermediate layers in comparison to full conventional pavement cores.

2.5.2. Dynamic Modulus Testing

The field cores were further cored to make small cylinder specimens to use to evaluate the dynamic modulus master curve following the AASHTO TP 133 standard. Two small cylinders were extracted from each of the inverted cores and each of the sections from the conventional cores. Example test specimens taken from the IC2 and IO2 cores are shown in Figure 14 and the corresponding bulk density values for the specimens are shown in Figure 15. Of note from Figure 15, is the relative consistency in inverted density and bottom layer density of the conventional site, but higher differences between the center and outer paths in the top layer of the conventional pavement. Again, the G_{mm} values were not measured for these sites, but using an estimated value

of 2.600 yields a maximum range in air void content across all specimens in the inverted site of 5.1-8.4%, a maximum range in the bottom layer of the conventional site of 3-5%, and a maximum range of 5.5-9.5% for the surface layer in the conventional site.

The values measured from the testing on each site are given in Appendix D along with the best fit master curve coefficients as determined from FlexMAT^{TM} 2.1.2. It is noted that the allowable repeatability limits in AASHTO T 378 were generally met in this testing, though in some cases the limits were exceeded. This outcome was anticipated since the tests were being done on field extracted (as opposed to lab prepared) specimens. It is also noted that the variation between test specimens extracted from the same core were all below the allowable limits.

Table 7. Impact Resonance Modulus for all Cores

Pavement	Location	Code	Depth (in.)	ANSYS Cons. (m/kg)	Mean Resonant Freq. (Hz)	Modulus (MPa)
Conventional	Center	CC1	4.6	0.07252	9486	17111
		CC2	4.7	0.07197	9576	17707
		CC3	4.7	0.07153	9482	17574
		CC1-T	2.2	0.05723	7453	16962
		CC2-T	2.1	0.05640	7283	16674
		CC1-B	2.3	0.05744	8385	21312
		CC2-B	2.4	0.05827	8556	21557
	Outer	CO1	5.2	0.06832	8734	16342
		CO2	5.1	0.06868	8648	15858
		CO3	5.1	0.06932	8924	16573
		CO1-T	2.2	0.05747	6804	14013
		CO2-T	2.1	0.05618	6522	13478
		CO1-B	2.7	0.06229	9205	21836
		CO2-B	2.9	0.06258	9213	21673
Inverted	Center	IC1	2.3	0.05815	7109	14950
		IC2	2.4	0.05934	7616	16474
		IC3	2.0	0.05430	6750	15452
	Outer	IO1	2.2	0.05704	7155	15736
		IO2	2.3	0.05821	7927	18543
		IO3	2.3	0.05855	7257	15363

The dynamic modulus master curves are shown along with the IR modulus estimates for each of the pavement types are shown in Figure 16. Time temperature superposition using the coefficients from the dynamic modulus testing were applied to the IR modulus results, which were obtained at a temperature of 22.7°C (the IR test temperature) for direct comparison with the master curves. The observations for the inverted and conventional pavement are summarized below.

Figure 14. Small cylinders extracted from cores IC2 and IO2.

- Inverted pavement
  - The average modulus from the outer cores was higher compared to the center cores by approximately 10% to 20% in the range of reduced frequencies measured.
  - The average IR modulus values for both the center and outer cores were higher compared to the master curve values by approximately 22% and 12% respectively.
- Conventional pavement
  - The average modulus from the top section of each core was lower compared to the bottom section of the same core for both the center and outer test locations.
  - The average modulus from the top section of the center location cores was higher compared to the top section of the outer location cores.
  - The modulus of the bottom sections for the center and outer location cores were statistically similar (p-value of 0.8) at higher reduced frequencies and statistically different (p-value of 0.0005) at lower reduced frequencies. Statistical significance was computed using a two-sided t-test.
  - The IR modulus estimated from the top sections was approximately 5% to 15% higher than the corresponding master curves.
  - The IR modulus from the bottom sections was approximately 3% to 5% higher than the corresponding master curve.
  - The IR modulus had a value between that of the top and bottom section moduli.

The IR modulus values are in general higher than the corresponding value from the AASHTO TP 132 testing for both the conventional and inverted cores. This result is expected as the strain rate in the IR test is much smaller than the mechanical testing, and the asphalt concrete modulus has been found to be strain dependent (Underwood and Kim 2012; Underwood and Kim 2013).

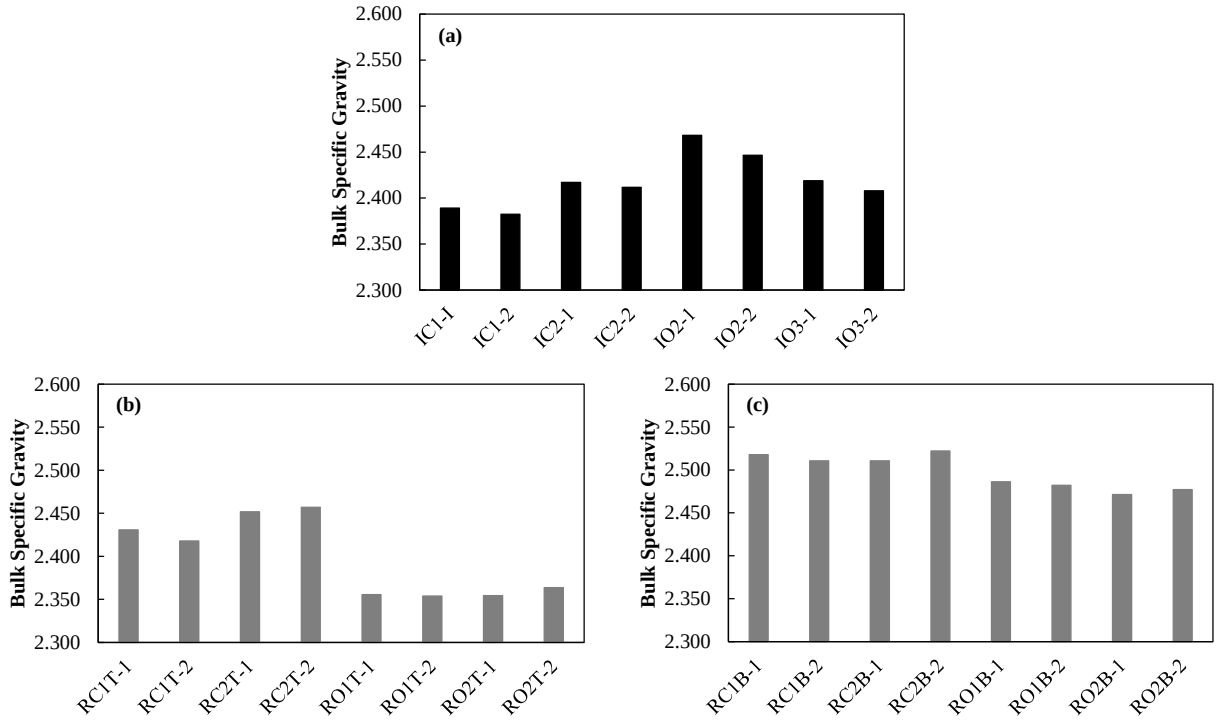

Figure 15. Small cylinder bulk specific gravity; (a) inverted pavement ,(b) conventional pavement top section, and (c) conventional pavement bottom section.

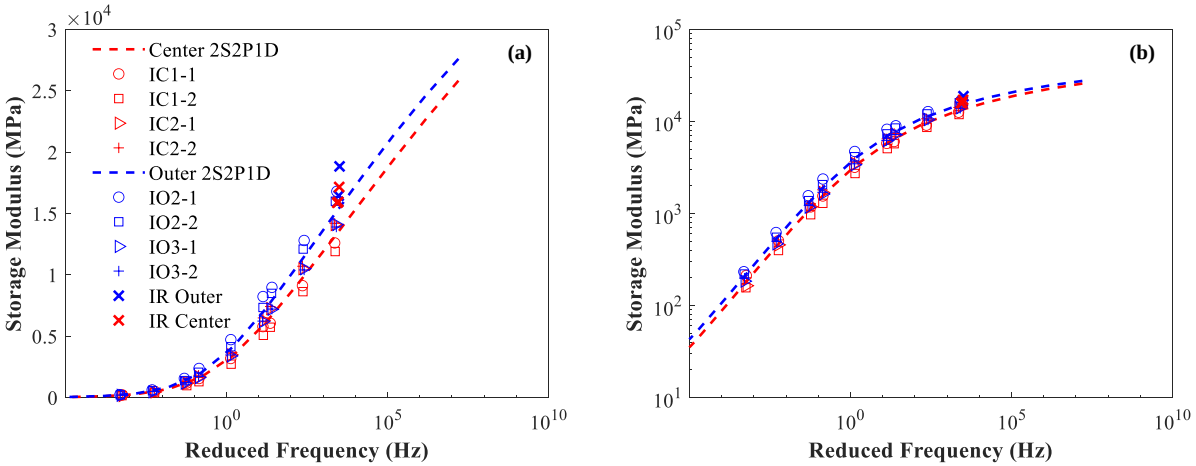

Figure 16. Dynamic modulus master curve from inverted pavement cores; (a) semi-log scale and (b) log-log scale.

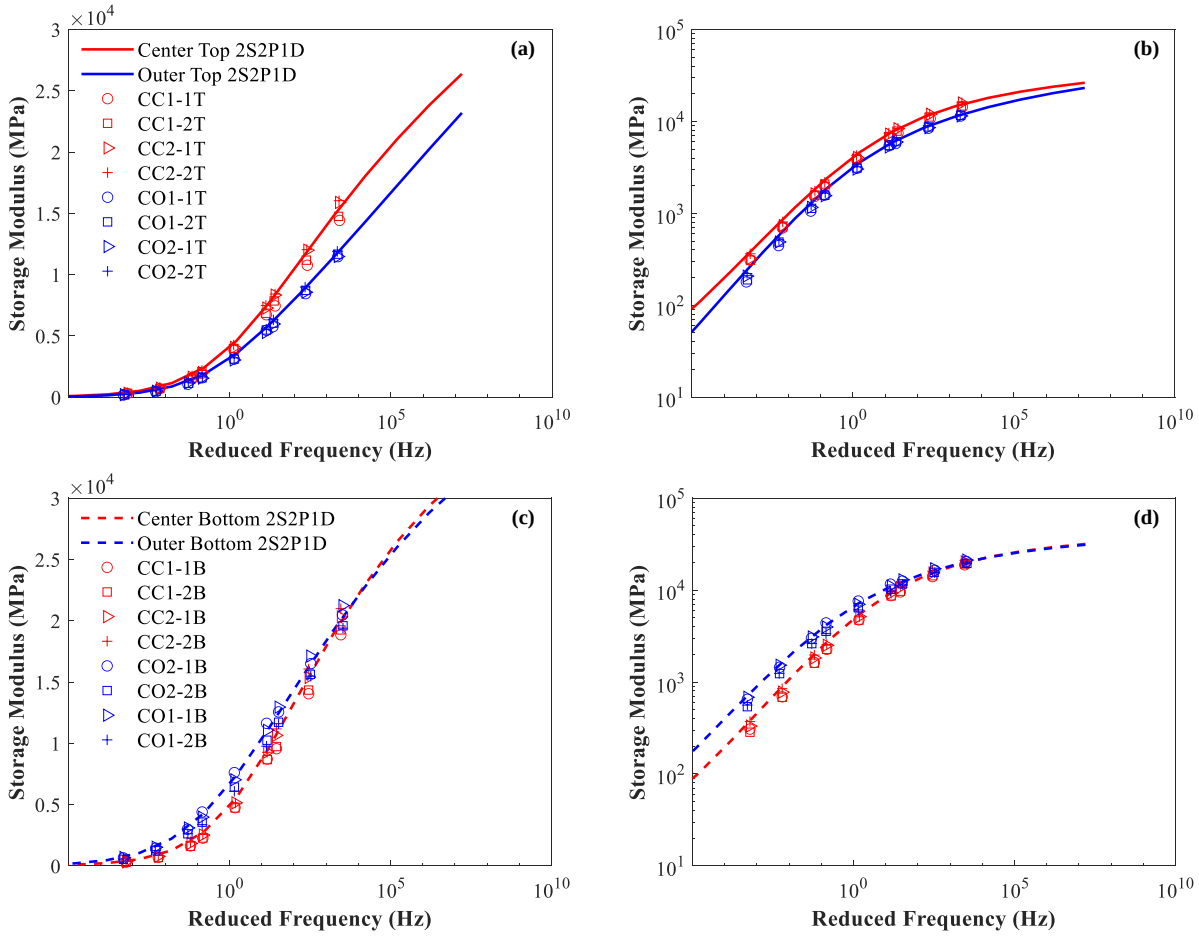

Figure 17. Dynamic modulus master curve from conventional pavement cores; (a) center top semi-log scale, (b) outer top log-log scale, (c) center bottom semi-log scale, and (d) outer bottom log-log scale.

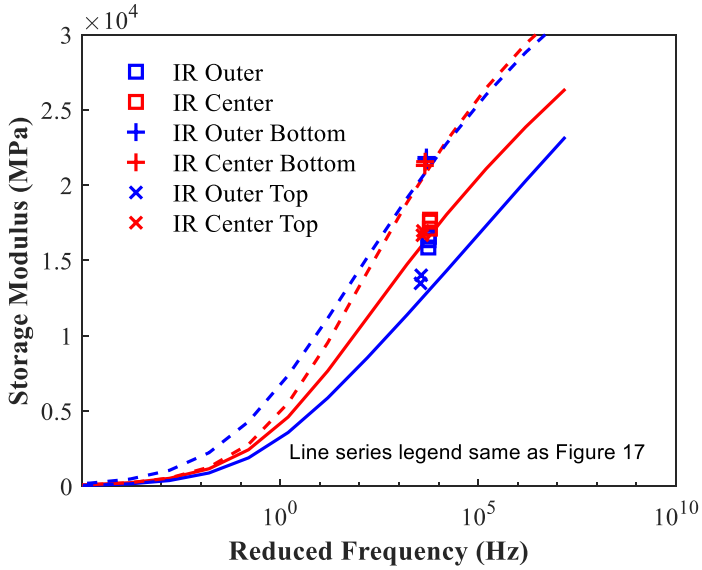

Figure 18. Dynamic modulus and impact resonance comparison.

2.6. Cost Benefit Analysis

Since to this point there is no clear evidence of the inverted pavement either outperforming or underperforming the conventional pavement, the cost-benefit analysis can be done solely on the basis of construction costs. To this end it was found that the conventional pavement, consisting 2.5 in. of S9.5B, 3.5 in. of I19B, and 10 in. of ABC cost $40.51 per square yard of pavement. The inverted pavement, consisting of 1.0 in. of S9.5A, 1.5 in. of S9.5B, 6 in. of ABC, and 8 in. of CTB cost $35.92 per square yard of pavement, 11.3% less expensive than the conventional pavement. However, it was noted that the distance to the ABC source may have contributed to some of these savings. Other published costs differences range from +20% (Louisiana) to -40% (Georgia). In the case of the Louisiana study it was noted that the longevity is likely to exceed a factor of 5 (Titi et al. 2003). South African estimates suggest a total net savings of inverted pavements compared with equivalent conventional pavements at 20-25% (SANRAL 1998). In short, there does appear to be a net cost-benefit savings potential for inverted pavements, but longer term performance measurements are needed to confirm these differences.

This page is intentionally blank

3. OVERVIEW OF SURFACE WAVE TESTING METHODOLOGY

3.1. Methodology

Based on the findings from the literature review (see Appendix A), the Multichannel Simulation using One Receiver (MSOR) has been adopted as the test methodology for this project. The surface wave testing method used with MSOR consists of three major steps,

1. Data acquisition – Inducing and measuring surface waves at sufficient resolution both in time and space. Several parameters influence the data such as hammer size, offset (distance between the sensors and the first impact), spacing between the impacts, and number of impacts.
2. Data analysis – Signal processing and data analysis to extract the dispersion curves from the recorded surface trace. Two different methods were used to extract the dispersion curves in this project.
3. Inversion – Back calculation of the layer properties by matching the experimental dispersion curves to theoretical dispersion curves from a forward model of the pavement layer system.

Each of the above steps in detailed in the following subsections.

3.1.1. Data Acquisition

A schematic of the data acquisition procedure using the MSOR method is shown below in Figure 19 (a) and a picture from one of the field tests with the equipment labelled is shown in Figure 19 (b). As mentioned earlier, an accurate trigger mechanism is critical for successfully using the MSOR method. An accelerometer attached to the hammer is used to trigger the data acquisition in the sensor attached to the pavement surface. National Instruments module NI-9234 with a NI-9171 chassis was used along with PCB 352C33 accelerometers for data acquisition. PCB 353B03 with a larger measurement range of ±500 g was attached to the hammer for triggering purposes. A laptop computer powers the entire data acquisition system and records the test data through a program developed using LabVIEW. An infrared thermometer was used to measure the pavement surface temperature over the duration of each test.

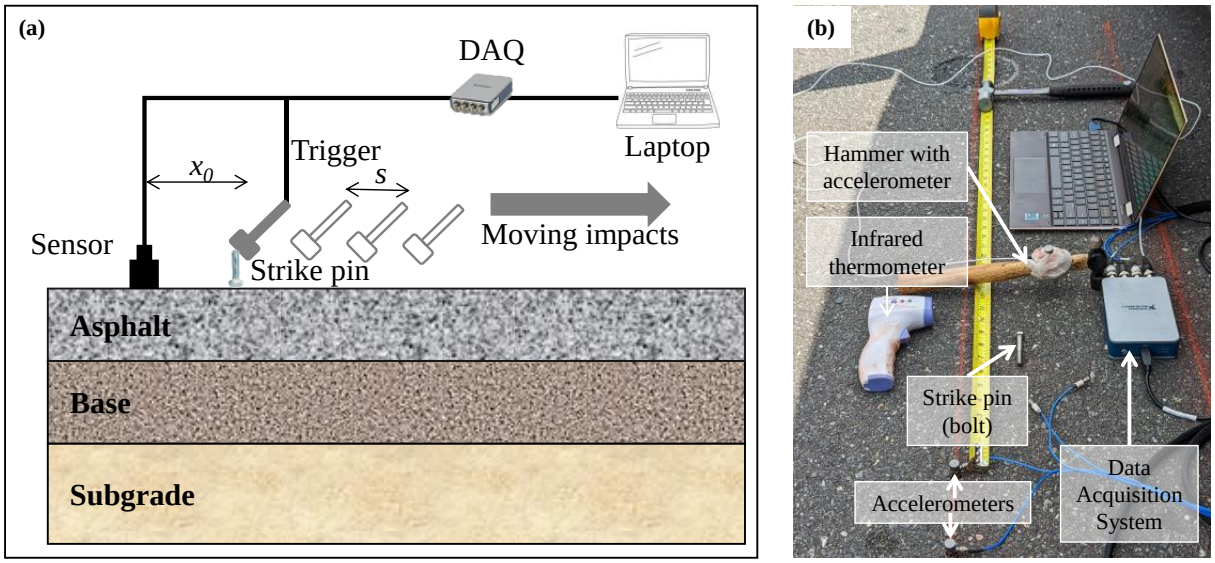

Figure 19. Surface wave testing setup; (a) test schematic and (b) test at field site.

At the project outset, the research team conducted a set of pilot experiments at a NCSU parking lot. On the basis of these pilot experiments and the literature review, the parameters that influence the data including source offset, impact spacing, number of impacts, and hammer characteristics were chosen. Since a four-channel data acquisition system was used, three sensors at increasing offset, typically ranging from 1 to 12 in., were used to build redundancy. A 225 g steel tip hammer along with a hex bolt was used to control the impact location.

A total of six test sites were investigated in this study (three inverted sites and three conventional sites) as shown in Table 8. Note that one site for each of the inverted and conventional pavements are labeled as 'core sites'. These sites correspond to the location of the cores that were taken on the pavements. The tests at these sites were conducted between each core location after the coring was done and no tests were conducted at the core sites prior to the coring. Each test site was located on the southbound lane and was laid out as shown in Figure 20. The motivation for the chosen test layout was to obtain as much data as possible so the data processing can be done at different offsets, spacing and number of impacts. Testing was conducted at approximately 30 in. from the pavement edge (referred to as the 'Outer' test location), approximately 72 in. from the pavement edge ('Center' test location), and in some sites, 114 in. from the pavement edge ('Inner' test location) to evaluate the potential differences in asphalt layer properties within a lane. It was originally believed that wheel loads were applied at each site on the 'Outer' location and that the 'Center' location was left largely unloaded. However, as the project proceeded it was found that this assumption was not necessarily true. Trucks using the roadway tended to more often travel through the 'Center' locations, but this varied considerably from test site to test site.

Table 8. Summary of all Surface Wave Testing

Site No.	Station	Code	Location	Average Surface Temp. (°C)			
				Test 1	Test 2	Test 3	Test 4
Conventional Pavement Section							
Site 1	10+35	CS1O	Outer	6	23	32	51
		CS1C	Center	6	22	29	41
		CS1I	Inner	7	25	27	40
Site 2	9+90	CS2O	Outer	13	17		
		CS2C	Center	16	19	37	
Core Site	10+75	CCS3C-CCS2C	Center cores 3 and 2	29			
		CCS2C-CCS1C	Center cores 2 and 1	28			
		CCS3O-CCS2O	Outer cores 3 and 2	27			
		CCS2O-CCS1O	Outer cores 2 and 1	28			
Inverted Pavement Section							
Site 1	4+00	IS1O	Outer	13	19	30	51
		IS1C	Center	14	28	53	
		IS1I	Inner	17			
Site 2	3+00	IS2O	Outer	10	18	27	44
		IS2C	Center	10	25	30	57
Core Site	3+60	ICS3C-ICS2C	Center cores 3 and 2	31			
		ICS2C-ICS1C	Center cores 2 and 1	33			
		ICS3O-ICS2O	Outer cores 3 and 2	29			
		ICS2O-ICS1O	Outer cores 2 and 1	38			

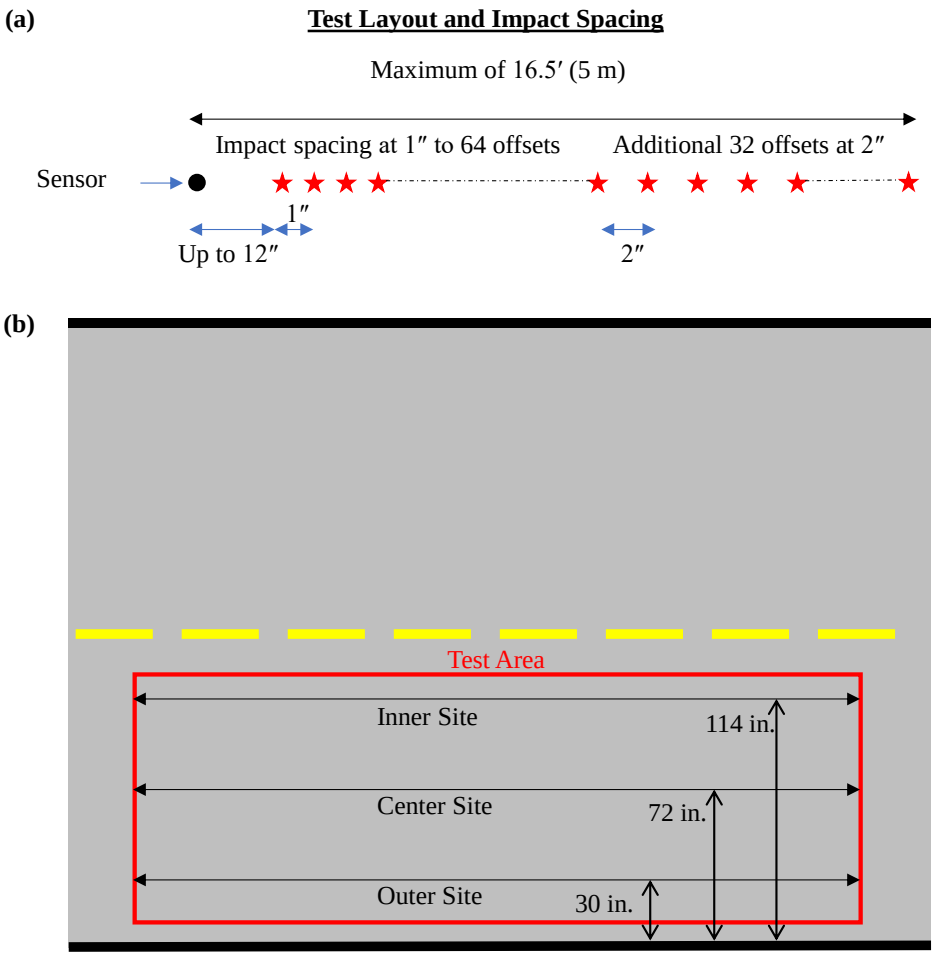

Figure 20. Test site layout for surface wave testing; (a) spacing of impacts at test location and (b) road schematic with typical test locations in a lane.

A typical recorded surface trace as a function of time and offset is shown in Figure 21. Each blue line represents the signal recorded in the accelerometer from a single surface strike as a function of time. The time at which the signal is first arrives at the accelerometer continually increases as the distance between the strike and the accelerometer increases. In total, four different site visits were made (Fall 2021, Winter 2021, Spring 2022, and Summer 2022) and sites were tested during one or more of these visits, as summarized in Table 8 based on the location and measured surface temperature at the time of the test. The initial setup of each site required approximately 15 minutes and a test (involving all 96 offsets) could be completed in approximately 30-40 minutes with a single operator. During the testing temperatures were taken at the beginning, at the half-way point, and at the end of each test. The temperatures shown in Table 8 are the average of these three measurements.

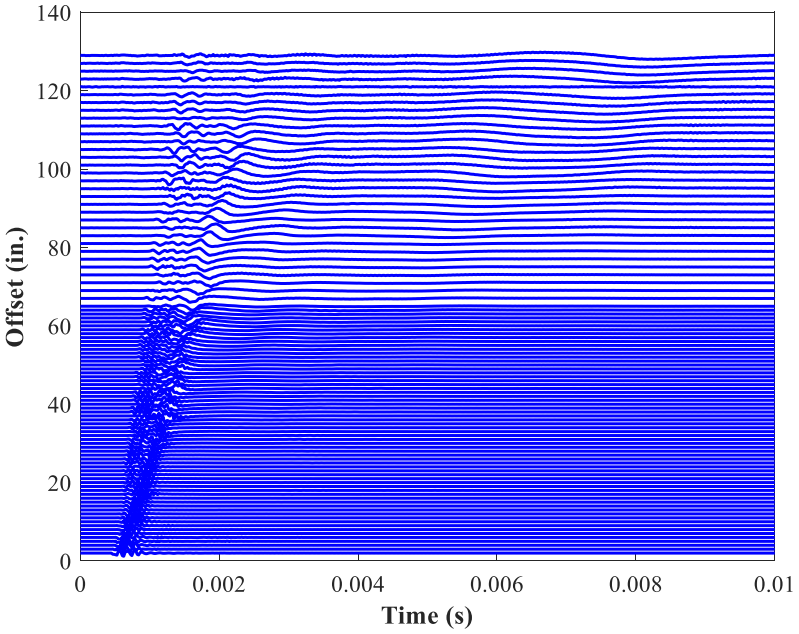

Figure 21. Typical surface trace from MSOR testing.

3.1.2. Data Analysis

Two methods, named FK (frequency-wavenumber) and FP (frequency-phase velocity), were used to obtain the dispersion curves from the recorded data. To compute the FK dispersion curves, the surface trace plots were Fourier transformed in both time and offset domain to obtain the frequency wavenumber plot. Data was preprocessed to include sufficient padding in both time and offset direction to extract accurate dispersion curves. The peak wavenumber at each frequency is used to calculate the phase velocity as the ratio of frequency and wavenumber. The FP spectrum was obtained by first applying the time Fourier transform and then evaluating the slant-stack amplitudes for a range of phase velocities to obtain a two-dimensional spectrum. Similar to FK, the peak phase velocity was calculated at each frequency to obtain the FP dispersion curve from the FP spectrum. Further details on the FK and FP processing techniques can be found in (Beaty and Schmitt 2003).

Typical dispersion curves from the conventional and inverted pavement sections are shown below in Figure 22. Dispersion curves from both the methods are comparable with minor differences. Unlike FK analysis, FP spectrum computation involves normalizing the signal at each frequency and offset and thus there are minor differences in the dispersion curves obtained from the two methods at the lower frequencies. A large portion of the computed dispersion curve is at phase velocities below 2000 m/s indicating the dominance of the fundamental bending mode of wave propagation. Several breaks are observed, especially from FP processing, with the curves jumping to a higher phase velocity. These higher phase velocity regions (above 2000 m/s) of the dispersion curves potentially correspond to the fundamental longitudinal mode of wave propagation although this information is not utilized in this study.

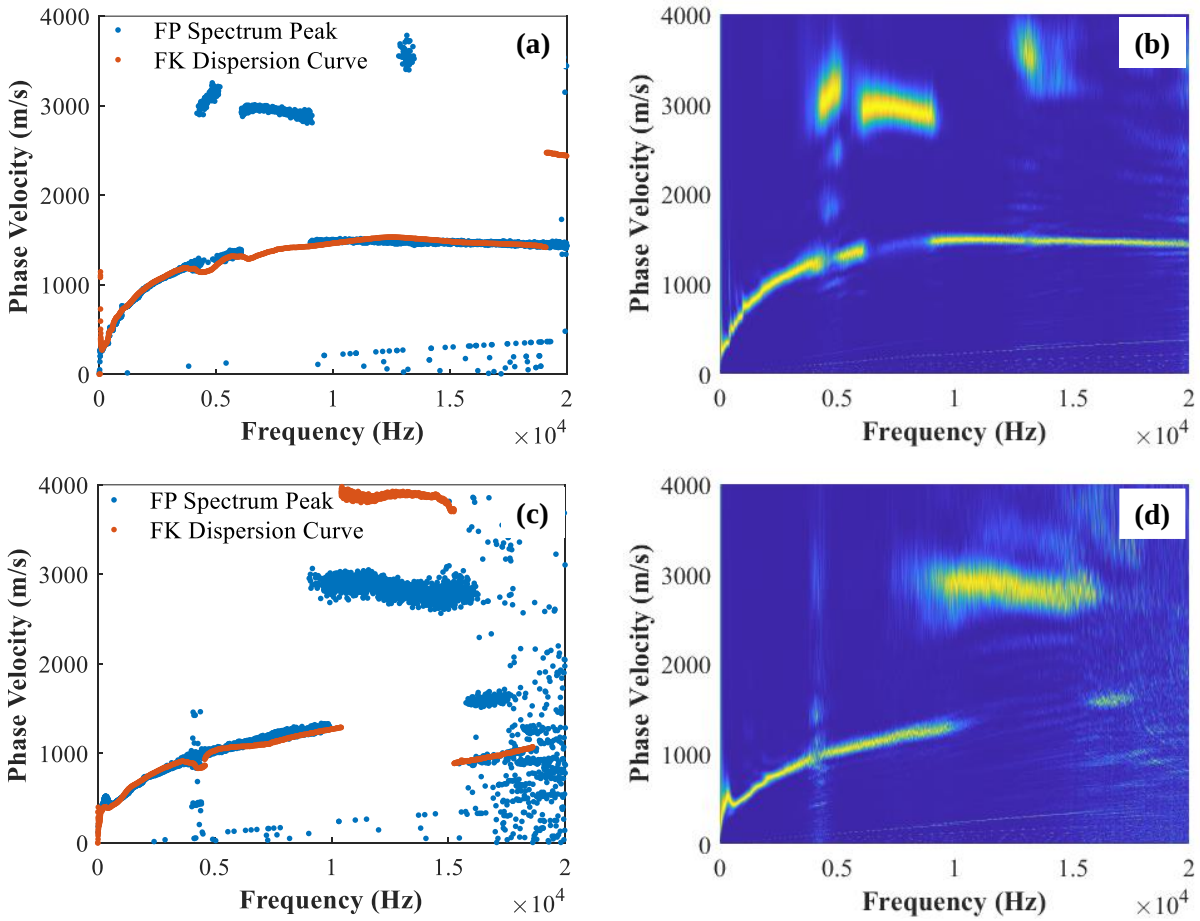

Figure 22. Representative dispersion curves; (a) conventional pavement site FP vs FK processing, (b) conventional pavement site FP spectrum, (c) inverted pavement site FP vs FK processing, and (d) inverted pavement site FP spectrum.

Assessment of Repeatability of the Test and Analysis Method

One concern with the MSOR method is the repeatability of the test since the impact is moving and small errors in positioning the strike pin are unavoidable. In this study, the repeatability of the test was important since measurements were to be taken repeatedly for the same test site at different pavement temperatures. To quantify the repeatability of the testing, an experiment was conducted wherein a test was performed at CS1C two different times, one week apart and at approximately the same time of day (i.e., when the surface temperatures were similar). The resulting dispersion curves from the tests were almost identical with minor differences in the higher frequencies, which could be due to slight changes in the impact locations.

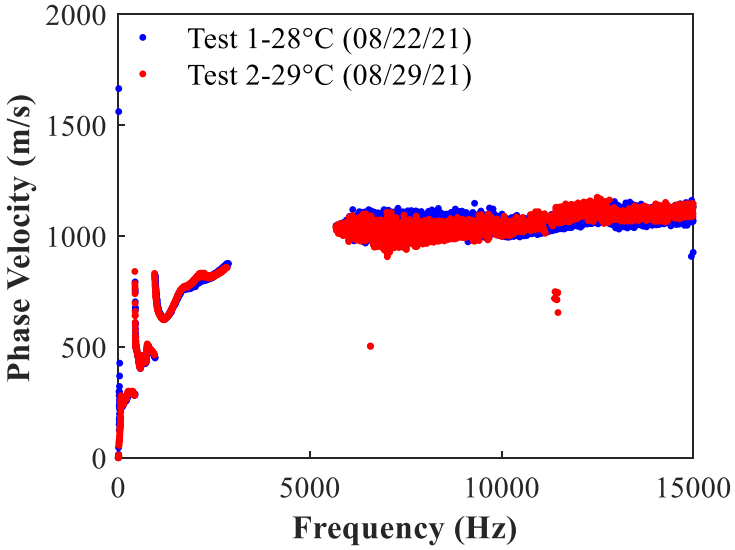

Figure 23. Repeatability of surface wave testing.

Assessment of Sensitivity of Test and Analysis Method to Structural Effects

A comparison of the dispersion curve obtained from a conventional pavement site and inverted pavement site at approximately the same surface temperature are shown in Figure 24. The dispersion curves are sensitive to the layering of the pavement structure and is clear from the different 'signatures' of the two curves. While the pavements are at a similar temperatures and thus comparable moduli, the significant difference observed at the higher frequencies is attributed to the difference in the thickness of the conventional and inverted pavement. On the contrary, the differences in the lower frequency are attributed to the structural difference in the deeper layers between the two pavement types. All these features, both at higher and lower frequencies, will be used to back calculate the layer properties in Section 3.3.

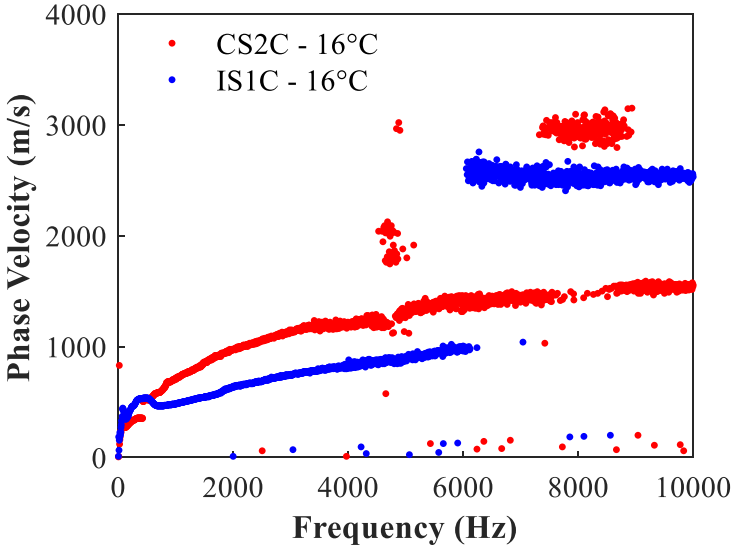

Figure 24. Dispersion curve comparison between conventional and inverted pavement.

Assessment of Sensitivity of Test and Analysis Method to Temperature Effects

It is well known that pavement materials are viscoelastic, and the modulus is a function of loading frequency and temperature. Surface wave testing can capture these effects as evidenced by the dispersion curves shown in Figure 25, which shows the curves for the CS1O and the IS1O sites measured on different days and at different surface temperatures. The following observations can be made from the figures,

1. The phase velocity at any given frequency is lower at higher temperatures indicating a reduction in the asphalt layer modulus at higher temperatures.
2. At lower temperatures, the dispersion curve is continuous and less noisy even up to frequencies of 10 kHz.
3. At higher temperatures, the dispersion curves become increasingly noisy and unstable at higher frequencies due to higher attenuation of the waves.

Thus, the usable frequency range for a given test depends on the test temperature. Since three sensors were used for each test, the repeatability within each test can be examined to identify the highest frequency that can be used for each temperature. This data analysis procedure results in the experimental dispersion curve, but an efficient forward model of the pavement system is critical to back calculate the layer properties.

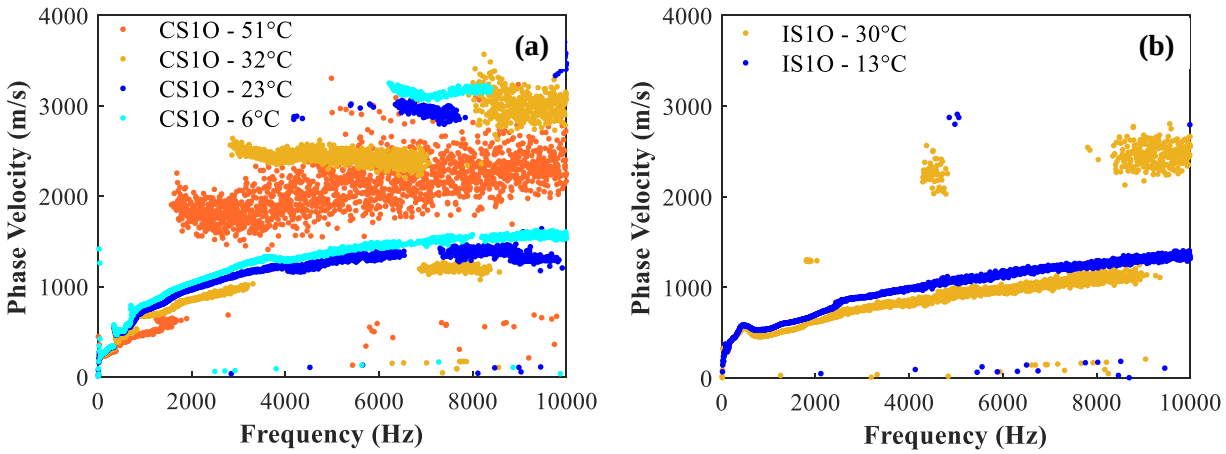

Figure 25. Seasonal variations captured from surface wave testing; (a) conventional pavement and (b) inverted pavement.

3.2. Modelling of Pavement Layers

Pavements are typically modelled as a set of finite layers (asphalt, base, etc.) on top of an infinite layer (subgrade). During surface wave testing of the pavement, the surface accelerations are measured through an accelerometer attached to the pavement surface. The fundamental idea for estimating the layer properties is to match the experimental dispersion curve to a theoretical dispersion curve computed from a model, i.e., by back calculation or inversion. Computation of the effective dispersion curve from the model is established in a two-step process.

1. Compute the theoretical dispersion curves using a semi analytic finite element approach, which will provide all possible modes of wave propagation that can exist in the layered pavement structure.

2. Compute the effective dispersion curve through Green's function and carefully chosen theoretical modes that influence the surface response at the same experimental sensor locations.

The method used in this study is adapted from similar efforts developed by the Co-PI for geophysical systems (Vaziri and Guddati 2016). Modelling the pavement layers involves using two newly developed methods for efficient modelling of finite pavement layers and infinite layers using Complex Length Finite Elements (CFEM) and Perfectly Matched Discrete Layers (PMDL) respectively.

The process starts by considering a two-dimensional layered elastic waveguide as shown in Figure 26. Each layer is assumed homogeneous and horizontally infinite with varying thickness and material properties across layers. Layer thickness, shear wave velocity, Poisson's ratio and density of each layer are required for the forward modeling. Viscoelasticity can be incorporated using complex valued wave velocities. Further details and mathematical derivations can be found in Appendix E and Vaziri and Guddati (2016). The important modifications and considerations for modelling pavement layers are summarized below.

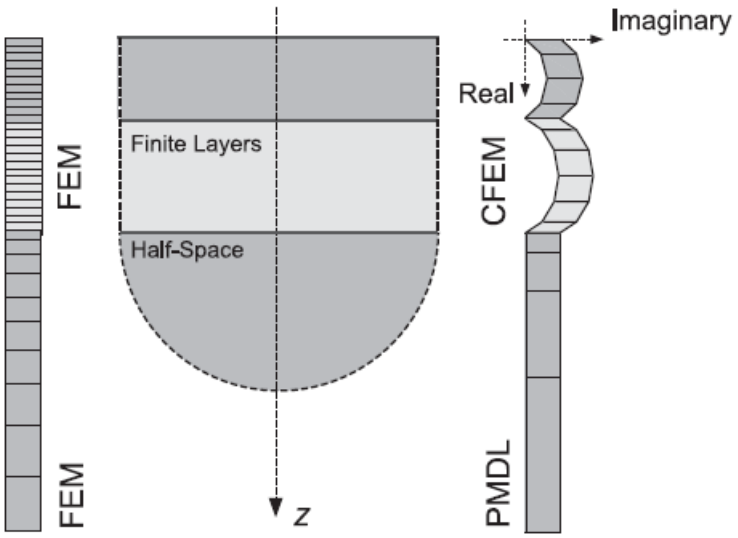

Figure 26. Schematic of pavement layer model using CFEM and PMDL in comparison to regular FEM (Vaziri and Guddati 2016).

- *CFEM* – Regular finite elements (FEM) require very fine discretization to achieve the required accuracy, which can be computationally prohibitive. To overcome this issue the finite layers are modelled through CFEM. CFEM is similar to regular FEM with two main modifications; (a) finite element discretization with linear midpoint integrated elements and (b) the element depths are chosen to be complex values and the value are chosen in a specific way to accurately capture the layer stiffness. With the above modifications, CFEM results in exponential convergence in comparison to polynomial convergence for regular finite elements.
- *PMDL* – The radiation of the wave energy through the unbounded half space layer needs to be accurately captured to compute the correct effective dispersion curve. Computational modelling of the half space is generally done through absorbing boundary layers. PMDL is a particular absorbing layer which efficiently models the half-space by using midpoint

integrated linear finite elements similar to CFEM and specific layer lengths that will absorb the radiating waves. Due to the way the pavement layers are structured with stiff layers on top of softer layers, wave propagation mechanics in pavements are fundamentally different in comparison to geophysical systems. These differences lead to the so-called *leaky waves* effects, which in simple terms means the energy generated from the surface impact radiates into the layers reducing the amplitude as it travels along the surface direction and increasing in amplitude as it travels along the depth direction. This effect greatly reduces the maximum distance at which discernable acceleration can be measured at the surface. More importantly it leads to the unusual choice of negative imaginary length for the PMDL layers to effectively absorb the radiating waves in the half space.

An efficient forward model for simulating the surface testing of pavements was developed based on the above procedure and used for the back calculation procedure detailed in the next section. Further details about the modelling, wave propagation characteristics and examples can be found in Appendix E.

3.3. Back Calculation of Layer Properties

3.3.1. Overview

Different regions of the dispersion curve are sensitive to different layer properties and a multistep procedure has been adopted for this project to back calculate the layer properties. In general, higher frequency waves have lower wavelength and thus, the depth of penetration of the waves is less. Thus, the higher frequency region of the dispersion curve is typically more sensitive to the top layer and the lower frequency regions are sensitive to the top and deeper layers. The specific frequency ranges depend on the thickness of the layers and differ for the conventional and inverted pavements. A simple sensitivity analysis to determine the inversion strategy followed by back calculation of the layer properties is presented in the following section for both the inverted and conventional pavements.

3.3.2. Inverted Pavement Section

Recall that the inverted pavement design consisted of a 2.5 in. asphalt layer, 6 in. ABC, 8 in. CTB on top of a subgrade. Due to the unconventional design consisting of a stiffer CTB on top of the subgrade, the fundamental wave propagation characteristics of this pavement type is different from the conventional pavements and thus the characteristics of the dispersion curve are different. The theoretical dispersion curve using layer properties given in Table 9 is shown in Figure 27 (a) and (b). Four different dispersion curves are shown in Figure 27 corresponding to models with; (i) only the asphalt layer, (ii) asphalt layer + ABC with a fixed bottom boundary, (iii) asphalt + ABC + CTB with a free boundary at the bottom, and (iv) the full four-layer inverted pavement system.

Table 9. Representative Layer Properties of an Inverted Pavement

Layer	Shear velocity (m/s)	Modulus (MPa)	Density (kg/m^3)	Poisson's ratio	Depth (m)
Asphalt	1900	23465	2500	0.30	0.0635
ABC	230	296	2000	0.40	0.1524
CTB	1700	15953	2400	0.15	0.2032
Subgrade	75	32	2000	0.40	∞

The motivation to look at dispersion curve with the progressive addition of layers from top to bottom is to understand the influence of different layers at different frequencies. Examining the dispersion curves from each variant, the first thing that is noticed is that when more than two layers are present there are vertical discontinuities (hereafter referred to as 'jumps') at frequencies of approximately 1400 Hz, 2300 Hz, 4250 Hz and 6200 Hz. These jumps in the theoretical dispersion curve occur due to the layering and the lack of material damping in the model. The magnitude of these jumps reduces as the frequency increases because in these cases, the wavelength is shorter and thus the waves only travel in the top layers. Further, it is found that the only region sensitive to the presence and properties of the ABC and CTB layers is the area between approximately 0 and 650 Hz, see Figure 27 (b), which shows the same data as Figure 27 (a) but is zoomed into the low frequency region. The three-layer- dispersion curve (grey) has a higher velocity at the lower frequencies (below 500 Hz) in comparison to the two-layer dispersion curve (blue) clearly indicating the presence of the stiffer CTB layer below the ABC layer. Additionally, the dispersion curve from the four-layer and three-layer models exhibits minor differences only at frequencies below 50 Hz indicating very low sensitivity of the subgrade layer. Given the low sensitivity of the subgrade and the difficulties involved in measuring data reliably at frequencies below 50 Hz, surface wave methodology in its current form lacks the ability to back calculate the subgrade layer properties for an inverted pavement section.

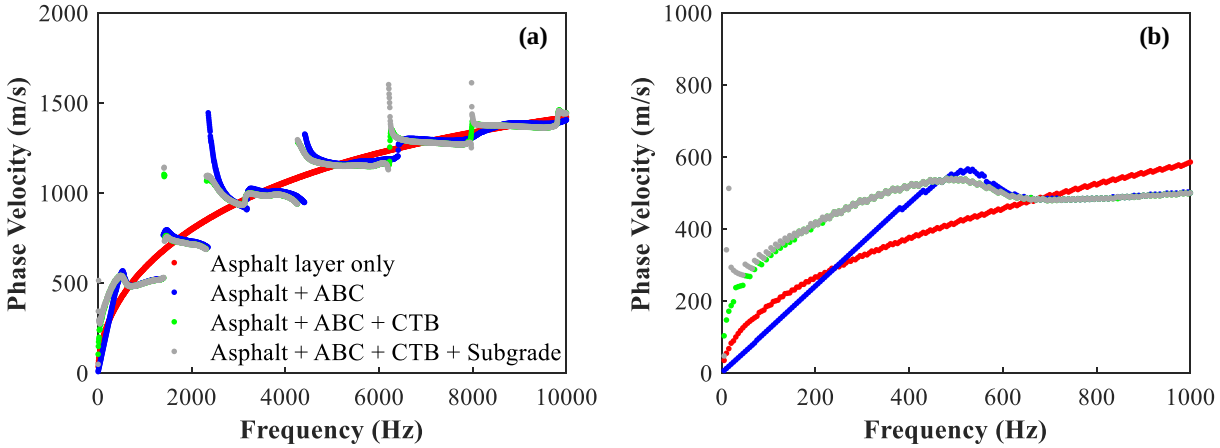

Figure 27. Dispersion curves for different scenarios; (a) theoretical curve comparisons for single layer, two-layer, three-layer and four-layer pavement and (b) theoretical curve comparisons at lower frequency range.

A typical dispersion curve obtained from field testing is shown in Figure 28. The characteristic feature of the curve highlighted at the lower frequency (up to 1,000 Hz) resembles the one observed from the three-layer theoretical model shown in Figure 27. It is also noted that the higher frequency region (above 1,000 Hz up to 10,000 Hz) of the curve closely follows a trend similar to asphalt layer only theoretical curve shown above. The jumps observed in the muti-layer theoretical dispersion curves are almost completely missing in the experimental dispersion curve, likely because of the geometric and material damping that occurs in the field which are difficult to capture accurately in the model. Based on these theoretical and experimental observations, a multi-step back calculation strategy is used based on separately analyzing the higher and lower frequencies back calculate the asphalt layer and deeper layer properties respectively.

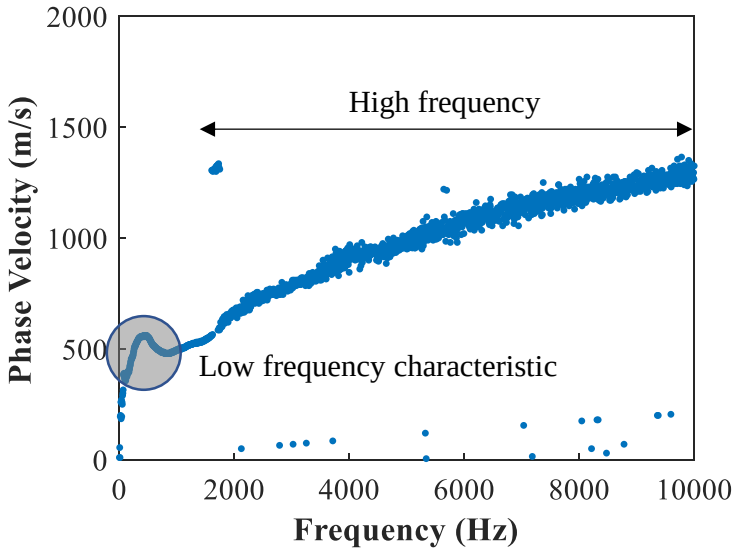

Figure 28. Typical dispersion curve for inverted pavement.

The first step for performing the back calculation is to estimate the asphalt layer properties using portions of the 'High frequency' region of the dispersion curve by assuming a single layer model. After examining the dispersion curves from multiple sensors from a single test and across different tests, a frequency range of 1.5 kHz to 3.0 kHz was chosen for this step. The objective function (E) is defined as the norm of the misfit between the measured and theoretical dispersion curves and is given by Equation (2).

$$E = y^T y \tag{2}$$

where; y is the difference between the experimental and theoretical dispersion curve. A typical fit between the experimental and theoretical dispersion curves is shown in Figure 29 (a). To evaluate the efficacy of this back calculation method, surface wave data from inverted core site is compared against the storage moduli values measured from the AASHTO TP 132 testing presented in Section 2.5.2. The results of this comparison are shown in Figure 29 where the TP 132 results are shown as master curves and the surface wave testing are shown as blocks representing the uncertainty in both back calculated moduli and reduced frequency. The uncertainty in moduli emerge because the actual pavement depth between the core sites is unknown and the back calculation has been performed assuming the test location has a depth equal to either IO3 or IO2 for the outer location or IC2 or IC1 for the center location. To calculate reduced frequency, the pavement temperature is input to the time-temperature factor function obtained from TP 132 testing and multiplied by the average frequency of the fitting range (2.25 kHz). However, since the pavement temperature is uncertain, there is a range of potential reduced frequencies that could exist. The lowest possible reduced frequency is the one that corresponds to the surface temperature taken at the time of testing. The highest possible reduced frequency is found by using the temperature at the bottom of the asphalt pavement layer. Since this value is not known, it was estimated using the Bells2 equation along with the surface temperature and previous day air temperature.

Accounting for these uncertainties, it is first observed that the modulus values back calculated from the surface wave testing are in general agreement with the magnitude of the moduli from the TP 132 experiments. However, it is also observed that the back calculated values have different

rankings (center greater than outer whereas the TP 132 testing suggested that the outer was stiffer than the center). One potential reason for this difference is the limited number of impacts at the core sites as the tests (recall core sites are only approximately 5 ft apart whereas the normal test locations cover more than 10 ft). While the surface wave method failed to capture the variation between the outer and center regions, the estimated modulus values compare well with the dynamic modulus values which is encouraging.

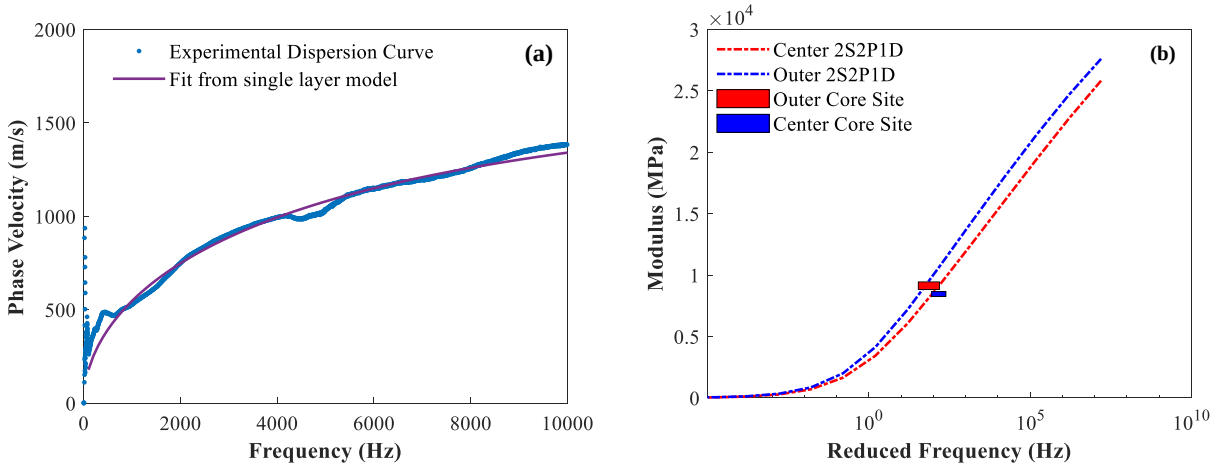

Figure 29. Back calculation results and comparison; (a) typical fit from matching a single layer model to the experimental dispersion curve and (b) inversion results from surface wave test at core site.

Unlike the core sites, accurate layer depth is not available for the tests at Sites 1 and 2. Thus, both the modulus and layer depths need to back calculated. Since the parameters are correlated, joint inversion using the objective function defined in Equation (2) can lead to potential errors. To overcome this issue, a regularization term is added to the misfit and the new objective function is given by Equation (3).

$$E = y^T y + \lambda (h_{design} - h_{model})^2 \tag{3}$$

where; λ is the regularization constant and h_{design} is the design thickness of the pavement (0.1524 m for conventional pavement and 0.0625 m for inverted pavement). The regularization constant is chosen based on trial and error. Though not shown here, it was found that this regularization greatly improved the ability to identify the two parameters. Asphalt layer modulus estimate from the surface wave test result is shown in Table 10. A frequency range of 1500 Hz to 3000 Hz is consistently used across all the data to back calculate the asphalt layer modulus. As was done for the core site, the measured surface wave temperature was used along with the BELLS2 prediction equation to compute the temperature variation along the pavement depth. An average frequency of 2250 Hz and the average temperature along the pavement depth from each test is used to compute the reduced frequency for each of the modulus estimate. Please note that, only a single reduced frequency is computed here from the average temperature and the uncertainty in the reduced frequency from the temperature variations are not shown for this set of data.

Table 10. Back Calculated Modulus and Depth of Inverted Pavement Asphalt Layer

Test Location	Average Temperature (°C)	Modulus (MPa)	Depth (m)	Depth (in.)
S1 Outer	14	20951	0.0579	2.28
	20	18277	0.0578	2.28
	29	13604	0.0582	2.29
S1 Center	15	12315	0.059	2.32
	17	12642	0.0588	2.31
	29	7486	0.0598	2.35
S2 Outer	12	17861	0.0582	2.29
	19	15955	0.0584	2.30
	27	12167	0.0577	2.27
S2 Center	12	16651	0.0586	2.31
	26	9979	0.0592	2.33
	29	9967	0.0590	2.32

A comparison of the surface wave estimates, and laboratory master curves is shown in Figure 30 (a) and (b) while the depth estimates are shown in Figure 31. Unlike the core sites, the trend from the inversion matches the trend observed in the master curves where the outer is at a higher modulus compared to center. It is important to note that the time-temperature shift is still approximate due to the use of BELLS2 prediction curve which may not be valid for inverted pavements and could potentially explain some of the differences between the master curve and surface wave estimates. More importantly, given the thin asphalt layer, the percentage difference between the maximum and minimum core thickness is 19% which would translate to a much higher difference in the modulus as they are correlated. Additionally, the core thicknesses measured within a distance of 10 ft. of one another (see Section 2.1) show substantial variation indicating that the depth over the entire region of the surface wave test is not uniform although it is assumed to be uniform in the forward model. Despite these limitations, the estimated moduli values still compare well to the laboratory modulus estimates, which is an encouraging result to further develop the method in the future.

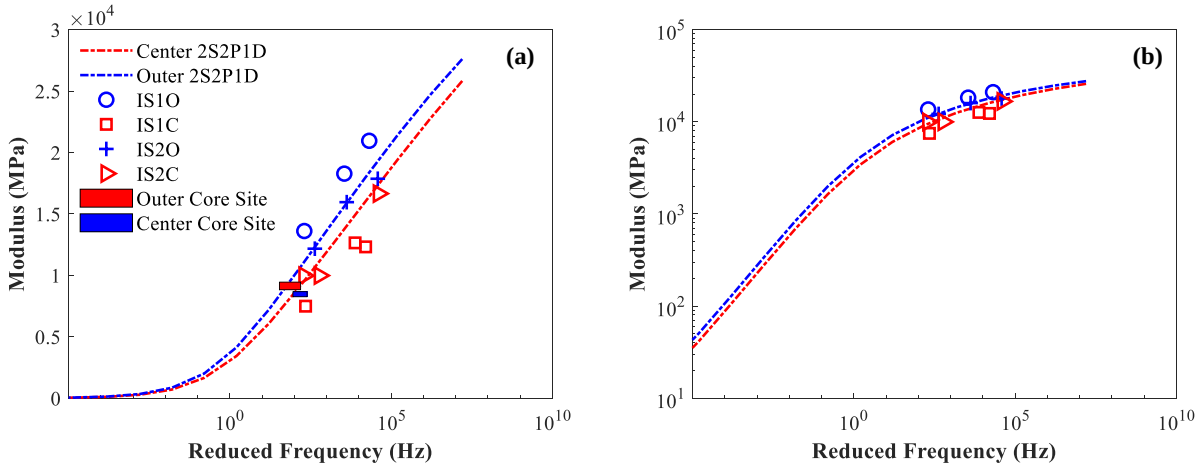

Figure 30. Comparison between back calculated and measured moduli of asphalt mixtures for inverted pavement sites in; (a) semi-log scale and (b) log-log scale.

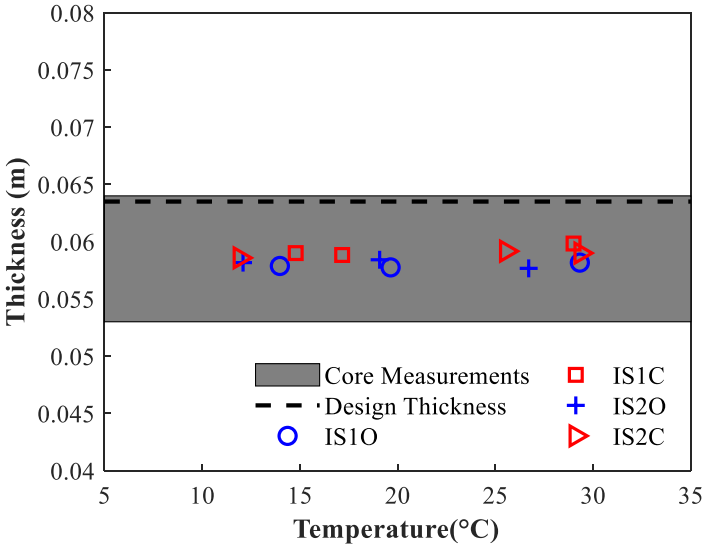

Figure 31. Comparison between back calculated layer thicknesses, core measurements, and design thickness.

Once the asphalt layer properties were estimated, the next step was to evaluate the deeper layer properties from the low frequency characteristic of the dispersion curve shown in Figure 28. Given that the ABC and CTB layer properties are not temperature dependent, it is expected that the dispersion curves especially around the low frequency characteristic remain similar across different tests. A comparison of the dispersion curves in this frequency range is shown for the center and outer sites in Figure 32. The center curves overlap with each other below 500 Hz irrespective of the pavement temperature at the center and inner site. On the contrary, the curves from the outer site differ in shape form the center site and also show substantial differences in the frequency ranges below 500 Hz. This phenomenon potentially arises due to the limitation of the MSOR method as we are close to the pavement boundary when testing at the outer site. Due to the reflections from the pavement sides, the reciprocity principle, which is the core of the MSOR methods, fails and thus the dispersion curves in this frequency range have additional artifacts that cannot be captured by the pavement model. The effect of this same phenomenon on the center and inner sites is expected to be less than the outer but hasn't been quantified.

As mentioned earlier, due to low sensitivity of the subgrade, the three-layer model is used to estimate only the modulus of the ABC and CTB layers by minimizing the same objective function shown in Equation (2) in a frequency range of 100 to 1000 Hz. The depth, Poisson's ratio, and density of the ABC and CTB layers are assumed known and shown in Table 11. A representative fit between the theoretical and experimental dispersion curves in shown in Figure 33 with the back calculated values for all the temperatures shown in Table 12. The best fit curve from the theoretical model still does not exactly match the experimental curve. The actual modulus of the ABC is unknown, but is expected to be higher than the typical value due to the higher compaction levels achieved in the inverted pavement and is also load dependent.

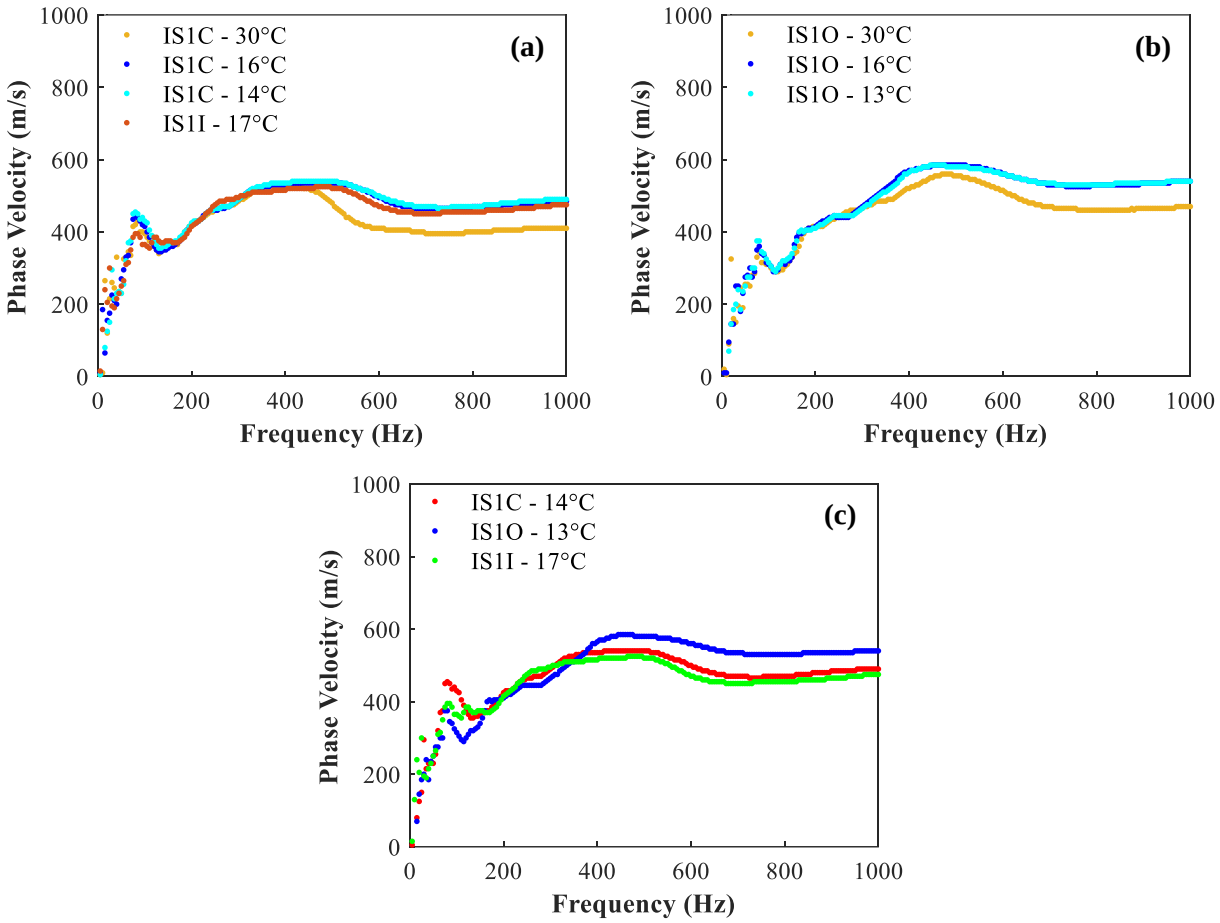

Figure 32. Dispersion curve comparison at low frequencies; (a) Center and Inner sites, (b) Outer site, and (c) Center vs Inner vs Outer sites.

The estimated values are in general higher than typical ABC modulus. The target strength of the CTB layer was around 400 psi but the field data provided by Vulcan Materials suggested that they ended up achieving a strength of 1400 psi with 4% cement. Using the ACI 318-08 equation to calculate modulus of elasticity from compressive strength with an assumption of 2400 kg/m^3 density results in a modulus of approximately 15 GPa. The ABC modulus values vary over a range of 307 to 402 MPa and the CTB modulus values vary over a range of 10 to 14 GPa. While the estimated deeper layer properties vary over a wide range, they can be used as a good starting point for more sophisticated back calculation algorithms in the future. Further work is required to achieve a better fit from the theoretical curve, improve the accuracy and estimate the layer depths in addition to the modulus estimates.

Table 11. Assumed Material Properties of ABC and CTB

Layer	Density (kg/m^3)	Poisson's Ratio	Depth (m)
ABC	2000	0.40	0.1524
CTB	2400	0.15	0.2032

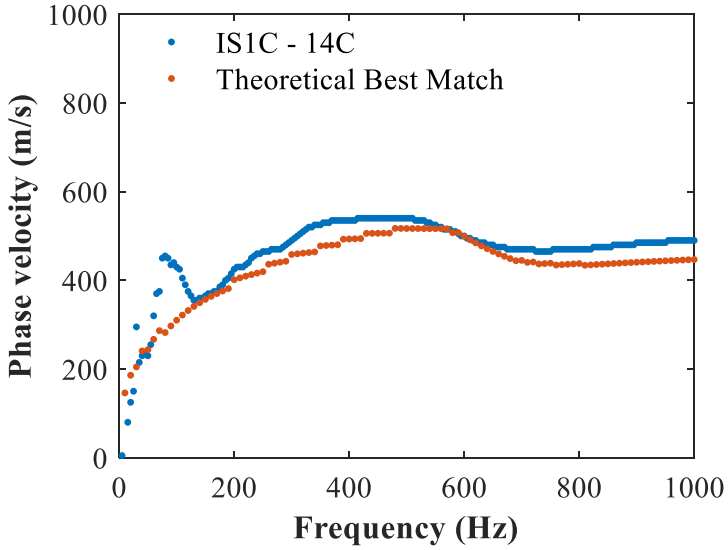

Figure 33. Representative experimental and best matching theoretical dispersion curve for ABC and CTB modulus back calculation.

Table 12. Back Calculated ABC and CTB Moduli

Site	Surface Temperature (°C)	ABC Modulus (MPa)	CTB Modulus (MPa)
IS1C	14	384	11383
	16	402	12026
	30	278	13973
IS1O	13	393	13763
	16	381	14008
	30	367	10897
IS1I	17	307	13885

3.3.3. Conventional Pavement Section

Recall that the conventional pavement design consisted of a 6 in. asphalt layer and a 10 in. ABC on top of a subgrade. The theoretical dispersion curve using the layer properties given in Table 9 is shown in Figure 34. Two different dispersion curves are shown in Figure 34 correspond to models with; (i) asphalt layer only and (ii) asphalt + ABC + subgrade. The three-layer dispersion curve overall follows the same trend as the asphalt layer dispersion curve. In addition, the three-layer model has multiple jumps in the entire frequency range due to the presence of multiple layers and lack of material damping in the model. The location and number of jumps are a function of the relative properties of the asphalt, ABC, and subgrade layers. As was seen in the example measured dispersion curve for the conventional pavement shown in Figure 24, jumps similar to the theoretical model can be observed in the low frequency region (up to 1000 Hz), but are not observed in the higher frequency regions (beyond 1000 Hz).

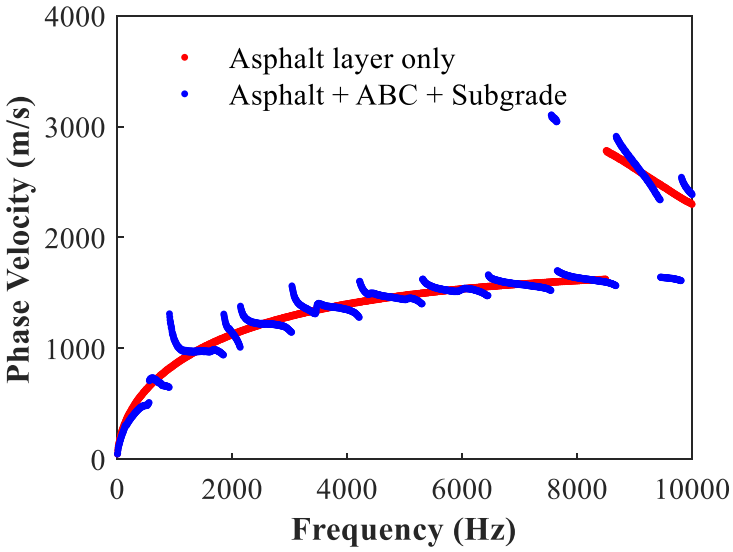

Figure 34. Theoretical dispersion curve for conventional pavement using a single layer and a three-layer pavement structure.

Thus, a back calculation strategy similar to the inverted pavement described in the previous section is followed here for the conventional pavement. First, the higher frequency region of the dispersion curve from 1500 to 3000 Hz is utilized to estimate the asphalt layer modulus. Subsequently, the lower frequency region (100-600 Hz) is used to estimate the ABC and subgrade modulus with a known asphalt layer modulus and assumed ABC thickness from design.

Asphalt moduli values estimated using the surface wave data from the conventional core site are compared to the storage modulus values measure from the AASHTO TP 132 testing presented in Section 2.5.2. A typical fit from a single layer model and the surface wave test estimates along with the master curves are shown in Figure 35 (a) and (b) respectively. Time-temperature shift coefficients obtained from TP 132 testing are used to calculate the reduced frequency for the surface wave estimates at an average frequency of (2250 Hz). Surface wave test estimates are shown as blocks representing the uncertainty in the modulus because of the difference in the measured core thickness and the uncertainty in the reduced frequency arising from the temperature distribution. There is a substantial overlap in the blocks and once again, the surface wave method fails to clearly capture the variations between the center and outer sites. Nevertheless, the back calculated moduli for the center and the outer sites fall within the range of the values from TP 132.

Unlike the core sites, accurate layer depth is not available for the tests at Sites 1 and 2. Thus, both the modulus and layer depths were calculated with the objective function defined earlier by Equation (3) and are summarized in Table 13. A comparison of the surface wave estimates, and laboratory master curves is shown in Figure 36 (a) and (b) while the depth estimates are shown in Figure 37. An average frequency of 2250 Hz and the average temperature along the pavement depth from each test is used to compute the reduced frequency for each of the modulus estimates. Note that, like for the inverted pavement tests, only a single reduced frequency is computed from the average temperature. Thus, the uncertainty in the reduced frequency from the temperature variations are not shown for this set of data. The trend from the inversion is opposite to the trend observed in the master curves. It is important to note that there are uncertainties including time-temperature shift, pavement depth variations that influence the estimates. Despite these limitations, overall the estimated modulus values and depths compare well with the master curves.

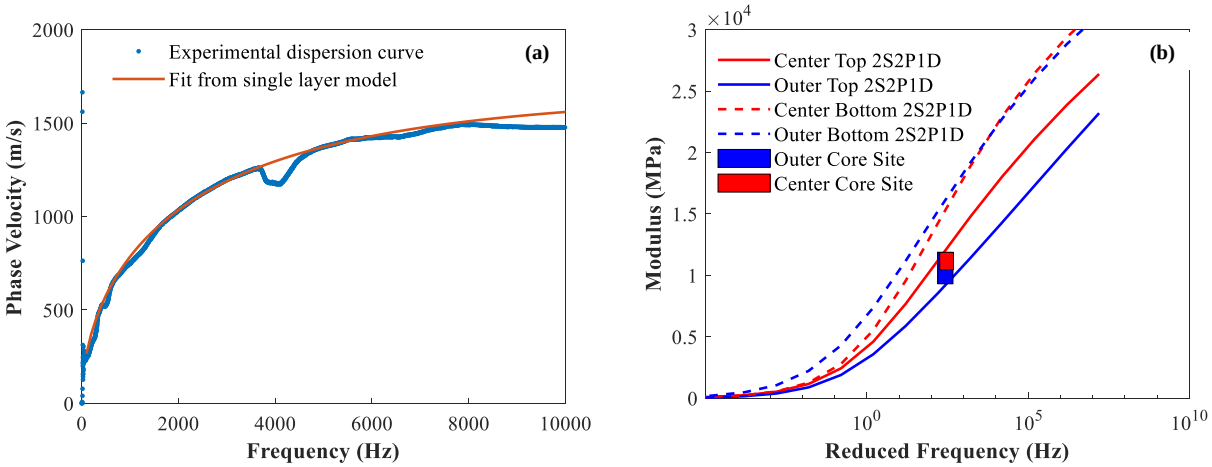

Figure 35. Back calculation result and comparison; (a) typical fit from matching a single layer model to the experimental dispersion curve and (b) inversion results from surface wave test at core site.

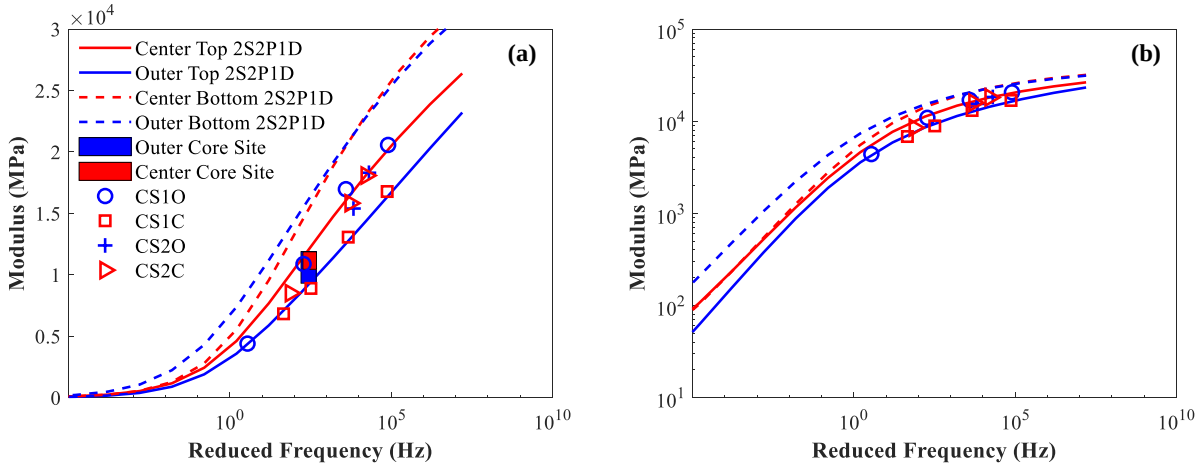

Figure 36. Comparison between back calculated and measured moduli of asphalt mixtures for conventional sites in; (a) semi-log scale and (b) log-log scale.

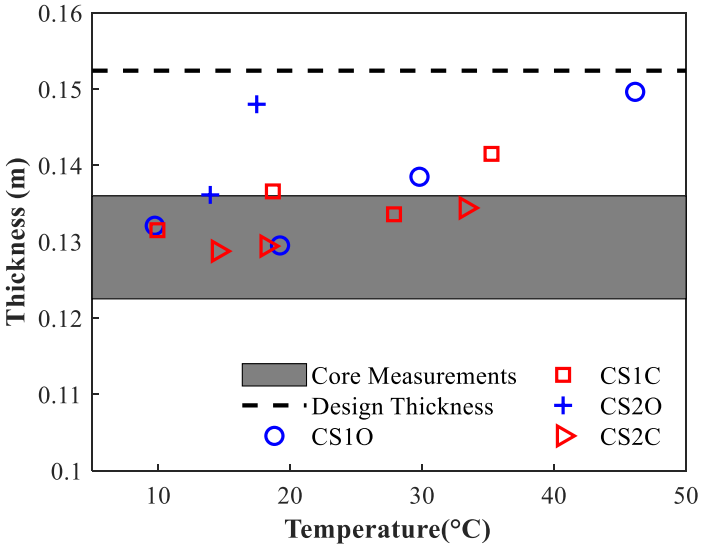

Figure 37. Comparison between back calculated layer thicknesses, core measurements, and design thickness.

Table 13. Back Calculated Modulus and Depth of Conventional Pavement Asphalt Layer

Test location	Average Temperature (°C)	Modulus (MPa)	Depth (m)	Depth (in.)
S1 Outer	10	20563	0.1321	5.20
	19	16962	0.1295	5.10
	30	10869	0.1385	5.45
	46	4390	0.1496	5.89
S1 Center	10	16772	0.1315	5.18
	19	13056	0.1366	5.38
	28	8882	0.1336	5.26
	35	6815	0.1415	5.57
S2 Outer	14	18299	0.1361	5.36
	17	15387	0.1480	5.83
S2 Center	15	18075	0.1288	5.07
	18	15821	0.1294	5.10
	33	8496	0.1344	5.29

Once the asphalt layer properties were estimated, the next step was to evaluate the deeper layer properties from the low frequency characteristic of the dispersion curve. As mentioned earlier, the jumps observed in the low frequency region are a function of the relative properties of asphalt, ABC and subgrade. Based on careful examination, it was observed that using the FP spectrum method with the entire set of 96 impacts resulted in consistent and less noisy dispersion curves at the low frequency with clear jumps. Typical signature of the low frequency characteristics of the dispersion curve is shown for center, outer and inner locations at conventional pavement site 1 in Figure 38.

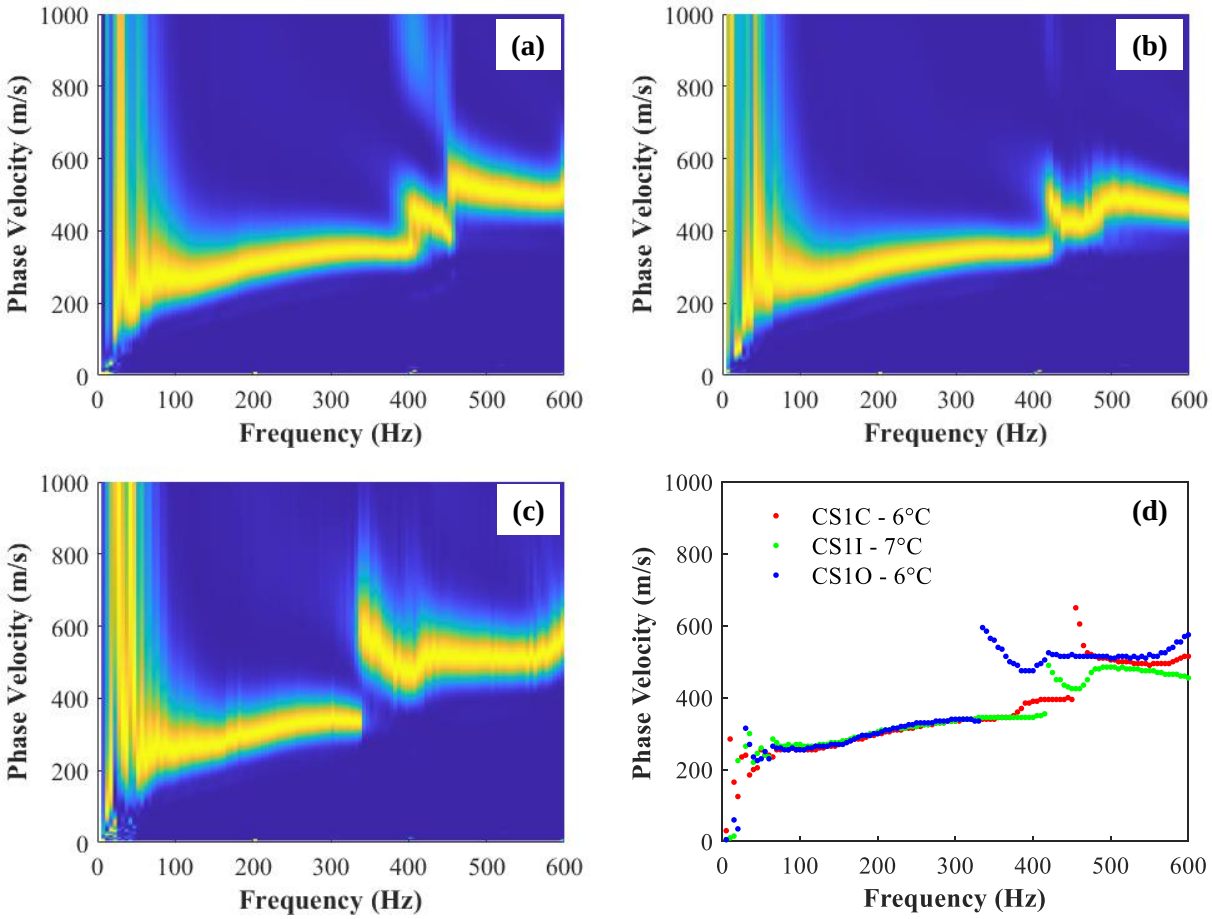

Figure 38. Dispersion curve comparison at low frequency at site 1; (a) CS1C FP spectrum, (b) CS1I FP spectrum, (c) CS1O FP spectrum, and (d) FP spectrum peak comparison.

Following the procedure described in Ryden and Park (2006), the FP spectrum was used along with a cross correlation based objective function defined by Equation (4).

$$M = \left(1 - \frac{\sum_{y=1}^{K}\sum_{z=1}^{N} \left| S_{obs} \right| \left| S_{pred} \right|}{\sum_{y=1}^{K}\sum_{z=1}^{N} \sqrt{S_{obs}^2} \sum_{y=1}^{K}\sum_{z=1}^{N} \sqrt{S_{pred}^2}} \right) \tag{4}$$

where; S_{obs} is the experimental FP spectrum, S_{pred} is the theoretical FP spectrum. M is the mismatch between the two spectra and can take a value between 0 and 1, where 0 represents a perfect match. Fast simulated Annealing (FSA) algorithm implemented in MATLAB is used to optimize for the ABC and subgrade modulus by minimizing the mismatch defined by Equation (4). The experimental FP spectrum, best fit from the optimization procedure and the difference between the experimental and best fit for conventional pavement site 1 is shown in Figure 39. While the best fit does not exactly match the experimental spectrum, the jump location is captured well in all the cases. The back calculated ABC and subgrade modulus are summarized in Table 14. The actual

properties of the ABC and subgrade at the site are not known, but the back calculated values fall within the typical moduli range for the two layers. This method is still considered a preliminary back calculation for the deeper layer properties and further work in needed to improve the results and include the ABC thickness as a parameter. Further analysis is required to explain the differences observed between the experimental and theoretical spectrum involving quantifying the uncertainties in the MSOR procedure in tandem with theoretical modelling. Nevertheless, this back calculation process is computationally fast resulting in an estimate for all three layers within a few minutes and the estimated values can be used as a starting point for more sophisticated inversion algorithms in the future.

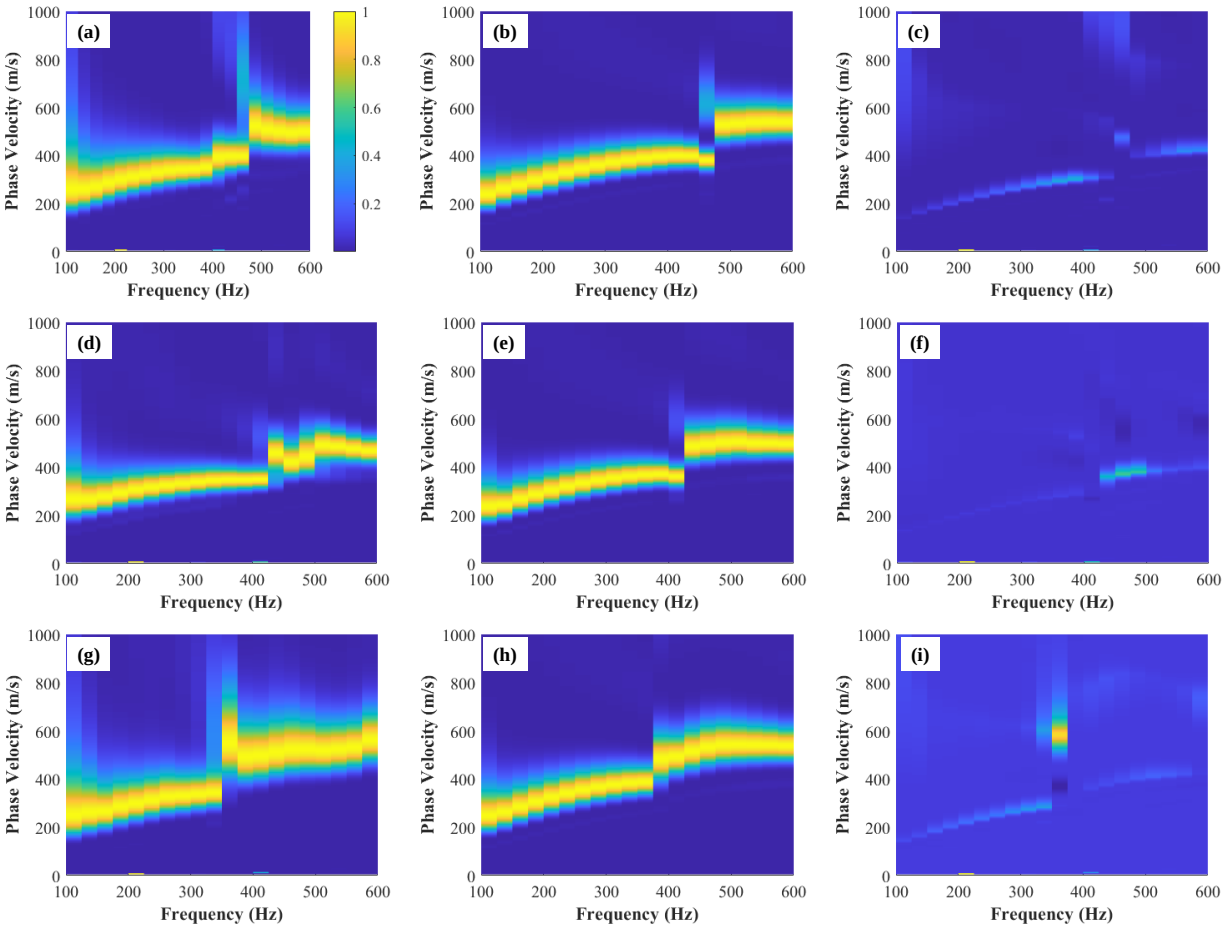

Figure 39. Experimental, best fit and mismatch comparison; (a) CS1C experimental, (b) CS1C best fit, (c) CS1C difference plot, (d) CS1I experimental, (e) CS1I best fit, (f) CS1I difference plot, (g) CS1O experimental, (h) CS1O best fit, and (i) CS1O difference plot.

Table 14. Back Calculated ABC and Subgrade Modulus

Site Code	Surface Temperature (°C)	ABC (MPa)	Subgrade (MPa)
CS1C	6	162	53
CS1I	7	134	47
CS1O	6	133	53

3.4. Summary and Discussion

The Pineville quarry site was tested using surface wave methodology, and simultaneously field cores were collected on which AASHTO TP 132 testing as well as impact resonance testing was conducted to characterize the different layers of the pavement. A summary of all the test estimates for both the conventional and inverted pavement asphalt layer are shown in Figure 40. The major observations are as follows.

- Figure 40 (a) shows the comparison of AASHTO TP 132 and surface wave for the conventional pavement. Surface wave estimates do not clearly capture the differences between the center and outer locations observed in the AASHTO TP 132 test. In general, surface wave estimates are withing the bounds of AASHTO TP 132 master curves. The surface wave estimates are closer to the top layer modulus and further work is required to evaluate their ability to capture different mixes within the asphalt layer.
- Figure 40 (b) shows the comparison of AASHTO TP 132 and surface wave for the inverted pavement. Surface wave testing captures the differences between center and outer observed in the AASHTO TP 132 test. Although more scatter compared to conventional pavement is observed owing to a thinner asphalt layer and a higher percentage of variation in thickness.
- Figure 40 (c) shows the comparison of AASHTO TP 132 test results from the inverted and conventional pavements. Given that the inverted pavement consists of only two surface mixes (RS9.5A and B) and no intermediate mix, the master curves follow closely the surface layer (RS9.5B) estimates from the conventional pavement.
- Figure 40 (d) shows the comparison impact resonance (IR) estimates with AASHTO TP 132 results. Overall, IR captures the trend observed between center and outer in both the conventional and inverted cores. The cut conventional cores also capture the difference between the surface and intermediate layers. In general, the IR estimates were slightly higher than the AASHTO TP 132 estimates. On the other hand, the trend between the center and outer locations is the opposite between the conventional and inverted pavements. The reasons for this behavior is not immediately clear but could potentially be attributed to the differences in the actual wheel path based on the location of the test sites in the overall pavement section.
- The surface wave testing does not distinguish between moduli of the inverted and conventional pavements; however, the AASHTO TP 132 testing also suggests similar moduli from the surface layers in these sections. Thus, the ability of the surface wave test method to distinguish between mixtures remains unclear.
- The average aggregate base layer (ABC) modulus obtained from the inverted section is more than 2 times higher than the modulus obtained from the conventional section as shown in Figure 41. Recall that the ABC layer in the inverted section was compacted to 103.4% in comparison to 99.8% in case of the conventional pavement which indicates a higher modulus in the inverted section in general but quantifying the modulus difference based on compaction is not straightforward. In addition, the ABC modulus in the inverted section is stress dependent and is expected to be higher under wheel loads.

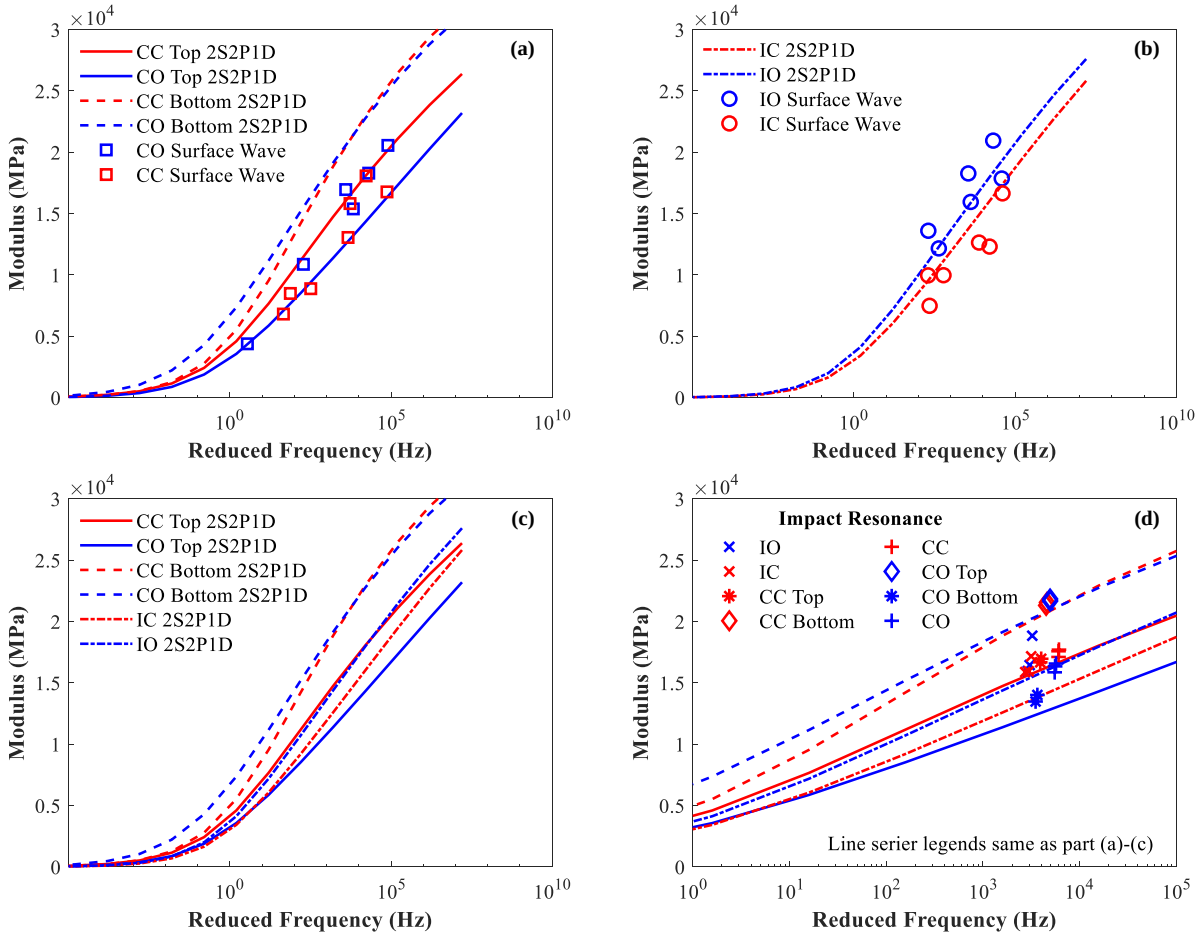

Figure 40. Overall comparison of AASHTO TP 132, IR and surface wave modulus estimates; (a) conventional pavement, (b) inverted pavement, (c) AASHTO TP 132 conventional vs inverted, and (d) AASHTO TP 132 and impact resonance estimates conventional vs inverted.

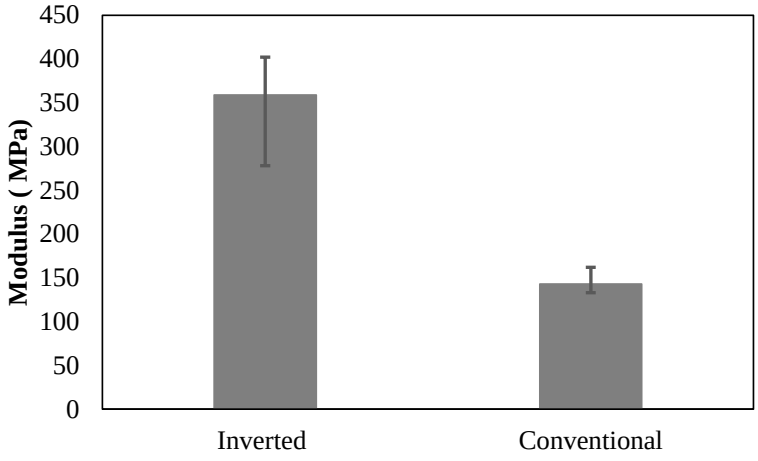

Figure 41. ABC modulus estimate – Inverted vs Conventional.

This page is intentionally blank

4. CONCLUSIONS AND RECOMMENDATIONS

4.1. Conclusions

The conclusions listed below are made based on the experiments and surveys conducted in this research project.

4.1.1. Condition Survey and In-Service Performance

- Condition survey concluded that the inverted pavement section is performing equally well, if not better than the conventional pavement section despite potential reflective cracking caused by an overly stiff cement treated base.
- The FWD and TSD deflection show less deflections in the inverted section and more importantly less variation in the inverted pavement over time compared against an up to 58% increase in the deflection in the conventional section. This finding confirms the conclusions from the condition survey.

4.1.2. Surface Wave Testing

As described in Section 3 of the report, a surface wave testing method was successfully developed and implemented on both inverted and conventional pavements.

- With respect to the surface wave testing on inverted pavements the following conclusions are made.
    - If the thickness of the asphalt layer is known at the surface wave test location, the asphalt layer moduli can be estimated with high confidence and the results compare well with the laboratory dynamic modulus master curve.
    - Back calculating both the modulus and thickness of the asphalt layer resulted in higher error between the back calculated values and those measured from the AASHTO TP 132 method. This difference can be attributed to the thin asphalt layer and the potential variation in the thickness at different locations along the pavement. The percentage difference between the maximum and minimum core thickness measured is 19%.
    - The modulus trend between the center and outer locations from the surface wave estimates match the observations from the laboratory AASHTO TP 132 test. While this result is encouraging, it needs to be reevaluated in cases where the accurate thickness of the asphalt layer is known.
    - Preliminary results from the back calculation of the ABC and CTB layer properties resulted in a wide range of values. The average ABC modulus from the surface wave testing was 359 MPa which is higher than the typical range of values for a regular ABC. The ABC layer in the inverted section is expected to be at a higher modulus due to the better compaction and the estimated values are in line with this. The compressive strength of the CTB used was estimated to be 9.65 MPa which results in an elastic modulus of 14844 MPa (using the ACI 318-08) which is 13.4% higher than the average modulus of 12854 MPa estimated from the surface wave methodology. Nevertheless, the estimated values can be used as good starting points for further analysis in the future.
- With respect to the surface wave testing of conventional pavements the following conclusions are made.

- Similar to the inverted pavements, the asphalt layer modulus can be estimated with high confidence with a known thickness.
- No clear trend is observed in the surface wave estimates between the center and outer locations. This result could be potentially due to the significant disparity in the surface and intermediate layer modulus and the frequency range in which the surface wave estimates are computed resulting in an average modulus value for the entire asphalt layer. However, the AASHTO TP 132 testing also did not show obvious differences in the moduli of the surface layer moduli between the inverted and conventional pavement sections. Further development of the method to increase the usable frequency range beyond 10 kHz could potentially lead to an improved surface wave method that can differentiate between different layers within the asphalt layer.
- Given the smaller variation in the asphalt layer thickness, back calculating both the modulus and thickness resulted in estimates that were within the laboratory dynamic modulus.
- Preliminary results from the back calculation of the ABC and subgrade layer properties resulted in estimates within the typical layer properties.

4.2. Recommendations

4.2.1. Use of Inverted Pavements as an Approved Pavement Design Method

The data gathered in this study showed no definitive evidence that the Vulcan inverted pavement was underperforming or had a high likelihood of impending failure. In fact, the performance data collected at the site suggests that the inverted pavement is outperforming the conventional one. As such, the inverted pavement design appears to be a viable design type for use on North Carolina roadways. There do still remain some unknown issues that neither this study nor the published literature have yet answered, especially with respect to long-term performance of inverted pavements in humid environments on high volume roadways and in situations where maintenance is not being performed carefully. As noted in the performance assessment of the Pineville site, transverse and longitudinal reflective cracking was identified early in the pavement life and Vulcan applied sealant to prevent/reduce the infiltration of water into the underlying layers. The overall effect of this early maintenance activities are not known, but are believed to be very important to the sustained success of the inverted pavement.

Given the sum total of these unknowns, the research team would not, at this time, recommend immediate and widespread adoption of inverted pavements. However, given the potential cost savings, performance benefits, and benefits to material suppliers it is recommended that the NCDOT work to identify two to three candidate projects where an inverted pavement design can be deployed and monitored. These sites should be at least 1,000 feet in length and preferably long enough to incorporate both a conventional pavement and an inverted one. It is also preferable that the sites be located near contractors who are already regularly producing CTB and can reliably produce a material with a compressive strength of approximately 500 psi. The South African material and pavement design guidelines appear to be adaptive to North Carolina and can be used to develop the structural designs for these sites. If test sites are constructed, the research team recommends that the NCDOT make every effort to carefully catalog the construction process and retain samples of the as constructed materials for mechanical investigation and for use in later performance assessments.

4.2.2. Surface Wave Testing

Surface wave testing methodology applied in this study for both conventional and inverted pavement resulted in estimates that are comparable to the laboratory tests for the asphalt layer and estimates for the deeper layer that are within the expected range. The asphalt layer modulus can be estimated with high confidence if the pavement thickness is known. Nevertheless, back calculating both the asphalt modulus and thickness still results in estimates often less than 15% error in comparison to AASHTO TP 132 modulus except a few cases. Further study and development is recommended before adoption of the surface wave testing for routine evaluation. If additional testing or studies are to be done with the surface wave testing, it is recommended that the testing be done at different times of the year encompassing a range of pavement temperatures to capture the viscoelastic behavior of the asphalt layer. The results for the asphalt layer can be further improved, especially for the inverted pavements, if surface wave testing is used in conjunction other techniques such as ground penetrating radar (GPR), which can provide a continuous pavement depth measurement. Such improvements could lead to the in-situ estimation of the asphalt mixture master curve for the asphalt layer, which could subsequently be used as an input for the mechanistic-empirical design and analysis. The deeper layer property estimates can be potentially improved by identifying and applying a more detailed back calculation approach for which the estimates from this study can serve as starting points. Overall, the surface wave test methodology has shown sufficient feasibility to be developed into a standard methodology that will benefit NCDOT and can provide critical and complementary information to evaluate pavement condition when applied alongside FWD.

This page is intentionally blank

5. IMPLEMENTATION AND TECHNOLOGY TRANSFER PLAN

The Materials and Test Unit of the NCDOT are the primary users of the products of this research. While the research team does not recommend immediate and widespread adoption of inverted pavements, it does believe that they can be available on a limited research basis for use on NCDOT pavements. In addition, the surface wave test method can be used immediately as a research tool for NCDOT to estimate the individual layer properties and subsequently investigate pavements for mechanistic-empirical design and analysis. The method is not yet ready for widespread use and a knowledgeable operator is needed in order to conduct the investigation. In addition, the developed test method can be used for forensic studies and/or a research tool for periodic evaluation of other experimental pavement sections across NC.

For follow-up activities the research team believes that the NCDOT could consider the following activities:

- allocating resources to deploy inverted pavement designs on a research basis, if followed resources would be needed to develop the inverted design given the specific site situations, monitor construction activities, sample and test the materials used in construction, and to monitor the long-term performance,
- allocating resources to document the thickness variation at the Pineville Quarry site using GPR technique to further develop the surface wave testing methodology based on the extensive set of data collected at multiple pavement temperatures as part of this project. Successful implementation of this step could open the possibility of using the surface wave method as a quality control tool at the time of construction.
- allocating resources to optimize the data collection process which currently requires between 30 to 40 minutes for the setup and data collection. This would involve data analysis, back calculation, uncertainty quantification and improvement of the test system and protocol.

This page is intentionally blank

6. REFERENCES

Ahlvin, R.G., Turnbull, W.J., Sale, J.P., and Maxwell, A.A. (1971). *Multiple-Wheel Heavy Gear Load Pavement Tests. Volume I. Basic Report*. U.S. Army Engineer Waterways Experiment Station, Vicksburg, Mississippi.

American Association of State Highway and Transportation Officials (AASHTO) (1993). *AASHTO Guide for Design of Pavement Structures, 1993*, Washington, D.C.

Beaty, K. S. and Schmitt, D.R. (2003). Repeatability of multimode Rayleigh-wave dispersion studies. *Geophysics*, 68(3), 782-790.

Buchanan, S. (2007). *Resilient Modulus: What, Why, and How?*, Online. <https://www.vulcan innovations.com/public/pdf/2-Resilient-Modulus-Buchanan.pdf> Accessed December 19, 2019.

Chen, X., Zhang, Z., and Lambert, J.R. (2014). Field Performance Evaluation of Stone Interlayer Pavement in Louisiana. *International Journal of Pavement Engineering*, 15(8), 708-717.

Department of Transport (DTSA) (1996). *Technical Recommendations for Highways (TRH) 4*. Committee of Land Transport Officials (COLTO), Pretoria, South Arica.

Foti, S., Parolai, S., Albarello, D., and Picozzi, M. (2011). Application of surface-wave methods for seismic site characterization. *Surveys in Geophysics*, 32(6), 777-825.

Freeme, C.R., Otte, E., and Mitchell, M.F. (1980). *Economics of Pavement Type Selection for Major Roads*. Pavement type selection committee for the National Transport Commission, Pretoria.

Heisey, J.S., Stokoe, K.H., and Meyer, A.H. (1982). Moduli of Pavement Systems from Spectral Analysis of Surface Waves. *Transportation Research Record: Journal of the Transportation Research Board*, 852, 22-31.

Johnson, C.W. (1961). Comparative Studies of Combinations of Treated and Untreated Bases and Subbases for Flexible Pavements. *Highway Research Board Bulletin*, 289, 44-61.

Kim, D. and Kim, Y.R. (2017). Determination of Dynamic Modulus Values of Asphalt Mixtures Using Impact Resonance Testing of Thin Disk Specimens. *Journal of Testing and Evaluation*, 45(2), 509-520.

Lewis, D.E., Ledford, K., Georges, T., and Jared, D.M. (2012). Construction and Performance of Inverted Pavements in Georgia. *Proceedings of the 91st Annual Meeting of the Transportation Research Board*, Washington, D.C.

Lin, S. (2014). *Advancements in Active Surface Wave Methods: Modeling, Testing, and Inversion*. Ph.D. Thesis, Iowa State University, Ames IA.

Metcalf, J.B., Roberts, F.L., Rasoulian, M., Romanoschi, S., Li, Y., and Djakfar, L. (2001). *Construction Comparison of Louisiana's Conventional and Alternative Base Courses under Accelerated Loading*. Final Report No. FHWA/LA-00/347. Louisiana Transportation Research Center.

Momen, M. (2004). *Complex Modulus Determination of Asphalt Concrete using Indirect Tension Test*. M.S. Thesis, North Carolina State University, Raleigh NC.

Papadopoulous, E. (2014). *Performance of Unbound Aggregate Bases and Implications for Inverted Base Pavements*. Ph.D. Thesis, Georgia Institute of Technology, Atlanta GA.

Rasoulian, M., Becnel, B., and Keel, G., (2000). Stone Interlayer Pavement Design. *Transportation Research Record: Journal of the Transportation Research Board*, 1709, 60-68.

Ryden, N. (2009). Determining the Asphalt Mastercurve from Free-Free Resonant Testing on Cylindrical Samples. In *Proceedings of the 7th International Symposium on Non-Destructive Testing in Civil Engineering (NDTCE09).* Nantes, France.

Ryden, N. and Park, C.B. (2006). Fast Simulated Annealing Inversion of Surface Waves on Pavement using Phase-Velocity Spectra. *Geophysics*, 71(4), R49-R58.

Rydén, N., Ulriksen, P., Park, C.B., Miller, R. D., Xia, J., and Ivanov, J. (2001). High Frequency MASW for Non-Destructive Testing of Pavements—Accelerometer Approach. In *Symposium on the Application of Geophysics to Engineering and Environmental Problems 2001* (pp. RBA5-RBA5). Society of Exploration Geophysicists.

South African National Road Agency Ltd (SANRAL) (1998). *High Performance Crushed Stone Based Used on South African Highways*, Pretoria, South Africa.

Titi, H., Rasoulian, M., Martinez, M., Becnel, B., and Keel, G. (2003). Long-Term Performance of Stone Interlayer Pavement. *Journal of Transportation Engineering*, 129(2), 118-126.

Tutumluer, E., Little, D.N., and Kim, S.H. (2003). Validated Model for Predicting Field Performance of Aggregate Base Courses. *Transportation Research Record: Journal of the Transportation Research Board*, 1837(1), 41-49.

Underwood, B.S. and Kim, Y.R. (2012). Comprehensive Evaluation of Small Strain Viscoelastic Behavior of Asphalt Concrete. *Journal of Testing and Evaluation*, *40*(4), 622-632.

Underwood, B.S. and Kim, Y.R. (2013). Nonlinear Viscoelastic Behavior of Asphalt Concrete and its Implication for Fatigue Modeling. *Transportation Research Record: Journal of the Transportation Research Board*, 2373(1), 100-108.

Vaughan, K., Personal communication over email, September 26, 2019.

Astaneh, A.V. and Guddati, M.N. (2016). Improved Inversion Algorithms for Near-Surface Characterization. *Geophysical Journal International*, 206(2), 1410-1423.

Weingart, R. (2010). *Inverted Base Pavement Design, The Virginia Experience*. Online < https://www.slideserve.com/uzuri/inverted-base-pavement-design-ju-ne-1-2010-the-virginia-experience> Accessed November 21, 2019.

APPENDIX A: DETAILED LITERATURE REVIEW

1. Introduction

This appendix presents a review and summary of a literature review on the current state of practice with inverted pavements in the U.S. and around the world and was the first step in the research project described in this report. The review is organized into eight separate sections. Section 1 (this section) is an introduction. Section 2 will explain the origins of this technology and its basic governing principles respectively. The next section will detail how inverted pavements have been used in the U.S. Then, design standards from across the U.S. and from South Africa will be compared. In the fifth section, comparisons will be made between material specifications in different areas and those that the NCDOT currently uses. Section 6 will do the same as Section 5, but focus on construction aspects. Section 7 reviews the basic technology and analysis for surface wave testing. Finally, the last section of this review will summarize the findings and enumerate the knowledge gaps that exist and are to be addressed in later tasks of this research project.

The true origin of the inverted pavement concept is unknown and has likely existed in the collective experience of some agencies for quite a long time. For example, there is documented evidence of experimental work in New Mexico as early as the 1950's (Johnson 1961) and the US Army Corp of Engineers in the early 1970's (Ahlvin 1971). Despite this uncertain history, most acknowledge South Africa as the predominant developer of modern inverted pavements. There the technology was developed during the 1970's as a strategy to better utilize high quality aggregate base materials, which exist in abundance in South Africa, and use less asphalt binder, which is not as readily available in the country (Rust et al. 1998). Today, this method represents the primary design for high-traffic roads in South Africa and designs are available for traffic volumes ranging from 1-50 million ESALs. The South African practices and design guidelines were shaped over the course of 10 or more years by a relatively few early experimental sections constructed throughout the country that were carefully tracked with respect to costs and detailed performance assessments as well as accelerated load facility testing (Freeme et al. 1980).

2. Inverted Pavement Principles

As mentioned in the introduction and shown later in the design guide of South Africa, a major key to the success of inverted pavements is the thin asphalt layer followed by a densely compacted aggregate base (GAB in the South African nomenclature or ABC in NCDOT nomenclature) layer on top of a cement treated base (CTB). The main principle of this design is the stress-state dependent modulus of the unbound aggregate layer. The resilient modulus of the aggregate layer is based on the recoverable strain under repeated loads (Huang 2003). This modulus can be shown to be a function of the bulk stress and the deviatoric stresses as shown with the universal model in Equation (4), where $k_{1\text{-}3}$ are material dependent coefficients, p_a is the atmospheric pressure, θ is the bulk stress and σ_d is the deviatoric stress.

$$M_r = k_1 p_a \left(\frac{\theta}{p_a} \right)^{k_2} \left(\frac{\sigma_d}{p_a} \right)^{k_3} \tag{5}$$

This equation describes what is typically observed in AASHTO T 307 testing of unbound aggregate materials, which is that the confining pressure or bulk stress increases, the resilient modulus of the aggregate base layer increases. In an inverted pavement this same phenomenon occurs due to the fact that the aggregate base layer is confined between a thin asphalt layer on top

and a cement treated base layer below. As the load on the pavement system increases, the confining pressure increases forcing the aggregate layer to compact thus increasing the density of the layer. Even though the aggregate base modulus is increasing as the load increases, it could not be possible without the cement treated base. The ABC cannot mobilize tension, so the CTB imparts a lateral constraint to help create compressive horizontal stresses on the ABC causing confinement.

A conventional flexible pavement system uses the asphalt layer to carry most of the stress, which is then distributed throughout the pavement system. This redistribution is done by having a thicker asphalt pavement layer that can spread the load to the rest of the pavement system. In a conventional pavement system, if the ABC was subjected to the high stresses at the surface it would fail because its modulus would not be high enough (due to a lack of confinement). The asphalt layer in this system makes up most of the structural capacity while the aggregate layer and other layers are assumed to have a lower structural capacity. Inverted pavement design uses the aggregate base in an entirely different way. The majority of an inverted pavement's structural capacity comes from the ABC layer. This layer feels large stresses, and as a result of the confinement effects, responds with a higher modulus. With the increasing modulus, less potential for strain accumulation results and the pavement can continue to function despite the fact that the asphalt concrete layer is relatively thin.

Along with this higher stiffness accumulating in the ABC layer, the thickness of the layers plays an important role in how they react to the loading on the surface. A conventional pavement has a thicker asphalt layer which performs like a beam that is bending and horizontal tensile stresses occur in the bottom of the layer. When an inverted pavement structure is used, the asphalt layer is very thin compared to a conventional pavement. Because the asphalt layer is so thin, the asphalt no longer acts as a beam but as a membrane. With the asphalt layer acting as a membrane, normal behavior is not exhibited by the structure. In a conventional pavement, reducing the asphalt layer will increase the tensile stresses, but in an inverted structure, because the layer is acting as a membrane, the stresses are being reduced. The thicknesses of the other layers affect the structure in various ways. By decreasing the thickness of the CTB layer, bending increases in the CTB, which also increases compressive stress at the top and tensile stress at the bottom of the layer. By increasing the ABC thickness, bending stresses are increased in the asphalt layer but the stresses in the CTB layer are decreased (Papadopoulos 2014).

Figure A.1 shows that this effect can be substantial. In the left panel of this figure the asphalt layer thickness is 75 mm (3 in.) and in the right panel it is 25 mm (1 in.). Comparing the horizontal stresses at the bottom of the asphalt layer it is seen that thinner layer has 25% less tensile stress than the thicker layer. This effect is counter-intuitive when thinking about the asphalt layer as a beam-like layer, wherein a thinner layer would equate to more bending and thus higher stresses.

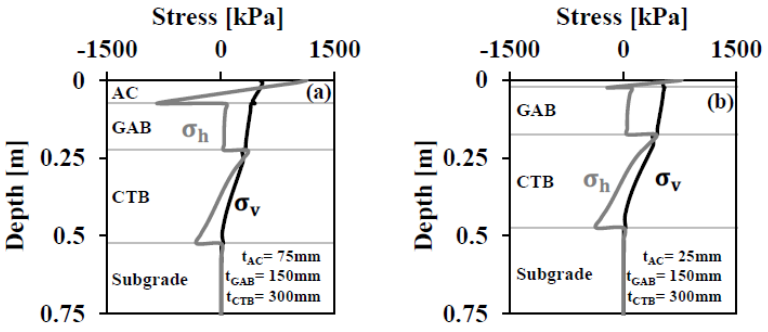

Figure A.1. Vertical and horizontal stress distribution vs. depth [Papadopoulous 2014].

Figure A.2 shows how changing the thickness of the asphalt layer inherently changes the way the layer reacts to loading. Each subsequent panel of this figure considers a different AC layer thickness from 100 mm (upper right panel) to 15 mm (lower left panel). With a 100 mm asphalt layer the maximum horizontal stress occurs near the center of the load. This horizontal stress distribution shows that this thicker layer acts like beam bending. A similar pattern exists for the 50 mm thickness, but at 25 mm a different behavior emerges. In this case, the maximum horizontal stresses are recorded near the edge of the load, meaning the layer no longer acting as a double supported beam and is instead behaving like a membrane. As a result, shear stresses are expected towards the edge of the load where the transition from compression to tension takes place.

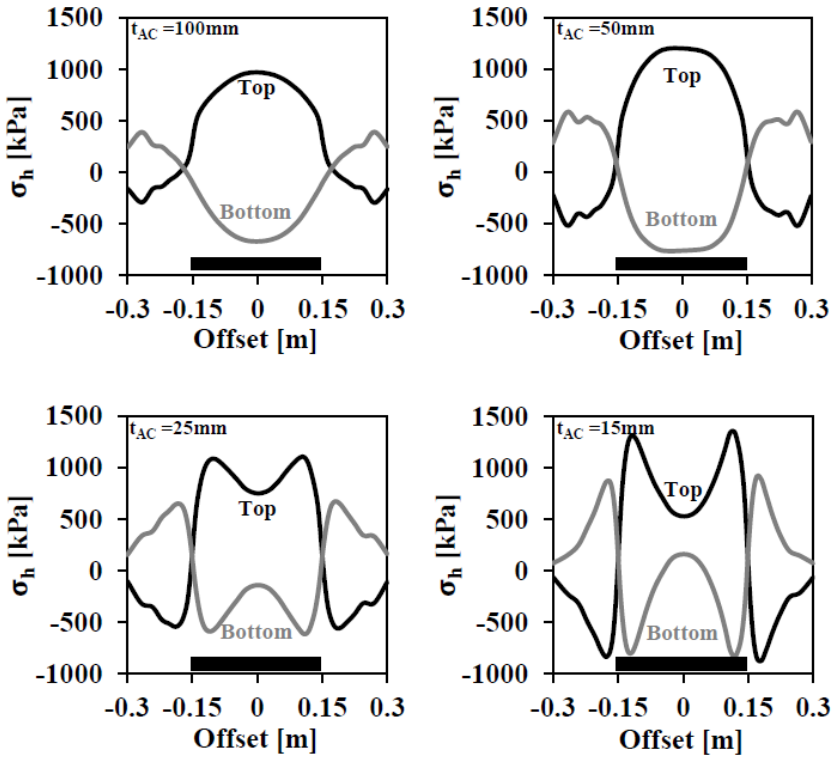

Figure A.2. Horizontal stress distribution along top and bottom of asphalt concrete layer [Papadopoulous 2014].

Also, by looking Figure A.2, it is seen that when the asphalt layer is reduced below 25 mm to 15 mm, the stresses increase. Thus, there exists a balance between the thickness of the asphalt and the ABC layers that will maximize the reduction in tensile stresses in the asphalt layer. Decreasing the thickness of the asphalt, increasing the stiffness of the ABC, or a combination of the two, will cause the central axis of the pavement to move vertically downward and reduce the bending strain at the bottom of the asphalt layer. The balance between the layers relative thickness is just as important as the thickness of the asphalt layer (Papadopoulous 2014).

3. Examples of use in the United States

3.1 Georgia

The Georgia DOT became interested in inverted pavements after meeting with the Georgia Construction Aggregate Association (GCCA) about the increasing costs of construction and the

need for more cost-effective materials. This meeting led to the construction of the first pilot project in Georgia at the Lafarge Quarry in Morgan County, Georgia in 2001. This project came to be known as the Morgan County project. The length of the haul road for the quarry was a total of 1,200 feet, consisting of 400 feet of conventional pavement, 400 feet of South African (SA) design inverted pavement, and 400 feet of "Georgia" (GA) design inverted pavement. The conventional section had 6 inches of surge stone, topped with 8 inches of graded aggregate base (GAB), topped with 3 inches of 19 mm Superpave hot mix asphalt. Both inverted pavement sections had 8 inches of cement treated base (CTB) and 6 inches of GAB, overlaid with 3 inches of 19 mm Superpave hot mix asphalt. This inverted section is shown in Figure A.3.

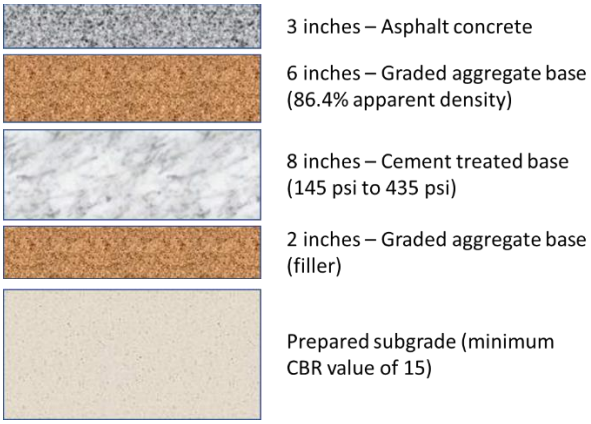

Figure A.3. Morgan County inverted pavement design [Lewis 2012].

The only difference between the SA inverted pavement and the GA inverted pavement was that the SA method compacted the GAB using a process called "slushing" while the GA method used conventional compaction methods. This difference was implemented because SA design procedures require the GAB to be compacted to 86-88% apparent density and the DOT wanted to evaluate whether the "slushing" process was needed to compact the GAB to this level. Note that based on the definition of apparent density for SA purposes, 86-88% apparent density is equivalent to 101-106% maximum dry density for a Georgia DOT Group II aggregate. The process of slushing creates an interlocked mass as the air voids are expelled from the aggregate and this pushes the fines to the surface of the base. These fines act as a lubricant upon saturation in the slushing process (Lewis 2012). After construction of both SA and GA GAB, the density was measured using the sand cone test and the results showed that both test sections reached 86% apparent density, therefore showing that the process of slushing is not needed in the construction of the GAB layer.

Testing was performed after 5 years and included visual inspection, rutting measurements, and falling weight deflectometer (FWD) testing. After 5 years approximately 854,000 ESAL's had travelled over the haul road, which totaled 63.4% of the design life for the pavement. Comparisons between the conventional test section and the inverted test sections showed that both inverted pavements had little to no rutting while the conventional pavement showed major rutting in some portions of the test section. The visual inspection showed that no cracking had appeared in the inverted pavement sections while extensive cracking formed within the conventional section. The FWD testing also showed lower deflections in the inverted pavement as compared to the conventional section. The FWD results were analyzed with MODTAG to estimate the pavement

remaining life (RL). The GA and SA sections had RL's of 99.3% and 94.6% while the conventional section had a RL of 67.9%.

After the success of the inverted pavement at the Morgan County Quarry, the Georgia DOT wanted to build its own test section on the South Lagrange Loop in Troup County starting in 2008. The project was a 2.03-mile-long road that included a 3,434 feet test section of inverted pavement. The remaining length of the roadway was a conventional portland cement concrete pavement structure. The two-lane stretch had Average Annual Daily Traffic (AADT) of 7,000 with an end of design life AADT of 11,700 with 3% multi-unit trucks and 4% single unit trucks. The inverted pavement included 1.5 inches of 12.5 mm nominal maximum aggregate size (NMAS) HMA, 2 inches of 19.0 mm NMAS HMA, 6 inches of GAB, 10 inches of CTB and then finally 6 inches of stabilized subgrade. The conventional pavement section included 9.5 inches of portland cement concrete, 10 inches of GAB, and 6 inches of stabilized subgrade. Both pavement structures are shown in Figure A.4.

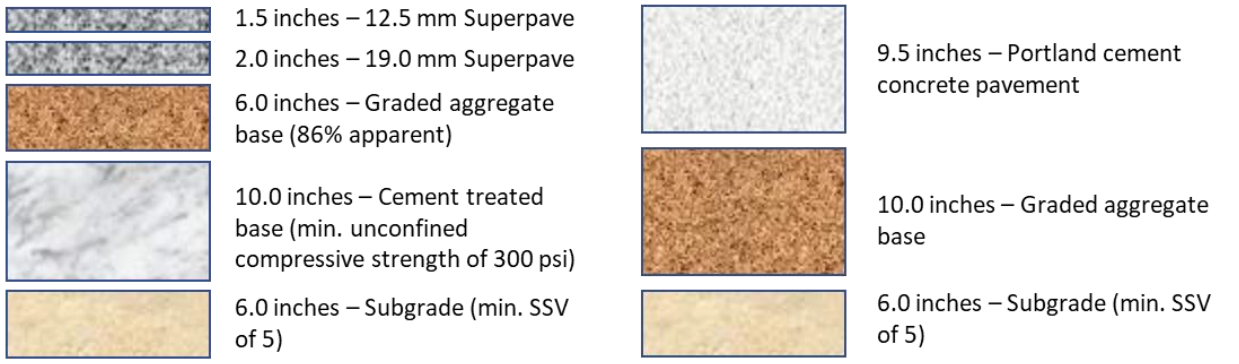

Figure A.4. South LaGrange Loop designs for; (a) inverted pavement section and (b) PCC section [Lewis 2012].

The subgrade of both sections was to be stabilized mechanically to obtain a California Bearing Ratio (CBR) of 15 in the top 6 inches of the subgrade. The CTB of the inverted pavement section was plant-mixed that had to be transported to the construction site. This varied from the onsite mixing of the CTB that took place in the Morgan County Project. The reasoning for this change was to ensure that a consistent mix was being used for construction. The GAB layer was constructed using typical construction equipment along with conventional practices. The apparent specific gravity of the GAB was measured using a South African test method along with AASHTO T-85, which is more commonly used by Georgia DOT. The apparent gravity obtained from each test respectively was 166.9 and then 165.4 pcf. The apparent specific gravity was then used along with the in-place density that was measured by a nuclear gauge to calculate the apparent gravity and the maximum dry density of the GAB. The desired apparent density was once again to be 86%. After using both test methods, the GAB passed with a median apparent density of 85.9% and a maximum dry density of 104.5%. These densities correspond to the South African method. The apparent density and maximum dry density associated with the apparent gravity obtained from AASHTO T-85 are 86.6% and 105.5%.After the end of construction, FWD testing took place, which suggested the section was in excellent condition with an average deflection of 8.54 mils (Lewis 2012). Avellaneda (2010) used the results from these two experiments to estimate that inverted pavements could yield an initial cost savings of 40% over the flexible pavement design for typical primary or secondary arterial routes.

3.2 Louisiana

Louisiana has been a front-runner in the use of inverted pavements. The Louisiana Department of Transportation and Development (DOTD) started pilot projects in 1991 with the LA-97 state highway project. Because of the lack of aggregate in southern Louisiana, soil-cement has been a cost-effective alternative for pavement designs. Louisiana's roadways consist of thousands of miles of soil-cement base (SCB) pavements because they improve the structural capacity when pavements are constructed on weak subgrade soils and they minimize the deflection of the pavement structure. The negative aspect of using these pavements is that reflective cracking from the SCB to the HMA surface layer. The Louisiana Transportation Research Center (LTRC) proposed an interlayer of crushed and graded aggregate between the HMA surface layer and the soil-cement layer. The reasoning for this interlayer was to decrease the tensile stresses at the bottom of the HMA layer by using the stone particles to absorb the movement transferred from the CTB (Titi 2003). The LA-97 project was a total of 4.7 miles long. A control section and test section of 1056 feet each were chosen from the total construction to conduct research. The control section had 3.5 inches of HMA on top of 8.5 inches of stabilized SCB. The test section was composed of 3.5 inches of HMA, 4 inches of crushed limestone, and 6 inches of stabilized SCB. The inverted pavement design is shown in Figure A.5.

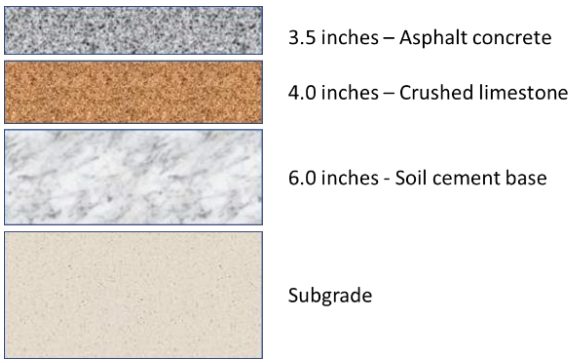

Figure A.5. LA-97 inverted pavement design [Titi 2003].

Each of these sections were constructed on a lime stabilized subgrade. The structural capacity was determined for each section by using the layer coefficients and the thickness of each layer. The test section had a structural number of 2.87 compared to the 2.66 for the control section. LA-97 at the time was considered a low volume rural collector highway with an AADT of 2,000. Following the construction of the pavements, surveys were completed to monitor the pavements' performance over the next several years. The final pavement survey was conducted in 1998 and included measurements of the total cracking, structural capacity, rideability and rutting. At this time, the control section had compiled 600 – 700 feet of total cracking, most of this being low severity with a few moderate and high severity cracks. The test section had 100 – 300 feet of total cracking all of which was low severity. Concerning the cracking, the control section mostly consisted of transverse, while the test section consisted of longitudinal cracking. Looking further into the evaluation of each pavement, the ride roughness and the average rut depth also remained consistent with one another over the evaluation period (Rasoulian 2000).

Although the initial results from the LA-97 study suggested equivalent performance, in the long-term the inverted pavement separated itself from the conventional pavement design. To examine this effect, Louisiana used an accelerated pavement testing experiment (begun in 1995) at the LTRC under a contract with Louisiana State University. This experiment used an accelerated

loading facility (ALF) machine to produce accelerated loading on test sections. The ALF machine uses a rolling dual-tire load assembly capable of applying a total load up to 18,950 lb and up to 8,100 passes per day on the test sections (Rasoulian 2000).

The initial experiment used nine total test sections with a goal to evaluate alternative SCB materials that would exhibit reduced shrinkage cracking but no loss of structural capacity. Lanes S-008 and S-009 resembled the control section and the inverted pavement section from the LA – 97 project respectively. The other test sections were combinations of soil cement and stone bases with different thicknesses. Based on the accelerated loading test results, the inverted pavement in test section S-009 outperformed all the other sections in every category. The number of ESALs accumulated before the failure criteria was reached was almost five times as much as any other design. Table A.1 and Figure A.6 through Figure A.8 from (Metcalf et al. 2001) show that the inverted pavement outperformed the other test sections in cracking, rutting, and serviceability (PSI). It was concluded during the study that the enhanced performance occurs because of the highly confined crushed stone layer that reduced the reflection of cracking from the soil cement base up to the asphalt layer and improves drainage between the two bound layers.

Table A.1. Pavement Life (x1000 ESAL); Results from ALF Testing [Metcalf 2001]

Lane #	Design (to PSI=2.5)	Rutting (to 25 mm)	Cracking (to 2.5 m/m^2)	Serviceability[a] (to PSI=2.5)
2	484	628	966	825
3	233	111	-	146
3A	233	883	467	1274
4	373	359	574	488
5	1038	351	235	269
6	1038	449	198	296
7	1038	725	231	305
8[b]	824	427	304	-
8A	824	383	196	400
9[c]	1095	1207	1138	1348
10	844	656	-	496

[a] Determined from quadratic regression fit of PSI against ESALs
[b] Control section replica from LA - 97
[c] Inverted pavement section replica from LA - 97

With this experiment there was also a cost-benefit analysis performed to compare the initial and long-term costs of the inverted pavement section and the regular soil cement base sections. This analysis showed that the conventional section with 26-foot-wide, 2 – lane road costs $173,000 per mile while the inverted section, with the same dimensions, costs $208,000 per mile (Titi 2003). This initial cost comparison showed that the inverted section costs almost 20% more, but since the section is expected to perform longer (almost five times) LTRC concluded that it might be worth the initial cost over the life-cycle of the pavement. Rasoulian (2000) using the same data showed that if the HMA layer was reduced to 2 inches instead of 3.5 inches that the initial cost per mile drops to $155,000 and suggested that even with this thinner layer of HMA, the inverted pavement would still outperform the conventional pavement.

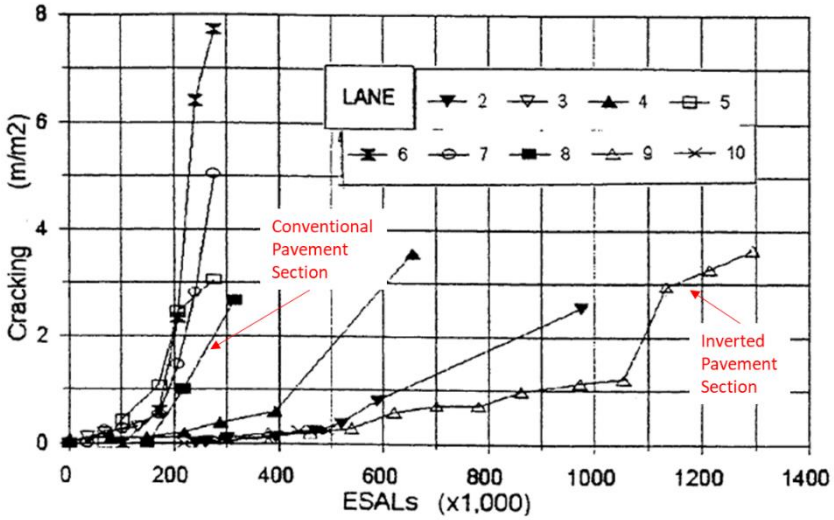

Figure A.6. Cracking development from all lanes [Metcalf 2001].

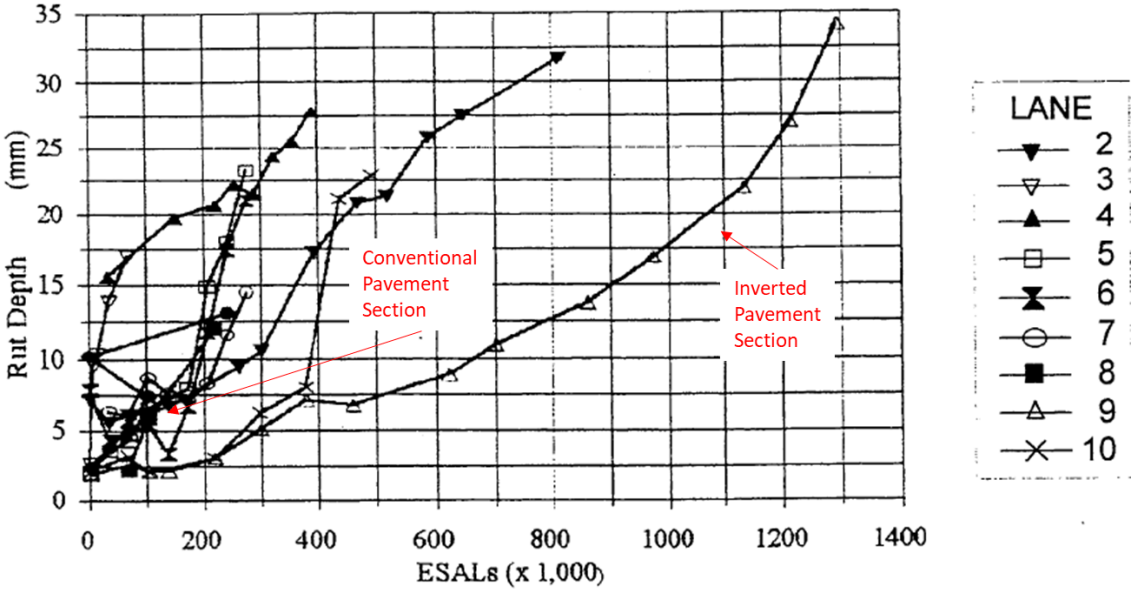

Figure A.7. Rutting development from all lanes [Metcalf 2001].

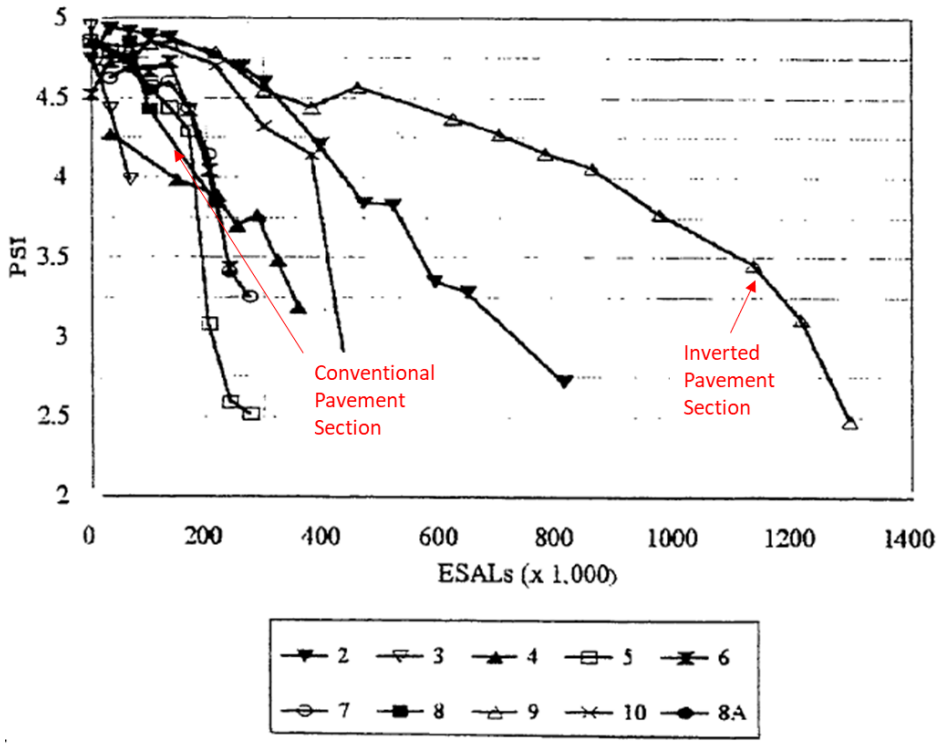

Figure A.8. PSI development for all lanes [Metcalf 2001].

3.3 New Mexico

New Mexico was among the first agency to experiment with inverted pavements in the United States. The project, referred to as I-010-1(8) Road Forks-East, established a foundation for experimental work on inverted pavements to take place. During the construction, the contractor noticed that the pavement's surface course began to show early cracking because the asphalt was directly on top of an aggregate layer. He petitioned to treat the subbase with cement and stated the four reasons of doing so: 1) immediate protection of the subgrade from the surface loading, 2) better compaction of the untreated base because of a firmer foundation, 3) alleviate reflective cracking in the surface course by using a "cushioning" intermediate layer, and 4) an overall smoother riding road is produced (Johnson 1961). After a year, the performance in the sections of the Road Forks – East project were examined. The two sections in this project that resembled "inverted pavement" were sections B and H, which are summarized in Figure A.9 and Figure A.10 respectively. Both sections had performed well and showed minimal rutting and little to no cracking, along with most of the other test sections. Essentially, the project found that while the inverted sections had not performed necessarily better, they did not perform worse either. According to Johnson, the cracking and rutting seemed to be more associated with the soil and moisture conditions rather than with the design of the base and subbase courses.

From the Road Forks – East project stemmed much concern over the combination of treated and untreated base and subbase that would perform best. As a result, the New Mexico DOT conducted project F-051-1(8), which constructed and evaluated nine test sections in order to determine the most efficient pavement design. Each test section was 2,000 feet long and was built with full stabilization, which in New Mexico is used based on the relationship between the traffic index and the California R values. The top 6 inches of the subgrade was specified to be compacted to a

minimum of 95 percent modified Proctor density. Each test section was designated by letters, A through I, with A being the control section. Upon the completion of the test sections, initial inspection took place. No sections showed any signs of rutting, but sections H and I, which used CTB directly below the HMA surface, exhibited surface cracking. Looking at the design of each test section, the Sections A and B are the designs that most closely resemble what is now referred to as inverted pavement design. These test sections are shown in Figure A.11 and Figure A.12. Inspection results from the F-051-1 (8) show the density, roughness readings, and deflection of each of the test sections. These results do not show much difference between the "inverted pavement" sections and the other test sections. As mentioned before, the rutting and cracking of the segments seemed to be more associated with the soil type and the moisture content of the soil.

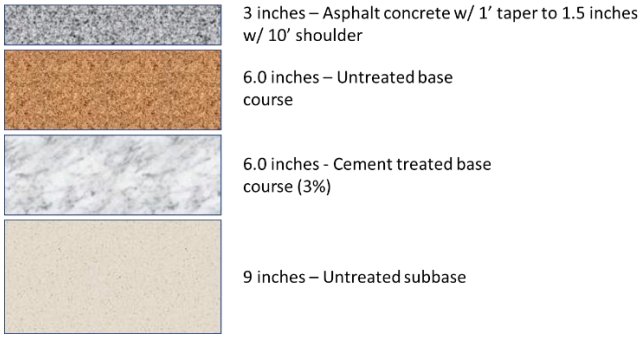

Figure A.9. Section B inverted pavement design from I-010-1(8) [Johnson 1961].

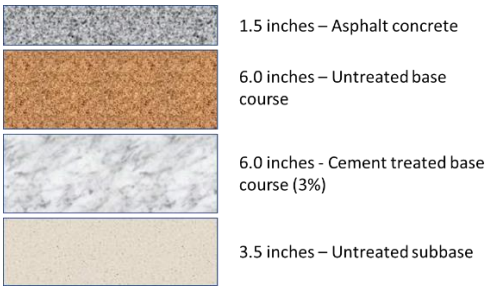

Figure A.10. Section H inverted pavement from I-010-1(8) [Johnson 1961].

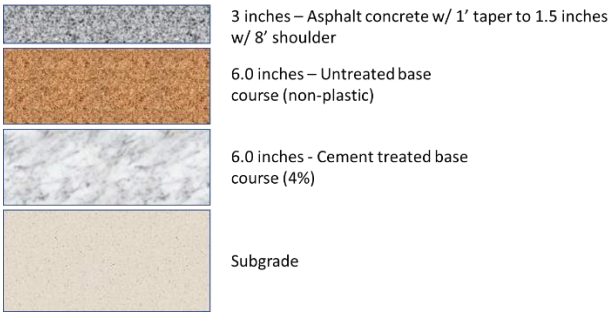

Figure A.11. Section A inverted pavement from F-051-1(8) [Johnson 1961].

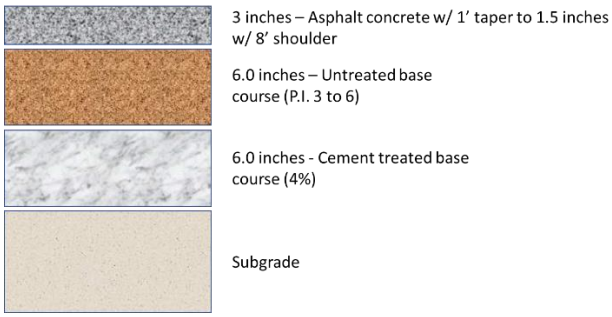

Figure A.12. Section B inverted pavement from F-051-1(8) [Johnson 1961].

In 2012, an inverted pavement design was used for a portion of I-25 in Raton, New Mexico. This is an interesting situation using inverted pavement since this area is susceptible to 54+ inches of snow per year. The as-constructed design can be seen in Figure A.13, and it shares many similarities with the other examples in New Mexico albeit with a thicker GAB and CTB.

Figure A.13. I-25 New Mexico inverted pavement design for I-25 study.

3.4 North Carolina

In 2015, Vulcan Materials constructed a new 1,600-foot road around their Pineville Quarry consisting of. The road was split into two sections, each 800 feet. The first section was an inverted pavement test section and the second was a conventional pavement design used as a control section. The inverted pavement section can be found in Figure A.14. Unlike in the New Mexico and Georgia pilot projects, these sections were built on top of the native compacted subgrade instead of a stabilized subgrade. The sections are relatively new so not much testing has been conducted to see the performance of each of the test sections. However, NCDOT conducted FWD testing on numerous occasions and found that there is less deflection and less seasonal variation in the inverted pavements. Looking at the density results of each section, the CTB greatly enhanced the density of the aggregate base in the inverted pavement test section (103.4% average achieved compaction) compared to the control section (99.8% average achieved compaction). Vulcan also ran its own economic analysis and found that construction costs were 11% lower in the case of the inverted pavement. It is noted that the distance to the ABC source may have contributed to these cost differences.

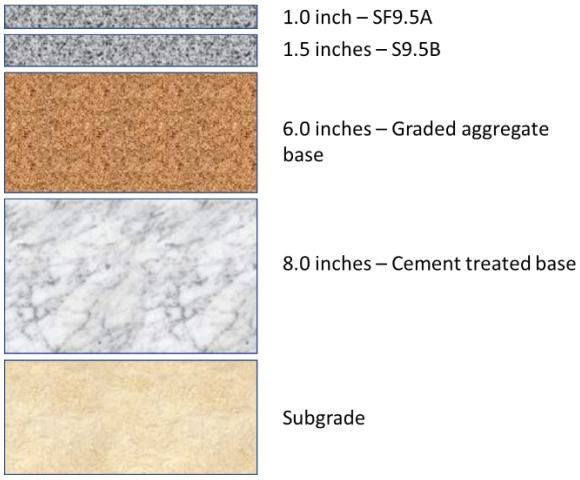

Figure A.14. Pineville Quarry haul road inverted design.

3.5 Virginia

The Virginia case study took place in Bull Run, Virginia with Luck Stone Corporation running the operation. The project consisted of an original design that was 500 feet long and an inverted pavement section that was 500 feet as well. Both pavement designs are shown in Figure A.15.

(a) **(b)**

Figure A.15. (a) Conventional pavement section, (b) Inverted pavement section from Bull Run, Virginia [Weingart 2010].

The original section was designed using the Mechanistic Empirical Pavement Design Guide (MEPDG), while the inverted pavement design was designed using the International Center Aggregate Research (ICAR) method. The ICAR method considers the unbound aggregate base as a nonlinear, stress sensitive material. This model accounts for the directional dependency of the stiffness values in the unbound layer meaning it accurately models the layer as anisotropic. The steps of the model are shown in Figure A.16. Thus, giving the layer realistic stress distribution and reducing significant horizontal tension. The predicted fatigue life for the inverted section was given as 19,583,009 ESALs while the rutting life was given as 17,700,146 ESALs. The original section cost $20,640 per 100 linear feet while the inverted section was $16,071 per linear feet, an estimated saving of 22.1% by utilizing the inverted pavement section. Detailed quantified performance data is not available for this project. However, informal discussions with engineers

familiar with the project suggest that the inverted pavement section seems to be in better condition than the traditional section, specifically that the control section is exhibiting more cracking than the inverted section (R. Ashtiani, personal communication, December 11, 2019).

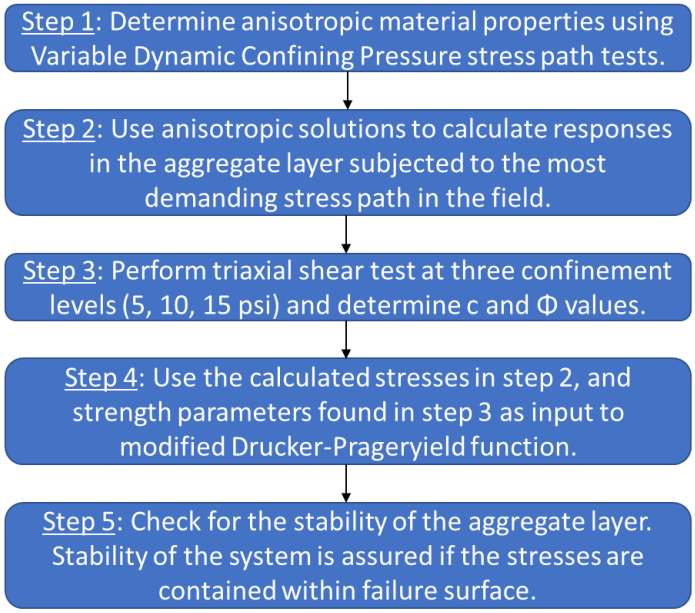

Figure A.16. Unbound aggregate base stability protocol [R. Ashtiani].

4. Inverted Pavement Design Standards

4.1 Louisiana DOT design standards for stone interlayer pavement

As mentioned above, Louisiana is one the states that most often uses inverted pavement designs, which they typically use for low trafficked roads. The Louisiana DOTD uses the AASHTO 1993 empirical method to design inverted pavements. Below is a comparison of the relevant differences between the implementation of the 1993 AASHTO empirical method for Louisiana (L.A.) and North Carolina (N.C.).

First, L.A. and N.C. vary with respect to their design period. Louisiana uses a 20 year design period for all facilities while the N.C. method adopts 30 years for all roads except when the AADT is less the 20,000 vehicles. For these low volume roadways the N.C. method uses 20 years. The two agencies also differ with respect to their design reliability, Table A.2. Louisiana uses a higher reliability for interstate and primary routes while N.C. has the same or higher values for collector and local routes. It is also found that the two agencies currently adopt different initial and terminal serviceability, Table A.3 and Table A.4. For N.C., the initial design serviceability index (p_o) is always 4.2, while for L.A. it is based on the road type and ranges from 3.5 (collectors) to 4.3 (interstates). For the terminal serviceability (p_t), L.A.'s is also based on road type, ranging from 1.5 (collectors) to 2.8 (interstates). For N.C., the p_t is based on the 20-year ADT and ranges from 2.5 (low AADT) to 3.0 (high AADT). The overall standard deviation (S_o) also is different (0.47 for L.A. and 0.45 for N.C.). Finally, the layer coefficients are slightly different between the two methods. The main components for stone interlayer pavement are the asphalt, unbound aggregate base, and cement treated base. For asphalt, the layer coefficients are the same except for an asphalt base course which in L.A. it is 0.33 and in N.C. it is 0.30. For SCB (stabilized) and soil cement (treated), the layer coefficients form the L.A. guide are 0.14 and 0.10, while the CTB layer

coefficient in N.C. is 0.23. The L.A. guide also gives the soil cement subbase layer coefficient as 0.14. N.C. does not distinguish between base and subbase values for layer coefficients.

Table A.2. Comparison of Reliability Levels Used for Pavement Design by the Louisiana DOTD and the North Carolina DOT

Road Type	Reliability Level		
	Louisiana		North Carolina
	Urban	Rural	
Interstate	99	97	95
Principal/Primary	97	95	90
Collector[a]	90	85	90
Local[b]	75	70	85

[a] For North Carolina DOT this considered as a Secondary with > 20,000 AADT
[b] For North Carolina DOT this is considered as a Secondary with < 20,000 AADT

Table A.3. Louisiana Serviceability Indices for Design

Road Type	p_o	p_t	ΔPSI
Interstate	4.30	2.80	1.50
Principal	4.30	2.50	1.80
Collector	4.00	2.00	2.00
Local	3.50	1.50	2.00

Table A.4. North Carolina Serviceability Indices for Design

20-year AADT	p_o	p_t	ΔPSI
> 80,000	4.20	3.00	1.20
> 40,000	4.20	2.75	1.45
Lowest Acceptable	4.20	2.50	1.70

4.2 ICAR Virginia Design Method

The Virginia Bull Run project was designed by using the International Center for Aggregates Research (ICAR) method of stress-dependent modeling for the unbound aggregate base (UAB) or the granular aggregate base (GAB). ICAR developed models for resilient and permanent deformation behavior of unbound layers based on the results from triaxial tests. The ICAR material models and testing protocol represents an improved method for analyzing the structural performance of unbound aggregates within pavement layers. The method utilizes an Uzan type model that relates the resilient modulus of the unbound material to the bulk and deviator stresses. However, it improves upon the Uzan type model by better accounting for higher stress values like those encountered in inverted pavements (Tutumluer et al., 2003). This new and improved anisotropic structural model correctly models critical pavement design parameters, such as the vertical compressive stresses and strains at the top of the GAB. This ICAR method uses three stress regimes and ten stress states within each regime to determine stress sensitivity and cross-anisotropy of the aggregate base. The specimens are tested with a rapid triaxial tester (RaTT), that simulates moving wheel loads. This machine uses variable dynamic confining pressure to

accurately account for moving loads on the pavement. The loading cycle of the dynamic stress consists of 1.5 s loading and 1.5 s unloading. This pattern is applied on a sample for 25 repetitions until a suitable resilient strain is obtained. With the resilient axial and radial strains determined for each stress regime, they are then implemented to calculate the five anisotropic elastic properties at that particular stress state (Kim et al. 2005). Experience with this method shows that the anisotropic ratio (ratio of vertical to horizontal moduli) can range from 2-5.

4.3 South African design standards catalogue (DTSA 1996)

The South African design standards as mentioned before are the only nationally recognized standards that could be found. The South African design guide is presented as a catalog and uses a nine-step process to determine the pavement design for a specified area. The process is broken down into the design philosophy, road category, pavement design, design traffic and pavement class, materials, environment, practical considerations, structural design and pavement type selections, and finally cost analysis. The flow chart of this design process can be seen in Figure A.17.

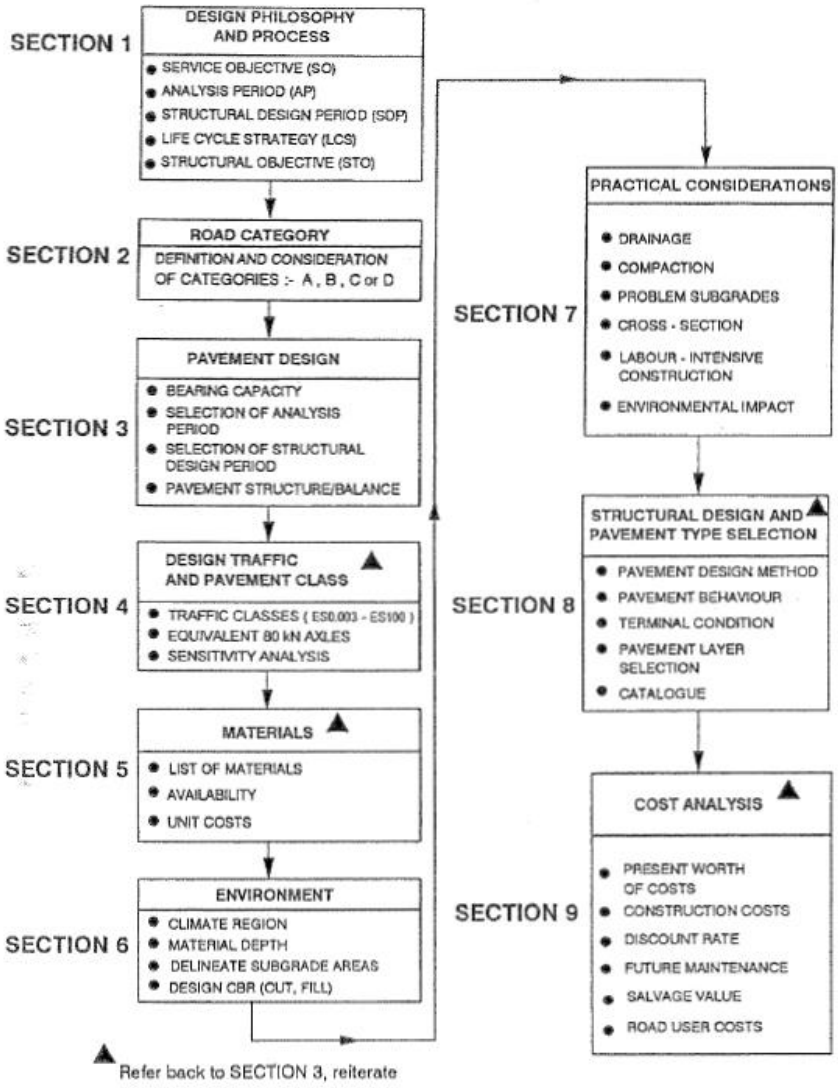

Figure A.17. Detailed Road Pavement Design Process [DTSA 1996].

The first step in the design process, design philosophy is essentially a planning process whereby the engineer identifies the functional service level of the road or facility improvement and the design life and analysis period that will be considered during design. This process incorporates factors such as traffic levels, speed, travel time, and safety. In the second step, the category of the road where the pavement is to be placed is determined. South African standards consider four categories for roads including: A, B, C, and D. These roads range from major interurban freeways to rural access roads. The road categories and their typical pavement characteristics can be seen in Table A.5.

Table A.5. Road Categories [DTSA 1996]

	Road Category			
	A	**B**	**C**	**D**
Description	Major freeways and major rural roads	Interurban collectors and rural roads	Lightly trafficked rural roads, strategic roads	Rural access roads
Importance	Very important	Important	Less important	Less important
Service level	Very high	High	Moderate	Moderate to low
Typical Pavement Characteristics				
Risk	**Very Low**	**Low**	**Medium**	**High**
Design Reliability, %	95	90	80	50
Total Lifetime E80s per lane[a,b]	3-100 x 10^6	0.3 - 10 x10^6	< 3 x10^6	< 1 x10^6
E80 Designation	ES10 - ES100	ES1 - ES10	ES0.003 - ES3	ES0.003 - ES1
Daily Traffic	> 4000	600 -10,000	< 600	< 500
Constructed riding quality				
p_o	3.5 - 4.5	3.0 - 4.5	2.5 -3.5	2.0 - 3.5
HRI[c], m/km (in./mi)	1.0 - 1.5 (64 – 95)	1.0 - 2.0 (64 – 127)	1.5 - 2.7 (95 – 171)	1.5 - 3.5 (95 – 222)
Terminal Riding Quality				
p_t	2.5	2	1.8	1.5
HRI[c], m/km (in./mi)	171	222	247	285
Warning Rut Level, mm (in.)	10 (0.4)	10 (0.4)	10 (0.4)	10 (0.4)
Terminal Rut Level, mm (in.)	20 (0.8)	20 (0.8)	20 (0.8)	20 (0.8)
Area/ Length exceeding terminal conditions, %	5	10	20	50

[a] E80 is on an 80 kN single axle load, 80 kN load is equal to 18 kips
[b] For road categories B, C, and D the design strategy impacts the E80 limit used for categorization
[c] HRI = half car roughness index

Step three focuses on identifying factors relevant to the pavement design including the necessary bearing capacity, analysis period, and structural design period. In the South African design guide, these three factors are selected based on the road category, but considerable latitude is granted to the engineer to select what they feel best balances the risks from under design and what best reflects the expected lifetime of the alignment (i.e., the design life for the geometric design). Table A.6 summarizes the range and recommended values for the design and analysis lifetimes used by South Africa for different road classifications.

Table A.6. Analysis Periods for Road Categories [DTSA 1996]

Road Category	Structural Design Period (years)		Analysis Period (years)		
	Range	Recommended	Range	Recommended	
				High Certainty	Low Certainty
A	15 - 30	25	20 - 40	30	----
B	15 - 25	20	15 - 30	30	25
C	10 - 20	15	10 - 30	30	20
D	7 - 15	10	10 - 20	20	10 - 15

Step four determines the traffic level to use for design. South Africa uses the same basic concept of equivalent axle loads as is used in the United States, but the basis for its calculation is slightly different. South Africa uses an 80 kN single axle load as its reference (referred to as E80), which is approximately equivalent to an 18-kip single axle load. The South African design guide identifies multiple ways that an engineer can determine the cumulative number of annual daily equivalent loads (ADE) and ultimately the cumulative number of E80s for the pavement lifetime. Method one takes a set of tabulated valuessadf that are based on heavy vehicle volumetric capacity or road category. An estimate of the type of heavy vehicle is made based on road category and a factor is chosen from Table A.7. The number of heavy vehicles is then multiplied by the chosen factor and summed to obtain the ADE. Method two is more detailed and requires the engineer to first obtain, or estimate, the number of trucks by type that will use the roadway. The engineer then uses Table A.8 to identify the truck factor for each type of truck, multiples it by the truck estimates for each type, and sums across truck type to obtain the ADE. Note that in this method the engineer must select whether to use low, average, or high equivalency values in their design calculations. The recommendation from the South African design guide is to use the third method which is the most accurate but requires load spectra data. The engineer would obtain static or dynamic load surveys that contain the number of repetitions of a given axle load (P). The loads are then used to calculate a load equivalency based on Equation (5).

Table A.7. Determination of E80s per Heavy Vehicle

Loading of heavy vehicles	E80/heavy vehicle
Mostly unladen	0.6
50% laden, 50% unladen	1.2
> 70% fully laden	2

Table A.8. South African Truck Factors used in Method 2

Type	Low E80	Avg E80	High E80
2-axle truck	0.30	0.70	1.10
2-axle bus	0.41	0.73	1.52
3-axle truck	0.80	1.70	2.60
4-axle truck	0.80	1.80	3.00
5-axle truck	1.00	2.20	3.00
6-axle truck	1.60	3.50	5.20
7 axle truck	3.80	4.40	5.00

$$F = \left(\frac{P}{80} \right)^n \tag{6}$$

where, F is the load equivalency factor, P is the load in question (in kN), and n is a damage coefficient. Within the South African design guide, the selection of n is up to the engineer. However, for inverted pavements, which have a granular base and cement treated subbase, the recommended value of n is 3, but the range can be 2-4. Table A.9 gives the values of the equivalency factor for each given single axle load for different damage coefficients. In Method three the engineer would compute F for each load in question and use these along with the traffic distribution to compute the ADE for the pavement.

For either of the three methods, once ADE is obtained it is used to compute the cumulative design E80s. The process closely resembles the method followed in North Carolina. First, the average annual daily equivalent (AADE) is obtained by applying monthly adjustments to the ADE, summing the results, and dividing by 365 days. This step may be omitted if the traffic count data used to compute ADE originally was taken over a sufficiently long period of time or if seasonal/monthly variations are known to be minor. Then, a lane distribution factor, L_D, is applied depending on the geometric design of the roadway, see Table A.10. This lane distribution factor is multiplied by the total AADE to find the design lane, base year, AADE value, Equation (6).

Table A.9. 80 kN Single-Axle Load Equivalency Factors [DTSA 1996]

Single Axle load, *P* (kN)	**80 kN axle equivalency factor, *F* for different relative damage coefficients, *n***			
	3	**4**	**5**	**6**
15-24	0.016796	0.004668	0.001331	0.000386
25-34	0.053642	0.021081	0.008423	0.003412
35-44	0.125058	0.064071	0.033178	0.017347
45-54	0.242763	0.153854	0.098220	0.063131
55-64	0.418476	0.316502	0.240635	0.183869
65-74	0.663915	0.58395	0.515640	0.457049
75-84	0.990800	0.993991	1.000239	1.009515
85-94	1.410849	1.590277	1.796889	2.035178
95-104	1.935780	2.42232	3.037161	3.815481
105-114	2.577313	3.545491	4.885401	6.742608
115-124	3.347167	5.021021	7.542392	11.34544
125-134	4.257060	6.915998	11.24902	18.31824
135-144	5.318710	9.303373	16.28993	28.55214
145-154	6.543837	12.26195	22.99720	43.16930
155-164	7.944159	15.87641	31.75397	63.55986
165-174	9.531396	20.23727	42.99817	91.42163
175-184	11.31726	25.44091	57.22610	128.8025
185-194	13.31349	31.58959	74.99615	178.1458
195-204	15.53178	38.79141	96.93245	242.3377

Table A.10. Lane Distribution Factors used in South African Design Guide [DTSA 1996]

Total Number of Lanes Per Direction	Lane Distribution Factor, L_D			
	Shoulder	Lane 1 (outer lane)	Lane 2	Lane 3
1	1	1	-	-
2	0.95	0.95	0.30	-
3	0.70	0.70	0.60	0.25

$$AADE_{design\ lane}^{base\ year} = AADE \times L_D \tag{7}$$

Next, a growth rate for the traffic distribution is obtained either from traffic data of a specific road or assumed from a typical rate (4% is often used). This growth rate is then used to compute a growth factor from Equation (7) or find the factor from Table A.11. In Equation (7), g_x is the growth factor, i is the growth rate in percent of E80s (per year), and x is the time in years between determination of axle load data and start of design period. The growth factor is multiplied by the design lane, base year AADE value to obtain the design lane, initial AADE, Equation (8).

$$g_x = \left(1 + 0.01i\right)^x \tag{8}$$

Table A.11. Traffic Growth Factor (g_x) [DTSA 1996]

Years before road opening	g_x for traffic increase, i (% per year)								
	2	3	4	5	6	7	8	9	10
1	1.02	1.03	1.04	1.05	1.06	1.07	1.08	1.09	1.10
2	1.04	1.06	1.08	1.10	1.12	1.14	1.17	1.19	1.21
3	1.06	1.09	1.12	1.16	1.19	1.23	1.26	1.30	1.33
4	1.08	1.13	1.17	1.22	1.26	1.31	1.36	1.41	1.46
5	1.10	1.16	1.22	1.28	1.34	1.40	1.47	1.54	1.61
6	1.13	1.19	1.27	1.34	1.42	1.50	1.59	1.68	1.77
7	1.15	1.23	1.32	1.41	1.50	1.61	1.71	1.83	1.95
8	1.17	1.27	1.37	1.48	1.59	1.72	1.85	1.99	2.14
9	1.20	1.30	1.42	1.55	1.69	1.84	2.00	2.17	2.36
10	1.22	1.34	1.48	1.63	1.79	1.97	2.16	2.37	2.59

$$AADE_{design\ lane}^{initial} = AADE_{design\ lane}^{base\ year} \times g_x \tag{9}$$

The design lane, initial AADE is multiplied by a growth factor, f_y, to compute the cumulative E80s for the design, Equation (9). The value of f_y is obtained from either Equation (10) or Table A.12. In Equation (10), i is the growth rate (%) and y is the structural design period. Finally, the cumulative E80s can be used to identify the pavement classification designation, Table A.13, and ultimately used in selecting a pavement design.

$$E80_{design} = AADE_{design\ lane}^{initial} \times f_y \tag{10}$$

$$f_y = 365 \times \left(1 + 0.01(i)\right)\left[\frac{\left(1 + 0.01(i)\right)^y - 1}{0.01(i)}\right] \tag{11}$$

Table A.12. Traffic Growth Factor (f_y) [DTSA 1996]

Design period, y (years)	f_y for traffic increase, I (% per year)								
	2	4	6	8	10	12	14	16	18
4	1534	1612	1693	1776	1863	1954	2048	2145	2246
5	1937	2056	2181	2313	2451	2597	2750	2912	3081
6	2349	2518	2699	2892	3098	3317	3552	3801	4067
7	2768	2998	3248	3517	3809	4124	4465	4833	5229
8	3195	3498	3829	4193	4592	5028	5506	6029	6601
9	3632	4017	4446	4923	5452	6040	6693	7417	8220
10	4077	4558	5100	5711	6399	7174	8046	9028	10131
11	4530	5119	5793	6562	7440	8444	9589	10895	12385
12	4993	5704	6527	7481	8586	9866	11347	13062	15045
13	5465	6312	7305	8473	9846	11458	13352	15575	18184
14	5947	6944	8131	9546	11232	13242	15637	18491	21887
15	6438	7601	9005	10703	12757	15240	18243	21873	26258
16	6939	8285	9933	11954	14434	17478	21213	25796	31415
17	7450	8996	10916	13304	16279	19984	24599	30346	37500
18	7972	9735	11957	14763	18308	22790	28459	35625	44681
19	8504	10504	13062	16338	20540	25934	32859	41749	53154
20	9046	11304	14232	18039	22996	29455	37875	48852	63153
25	11925	15809	21227	28818	39486	54507	75676	105517	147559
30	15104	21290	30588	44656	66044	98657	148459	224534	340661
35	18613	27958	43114	67927	108816	176464	288596	474510	782432
40	22488	36072	59877	102120	177701	313587	558417	999545	1793096

Table A.13. Classification of Pavements [DTSA 1996]

Pavement Class	$E80_{design}$ x 1×10^6	Volume and type of traffic	
		Approximate v.p.d per lane [a]	Description
ES0.003	< 0.003	< 3	Very lightly trafficked roads, very few heavy vehicles. These roads could include transition from gravel to paved roads and may incorporate semi-permanent and all weather surfacings
ES0.01	0.003 - 0.01	3 - 10	
ES0.03	0.01 - 0.03	10 - 20	
ES0.1	0.03 - 0.10	20 - 75	
ES0.3	0.10 - 0.30	75 - 220	
ES1	0.3 - 1	220 - 700	Lightly trafficked roads, mainly cars, light delivery and agriculture vehicles; very few heavy vehicles
ES3	1 - 3	> 700	Medium volume of traffic, few heavy vehicles
ES10	3 - 10	> 700[b]	High Volume of traffic and many heavy vehicles
ES30	10 - 30	> 2200[b]	Very high volume of traffic and a high proportion of fully laden heavy vehicles
ES100	30 - 100	> 6500[b]	

[a] v.p.d = vehicles per day

[b] v.p.d is total per direction with 20% vehicles having 2 E80s per vehicle

Material selection is the next process in determining the pavement type and design. The selection of the materials for a pavement design is based on a combination of availability of suitable materials, environmental considerations, construction methods to be used, economics, and previous experience. A multitude of materials are listed in the design guides for South Africa but as mentioned later in the material comparison, the focus is placed on those that are used in inverted pavements.

After taking into consideration the availability of the engineered materials (asphalt, aggregate, and CTB), the climate and its effect on the subgrade is examined. In South Africa, the subgrade is classified using soaked CBR values. To determine the design CBR of the pavement structure, the "material depth" must be examined. The material depth is defined as the depth below the finished level of the road to which soil characteristics have a significant effect on the pavement behavior. The strength and density of the soils below this depth are considered negligible for the pavement structure. The depth denotes the approximate cover required for a soil of 1 – 2% soaked CBR value. Typical material depths are given in Table A.14 based on the road category. The depth given is the total thickness of the pavement above the roadbed. The bear capacity of the subgrade is improved by overlaying it with the necessary layers of material to achieve a structurally balanced pavement system. With this being said, the final pavement should have the design bearing capacity to ensure that the structure can perform over the structural design period. The design subgrade bearing capacity is given by Table A.15. SG1, SG2, and SG3 are appropriate subgrade classifications, but if a subgrade obtains a classification of SG4, the soil must be modified.

Table A.14. Typical Material Depths [DTSA 1996]

Road Category	Material Depth (mm)
A	1000 - 1200
B	800 - 1000
C	800
D	700

Table A.15. Subgrade CBR Classification [DTSA 1996]

Class	Subgrade CBR (%)
SG1	> 15
SG2	7 to 15
SG3	3 to 7
SG4	< 3[a]

[a] requires modification and/or stabilization

Practical considerations are then considered including drainage, compaction, subgrade below material depth, pavement cross-section, and construction impacts. Drainage design is implemented to provide effective drainage to at least material depth so that the pavement structure is prevented from becoming saturated. Surface runoff is important, but subsurface drainage is more problematic in the pavement structure. Impermeable layers may be introduced to keep layers from trapping moisture and causing the pavement layers to become saturated, thus resulting in a loss of strength. Compaction is a major step in the construction process of the pavement structure. The higher the construction density of the layer, the higher the strength, and hence, the resistance to permanent deformation. The minimum compaction requirements for various layers are discussed later in the

material comparison and given in Table A.16. For the South African method, the subgrade below the material depth should be examined before looking at minimum compaction requirements to check for any abnormalities such as excessive volume changes due to moisture change, flaws in structural support, non-uniform support, soluble salts, excessive deflection and rebound of highly resilient soils during and after loading, and finally impact of burrowing animals beneath the structure. Construction impacts that are mentioned include considerations of manual labor-intensive road pavement construction and integrated environmental management of road construction. Manual labor construction is mentioned because labor-intensive projects affect the selection of the road category, pavement layer types and other practical considerations. For the labor-intensive projects, it would be more economically feasible to use labor-intensive construction on lightly trafficked roads, thus affecting the selection of the road category. Integrated environmental management of road construction is a process designed to minimize the negative environmental consequences of development.

Table A.16. Nominal Field Compaction of Pavement Layers [DTSA 1996]

Pavement Layer	Material or layer	Target density (Relative Compaction)
Base	Hot - mix asphalt:	97% minus design voids-in-mix
	Crushed stone:	
	G1	86 - 88 % apparent relative density
	G2	100 - 102% mod. AASHTO or 85% bulk relative density
	G3	98 - 100% mod. AASHTO
	G4	98 - 100% mod. AASHTO
	Waterbound macadam:	
	WM1	88 - 90 % apparent relative density
	WM2	86 - 88 % apparent relative density
	Cemented(C3/C4):	97 - 98% mod. AASHTO
Subbase	Gravel (G4/G5):	
	Upper	95 - 97% mod. AASHTO
	Lower	95% mod. AASHTO
	Cemented(C3/C4):	
	Upper	96% mod. AASHTO
	Lower	95% mod. AASHTO
Other	Select layers:	
	Upper	93 - 95% mod. AASHTO
	Lower	90 - 93% mod. AASHTO
	Fill (within material depth):	
	Gravel	90% mod. AASHTO
	Sand	100% mod AASHTO
	Roadbed (within material depth):	
	Gravel	90% mod. AASHTO
	Sand	100% mod AASHTO
	Shoulder gravel:	93% mod AASHTO

The next step in the South African design process is, “Pavement Type Selection and Structural Design”. Factors influencing pavement layer selection including traffic class, category and layer type are shown in Table A.17. In Table A.17, each type of base is given and then either a granular or cemented base is given. Looking at each combination, a granular base with a cemented subbase is recommended for each type of traffic class. South Africa permits engineers to use a number of different methods for pavement design, including AASTHO empirical, the South African Mechanistic Design Method (SAMDM) and other mechanistic-empirical approaches, but the default process involves using a catalog. The catalog designs for a dry region in South Africa are given in Table A.18. The catalog designs for a wet region are given in Table A.19. The major difference in the wet region designs are that the highest traffic level there are no designs, the granular bases are typically of higher quality, and the bases/subbases are typically thicker. These designs are to be used a guide but may not take into account special considerations that have been listed above. The pavement designs listed in the catalog are considered to be of adequate capacity to carry the total equivalent design traffic over the structural design period. Once a design is chosen, it is preferred that it is validated mechanistically using the SAMDM.

Table A.17. Suggested Pavement Types for Road Categories and Traffic Class [DTSA 1996]

Pavement Types		**Road Category and Traffic Class**								**Reasons why pavement types are not recommended**
Base	**Subbase**	**A**		**B**			**C and D**			
		ES100	ES3	ES10	ES3	ES1	ES3	ES1	<ES0.3	
Granular	Granular	×	✓	✓	✓	✓	✓	✓	✓	Uncertain behavior
	Cemented	✓	✓	✓	✓	✓	✓	✓	✓	----
Hot-mix asphalt	Granular	✓	✓	✓	✓	×	✓	×	×	Cost effectiveness
	Cemented	✓	✓	✓	✓	×	✓	×	×	cost effectiveness
Cemented	Granular	×	×	×	×	×	×	×	✓	Fatigue cracking, crushing, pumping and rocking blocks
	Cemented	×	×	✓	✓	✓	✓	✓	✓	Shrinkage cracks unacceptable

Table A.18. Summary of South African Inverted Pavement Design (dry region only) [DTSA 1996]

Road Category	Layer No.	E80s						
		3-10 x 10^4	*0.1-0.3 x 10^6*	*0.3-1 x 10^6*	*1-3 x 10^6*	*3-10 x 10^6*	*10-30 x 10^6*	*30-100 x10^6*
Major interurban freeways and major rural roads	1	-	-	-	1.5 in. – HMA[1]	1.5 in. - HMA[1]	2.0 in. - HMA[1]	2.0 in. - HMA[1]
	2				5.0 in. – ABC[3]	6.0 in. - ABC[3]	6.0 in. - ABC[2]	6.0 in. - ABC[2]
	3				6.0 in. – CTB[4]	10.0 in. - CTB[4]	10.0 in. - CTB[4]	12.0 in. - CTB[4]
	4				6.0 in. - AGS[5]			
	5				6.0 in. - AGS[6]			
Interurban collectors and rural roads	1	-	-	ST[7]	1.25 in. HMA[1] or ST[7]	1.5 in. – HMA[1]	-	-
	2			5.0 in. - CAB[8]	6.0 in. ABC[3] or 8.0 in. ABC[3]	6.0 in. - ABC[3]		
	3			6.0 in. – CTB[9]	6.0 in. CTB[9] or 8.0 in. CTB[9]	10.0 in. - CTB[9]		
	4			6.0 in. - AGS[5]				
	5			6.0 in. - AGS[6]				
Lightly trafficked rural roads, strategic roads	1	ST[7]				-	-	-
	2	4.0 in. - NG[10]	5.0 in. – NG[10]	5.0 in. - CAB[8]	5.0 in. - ABC[3]			
	3	5.0 in. - CTB[9]	5.0 in. - CTB[9]	5.0 in. - CTB[9]	6.0 in. - CTB[9]			
	4	6.0 in. - AGS[5]						
	5	6.0 in. - AGS[6]						
Rural access roads	1	ST[7]			-	-	-	-
	2	4.0 in. - NG[10]	4.0 in. - NG[10]	5.0 in. - NG[10]				
	3	4.0 in. - CTB[9]	5.0 in. - CTB[9]	6.0 in. - CTB[9]				
	4	6.0 in. - AGS[6]						

[1] Hot Mix Asphalt
[2] Well graded crushed aggregate base with Plasticity Index < 4
[3] Well graded crushed aggregate base with Plasticity Index < 6
[4] Cement Treated Base with Unconfined Compressive Strength at 7 days = 200 – 500 psi
[5] Aggregate soil with CBR > 15
[6] Aggregate soil with CBR > 7
[7] Surface Treatment
[8] Crushed aggregate base with CBR > 80
[9] Cement Treated Base with Unconfined Compressive Strength at 7 days = 100 – 200 psi
[10] Natural Gravel with CBR > 45

Table A.19. Summary of South African Inverted Pavement Design (wet region only) [DTSA 1996]

Road Category	Layer No.	E80s					
		3-10 x 10^4	***0.1-0.3 x 10^6***	***0.3-1 x 10^6***	***1-3 x 10^6***	***3-10 x 10^6***	***10-30 x 10^6***
Major interurban freeways and major rural roads	1	-	-	-	1.2 in. – HMA[1]	1.5 in. - HMA[1]	2.0 in. - HMA[1]
	2				6.0 in. – ABC[2]	6.0 in. - ABC[2]	6.0 in. - ABC[2]
	3				8.0 in. – CTB[4]	12.0 or 10.0 in.- CTB[4,11]	16.0 or 12.0 in. - CTB[4,11]
	4				6.0 in. - AGS[5]		
	5				6.0 in. - AGS[6]		
Interurban collectors and rural roads	1	-	-	ST[7]	1.25 in. HMA[1] or ST[7]	1.5 in. – HMA[1]	-
	2			6.0 in. - ABC[2]	5.0 in. ABC[2] or 6.0 in. ABC[2]	6.0 in. - ABC[2]	
	3			6.0 in. – CTB[9]	8.0 or 10.0 in. CTB[9]	12.0 or 10.0 in. - CTB[9,11]	
	4			6.0 in. - AGS[5]			
	5			6.0 in. - AGS[6]			
Lightly trafficked rural roads, strategic roads	1	ST[7]				-	-
	2	4.0 in. - NG[10]	5.0 in. – NG[10]	5.0 in. - ABC[2]	5.0 in. or 6.0 in. - ABC[2]		
	3	5.0 in. - CTB[9]	5.0 in. - CTB[9]	6.0 in. - CTB[9]	8.0 in. or 10 in. - CTB[9]		
	4	6.0 in. - AGS[5]					
	5	6.0 in. - AGS[6]					
Rural access roads	1	ST[7]			-	-	-
	2	4.0 in. - NG[10]	4.0 in. - NG[10]	6.0 in. - NG[10]			
	3	4.0 in. - CTB[9]	5.0 in. - CTB[9]	6.0 in. - CTB[9]			
	4	6.0 in. - AGS[6]					

[1] Hot Mix Asphalt
[2] Well graded crushed aggregate base with Plasticity Index < 4
[3] Well graded crushed aggregate base with Plasticity Index < 6
[4] Cement Treated Base with Unconfined Compressive Strength at 7 days = 200 – 500 psi
[5] Aggregate soil with CBR > 15
[6] Aggregate soil with CBR > 7
[7] Surface Treatment
[8] Crushed aggregate base with CBR > 80
[9] Cement Treated Base with Unconfined Compressive Strength at 7 days = 100 – 200 psi
[10] Natural Gravel with CBR > 45
[11] If water is prevented from entering the base, the subbase thickness may be reduced to the values indicated in brackets

With a design structure selected and validated, the design subgrade for categories A, B, and C assume that all subgrades are brought to equal (G7) support standards, unless otherwise stated. The G7 materials' minimum CBR is 15% at 93% Modified AASHTO and the plasticity index is less than 12. While category D are assumed to be supported by G9/G10 foundations. The G9 materials' minimum CBR is 7% at 93% Modified AASHTO and the plasticity index is less than 12. The G10 materials' minimum CBR os 3% at 93% Modified AASHTO. Table A.20 shows the techniques used to prepare subgrades and the select materials that may be required to do so. With a design chosen and the subgrade preparation selected, multiple designs can then be compared using a general cost analysis to see which is more economically feasible over the analysis period. This cost analysis compares the present worth of each design using Equation (11). In this equation, C is the present cost of initial construction, M_j is the cost of the j^{th} maintenance measure expressed in terms of current costs, r is the real discount rate (8% recommended, unless otherwise noted), x_j is the number of years from the present to the j^{th} maintenance measure, within the analysis period, z is the analysis period and S is the salvage value of the pavement at the end of the analysis period expressed in terms of present values (usually taken as 0, unless analysis period varies considerably between two designs). The present worth of costs, *PWOC*, is used to determine the relative cost difference between pavement structures. If the difference between two designs is 10% or less, then it is assumed to be insignificant.

Table A.20. Preparation of Subgrade for Different Subgrade Design CBRs [DTSA 1996]

	Subgrade CBR Class			
	SG4	**SG3**	**SG2**	**SG1**
Design CBR of Subgrade	< 3	3 - 10	7 - 15	> 15
Add selected layers:				
Upper	not applicable	150 mm G7	150 mm G7	---
Lower		150 mm G9	---	---
Treatment of in-situ subgrade	Special treatment required	RR-C[a] to 150 mm G10	RR- C[a] to 150 mm G9	RR- C[a] to 150 mm G7

[a] Remove and Re-compact

[b] If the in-situ subgrade is expected to be wet, an additional 150 mm layer of G9 could be used

$$PWOC = C + \left(M_1\left(1+r\right)\right)^{-x_1} + .. + \left(M_j\left(1+r\right)\right)^{-x_j} - S\left(1+r\right)^{-z} \quad (12)$$

4.4 Comparison of Methods

The Louisiana DOTD and North Carolina DOT pavement design procedures are similar. Both use the 1993 AASHTO Design Guide but differ slightly in the layer coefficients and other inputs that they use. The ICAR method used to design the granular aggregate base relies on variable dynamic confining pressure testing, which can be compared to AASHTO T 307. AASHTO T 307 is a standard method that covers procedures for preparing and testing untreated base materials for the determination of the resilient modulus. The value of the resilient modulus from this procedure is a measure of the elastic modulus of the untreated base recognizing certain nonlinear characteristics. The AASHTO T 307 test uses cyclic loading similar to the variable dynamic loading of the ICAR method. In this case, the specimen receives an axial stress applied for 0.1 second followed by a 0.9 second rest period. This loading and unloading is where the methods differ. For T 307 granular materials are tested at five levels of confinement (3, 5, 10, 15, 20 psi) with varying levels of axial stress for each confinement level. The bulk stress is then calculated for each test sequence and represents the total specimen stress state. The resilient modulus is then calculated at each of the 15

test sequences (Buchanan 2007). The number of test sequences also varies from the ICAR method. Multiple models have been used for the resilient modulus, but the universal model is used by the mechanistic-empirical design guide, which is shown in Equation (12). As mentioned before the ICAR method utilizes the Uzan model which is shown in Equation (13).

$$M_r = k_1 P_a \left(\frac{\theta}{P_a} \right)^{k_2} \left[\frac{\tau_{oct}}{P_a} + 1 \right]^{k_3} \tag{13}$$

$$M_R = K_A \left(\frac{\theta}{P_o} \right)^{K_B} \left(\frac{\sigma_d}{P_o} \right)^{K_C} \tag{14}$$

The overall methodology for South Africa also shares many similarities with the North Carolina DOT pavement design method. Both methods follow a step-by-step process involving project characterization, traffic evaluation, and a design heuristic that assigns different levels of certainty and conservatism based on the traffic level and functional classification. However, while both methods use loading equivalency for pavement design (ESALs in the case of the North Carolina DOT and E80's in South Africa), it is not clear that they are equivalent. That is, 1,000,000 ESALs may not represent the same amount of loading/pavement damage as 1,000,000 E80's. Understanding this equivalency, or lack thereof, is important in adapting the South African design methodology to North Carolina. For certain, the underlying mathematics of load equivalency are not the same between North Carolina and South Africa. The North Carolina DOT truck factors were established based largely on the AASHTO empirical model for relating performance to load level and axle configuration. South Africa, by comparison, bases its load equivalency factors on the ratio of applied forces and a power-law based assumption of damage growth, Equation (6)Comparing the truck factors for South Africa, Table A.8, to those used by North Carolina DOT, Table A.21, it is seen that the South African factors are considerably higher than the North Carolina DOT factors in all cases. This observation alone suggests that if using the Average or High values for calculation, that a South African E80 is not equivalent to a North Carolina ESAL. In fact it would suggest that for the same mixed traffic the South African E80 could be more than 7 times larger than an ESAL (i.e., a mixed traffic stream that results in a calculated ESALs of 1,000,000 could result in an E80 of 7,000,000 or more). If using the low E80 truck factors, then the two values are similar.

Table A.21. Summary of North Carolina DOT Truck Factors for Flexible Pavement Design [AASHTO 1993]

Description	Truck Factor	
	DUALS	TTST
Rural Freeway and Interstates	0.30	1.15
Rural Other	0.30	0.95
Urban Freeway and Interstates	0.30	0.85
Urban Other	0.25	0.80

The differences in truck factors may also be related to differences in load levels since the legal limits for truck weights in South Africa are larger than in North Carolina (123,600 lbs versus 80,000 lbs). As a result of these differences, direct comparisons of truck factors are somewhat misleading. Thus, comparisons between the underlying functions that govern the truck factor

selection have been performed. In this analysis, F was first calculated for pre-defined load levels (from 5 to 23 kips) using Equation (6) with n equal to 3. Then, the load equivalency factor (LEF) was calculated using the AASHTO function, Equation (14), by assuming a p_t equal to 2.5, a structural number of 3, and axle code configuration, L_{2x}, of 1.

$$LEF = \left(\frac{18+1}{L_x + L_{2x}} \right)^{-4.79} \frac{10^{G/\beta_{18}}}{10^{G/\beta_x}} \left(L_{2x} \right)^{-4.33} \tag{15}$$

$$G = \log\left(\frac{4.2 - p_t}{4.2 - 1.5} \right) \tag{16}$$

$$\beta = 0.4 + \frac{0.081\left(L_x + L_{2x} \right)^{3.23}}{\left(SN + 1 \right)^{5.19} L_{2x}^{\ 3.23}} \tag{17}$$

Figure A.18 and Figure A.19 show the comparison of the factors for low force and high force levels respectively. As shown, the factors are indistinguishable until the axle load is quite high. The North Carolina LEF is slightly lower with lower single axle loads and as the load increases you see this switch, making the factors for South Africa lower. Comparing these factors shows they are basically equivalent overall. The data in Figure A.18 and Figure A.19 suggest that the underlying equivalency principles between South Africa and the North Carolina DOT are the same and that the aforementioned differences in truck factors are the consequence of higher load levels in South Arica. Thus, it is reasonable to equate ESALs and E80s and directly translate the South African design catalog, Table A.17, to North Carolina traffic levels.

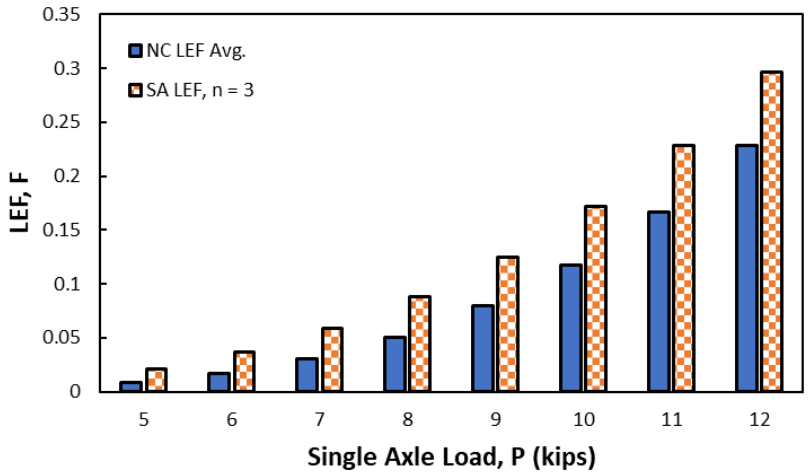

Figure A.18. LEF comparison between NCDOT values and South African values for low load levels.

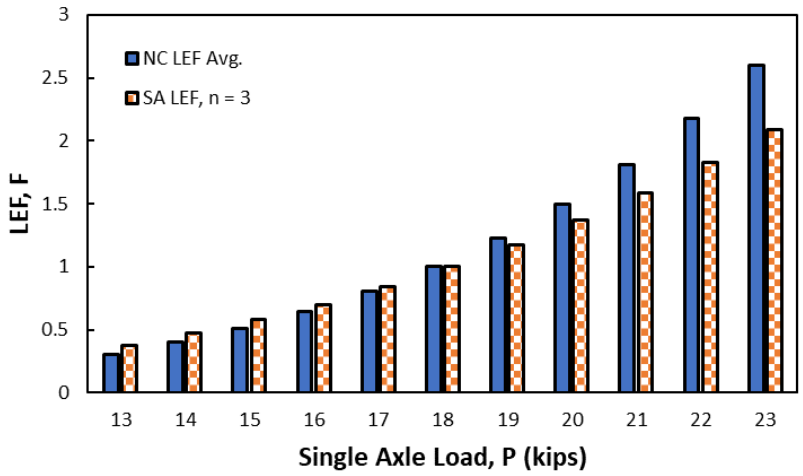

Figure A.19. LEF comparison between NCDOT values and South African values for high load levels.

5. Material Comparison

Inverted pavements use three basic materials: asphalt concrete, aggregate base, and cement treated base. In this section the material specifications for agencies that use inverted pavements are compared against the existing North Carolina DOT materials.

5.1 Asphalt Concrete

In North Carolina, asphalt concrete is specified according to the location in the pavement where it is to be used (surface, intermediate, or base layer). On most roadways, surface layers use asphalt mixtures with NMAS of 9.5 mm. Intermediate and base layer mixtures have NMAS of 19 and 25 mm respectively. The asphalt mixtures for North Carolina DOT are designed according to the Superpave method and, with the exception of S9.5D mixtures, have an asphalt binder pay grade of PG 64-22 (NCDOT 2018).

In South Africa, asphalt concrete is designed and produced from various combinations of aggregate types, aggregate sizes, and binder grades. Each mix has its own specific conditions of use determined from combinations of certain properties. The asphalt concrete mixes are specified according to aggregate grading. Overall there are five broadly classified mix types, gap-graded, semi-gap-graded, continuously graded, dense bitumen macadam (DBM), and open-graded. Most of the mixes in South Africa include a NMAS of 13.2 mm including gap-graded, continuously graded course mix, open-graded, and semi-gap-graded. The fine and medium mixes of the continuously graded designation have a NMAS of 9.5 mm along with the fine open-graded mix. The binder grade for these mixes was not given, but the typical asphalt binder content ranges from 5.5% for the continuously graded mix to 7% for the gap-graded mix (TRH 8 1987).

In Louisiana, asphalt concrete is specified according to the location in the pavement but not in as much detail as the North Carolina DOT specifies. The location is described as the mainline wearing course, mainline binder course, and base course. The mainline wearing and binder courses are given by mix levels 1 and 2. The base course also has a mix level of 1. For the case studies mentioned in the prior section of the literature review, the asphalt concrete is described as Type 3 and 8 wearing and base courses (Titi 2003, Rasoulian 2000, and Metcalf 2001). These designations were used when Marshall design was used instead of Superpave design. The Type 3 and Type 8

mixes are most closely related to the Level 1 and 2 mixes designated by Superpave design. The Type 3 and 8 wearing courses have NMAS of 19 mm while the binder course has a NMAS of 25 mm. Compared to the mix designations given today, these mixes signify that a Level 2 wearing course has a NMAS of 19 mm and that a Level 1 or 2 binder course has a NMAS of 25 mm. The Level 1 mainline wearing and binder courses have an asphalt binder pay grade of PG 70-22. The Level 2 mainline wearing and binder course have an asphalt binder pay grade of PG 76-22. While the base course has an asphalt pay grade of PG 67-22 (LADOTD 2016).

The most comparable South African mix to what is typically used in North Carolina is the continuously graded mix with a NMAS of 9.5 mm. The Louisiana DOTD mixes all have a NMAS higher than the South African and North Carolina DOT mixes. To compare the gradations, it is practical to pair the mixes with similar NMAS. Thus, the gradation of South Africa's continuously graded mix and North Carolina DOT's S9.5B, C, and D are shown in Figure A.20. S9.5C and D mixtures are seemingly interchangeable with South Africa's continuously graded mix. The S9.5B has a smaller range in its gradation due to the change of percent passing of 32-67% to 60-70% on the 2.36 mm sieve. Figure A.21 shows the comparison of gradations of NCDOT's 19.0 mm mix and the Type 3 and 8 wearing course mixes. These gradations are generally the same. Figure A.22 shows the comparison of gradations of NCDOT's 25.0 mm mix and the Type 3 and 8 binder course mixes. Again, these mixes have essentially the same gradation.

Based on the literature, it is also found that the typical asphalt binder contents for each mix are similar suggesting that the mixes have similar strength, stiffness, fatigue life, and performance against rutting and cracking. This is especially true for the South African and North Carolina DOT 9.5 mm mixes. The South African mixes: gap-graded, continuously graded and open-graded have a typical binder content of 7%, 5.5% coarse and 6% medium/fine, and 6% respectively. For the North Carolina DOT mixes: S9.5B, C, and D the typical asphalt binder content for each is given as 6.7%, 6%, and 5.7% respectively. The typical binder content of the Louisiana DOTD mixes is not given, but the binder grades are given as shown in the paragraph summarizing asphalt concrete in Louisiana.

Other properties of the aggregate used in each mixture are compared in Table A.22. The coarse aggregate angularity does not show up in the South African mix design, but the mixture design protocols suggest that crushed stone must be used. The fine aggregate angularity can be compared between the North Carolina DOT and Louisiana DOTD mixes, which shows they typically have the same fine aggregate angularity. For the South African mixes, the percent of fine angularity is not mentioned, but the mixture procedures do specify the types of sands that are allowed. The sand equivalent in all the mixes varies very little across the different departments of transportation. Although the South African mixes have less fines than the North Carolina DOT and Louisiana DOTD mixes. The shape of the aggregates is the same for the North Carolina DOT and Louisiana DOTD mixes. It is more difficult to make direct comparisons on aggregate shape with South African mixes because the South African method uses a dimensional ratio of 3:1 whereas the North Carolina DOT and Louisiana DOTD mixes are based on a ratio of 5:1. Finally, looking at the percentage of air voids for each mixture, the North Carolina DOT mixes, and the South African continuously graded mixtures have the same percentage of air voids, while the Louisiana DOTD mixes are just below the range at 2.5 – 4.5%.

Georgia, New Mexico, and Virginia do not have as developed of an inverted pavement program, but in their pilot projects these states used typical asphalt mixtures available in their respective states. For Georgia, they utilize 9.5 mm Superpave mixes just like in North Carolina and the typical

asphalt content consists of 5.50 – 7.25% (GDOT 2016). New Mexico's equivalent asphalt is SP-V which has a similar gradation to in North Carolina DOT's 9.5C and D mixes. This mix also has a minimum asphalt content of 5.5% (NMDOT 2019). Virginia's equivalent mix to S9.5B is SM-9.5D (VDOT 2016). The typical asphalt content is not given, but the performance grade of the binder is given as 64H-16, which is similar to the mixes of North Carolina.

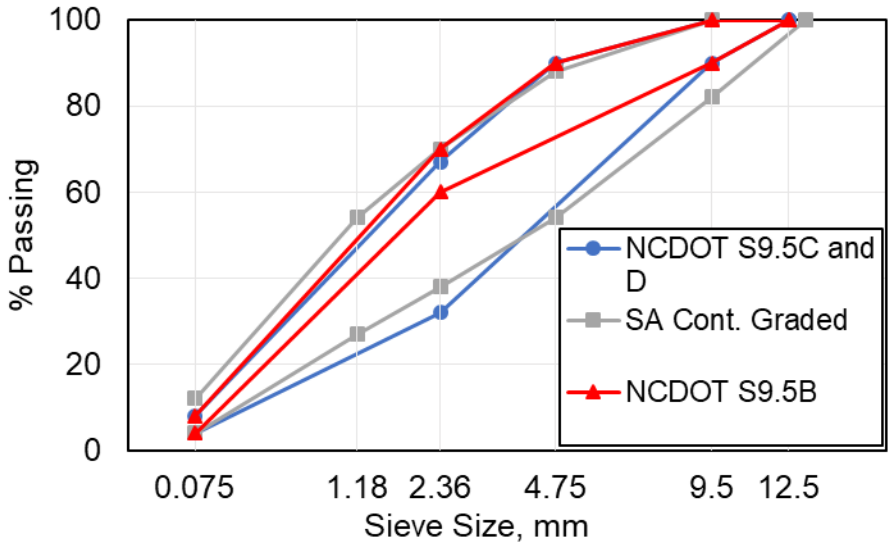

Figure A.20. Gradation of 9.5 mm nominal maximum aggregate size.

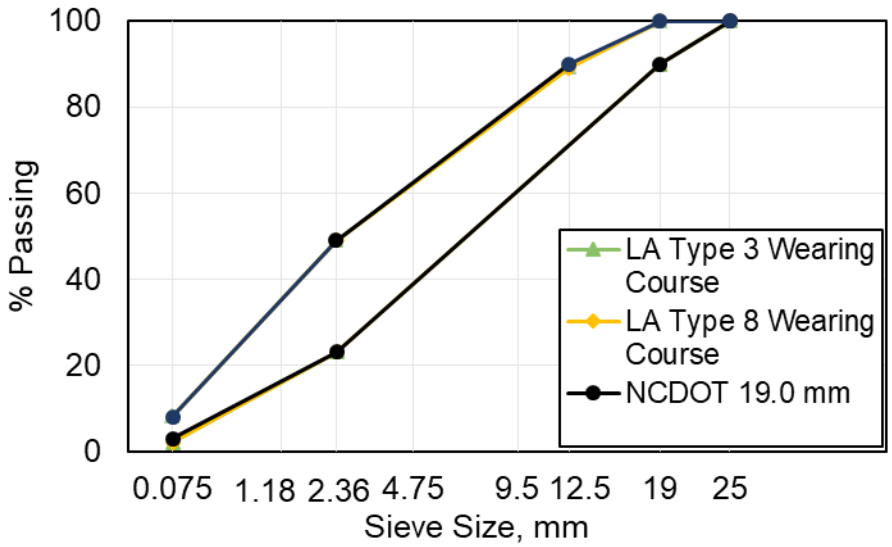

Figure A.21. Gradation of 19.0 mm nominal maximum aggregate size.

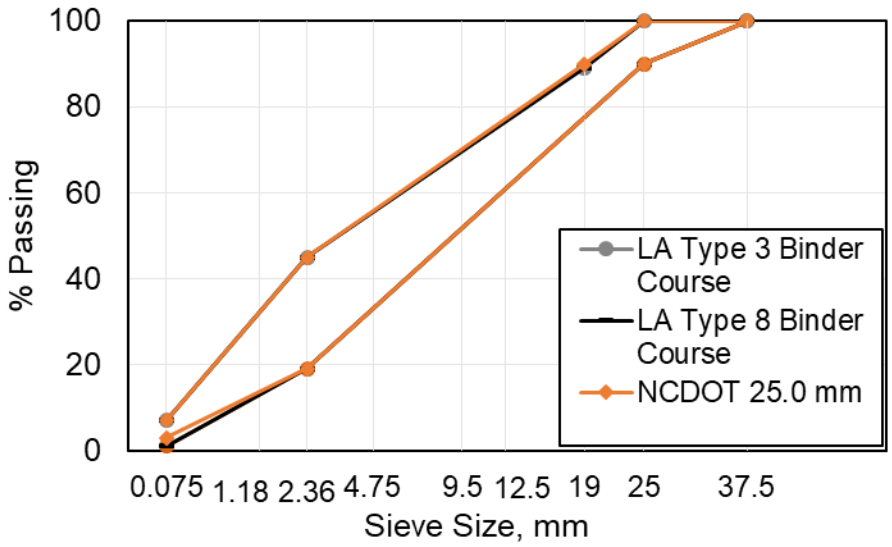

Figure A.22. Gradation of 25.0 mm nominal maximum aggregate size.

Table A.22. Asphalt Aggregate Properties

	NCDOT mixes			South African mixes				LaDOTD mixes		
	S9.5B	S9.5C	S9.5D	AG	AS	AC	AO	Level 2 WC[f]	Level 1 BC[f]	Level 2 BC
CAA[a]	75/-	95/90	100/100	crushed[d] stone				95	75	95
FAA[b]	40	45	45	sands[e]				45	40	45
SE % Min.	40	45	50	35	35	35	35	45	40	45
F&E[c]	-	10	10	30	30	30	30	10	10	10
AV (%)	3.0 - 5.0			2.0 - 12.0		3.0 - 5.0	-	2.5 - 4.5		

[a] Coarse Aggregate Angularity, for NCDOT mixes, 95 / 90 denotes that 95% of the coarse aggregate has one fractured face and 90% has 2 or more fractured faces.
[b] Fine Aggregate Angularity
[c] Table value represents maximum allowed flat and elongated at 5:1 ratio except for South Africa, which standardizes a 3:1 ratio
[d] The percentage of coarse aggregate angularity was not listed in the South African design guide but crushed stone with multiple fracture faces is preferred
[e] Crusher sand, clean natural sand, mine sand, selected river gravel or a blend of these
[f] WC = wearing course and BC = bearing course

5.2 Aggregate Base

In North Carolina, aggregate bases are used characterized by the size of aggregate present. Various aggregate bases can be used for different designs, but for inverted pavement, an aggregate base course is proposed. An aggregate base course has a NMAS of 37.5 mm. The aggregate base course consists of crushed stone, crushed gravel, uncrushed gravel or other similar materials. These materials have hard, strong, durable particles free of adherent coatings (NCDOT 2018).

In South Africa, the graded aggregate bases are described by a "G" for graded and then followed by a number representing the quality of the base, with being the best and 10 being the worst. Under higher traffic volumes, usually G1, G2, and G3 bases are used for the interlayer of the pavement. G1 is the most comparable to an aggregate base course and gives the best compaction while also providing the highest strength in the inverted pavement. A G1 base is obtained from solid,

unweathered rock with all the faces of the aggregate particle being fractured. The gradation of this material is only adjusted by adding fines that are produced by crushing the parent rock. G2 and G3 is obtained from crushing rock, boulders or coarse gravel. At least 50 percent of the particles by mass should have at least one fractured face and the material may include natural fines from other materials other than the parent rock. Other materials used for bases include G4, G5, G6 bases which can be obtained from natural gravel and boulders that could require crushing. But these bases are used mainly for low volume roads. The G4 material is sometimes included as a base material with G1, G2, G3 while G5 and G6 materials are mostly used for subbases. The G1, G2, and G3 bases have a NMAS of 37.5 mm (DTSA 1996).

In Louisiana, base courses are classified as either a Class 1 or Class 2 base. The primary difference between these two is that the Class 1 base courses are placed on a subgrade layer that is built in accordance with section 305 of the Louisiana Standard Specifications for Roads and Bridges. An aggregate base course is in included in the specification of base courses. The aggregate base course is usually made up of limestone, but can be any stone from the State's approved materials list. The stone for the base coarse aggregates also includes a 37.5 mm NMAS (LADOTD 2016).

Looking at Figure A.23, the gradations of coarse aggregate from North Carolina DOT, G1, G2, G3 from South Africa, limestone from Louisiana DOTD, and group two aggregate from GDOT are shown. The Georgia DOT aggregate is included because this aggregate was tested against the G1 base in the Morgan County Project (Lewis 2012). The gradation of ABC with a nominal maximum aggregate size of 37.5 mm and the gradation of G1, G2, and G3 with a nominal maximum aggregate size of 37.5 mm are almost identical. The Louisiana DOTD limestone has a similar gradation with a nominal maximum aggregate size of 37.5 mm, but the gradation shows a wider range in the upper bound. The Georgia DOT Group II aggregate gradation is similar as well but has a wider range at the 0.25 mm sieve. This sieve was not listed for the other three materials, but if it was taken out of the Group II aggregate, the gradations would be almost identical.

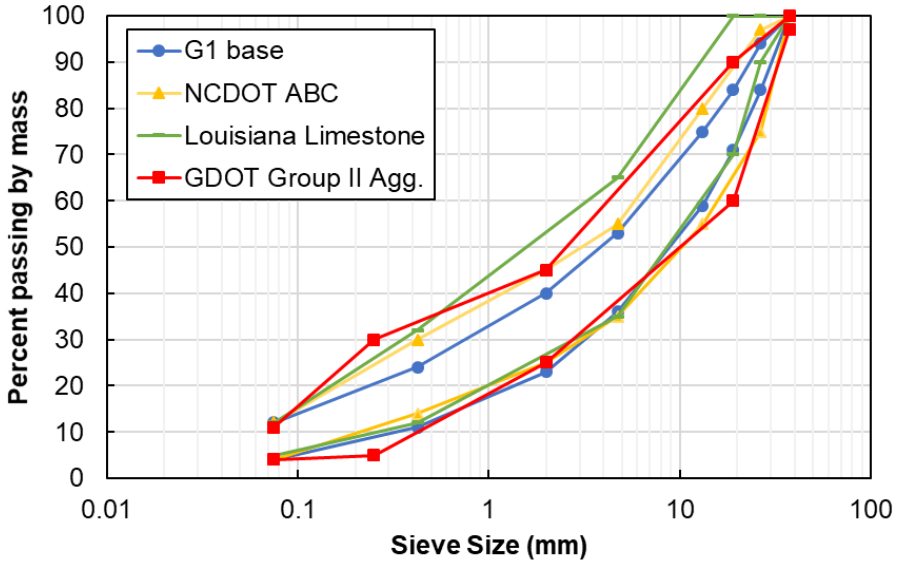

Figure A.23. Gradation of coarse aggregate material.

Next looking at Table A.23, the fines of each material, the shape and the required density are compared. The figure also includes these properties of a Georgia DOT Group II aggregate. The

limestone base course that is used in Louisiana as the interlayer course is also included. The Georgia DOT Group II aggregate performed just as well as the G1 base. The liquid limit and plasticity index of the North Carolina DOT ABC, the G1 base, and the Louisiana DOTD limestone are almost identical. The flakiness index represents the length to width ratio of the aggregate particles. The elongated particles are determined a bit differently compared to the South African Method. But the percent elongated particles are identical to that the GDOT Group II aggregate and the Louisiana DOTD limestone has a slightly higher percentage. Because the Group II aggregate performed similarly to the G1 base, the percent elongated particles from the North Carolina DOT look to be sufficient.

Going back to the Morgan County Project, the biggest concern about the aggregate was the compaction under conventional methods compared to South African methods. As shown earlier in the literature review, each method compacted the material to 86 – 88% of apparent solid density which is the required compaction of a G1 base. Looking at the table, North Carolina DOT is 100% density of that obtained by compacting a sample. The 86 – 88% apparent solid density is equivalent to 101 – 106% max dry density of Georgia DOT or 98% modified proctor. Louisiana DOTD base requires a slightly lower percentage of compaction compared to the other three aggregates. Comparing these four densities shows that the ABC of the North Carolina DOT will most likely achieve the required compaction, but as with the Georgia DOT aggregate it will probably be due to the extremely compact and stable cement treated base underneath the aggregate (Lewis 2012, Papadopoulous 2014). Looking at the comparison of the materials, North Carolina DOT ABC should be qualified to be used in place of the South African G1 base.

As before Georgia, New Mexico, and Virginia do not have as developed of an inverted pavement program, but in their pilot projects these states used typical aggregate bases available in their respective states. But for the aggregate base, Georgia's Group II aggregate is included along with North Carolina, South Africa and Louisiana's because it was tested against the G1 base of South Africa as mentioned above. For New Mexico, a Type I aggregate is the comparable equivalent to the G1 South African base and North Carolina DOT's ABC based on gradation (NMDOT 2019). This base has maximum liquid limit of 25% and a maximum plasticity index of 6%. Virginia's comparable equivalent base is called 21B (VDOT 2016). The gradation is similar to the G1 base and ABC. The maximum liquid limit is 25%, the maximum plasticity index is 6% and the elongated particles ratio 5:1 has a maximum of 30%.

Table A.23. Comparison of Aggregate Bases

	South African G1 Base	NCDOT ABC	GDOT Group II Aggregate	LaDOTD Aggregate
Fines	LL < 25%, PI < 4	LL < 30%, PI < 4[a]	SE[b] < 20	LL < 25%, PI < 5
Shape	flakiness < 35%	5:1 ratio: < 10%	EP[c] < 10%	5:1 ratio: < 15%
Density	86 - 88% of apparent solid density	100% modified proctor	98% modified proctor	95% modified proctor

[a] material passing 40%
[b] Sand Equivalent
[c] Elongated Particles

Finally, a major issue to consider when evaluating ABC materials for inverted pavement is the overall toughness of the aggregate. In inverted pavements the ABC materials are subjected to substantially greater stresses than a traditional design. As such, the likelihood of aggregate wear and breakdown is greater. Thus, strong, wear resistant, and sulfate resistant aggregates should be used (R. Ashtiani, personal communication, December 11, 2019). Currently the North Carolina DOT does not perform strength or wear testing as part of the standard specification for the aggregate base course. In the section for asphalt surface treatments a maximum LA abrasion loss of 45% is given for lightweight aggregates. Looking at the other states, Louisiana lists a maximum of 40% for course natural aggregates and recycled portland cement concrete material, Georgia lists a maximum of 50% for Group II Class A aggregates, and Virginia lists a maximum of 50% for Grade B stone. For New Mexico, a maximum of 35% is listed for the aggregate index which is found by using the test values from the LA abrasion test, soundness loss test and absorption test.

5.3 Cement Treated Base

In North Carolina, cement treated bases are composed of aggregate, Type 1 portland cement, and then water. There are no classifications for different levels of cement treated bases. The only differences allowed are how the aggregate, cement and water can be mixed. There can be multiple types of plant mixes, and the base can also be mixed in place. These details are discussed more in the construction portion of the literature review. The aggregate for the cement treated base is the same aggregate base course described in the previous section (NCDOT 2018).

In South Africa, the cement treated bases are specified by the aggregate bases used in creating the mixture. The three specifications include C1, C2, C3, and C4 (DTSA 1996). C1 and C2 cement treated bases meet specifications of at least G2 for C1 or G2 to G4 for C2 before treatment. Thus, the gradation of the two cement treated bases have the same gradation that is shown for the G1 base in Figure A.23. The NMAS for each is also 37.5 mm like the G1, G2, and G3 bases. C3 and C4 represent cemented natural gravel instead of cemented crushed stone or gravel. The mixes C3 and C4 meet G5 and G6 material requirements. Unfortunately, the gradation for these two aggregate bases were not found, but the NMAS for these two are both 63 mm (DTSA 1996).

In Louisiana, there are multiple bases or subbases that utilize cement. In base courses, the DOTD specifies a soil cement that is either stabilized or treated. As discussed before in the design portion of the paper, the layer coefficients of these two materials are slightly different being 0.14 and 0.10 respectively. But for the subbase layer which is where soil cement is used in inverted pavement, they specify just soil cement with a layer coefficient of 0.14. Thus, the subbase seems to use the cement stabilized soil cement base instead of the treated soil cement (LADOTD 2016).

Comparing the cement treated bases from North Carolina DOT, Louisiana DOTD, and the South African design guide starts with the comparison of the aggregate used in the mixes. As shown before, the aggregates from North Carolina DOT and the South African design guide are very similar. The limestone, which is most commonly used in Louisiana, is very similar to the 37.5 mm aggregate from North Carolina DOT. Each CTB uses a specified portland cement which differs very little. The main difference between each cement treated base or soil cement is the unconfined compression strength. For North Carolina DOT, an unconfined compression strength of 500 psi at a seven-day cure is required. This test is done with the material compacted to at least 97% modified AASHTO density. Looking at Table A.24, the unconfined compressive strengths are given for the South African C1 to C4 materials. With the material cured 7 days at 100% modified AASHTO density, the unconfined compressive strength for the C1 material is substantially greater than the

requirement for the North Carolina DOT. However, the C2 material is borderline if using 100% modified density as the comparison case and about the same as the requirement from North Carolina DOT if using the 97% modified density. For the Louisiana soil cement base, which was established as stabilized and not treated, the unconfined compressive strength is determined to be 300 psi. This soil cement base is compacted to a minimum of 95% maximum dry density. Thus, the soil cement base from Louisiana is compacted to a less dense state which results to a lower unconfined compression strength compared to the mixtures from North Carolina and South Africa. In the Pineville, North Carolina test road, it was proven that the cement treated base could easily obtain the unconfined compressive strength required by North Carolina DOT, South Africa and Louisiana. Even though the percent cement used is not mentioned in the South African design standards, the unconfined compressive strength is correlated with the percent cement in the data from the Pineville Quarry project, given in Table A.25. From this data, it is shown that the South African requirements can easily be matched using North Carolina DOT materials and methods for cement treated bases.

As mentioned before Georgia, New Mexico, and Virginia do not have as developed of an inverted pavement program, but in their pilot projects these states used typical cement treated bases available in their respective states. For Georgia, this meant that CTB is compacted to 98% of maximum dry density (GDOT 2016). They do not have much other information regarding the strength of the CTB layer. But in the Morgan County case study, the unconfined compression strength ranged from 145 psi to 435 psi. For the Lagrange case study, the unconfined compression strength had a minimum of 300 psi. For New Mexico, the case studies did not list the unconfined compression strength of the CTB layers, but the percentage of cement ranged from 3% – 4%. The standard specifications from New Mexico also did not have much information on the CTB, just the portland cement that may be used in the treatment of the layer (NMDOT 2019). For Virginia, cement treated bases is mentioned scarcely in the specifications, but they do mention a hydraulic cement concrete and that 4% cement was used for the construction of the CTB layer in the Bull Run case study in Virginia.

Table A.24. Design Strength for Cemented Materials [TRH 14, 1985]

Property	Cemented Material							
	C1		C2		C3		C4	
	min	max	min	max	min	max	min	max
unconfined compressive strength at 7 days (psi) 100% Mod. AASHTO density	870	1740	435	870	220	435	110	217
unconfined compressive strength at 7 days (psi) 97% Mod. AASHTO density	580	1160	290	580	145	290	73	145

Table A.25. Pineville Quarry CTB Data [K. Vaughn 2015]

Sample ID	Dry Unit Weight (pcf)	Average Moisture (%)	Compressive Load (lbs)	7-Day Compressive Strength (psi)
2% Cement	154.7	5.3	15790	560
	153.6	5.3	15890	560
Average	154.2	5.3	15840	560
3.5% Cement	155.2	5.3	36380	1290
	154.5	5.3	39400	1390
Average	154.9	5.3	37890	1340
4.5% Cement	154.6	5.3	46050	1630
	156.6	5.3	53810	1900
Average	155.6	5.3	49930	1765

6. Construction

Inverted pavement construction mostly requires standard methods of construction for the various layers. In most cases each state has used their own methods of construction whether it be from standards for conventional asphalt pavement or new standards. In Georgia's case, they created a Special Provision #320, just for the construction of inverted pavements. This provision was used in the case studies mentioned previously. For the asphalt, cement treated base, and subgrade normally standard methods of construction from each state's standards will suffice. The unbound aggregate base course layer is where there is uncertainty whether conventional compaction techniques will work, or South African methods need to be introduced.

Starting with the subgrade, standard subgrade requirements can generally be used to ensure that the pavement structure has a sound and stable base. Multiple techniques have been used throughout the country and in South Africa. The variation of the subgrade construction techniques is mainly due to the various soil types found at each location. In North Carolina typical standards have been used which include using lime, cement or aggregate whenever needed to stabilize subgrade. If none is needed, the subgrade is compacted to 100% of that obtained by compacting a sample of the material in accordance with AASHTO T 99. If lime stabilization is needed, then mix in lime to a depth of at least 8 inches and compact to at least 97% of that obtained by compacting a sample of the soil lime mixture in accordance with AASHTO T 99. If an aggregate subgrade is used, then class IV subgrade stabilization (ABC) is used. This soil is then compacted to 92% of modified proctor (NCDOT 2018).

For Louisiana the subgrade can be treated or untreated. The roadbed in general should be compacted to at least 95% of the maximum dry density if a subbase is used or 98% if a base is used. If the subgrade is treated, portland cement or lime can be utilized. For a plasticity index (PI) of 0 – 15, 6% cement is recommended. If a PI of 16 -25 is present, 6% lime and 6% cement are recommended. Then if the soil has a PI of 26 – 35, 9% lime and 6% cement are recommended (LADOTD 2016). In South Africa, the subgrade has been compacted to a range of 90 – 93% modified Proctor in many cases. For Georgia, the subgrade whether it is stabilized or mechanically treated should have a SSV of 5 or CBR of 15. The subgrade when stabilized whether lime or cement is used should be mixed to a depth of at least 6 inches. For New Mexico, in one of the case studies the subgrade went untreated, but in many cases in New Mexico, the subgrade is treated with lime. But in all cases for New Mexico the subgrade is compacted to 95% Modified Proctor

(NMDOT 2019). For Virginia, the subgrade as the others can be treated or untreated. The subgrade regardless is scarified to a depth of 6 inches. The compaction of the subgrade is based on the percentage retained on the No. 4 sieve of the material. For 0 – 50% the minimum density is 100%, for 51 – 60% the minimum distance is 95%, and for 61 – 70% the minimum density is 90%. For lime stabilized mixtures the subgrade is compacted to 95% and for cement stabilized 100% (VDOT 2016).

For the cement treated base, traditional requirements from each state are typically used. The construction of the cement treated base can be mixed in a variety of ways: batch type plant, continuous flow type plant or road mixed. The road mixed method is done by placing the aggregate on the prepared subgrade and then applying the required amount of cement. Then the aggregate and cement are blended in a uniform manner. After mixing, compaction may begin immediately after mixing. Self-propelled rollers are used to compact the material to at least 97% the maximum density of Modified Proctor. The compacted mixture should then be kept moist until a curing seal can be placed over the cement treated base. The base should be cured for 7 days. The South African design follows basically the same standard procedure of mixing, placing and curing. A lot of detail on the process of the actual construction of this layer is not provided but the required density and curing strength was discussed in the materials section under cement treated base. In Louisiana, as determined before the cement treated base used there is a soil cement. The mixing of this layer consists of mixing in place with a spreader or stabilizer and add water as needed. Then the mixture is compacted using a sheepsfoot-type roller or a self-propelled tamping foot compactor-type roller. The final compaction should be done with a pneumatic tire roller. Then as the other cases, keep the compacted mixture moist until it is cured and sealed with an asphalt curing membrane.

In Georgia, either mixing in place or plant style mixing is also used. They also use a mixture spreader to apply the cement mixture to the prepared subgrade. Then the cement treated base should be compacted using sheepsfoot roller or steel wheel roller as before (LADOTD 2016). Georgia's special provision for construction of inverted pavements provides that the maximum thickness to a compacted layer of CTB shall be 8 inches and if the specified thickness on the plans exceeds this thickness, then it is necessary to construct two or more courses of equal thickness to achieve the correct depth. Just as in other states, a pneumatic-tired roller should be used to finish the compaction effort. The CTB should be compacted to at least 98% the maximum dry density established on the Job Mix Design. Then the CTB is to be cured (GDOT 2007). New Mexico does not include cement treated bases in their standard specifications per say, but they include cement treated subgrades and portland cement concrete (NMDOT 2019). Their construction methods seem to be similar to other DOTs except that they have an asphalt paver to spread the cement mixture evenly. This has been reported to eliminate segregation and control the depth well. In Virginia, typical construction methods were used as well. From the case study of Bull Run, there was high variability in the unconfined compressive strength which they believe resulted from unknown construction mishaps or methods. The mixture also differed in that the there was a 14-day moisture cure instead of a 7-day cure.

Overall the aggregate base layer is the most important layer within the inverted pavement structure because it takes on most of the structural capacity with the decrease in asphalt layer thickness. But without the aforementioned CTB, the aggregate base layer could not respond the way it does to loading. For North Carolina, it is specified to spread the aggregate with a mechanical box spreader. Once this is done the compacting is done with a pneumatic roller or vibratory roller. Optimum water content is be maintained so that maximum density can be achieved for the aggregate layer.

From the U.S. case studies, every state's construction of the aggregate layer involves the same principles. The only difference may be in the specified thickness of the lifts. South Africa does use a slightly different method when it comes to their aggregate bases, which is called slushing. This process was described in the Georgia case studies but as a basic overview, the base is placed as it would normally be placed and then compacted with a vibratory roller. Next the base is flooded with water and compacted again using static rollers. The base is compacted at a high speed to which brings the fines to the top. These fines are then brushed away. This technique forms a tight interlocked matrix of the coarse aggregate (Papadopoulous, 2014). This technique supposedly increases the density of the aggregate base more than the conventional technique of compacting the aggregate base.

For the asphalt construction, in each case a mix is prepared pertaining the specific mix design. Once this is complete, the asphalt is transported from the plant to the site via asphalt mixing truck then placed with an asphalt paver along with a tack coat. The methods of construction for asphalt pavement vary little amongst the states that have dabbled in inverted pavements and South Africa.

7. Surface Wave Testing of Asphalt Pavements

Surface wave testing is an extensively used method for near surface geophysical imaging and geotechnical site characterization (Foti et al. 2011). The surface is excited with an impact source such as hammer, and the response is measured using sensors often at multiple locations. Geophones are used in soil site characterization and accelerometers are used in pavement application as the frequency range of interest is generally much higher than the operating ranges of geophones. The measured responses are processed to calculate the dispersion properties of the system which is a relationship between the phase velocity and the frequency. Dispersion characteristics of a system are sensitive to the layer thickness and layer moduli and can be used to back calculate the system properties.

Predominantly, the stiffness of soil layers increases with depth and in such systems, the fundamental mode dominates the surface wave response. Recently, (Vaziri and Guddati 2016) have developed an improved forward model and inversion algorithm for soil systems with soft layers sandwiched between stiff layers which leads to influence of higher modes of wave propagation. While this phenomenon is not common in soil characterization, it is almost universal in pavement systems and makes the surface wave characterization more complex than soil systems.

Heisey et al. (1982) first introduced the Spectral Analysis of Surface Waves (SASW) to nondestructively estimate the moduli of pavement layers. Since then, SASW has been widely used and investigated by several researchers (for example, Roesset et al. 1990; Al-Adhami 2019; Aouad 1993). Figure A.25 shows the experimental setup of a typical SASW test and Figure A.24 shows a schematic of the various steps involed in the procedure. The phase difference measured between the two receivers as a function of frequency can be used to estimate the phase velocity. A coherence function between the two sensors signals is used to identify the usable frequency range for dispersion curve computation. The inversion process for the SASW method is a challenging due to the phase unwrapping required. Several authors have reported on the limitations of the two-receiver method such as inability to resolve higher modes, contamination from reflected waves (Sheu et al. 1998) among several others. The major drawback of the SASW method is that only one phase difference can be evaluated at each frequency and thus the different modes of wave propagation cannot be separated.

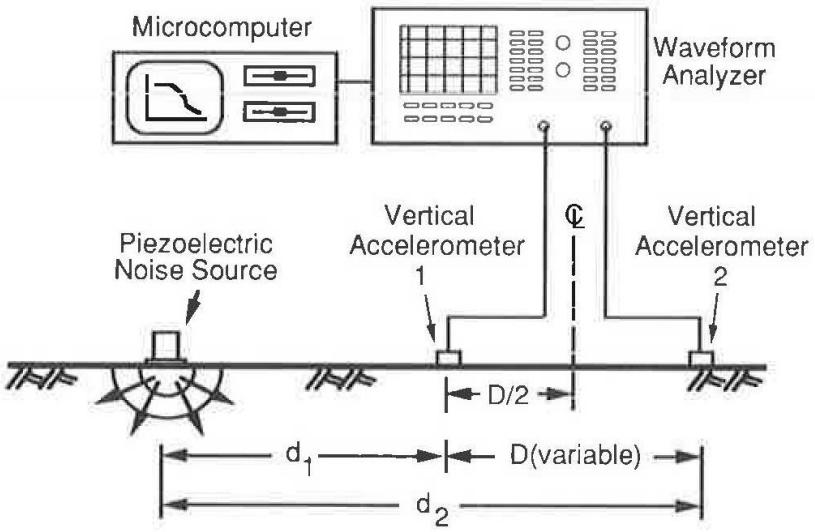

Figure A.25. SASW test setup (Roesset et al. 1990)

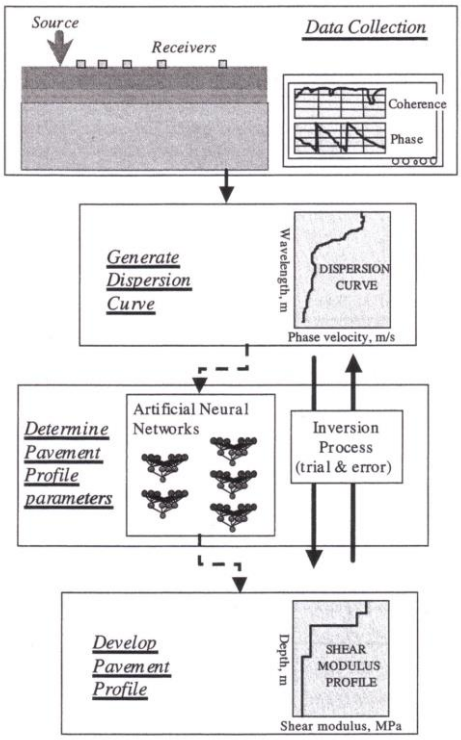

Figure A.26. SASW procedure (Wu et al. 2002)

In order to overcome the limitations of SASW, Multichannel Analysis of Surface Waves (MASW) was introduced in the early 1980's for soil site characterization. MASW is an extension of the SASW technique more than two receivers are used to record a two-dimensional wave field. This 2-D wave field is transformed using Fourier transform in both time and space also known as *f-k* transformation (Vaziri and Guddati 2016) to obtain effective dispersion curve in which the different modes can be separated. The layer model is used to match the effective dispersion curve

to estimate the layer thickens and mechanical properties. The overall process of surface wave testing through MASW technique is shown in Figure A.27 and is similar in principle for both soil and pavement layers. MASW has been successfully applied to applications such as geotechnical sites to map the soil layers, locate buried objects, geophysical explorations.

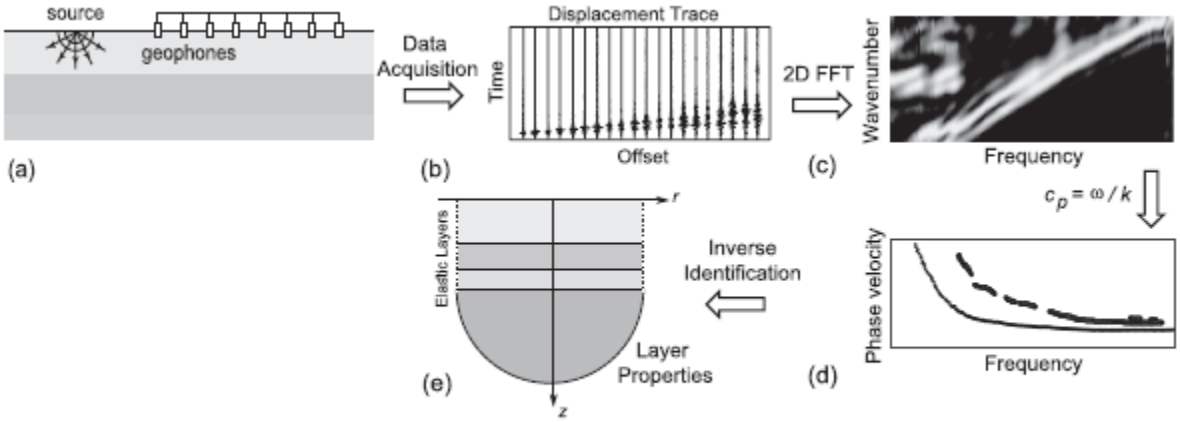

Figure 1. Schematic of multistation surface wave inversion: (a) experimental setup where the surface waves are generated and recorded at the surface; (b) surface trace representing the measured response histories; (c) transformed signal in frequency–wavenumber (f–k) domain; (d) dispersion curves obtained by processing the f–k signal; and (e) layer properties estimated through inversion.

Figure A.27. Overall process of MASW (Vaziri and Guddati 2016).

A traditional MASW method requires costly and bulky data acquisition systems with multiple sensors attached to the surface. Sufficient care is required to ensure proper coupling between the sensors and the surface for reliable measurements. Traditionally, geophones are used for soil exploration, but they are limited in their frequency bandwidth. Therefore, accelerometers are preferred as they provide a much wider bandwidth and measurement range very suitable for pavement testing. The cost of geophones is a fraction of the accelerometer cost and thus the entire MASW test system cost can be very high. To overcome the above limitations, Multichannel Simulation with One Receiver (MSOR) was developed (Rydén et al. 2001). MSOR uses a single receiver (accelerometer) and the source (hammer impact) is moved along a line to simulate the effect of MASW thus reducing the need for bulky and costly equipment as shown in Figure A.28. While this technique is simple, the response can be sensitive to local changes and the reliable frequency range is smaller compared to the MASW method (Lin and Ashlock 2015). An accurate trigger is critical for the MSOR method to synchronize the impact and data acquisition as the source is moving along the pavement. The frequency content of the waves generated are dependent on the hammer characteristics and Table A.26 summarizes some of the source, offset and receiver spacing used in the past (Davis 2016).

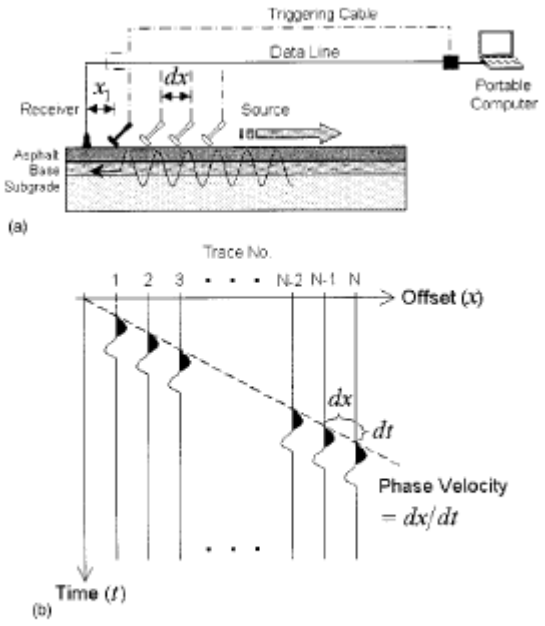

Fig. 3. (a) Schematics illustrating multichannel simulation with one receiver survey with fixed receiver and moving source. In (b), true (or simulated) multichannel record is schematically illustrated.

Figure A.28. MSOR schematic (Ryden et al. 2004).

Table A.26. Summary of Source, Offset and Receiver Spacing used for Pavement MASW (Davis 2016)

Citation	Source Type	Number of Receivers (Real or Simulated)	Receiver to Pavement Coupling	Receiver Spacing	Source Offset	MASW or MSOR
(Ryden et al. 2004)	225 g Hammer with Steel Spike	80	Sticky Grease	2.5 cm	2.5 cm-200 cm	MSOR
(Lin and Ashlock 2015)	225 g Hammer	9	Plumber's Putty	4 cm	Not specified	MASW
(Ryden et al. 2002)	500 g Hammer	24	Sticky Grease	2.5 cm	10 cm - 70 cm	MSOR

(Ryden et al. 2004) worked extensively on the application of MSOR to pavements. Ryden and Lowe (2004) further studied a three-layer pavement system through theoretical modelling to understand the various modes that are dominant in different frequency regions. It is concluded that due to the stiffness profile of pavement, leaky guided waves dominate the majority of the frequency spectrum instead of Rayleigh surface waves. Predominantly, a quasi-antisymmetric Lamb wave mode is generated in the top pavement layer, and this dominates at the higher frequencies. Mode separation was possible in the lower frequency ranges where there is greater influence from the base and subgrade layers. Ryden and Park (2006) used the Fast Simulated Annealing (FSA) inversion scheme to obtain the layer properties from the field measured dispersion curve. FSA is a global inversion algorithm and is less likely to return local minima. The inversion of the thickness

and stiffness of the top layers are the most efficient and accurately measured but there are still several challenges with identifying the deeper embedded layer properties.

8. Knowledge Gaps

Overall inverted pavements seem to perform well under many conditions, making them a technology that requires some additional study for North Carolina. The various layers that make up the pavement structure can be constructed using North Carolina DOT specifications in many cases. The surface mixes of the North Carolina DOT compare well against the mixes used by South Africa in their inverted pavement. For the aggregate base layer, stress dependency needs to be considered as well as the makeup of the aggregate. Tougher aggregates can withstand more stress and will not fail under greater loads. North Carolina DOT's ABC stone compared well to the G1 base of South Africa. The South African technique of slushing has been compared to conventional methods in multiple case studies and both achieved the required density (Lewis et al. 2012). In the Pineville Quarry case study, the density of the aggregate was easily achieved without using the slushing technique. Next the modulus and strength of the cement treated layer should be taken into consideration as well. But the strength of the CTB layer is important to be able to support and stabilize the aggregate base layer above. The design process used in South African mainly follows the principles laid out by the 1993 AASHTO design guide. The calculated design traffic is very similar but as shown in the comparison of the designs, the trucks of South Africa seem to be loaded more heavily than those in North Carolina. Thus, the loading difference needs to be corrected when designing a pavement if the South African methodology is used.

So, while the literature shows the efficacy of the technology, it also demonstrates some caution should be exercised before fully adopting the technique. In North Carolina, a single case study has been performed, but not within the control of the North Carolina DOT. The literature review supports the overall research plan as described in the proposal and shows that knowledge gaps remain with respect to the long-term performance of inverted pavements in the United States. The use of full-scale studies to fill in knowledge gaps on the use and performance of inverted pavements represents the state of practice and has been used successfully by other states. In conducting the full scale study the research team will need to consider the following aspects; stress dependency of aggregate base and its toughness to withstand the higher stresses that will exist in inverted pavements, the modulus and strength of CTB as this affects the level of confinement that is achieved when compacting the aggregate base, the traffic that will use the roadway, adapting existing material specifications for proper material selection, and careful control during construction to produce a high quality pavement and informative outcomes.

The literature review for the application of surface wave testing on pavements indicated a good potential of the methodology to estimate the individual layer properties but has been primarily applied on conventional pavement design in controlled settings. Surface wave testing has not been applied to inverted pavements, which will potentially exhibit different wave propagation phenomenon compared to conventional pavement design due to the presence of cement treated base in between the aggregate base and subgrade layers and a thinner asphalt layer. The research team will study the wave propagation characteristics on inverted pavements while also testing and identifying the different parameters that influence the data collection, analysis and the back calculation procedures.

9. Appendix A References

Ahlvin, R.G., Turnbull, W.J., Sale, J.P., and Maxwell, A.A. (1971). *Multiple-Wheel Heavy Gear Load Pavement Tests. Volume I. Basic Report*. U.S. Army Engineer Waterways Experiment Station, Vicksburg, Mississippi.

American Association of State Highway and Transportation Officials (AASHTO) (1993). *AASHTO Guide for Design of Pavement Structures, 1993*, Washington, D.C.

Al-Adhami, H.H. (2019). *Air-Coupled Surface Wave Testing of Pavements*. Ph.D. Thesis, Rutgers University, New Brunswick NJ.

Aouad, M.F. (1993). *Evaluation of Flexible Pavements and Subgrades Using the Spectral Analysis of Surface Waves Method*, Ph.D. Thesis, The University of Texas at Austin.

Ashtiai, R., Personal communication over phone, December 11, 2019.

Avellaneda, D.D.C. (2010). *Inverted Base Pavement Structure*. Ph.D. Thesis, Georgia Institute of Technology, Atlanta GA.

Buchanan, S. (2007). *Resilient Modulus: What, Why, and How?*, Online. <https://www.vulcan innovations.com/public/pdf/2-Resilient-Modulus-Buchanan.pdf> Accessed December 19, 2019.

Chen, X., Zhang, Z., and Lambert, J.R. (2014). Field Performance Evaluation of Stone Interlayer Pavement in Louisiana. *International Journal of Pavement Engineering*, 15(8), 708-717.

Davis, B. (2016). *Development of the MASW Method for Pavement Evaluation*. Ph.D. Thesis, University of Arkansas, Fayetteville AR.

Department of Transport (DTSA) (1985). *Technical Recommendations for Highways (TRH) 14*, Guidelines for Road Construction Materials. Committee of Land Transport Officials (COLTO), Pretoria, South Arica.

Department of Transport (DTSA) (1987). *Technical Recommendations for Highways (TRH) 8, Design and Use of Hot-Mix Asphalt in Pavements*. Committee of Land Transport Officials (COLTO), Pretoria, South Arica.

Department of Transport (DTSA) (1996). *Technical Recommendations for Highways (TRH) 4*. Committee of Land Transport Officials (COLTO), Pretoria, South Arica.

Foti, S., Parolai, S., Albarello, D., and Picozzi, M. (2011). Application of Surface-Wave Methods for Seismic Site Characterization. *Surveys in geophysics*, 32(6), 777-825.

Freeme, C.R., Otte, E., and Mitchell, M.F. (1980). *Economics of Pavement Type Selection for Major Roads*. Pavement type selection committee for the National Transport Commission, Pretoria.

Georgia Department of Transportation (GDOT) (2007) *SP320 – Inverted Pavements.* Atlanta, GA.

Georgia Department of Transportation (GDOT) (2016). *State of Georgia's Supplemental Specifications Modifying the 2013 Standard Specifications Construction of Transportation Systems.* Atlanta, GA.

Heisey, J.S., Stokoe, K.H., and Meyer, A.H. (1982). Moduli of Pavement Systems from Spectral Analysis of Surface Waves. *Transportation research record: Journal of the*

Transportation Research Board, 852, 22-31.

Huang, Yang H. (2003). *Pavement Analysis and Design*, 2nd Edition, Pearson.

Johnson, C.W. (1961). Comparative Studies of Combinations of Treated and Untreated Bases and Subbases for Flexible Pavements. *Highway Research Board Bulletin*, 289, 44-61.

Kim, S., Little, D.N., Masad, E., and Lytton, R.L. (2005). Estimation of Level of Anisotropy in Unbound Granular Layers Considering Aggregate Physical Properties. *International Journal of Pavement Engineering*, 6(4), 217-227.

Louisiana Department of Transportation and Development (LADOTD) (2016). *The Louisiana Department of Transportation's Pavement Management System manual (2016 edition).* Baton Rouge, LA.

Lewis, D.E., Ledford, K., Georges, T., and Jared, D.M. (2012). Construction and Performance of Inverted Pavements in Georgia. *Proceedings of the 91st Annual Meeting of the Transportation Research Board*, Washington, D.C.

Lin, S. (2014). *Advancements in Active Surface Wave Methods: Modeling, Testing, and Inversion*. Ph.D. Thesis, Iowa State University, Ames IA.

Metcalf, J.B., Roberts, F.L., Rasoulian, M., Romanoschi, S., Li, Y., and Djakfar, L. (2001). *Construction Comparison of Louisiana's Conventional and Alternative Base Courses under Accelerated Loading*. Final Report No. FHWA/LA-00/347. Louisiana Transportation Research Center.

North Carolina Department of Transportation (NCDOT) (2018). *North Carolina Department of Transportation's Standard Specifications for Roads and Structures (NCDOT).* Raleigh, NC.

New Mexico Department of Transportation (NMDOT) (2019). *Standard Specifications for Highway and Bridge Construction.* Sante Fe, NM.

Papadopoulous, E. (2014). *Performance of Unbound Aggregate Bases and Implications for Inverted Base Pavements*. Ph.D. Thesis, Georgia Institute of Technology, Atlanta GA.

Rasoulian, M., Becnel, B., and Keel, G., (2000). Stone Interlayer Pavement Design. *Transportation Research Record: Journal of the Transportation Research Board*, 1709, 60-68.

Roesset, J.M., Chang, D. W., Stokoe II, K.H., and Aouad, M. (1990). Modulus and Thickness of the Pavement Surface Layer from SASW Tests. *Transportation Research Record: Journal of the Transportation Research Board*, 1260, 53-63.

Rust, F.C., Mahoney, J.P., and Sorenson, J.B. (1998). *An International View of Pavement Engineering." Trondheim: Bearing Capacity of Roads and Airfields*. Online. < http://researchspace.csir.co.za/dspace/bitstream/handle/10204/1369/Rust_1998.pdf?sequence=1&is Allowed=y>. Accessed October 2018.

Ryden, N. and Lowe, M.J. (2004). Guided Wave Propagation in Three-Layer Pavement Structures. *The Journal of the Acoustical Society of America*, 116(5), 2902-2913.

Ryden, N. and Park, C.B. (2006). Fast Simulated Annealing Inversion of Surface Waves on Pavement using Phase-Velocity Spectra. *Geophysics*, 71(4), R49-R58.

Ryden, N., Park, C.B., Ulriksen, P., and Miller, R. D. (2004). Multimodal Approach to Seismic Pavement Testing. *Journal of Geotechnical and Geoenvironmental Engineering*, 130(6), 636-645.

Rydén, N., Ulriksen, P., Park, C.B., Miller, R. D., Xia, J., and Ivanov, J. (2001). High Frequency MASW for Non-Destructive Testing of Pavements—Accelerometer Approach. In *Symposium on the Application of Geophysics to Engineering and Environmental Problems 2001* (pp. RBA5-RBA5). Society of Exploration Geophysicists.

Ryden, N., Ulriksen, P., Park, C., and Miller, R. (2002). Portable Seismic Acquisition System (PSAS) For Pavement MASW. In *15th EEGS Symposium on the Application of Geophysics to Engineering and Environmental Problems* (pp. cp-191). European Association of Geoscientists & Engineers.

Sheu, J.C., Stokoe II, K.H., and Roesset, J.M (1988). Effect of Reflected Waves in SASW Testing of Pavements. *Transportation Research Record: Journal of the Transportation Research Board*, 1196, 51-61.

Titi, H., Rasoulian, M., Martinez, M., Becnel, B., and Keel, G. (2003). Long-Term Performance of Stone Interlayer Pavement. *Journal of Transportation Engineering*, 129(2), 118-126.

Tutumluer, E., Little, D.N., and Kim, S.H. (2003). Validated Model for Predicting Field Performance of Aggregate Base Courses. *Transportation Research Record: Journal of the Transportation Research Board*, 1837(1), 41-49.

Vaughan, K., Personal communication over email, September 26, 2019.

Vaziri, A.A. and Guddati, M.N. (2016). Improved Inversion Algorithms for Near-Surface Characterization. *Geophysical Journal International*, 206(2), 1410-1423.

Weingart, R. (2010). *Inverted Base Pavement Design, The Virginia Experience*. Online < https://www.slideserve.com/uzuri/inverted-base-pavement-design-ju-ne-1-2010-the-virginia-experience> Accessed November 21, 2019.

Wu, H., Wang, S., Abdallah, I., and Nazarian, S. (2002). A Rapid Approach to Interpretation of SASW Results. In *Bearing Capacity of Roads, Railways and Airfields* (pp. 761-770). CRC Press.

APPENDIX B: DETAILED PCR AND PCI CALCULATIONS FROM FIELD CONDITION ASSESSMENTS

Pavement Condition Index (PCI) calculation details

The Pavement Condition Index was calculated according to the ASTM D6433-18 with the exception that the entire pavement section (either inverted or conventional) in both directions were treated as a single sample unit. All distresses called for in the ASTM standard were measured during the August 2021 and July 2022 site visits with the exception of rutting. However, as noted in the report, the traffic speed deflectometer test conducted in September of 2021 confirmed that all rutting on the site was below the low severity threshold and would thus not factor into the deduct calculations.

Following the standard procedure the cumulative extent of each distress was first cumulated by severity level. Then the cumulative distress density of each distress and severity level was calculated by dividing the extent by the total area of the site, approximately 19,200 ft^2 (800 ft x 12 ft lane width x 2 directions). Finally, the corresponding deduct values were obtained by using the curves shown in Appendix X3 of ASTM D6433-18. Table B.1 summarizes the cumulative extent, density, and individual deduct values for both pavements and for the surveys conducted in August 2021 and July 2022. Note that for this calculation, the random cracking observed in the southbound conventional pavement sites (approximately stations 8+32 and 9+75) were added to the low severity fatigue cracking for deduct calculation purposes.

Table B.1. Summary of Distress Severity, Extent, and Deduct Values from ASTM D6433-18 PCI Procedure.

Pavement	Distress	Severity	Cumulative Extent (ft/sq ft)	Cumulative Density	DV
Conventional (Aug. 2021)	Edge Cracking	Low	46	0.24	1.9
	Fatigue Cracking	Low	239	1.24	12.3
	Fatigue Cracking	Moderate	36	0.19	10
	Transverse/Lon. Cracking	Low	27	0.14	0.0
	Shoulder Dropoff	Low	97	0.51	2.7
	Shoulder Dropoff	Moderate	397	2.07	5.7
	Slippage	Low	0	0.00	0
Conventional (July 2022)	Edge Cracking	Low	92	0.48	3
	Fatigue Cracking	Low	110.5	0.57	6
	Fatigue Cracking	Moderate	108	0.56	16.3
	Transverse/Lon. Cracking	Low	13	0.07	0.0
	Shoulder Dropoff	Low	175	0.91	2.7
	Shoulder Dropoff	Moderate	398	2.07	5.7
	Slippage	Low	31.5	0.16	0.0
Inverted (Aug. 2021)	Transverse/Lon. Cracking	Low	378.5	1.97	5.4
	Shoulder Dropoff	Low	62	0.32	2.7
Inverted (July 2022)	Transverse/Lon. Cracking	Low	510	2.66	7.4
	Shoulder Dropoff	Low	100	0.52	2.7

Since multiple distresses were present in the study sites, the final deduct values were calculated using the corrected deduct value (CDV) method where the allowable number of deduct values, *m*, was first determined using the maximum individual deduct values (*MaxDV*) according to Equation

(17). For all cases the number of allowable deduct values exceeded the number of actual distress deducts and so none were eliminated or adjusted. Then, the iterative CDV approach described in Section 9.5 was performed to identify the maximum (and thus reported) CDV after iteratively eliminating distresses, calculating the total deduct value (TDV) and using the relevant correction curves. For this study, the correction values were calculated based on the regression analysis of Figure X3.27 in ASTM D6433 that was performed by Wu (2015). These regression functions are are summarized in Equation (18) and Table B.2. Table B.3 through Table B.6 summarize the results of the iterative calculation and the final reported deduct value for each pavement and for each survey.

$$m = 1 + \left(\frac{9}{98}\right)\left(1 - MaxDV\right) \le 10 \tag{18}$$

$$CDV = B0 + B1 \times TDV + B2 \times TDV^2 + B3 \times TDV^3 \tag{19}$$

Table B.2. Summary of CDV Function Coefficient Values (Wu 2015)

q[1]	B_0	B_1	B_2	B_3	R^2
0	0	0	0	0	1
1	0	1	0	0	1
2	-1.9070	0.8190	-0.0006	-0.000004	0.9999
3	-6.1516	0.8016	-0.0009	-0.000002	0.9999
4	-7.9770	0.6844	0.0002	-0.000005	0.9999
5	-7.8998	0.6105	0.0003	-0.000004	0.9999
6	-6.6359	0.5140	0.0009	-0.000005	0.9999
7	-7.2983	0.5192	0.0012	-0.000008	0.9999

[1] q = number of deduct values that are not discounted for the purposes of CDV calculation

Table B.3. Summary of CDV Calculation for Conventional Pavement Section from August 2021 Survey

m	9.1	← Use All Distresses				
Distress	**Severity**	**Individual DV**				
Transverse/ Lon. Cracking	Low	0	0	0	0	0
Edge Cracking	Low	1.9	2.0	2.0	2.0	2.0
Shoulder Dropoff	Low	2.7	2.7	2.0	2.0	2.0
Shoulder Dropoff	Moderate	5.7	5.7	5.7	2.0	2.0
Fatigue Cracking	Moderate	10.0	10.0	10.0	10.0	2.0
Fatigue Cracking	Low	12.3	12.3	12.3	12.3	12.3
TDV		32.6	32.7	32	28.3	20.3
q		5	4	3	2	1
CDV		12.2	14.4	18.5	20.7	20.3
PCI				**79.3**		

Table B.4. Summary of CDV Calculation for Conventional Pavement Section from July 2022 Survey

m	8.7	← Use All Distresses				
Distress	**Severity**	**Individual DV**				
Transverse/ Lon. Cracking	Low	0	0	0	0	0
Edge Cracking	Low	2.7	2.0	2.0	2.0	2.0
Shoulder Dropoff	Low	3.0	3.0	2.0	2.0	2.0
Shoulder Dropoff	Moderate	5.7	5.7	5.7	2.0	2.0
Fatigue Cracking	Moderate	6.0	6.0	6.0	6.0	2.0
Fatigue Cracking	Low	16.3	16.3	16.3	16.3	16.3
TDV		32.6	33.7	33	32	28.3
q		5	5	4	3	2
CDV		12.9	14.6	18.5	20.7	24.3
PCI				**75.7**		

Table B.5. Summary of CDV Calculation for Inverted Pavement Section from August 2021 Survey

m	9.4	← Use All Distresses	
Distress	**Severity**	**Individual DV**	
Shoulder Dropoff	Low	2.7	2
Transverse/ Lon. Cracking	Low	5.4	5.4
TDV		32.6	8.1
q		2	1
CDV		4.7	7.4
PCI		**92.6**	

Table B.6. Summary of CDV Calculation for Inverted Pavement Section from July 2022 Survey

m	9.3	← Use All Distresses	
Distress	**Severity**	**Individual DV**	
Shoulder Dropoff	Low	2.7	2
Transverse/ Lon. Cracking	Low	7.4	7.4
TDV		32.6	10.1
q		2	2
CDV		6.3	9.4
PCI		**90.6**	

Pavement Condition Rating (PCR) calculation details

The PCR value was calculated by applying the deduct functions shown in Equations (19) through (26). Table B.7 summarizes the ratings given and the cumulative PCR value calculated.

$$PCR = 100 - A - T - Ru - Ra - B - P - O \tag{20}$$

where the deduct indices are defined by;

A = alligator (fatigue) cracking, Equation (20),
T = transverse cracking, Equation (21),
Ru = rutting, Equation (22),
Ra = raveling, Equation (23),
B = bleeding, Equation (24),
P = patching, Equation (25), and
O = oxidation, Equation (26).

$$A = \begin{cases} 3.3 \quad \text{for distress} = L - 10\% \text{ to } 90\% & 1 \quad \text{for distress} = L - > 90\% \\ 7.5 \quad \text{for distress} = \text{M} - 10\% \text{ to } 40\% & 2 \quad \text{for distress} = \text{M} - > 40\% \\ 15 \quad \text{for distress} = \text{S} - 10\% \text{ to } 20\% & 3 \quad \text{for distress} = \text{S} - > 20\% \end{cases} \tag{21}$$

For the alligator distress two different deduct values are used. The larger deduct values are used until a total of 30 deduct points are accumulated after which the smaller values are used.

$$T = \begin{cases} 5 \quad \text{for distress} = L \\ 15 \quad \text{for distress} = \text{M} \\ 30 \quad \text{for distress} = \text{S} \end{cases} \tag{22}$$

$$Ru = \begin{cases} 5 \quad \text{for distress} = L \\ 20 \quad \text{for distress} = \text{M} \\ 30 \quad \text{for distress} = \text{S} \end{cases} \tag{23}$$

$$Ra = \begin{cases} 2 \quad \text{for distress} = L \\ 5 \quad \text{for distress} = \text{M} \\ 15 \quad \text{for distress} = \text{S} \end{cases} \tag{24}$$

$$B = \begin{cases} 10 \quad \text{for distress} = L \\ 20 \quad \text{for distress} = \text{M} \\ 30 \quad \text{for distress} = \text{S} \end{cases} \tag{25}$$

$$P = \begin{cases} 5 \quad \text{for distress} = L \\ 10 \quad \text{for distress} = \text{M} \\ 20 \quad \text{for distress} = \text{S} \end{cases} \tag{26}$$

$$O = \begin{cases} 0 \quad \text{for distress} = \text{N} \\ 5 \quad \text{for distress} = \text{S} \end{cases} \tag{27}$$

Table B.7. Summary of PCR Calculation Results for Conventional and Inverted Pavement Sections

Section and Date		Alligator Cracking (01, 02, 03….10)				Fatigue Portion	Trans. Crack.	Rutting	Raveling	Oxidation	Bleeding	Ride Qual.	Patching	PCR
		N	L	M	S									
Conventional	August 2021	9.24	0.56	0.2	0	3.3	N	N	N	N	N	N	N	96.7
	July 2022	9.4	0.16	0.44	0	3.8	N	N	N	N	N	N	N	96.2
Inverted	August 2021	10	0	0	0	0.0	L	N	N	N	N	N	N	95.0
	July 2022	10	0	0	0	0.0	L	N	N	N	N	N	N	95.0

Appendix B References

Wu, K. (2015). *Development of PCI-based pavement performance model for management of road infrastructure system*. M.S. Thesis, Arizona State University, Tempe, AZ.

This page is intentionally blank

APPENDIX C: IMPACT RESONANCE TESTING OF FIELD CORES

Impact Resonance Testing of Field Cores

A comprehensive test plan consisting of two different impact locations and two different accelerometer locations as shown in Figure C.1 was used for testing the cores. Multiple impact repetitions (4 to 5) for each impact case were conducted to quantify the repeatability.

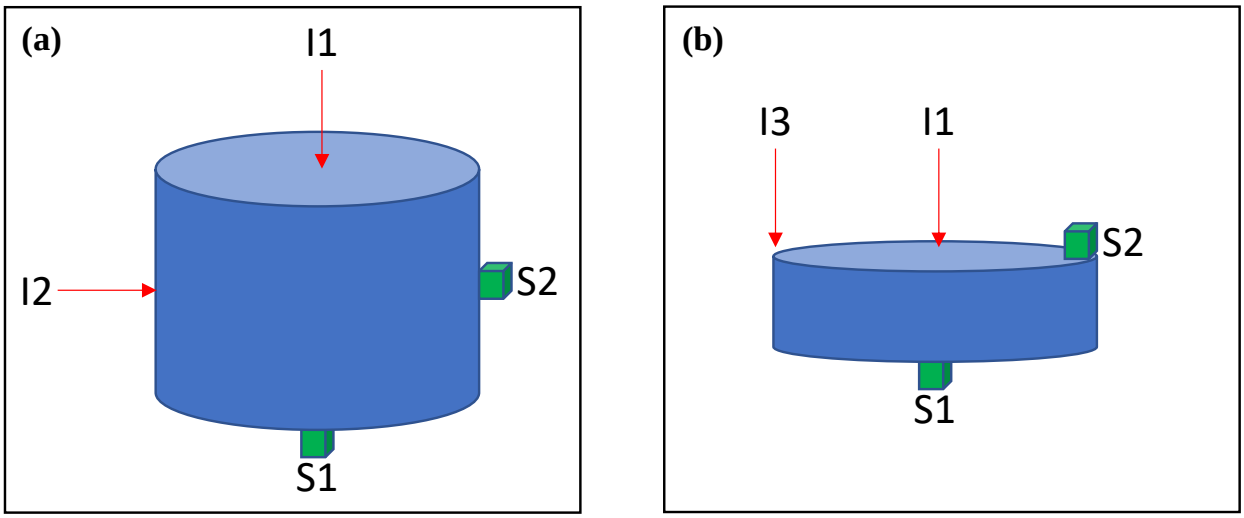

Figure C.1. Impact resonance test schematic; (a) conventional cores and (b) inverted cores.

After testing the conventional pavement cores, they were sliced into two thinner layers to approximately separate the surfaced and intermediate layer materials. The raw and cut specimen dimensions can be found in Table 1 and Table 7 respectively.

ANSYS Modelling

The average dimensions of the cores were used to develop an ANSYS model of the impact cylinders to compute the free-free resonant modes of vibration and corresponding resonant frequencies. The typical mesh used for the conventional and inverted section are shown in Figure C.2. The element size was chosen after performing a convergence analysis based on the first six resonant frequencies. The elastic modulus, density and Poisson's ratio are required as inputs for the ANSYS model. The bulk density values estimated for each core is used along with an assumed Poisson's ratio of 0.3 which is typical for asphalt. It is important to note that the Poisson's ratio is not a constant in reality and could have an influence on the IR modulus computed. A brief study on the effect of Poisson's ratio on different modes is presented later. A unit value for the modulus is assumed to facilitate the direct computation of the constant of proportionality from the ANSYS modelling, which along with the resonant frequency calculated from the IR test, is used to estimate the modulus of the core. The first six independent modes of vibration are extracted for a model of CC1 and shown in Figure C.3.

The critical step is to identify the mode of vibration for each of the impact scenarios and match them with the correct mode form ANSYS. The first step for this assessment is to visually identify the modes that correspond to each of the impact cases. For example, for Case I1, Mode 6 shown in Figure C.3 is the most likely mode that is predominantly excited based on the displacement observed. In order to further confirm the initial hypothesis, the phase and amplitude from the two

sensors measurements are further examined as a second step. Figure C.45 (a) and (b) correspond to the Case I1 and (c) and (d) correspond to Case I2. Firstly, the amplitude at the dominant frequency is higher for S1 in I1 and S2 in I2 as the sensors are in the opposite faces and at diametrically opposite locations respectively. Further, the phase for both the case at S1 and S2 are out of phase when examined around the dominant frequency. Comparing the phase with the displacement contours shown in Figure C.3, it is clearly evident that I1 corresponds to Mode 6 and I2 corresponds Mode 3.

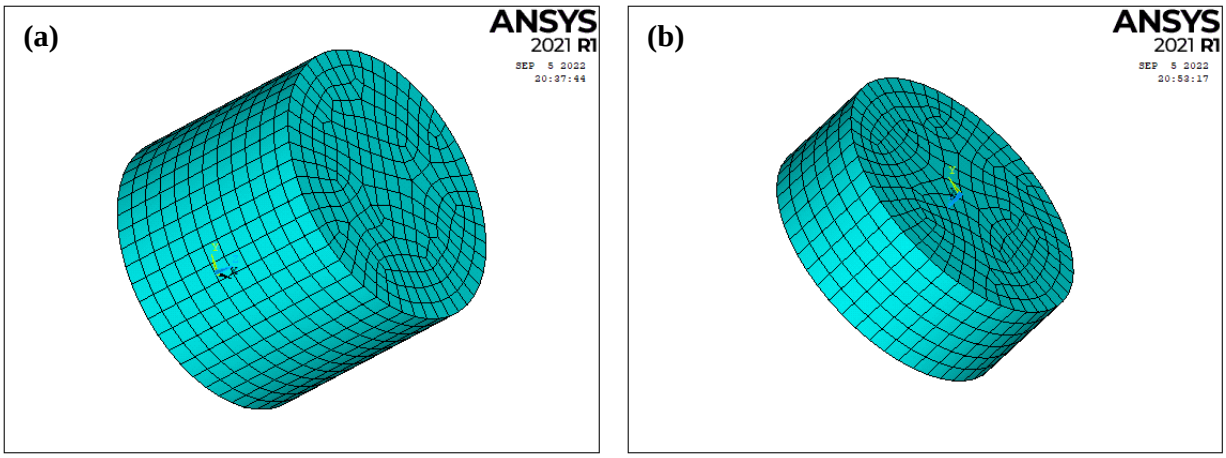

Figure C.2. Typical mesh for ANSYS modal analysis.

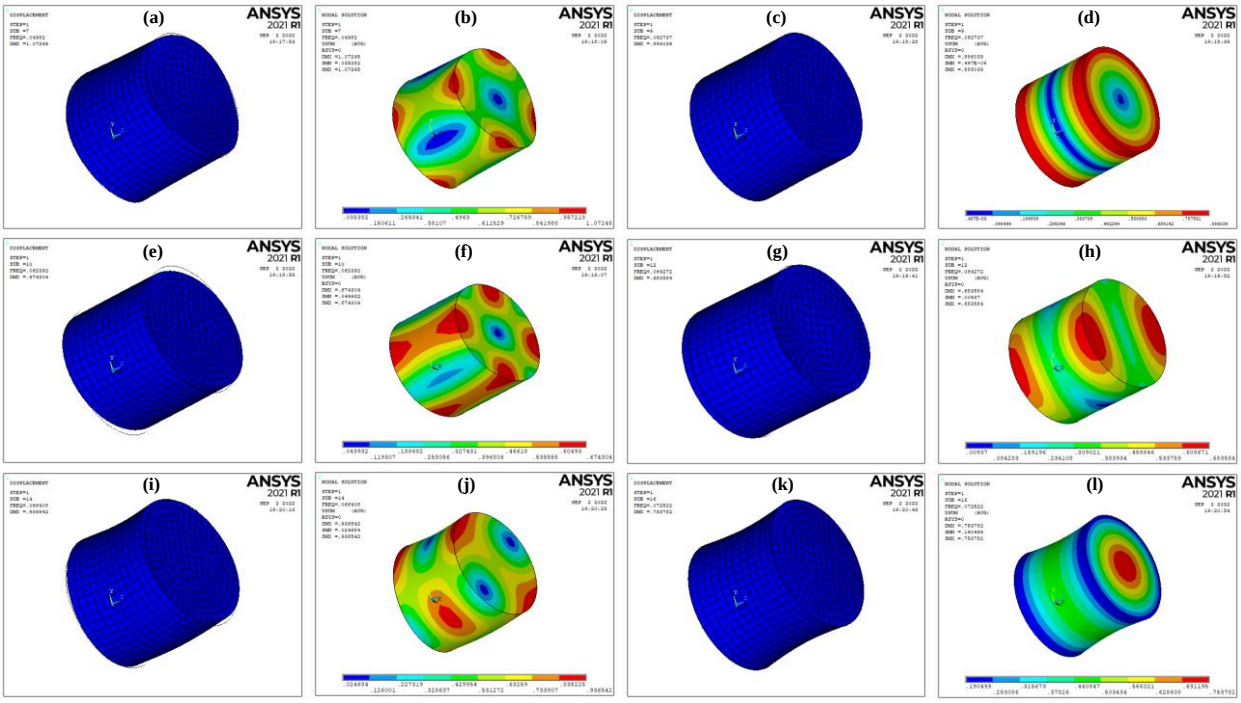

Figure C.3. First six resonant modes of CC1; (a) Mode 1 deformed shape, (b) Mode 1 displacement contour, (c) Mode 2 deformed shape, (d) Mode 2 displacement contour, (e) Mode 3 deformed shape, (f) Mode 3 displacement contour, (g) Mode 4 deformed shape, (h) Mode 4 displacement contour (i) Mode 5 deformed shape, (j) Mode 5 displacement contour, (k) Mode 6 deformed shape, and (l) Mode 6 displacement contour.

A similar analysis is conducted for the inverted cores as well to match the corresponding modes to the impact scenarios. Owing to thinner specimen, the first two modes from the inverted cores modelling, match with I3 and I1 respectively. Based on this analysis, the correct constant of proportionality, which is the resonant frequency from the ANSYS model since a unit modulus was used, is identified and the corresponding estimated modulus values are shown in Figure C.5. A comparison of the estimated IR moduli with the AASHTO TP 132 test results are shown in Figure C.6. In case of the conventional cores, it is observed that there is an average difference of 23% between I1-S1 and I2-S2 modulus. Comparing these values with the laboratory master curves in Figure C.6 (a) mode I1-S1 results in an average modulus for the entire section while the I2-S2 results in modulus values closer to the intermediate layer. This result could be occurring due to the substantial disparity in between the surface and intermediate layer moduli, impact locations, and the sensor placement. However, further work is needed to gain a deeper understanding. It is possible that the impact and sensor were placed both on the intermediate portion of the core for the I2-S2 case. On the contrary, inverted pavement having two surface mixes of comparable properties, both the impact scenarios results in similar modulus values with an average difference of only 4% between the impact scenarios.

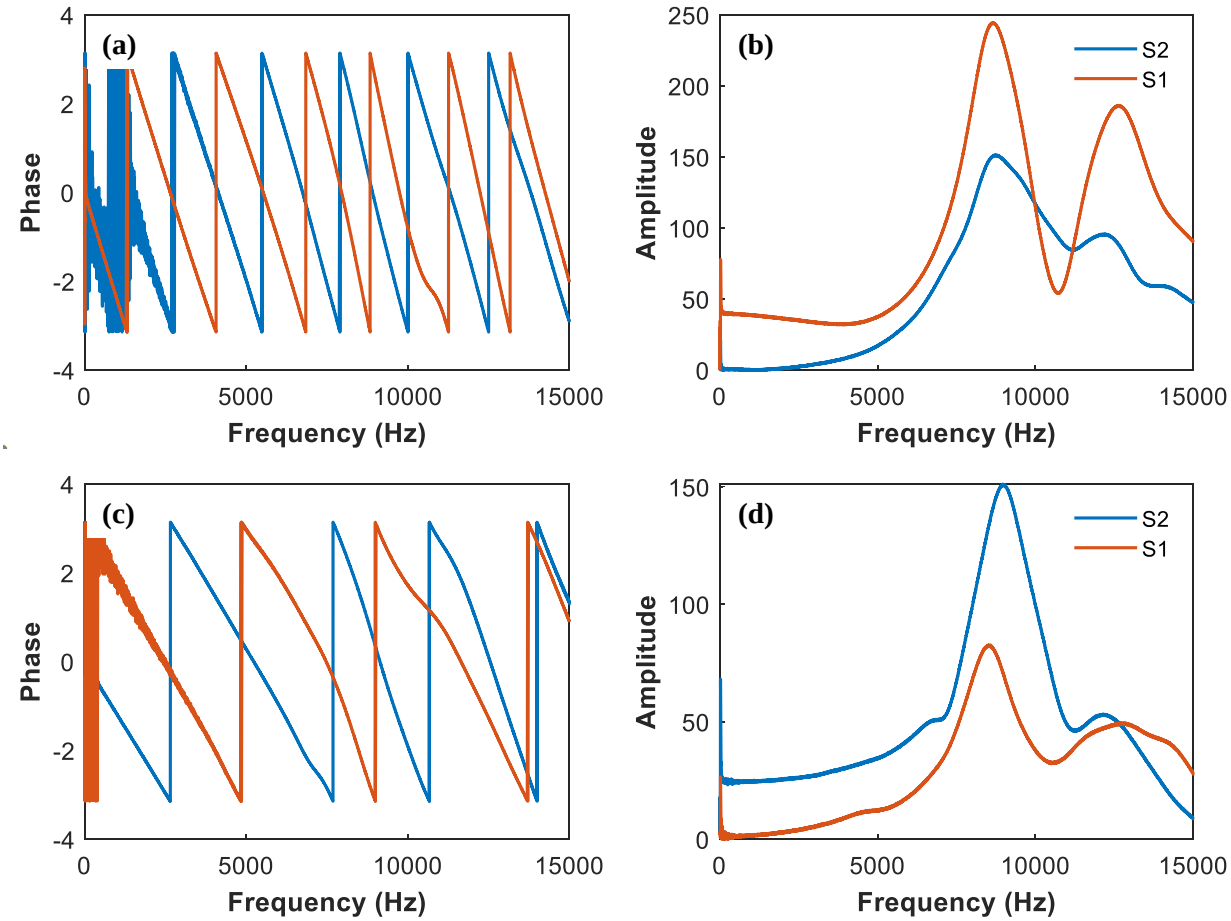

Figure C.4. IR mode matching with ANSYS; (a) I1 phase, (b) I1 amplitude, (c) I2 phase, and (d) I2 amplitude.

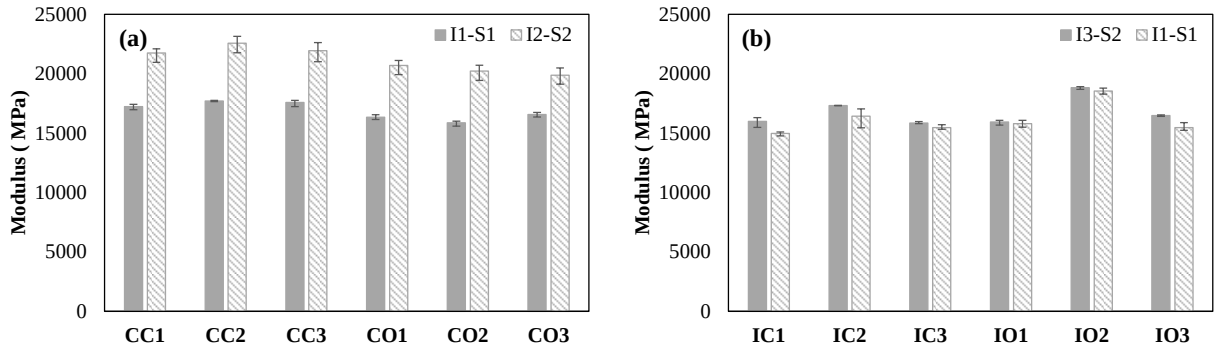

Figure C.5. IR modulus estimates from different impact scenarios; (a) conventional cores and (b) inverted cores.

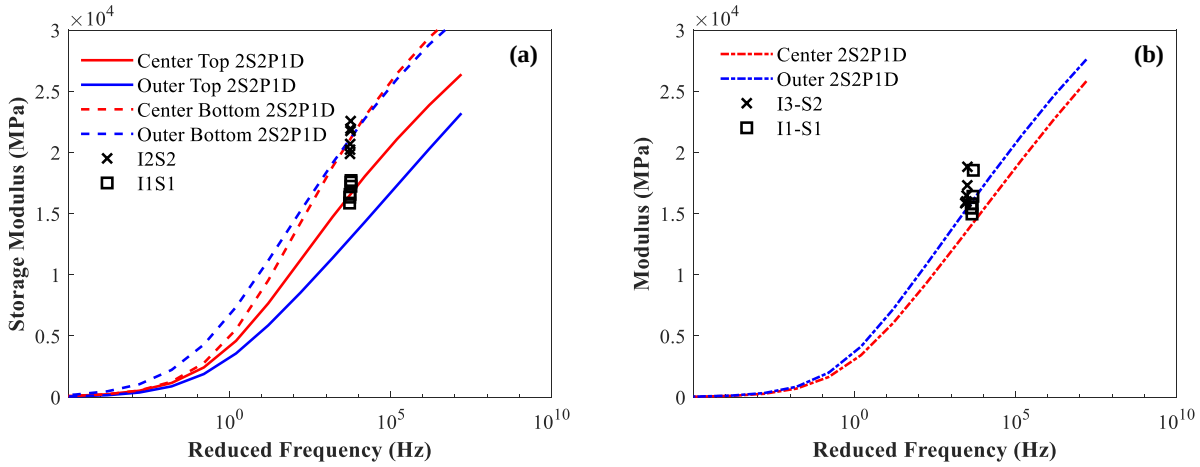

Figure C.6. IR modulus comparison with AASHTO TP 132 test results; (a) conventional pavement and (b) inverted pavement.

Effect of Poisson's Ratio

The effect of Poisson's ratio is studied using the ANSYS model and preliminary results are presented for the CC2 cores. The variation of the computed modulus as a function of Poisson's ratio for both the impact scenarios is shown in Figure C.7. It is observed that the I1-S1 mode, which is the most widely used scenario for IR testing, results in a nonlinear relationship between Poisson's ratio and modulus. On the contrary, the I1-S1 mode resulted in a linear relationship. While these are preliminary observations, further investigation of the I2-S2 modes could potentially lead to an improved IR test methodology that can be directly applied to field cores without the need to slice into thinner sections. Additionally, different impact and sensor locations for the I2-S2 scenario could be studied to potentially be able to identify the individual asphalt layer modulus from the IR test.

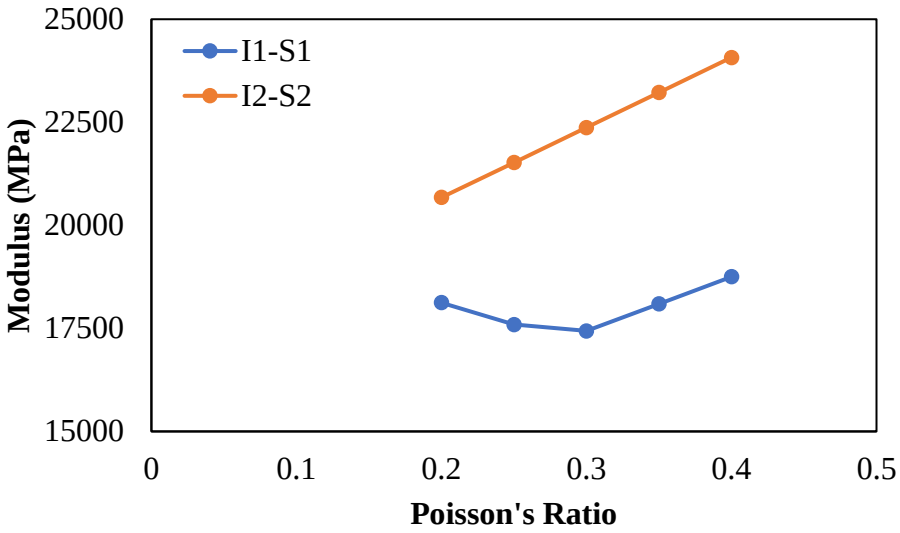

Figure C.7. IR modulus variation as a function of Poisson's ratio.

This page is intentionally blank

APPENDIX D: SUMMARY OF AASHTO TP 133 TEST RESULTS FROM FIELD CORES

Table D.1. Dynamic Modulus Results for Inverted Site Specimens

Specimen	Dynamic Modulus (MPa)								
	4°C-10Hz	4°C-1Hz	4°C-0.1Hz	20°C-10Hz	20°C-1Hz	20°C-0.1Hz	40°C-10Hz	40°C-1Hz	40°C-0.1Hz
IC1-1	12785	9409	6386	6179	3535	1793	1398	588.2	240.4
IC1-2	12083	8908	6044	5449	3051	1507	1169	470.1	181.0
IC2-1	14302	10797	7581	6706	3870	1967	1447	564.2	200.9
IC2-2	14440	10958	7748	6895	4033	2087	1559	630.7	238.9
IO2-1	17043	13073	9343	8694	5200	2737	1925	772.3	282.2
IO2-2	16196	12362	8823	7781	4576	2387	1698	686.3	266.2
IO3-1	14334	10810	7532	6612	3792	1912	1454	583.7	224.5
IO3-2	14089	10691	7542	6642	3859	1987	1508	620.4	242.8

Table D.2. Phase Angle Results for Inverted Site Specimens

Specimen	Phase Angle (°)								
	4°C-10Hz	4°C-1Hz	4°C-0.1Hz	20°C-10Hz	20°C-1Hz	20°C-0.1Hz	40°C-10Hz	40°C-1Hz	40°C-0.1Hz
IC1-1	10.97	14.26	18.34	20.69	25.96	29.98	32.46	30.68	28.09
IC1-2	11.25	14.47	18.63	21.53	26.91	30.79	33.89	32.54	30.76
IC2-1	10.08	13.08	17.10	20.19	25.98	31.02	35.61	36.06	35.18
IC2-2	10.12	13.00	16.85	19.76	25.23	29.99	34.71	35.06	33.29
IO2-1	9.44	12.24	15.94	18.80	24.83	30.21	35.77	36.51	34.49
IO2-2	9.60	12.34	15.84	19.36	25.19	30.36	35.78	36.48	34.42
IO3-1	10.25	13.34	17.44	20.61	26.57	31.74	36.21	36.75	35.04
IO3-2	9.93	13.00	16.99	20.21	26.03	31.07	36.00	36.62	35.37

Table D.3. Dynamic Modulus Results for Top Layer in Conventional Site Specimens

Specimen	Dynamic Modulus (MPa)								
	4°C-10Hz	4°C-1Hz	4°C-0.1Hz	20°C-10Hz	20°C-1Hz	20°C-0.1Hz	40°C-10Hz	40°C-1Hz	40°C-0.1Hz
CC1-1T	14654	11064	7798	7144	4211	2255	1859	850.3	369.6
CC1-2T	14942	11422	8135	7188	4322	2358	1896	865.9	373.7
CC2-1T	16071	12222	8591	7711	4500	2347	1989	900.6	386.9
CC2-2T	16264	12348	8791	7972	4742	2537	2110	977.6	427.7
CO1-1T	11664	8698	6034	5797	3416	1807	1292	551.1	219.2
CO1-2T	11846	8932	6288	5831	3437	1812	1366	590.4	230.1
CO2-1T	11623	8731	6139	5525	3257	1726	1394	596.7	252.2
CO2-2T	12069	9189	6539	5824	3487	1884	1472	636.3	273.2

Table D.4. Phase Angle Results for Top Layer in Conventional Site Specimens

Specimen	Phase Angle (°)								
	4°C-10Hz	4°C-1Hz	4°C-0.1Hz	20°C -10Hz	20°C-1Hz	20°C-0.1Hz	40°C-10Hz	40°C -1Hz	40°C -0.1Hz
CC1-1T	10.09	13.27	17.14	19.63	25.24	29.92	34.63	35.3	33.01
CC1-2T	8.96	11.67	15.04	17.59	22.89	27.84	33.69	34.55	33.94
CC2-1T	8.48	10.97	13.99	19.38	25.53	31.08	34.83	35.07	33.47
CC2-2T	9.63	12.72	16.72	20.07	25.89	30.83	34.31	34.38	31.80
CO1-1T	10.55	13.66	17.36	19.60	24.65	28.88	34.94	35.91	34.93
CO1-2T	9.81	12.61	16.06	19.80	25.00	29.43	33.86	34.31	34.62
CO2-1T	8.89	11.04	13.22	17.05	21.23	25.54	33.48	35.01	34.44
CO2-2T	9.52	11.99	15.11	18.09	22.88	27.93	33.54	35.76	35.63

Table D.5. Dynamic Modulus Results for Bottom Layer in Conventional Site Specimens

Specimen	Dynamic Modulus (MPa)								
	4°C-10Hz	4°C-1Hz	4°C-0.1Hz	20°C -10Hz	20°C-1Hz	20°C-0.1Hz	40°C-10Hz	40°C -1Hz	40°C -0.1Hz
CC1-1B	19141	14440	10076	9336	5378	2713	2048	851.1	355.4
CC1-2B	19554	14754	10262	9319	5340	2703	2003	836.1	331.6
CC2-1B	20599	15775	11171	9944	5786	2979	2269	947.8	385.9
CC2-2B	21274	16462	11703	9942	5775	3020	2425	1020	426.2
CO1-1B	21443	17383	13311	11530	7539	4452	3560	1776	796.9
CO1-2B	19597	15731	11940	10188	6555	3789	3051	1472	662.0
CO2-1B	20663	16751	12906	12051	8099	4880	3483	1722	774.2
CO2-2B	19791	15886	12062	10678	6912	4010	3049	1466	642.1

Table D.6. Phase Angle Results for Bottom Layer in Conventional Site Specimens

Specimen	Phase Angle (°)								
	4°C-10Hz	4°C-1Hz	4°C-0.1Hz	20°C -10Hz	20°C-1Hz	20°C-0.1Hz	40°C-10Hz	40°C -1Hz	40°C -0.1Hz
CC1-1B	9.82	13.41	18.46	20.88	27.85	33.35	37.08	35.68	29.96
CC1-2B	10.01	13.50	18.36	21.54	27.80	32.72	36.78	35.24	30.81
CC2-1B	9.55	12.85	17.60	20.85	27.22	32.34	36.22	35.02	30.58
CC2-2B	9.39	12.57	17.25	21.18	27.43	31.96	35.86	33.84	29.31
CO1-1B	7.85	9.96	13.23	16.29	21.27	26.75	29.44	30.71	30.90
CO1-2B	8.11	10.29	13.64	16.55	21.70	27.37	30.64	32.35	31.98
CO2-1B	7.80	9.90	13.18	15.11	19.96	25.65	30.73	32.78	32.91
CO2-2B	8.11	10.27	13.64	16.22	21.43	27.23	30.81	32.5	32.78

The model coefficients obtained from optimization of the measured dynamic modulus and phase angle data using FlexMAT version 2.1.2 are summarized in Table D.7. The 2S2P1D model function for the complex modulus is shown in Equation (27) below. The dynamic modulus can be computed by decomposition of this function into the real and imaginary components (storage and loss moduli respectively) as shown in Equations (28) through (31) and then combining these via

Equation (32). Likewise the phase angle can be computed using the definition shown in Equation (33). For the analysis shown in this report, the time-temperature shift factor function was expressed as shown in Equation (34).

$$E^*_{2S2P1D} = E_{00} + \frac{E_0 - E_{00}}{1 + \delta\left(j\omega_r\tau_E\right)^{-k} + \left(j\omega_r\tau_E\right)^{-h} + \left(j\omega_r\beta\tau_E\right)^{-1}} \tag{28}$$

$$E'_{2S2P1D} = E_{00} + \frac{E'_1}{\left[\left(\frac{E'_1}{\left(E_0 - E_{00}\right)}\right)^2 + \left(\frac{E'_2}{\left(E_0 - E_{00}\right)}\right)^2\right]} \tag{29}$$

$$E''_{2S2P1D} = \frac{E'_2}{\left[\left(\frac{E'_1}{\left(E_0 - E_{00}\right)}\right)^2 + \left(\frac{E'_2}{\left(E_0 - E_{00}\right)}\right)^2\right]} \tag{30}$$

$$E'_1 = \left(E_0 - E_{00}\right)\left[1 + \delta\left(\omega_r\tau_E\right)^{-k}\cos\left(\frac{k\pi}{2}\right) + \left(\omega_r\tau_E\right)^{-h}\cos\left(\frac{h\pi}{2}\right)\right] \tag{31}$$

$$E'_2 = \left(E_0 - E_{00}\right)\left[\delta\left(\omega_r\tau_E\right)^{-k}\sin\left(\frac{k\pi}{2}\right) + \left(\omega_r\tau_E\right)^{-h}\sin\left(\frac{h\pi}{2}\right) + \left(\omega_r\beta\tau_E\right)^{-1}\right] \tag{32}$$

$$\left|E^*\right| = \sqrt{\left(E'\right)^2 + \left(E''\right)^2} \tag{33}$$

$$\phi = \arctan\left(\frac{E''}{E'}\right) \tag{34}$$

$$\log a_T = a_1\left(T^2 - T_{ref}^2\right) + a_2\left(T - T_{ref}\right) \tag{35}$$

Table D.7. Summary of Master Curve Function Coefficients for All Locations and Layers

Coefficient	Inverted		Conventional - Top Layer		Conventional - Bottom Layer	
	Center	Outer	Center	Outer	Center	Outer
δ	2.985	2.642	1.946	3.296	1.467	1.902
k	0.136	0.137	0.111	0.124	0.136	0.134
h	0.438	0.441	0.388	0.420	0.409	0.391
β	1E+12	1E+12	1E+12	1E+12	1E+12	1E+12
E00 [MPa]	3.13	4.94	17.56	3.16	22.44	11.08
E0 [MPa]	40000	40000	40000	40000	40000	40000
log(τE)	-2.62	-2.40	-2.78	-2.71	-2.51	-1.84
a_1	0.0005	0.0005	0.0007	0.0004	0.0007	0.0007
a_2	-0.152	-0.155	-0.156	-0.147	-0.159	-0.166
T_{ref}	21.1	21.1	21.1	21.1	21.1	21.1

This page is intentionally blank

APPENDIX E: MODELLING PAVEMENT LAYERS

Overview

This section consists of examples of conventional and inverted pavement, theoretical dispersion curve computed from the modelling technique and displacement shape at different regions which helps understand the wave propagation behavior of the system. The pavement system is modelled as a layered system that is transversely isotropic half-space under axisymmetric excitation as shown in Figure E.1.

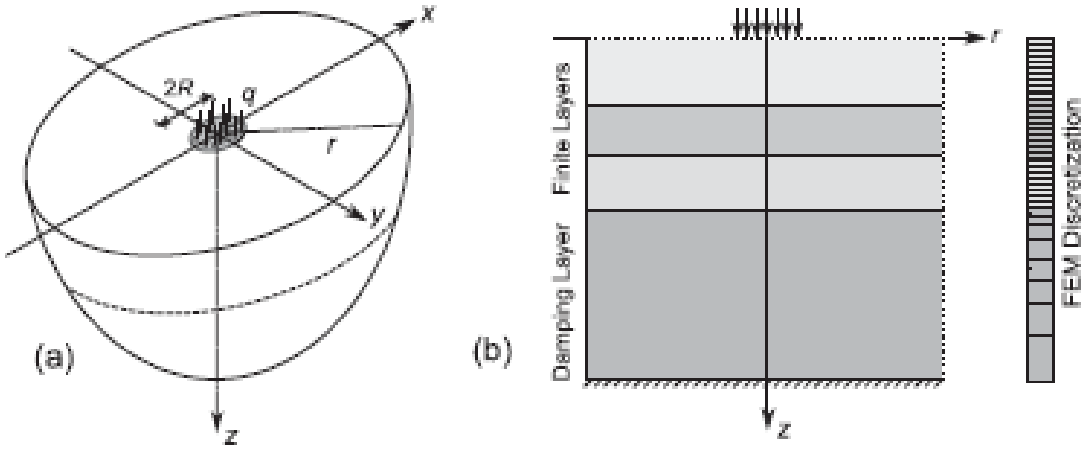

Figure E.1. Layered pavement model; (a) layered half-space with vertical load, and (b) mathematical model of the finite layers and semi-infinite bottom layer (Vaziri and Guddati 2016).

A semi-analytical finite element (SAFEM) procedure which employs Fourier transformation in the horizontal direction and finite element formulation in the vertical direction is adopted for modelling the wave propagation behavior. The back calculation procedure described in this report employs complex length finite elements (CFEM) which uses midpoint integrated linear finite elements with specially chosen complex valued length. CFEM results are accurate at the nodes but not inside each element. Quartic (5-noded) finite elements (FEM) can be used in the vertical direction for computing reference solutions as well as to study the wave propagation characteristics as the solution can be interpolated between the nodes. However, using higher order FEM will result in high computational costs. Perfectly Matched Discrete Layers (PMDL) is used to model the semi-infinite half-space layers in both the above cases. The finite element formulation is an eigen value problem that results in all the theoretical dispersion modes of wave propagation. Following a similar procedure to (Vaziri and Guddati 2016), the surface displacement is obtained assuming an idealized disk load of radius *R* and computed from the theoretical dispersion modes (Kausel and Peek 1982) using Equation (36).

$$u^{surface}(r,\omega) = \sum_{j=1}^{N_R} \frac{-iqR\pi}{2k_j} \phi_z^2 J_1(k_j R) H_0^{(2)}(k_j r) \tag{36}$$

where; N_R is the number of included modes, r is the offset, q is the load density, $H_0^{(2)}$ is the Hankel function of the second kind of zeroth order, J_1 is the Bessel function of first kind of the first order, and ϕ_z denoted the vertical component of the normalized right eigenvector at the surface. The surface displacement is computed at the same locations as those used in the experiment and then the same data processing procedure (FK or FP) is used to compute the theoretical effective dispersion curve that can be directly compared with the experimental dispersion curve.

Modelling examples

9.1 Conventional pavement

A conventional pavement system as shown in Table E.1 is modelled and the computed dispersion curve is shown in Figure E.2. The effective dispersion curves are computed with an initial offset of 3 in., receiver spacing of 1 in. and 128 receivers. The theoretical dispersion curves are plotted on a grayscale based on the imaginary part of the wavenumber. Effective dispersion curve computed from the surface displacement calculated using Equation (36) is plotted in red. Higher the imaginary part of the wavenumber, higher the attenuation. Thus, only the darker curves are identifiable at the surface where the measurements are taken during the test. The lower portions of the theoretical dispersion curves roughly below 500 m/s phase velocity are potentially from interface waves at the different layers and do not have an influence in the surface displacement. Other than those, the regions of the dispersion curves that are darker closely correspond to the dispersion curve of the top layer only as shown in Figure 34. This behavior is expected as the wave are leaky, dissipate quickly into the deeper layers as they travel. A few jumps in the effective dispersion curve (red) are observed in the lower frequencies (below 1000 Hz) which is due to the deeper layers and these jump locations are used during the back calculation of the deeper layer properties in Section 3.3. It is also observed that the effective dispersion curve jumps to a higher mode around 8000 Hz in this example. A similar behavior is observed in the experimental results and this jump location is dependent on the asphalt layer properties. A brief study on the influence of asphalt layer viscoelasticity is presented at the end of this appendix.

Table E.1. Conventional Pavement Modelling Example Layer Properties

Layer	Shear velocity (m/s)	Modulus (MPa)	Density (kg/m^3)	Poisson's ratio	Depth (m)
Asphalt	1700	18727	2400	0.35	0.1524
ABC	160	143	2000	0.4	0.254
Subgrade	95	51	2000	0.4	∞

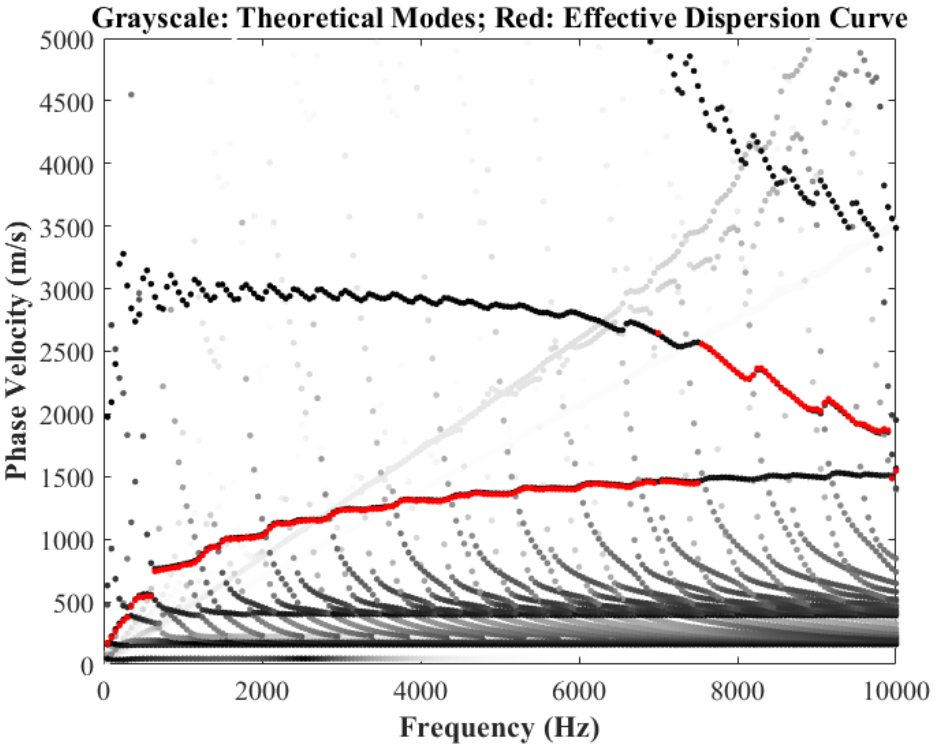

Figure E.2. Theoretical (grayscale) and effective dispersion curve (red) for conventional pavement example.

9.2 Inverted Pavement

An inverted pavement system as shown in Table E.2 is modelled and the computed dispersion curve is shown in Figure E.3. The effective dispersion curves are computed with an initial offset of 3 in., receiver spacing of 1 in. and 128 receivers. Similar to the conventional pavement, the theoretical modes are plotted in grayscale based on the imaginary part of the wavenumber. The theoretical dispersion curves are completely different in comparison to the conventional pavements owing to the existence of the stiff cement treated base and thinner asphalt layer. The effective dispersion curve (red curve) has multiple jumps unlike the conventional pavement.

Table E.2. Inverted Pavement Modelling Example Layer Properties

Layer	Shear velocity (m/s)	Modulus (MPa)	Density (kg/m^3)	Poisson's ratio	Depth (m)
Asphalt	1700	18727	2400	0.35	0.0635
ABC	160	143	2000	0.4	0.1524
CTB	1500	12420	2400	0.15	0.2032
Subgrade	95	51	2000	0.4	∞

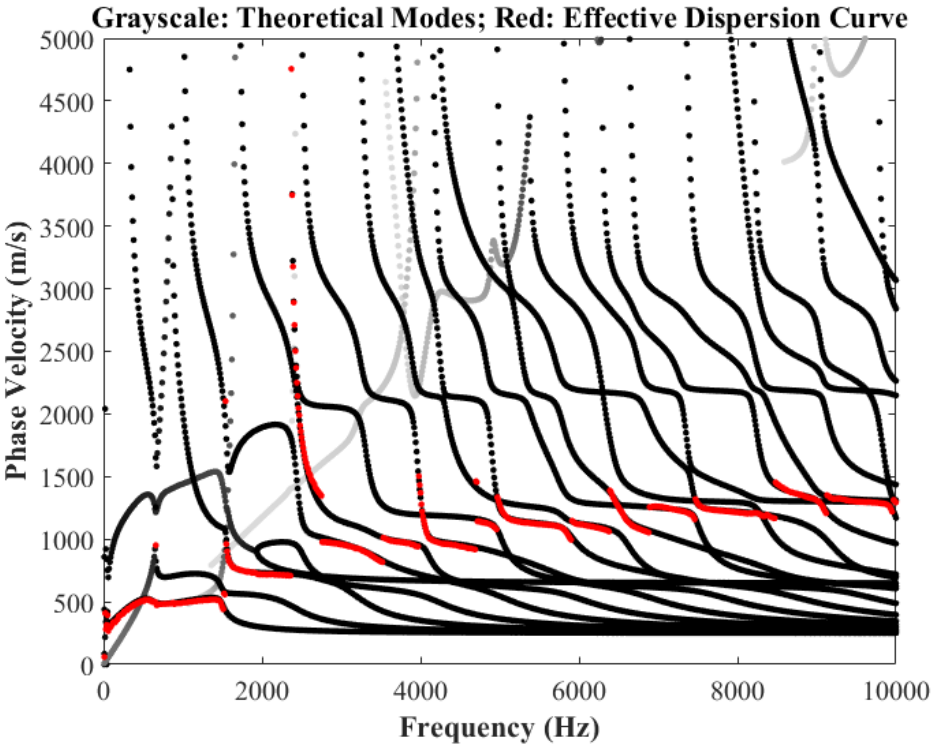

Figure E.3. Theoretical (grayscale) and effective dispersion curve (red) for inverted pavement example.

9.3 Effect of Viscosity

It is well known that asphalt is a viscoelastic material, and its complex modulus is frequency dependent. Viscoelastic behavior can potentially have a significant effect on the computed effective dispersion curve and needs to be evaluated. In this section a freestanding pavement layer is evaluated with elastic and viscoelastic properties at different temperatures (10°C, 20°C, and 30°C) and is shown in Figure E.4. Dynamic modulus was computed as function of frequency at each temperature using 2S2P1D model parameters fitted through laboratory tests conducted on typical NC pavement mix, RS9.5C. Viscoelasticity increases the damping of certain modes in specific frequency ranges leading to their addition or disappearance in the effective dispersion curve. At lower frequencies, the shape of the higher velocity modes is different for the viscoelastic layer in comparison to the elastic layer. Additionally, adding viscoelasticity changes location of the jump seen in the red curve and is also a function of the pavement temperature. While forward modelling with added viscoelasticity is simple, complexity of inverting for the asphalt layer properties from the experimental dispersion curve depends on the viscoelastic model assumed. The simplest model reported in the literature is the use of power law to approximate the shear wave velocities dependence on frequency but extrapolating this over other frequency ranges will not provide accurate results (Barnes and Trottier 2009; Ryden and Park 2016). But just two parameters are required for the power law description of the shear wave velocity which is an advantage from the inversion perspective. More complicated models such as the sigmoidal curve or the 2S2P1D models require more parameters and it may not be possible to invert for all the parameters from surface wave testing data. Nevertheless, addition of viscoelasticity and inclusion of the higher

modes observed in the experimental data could lead to a more accurate estimates of the layer moduli.

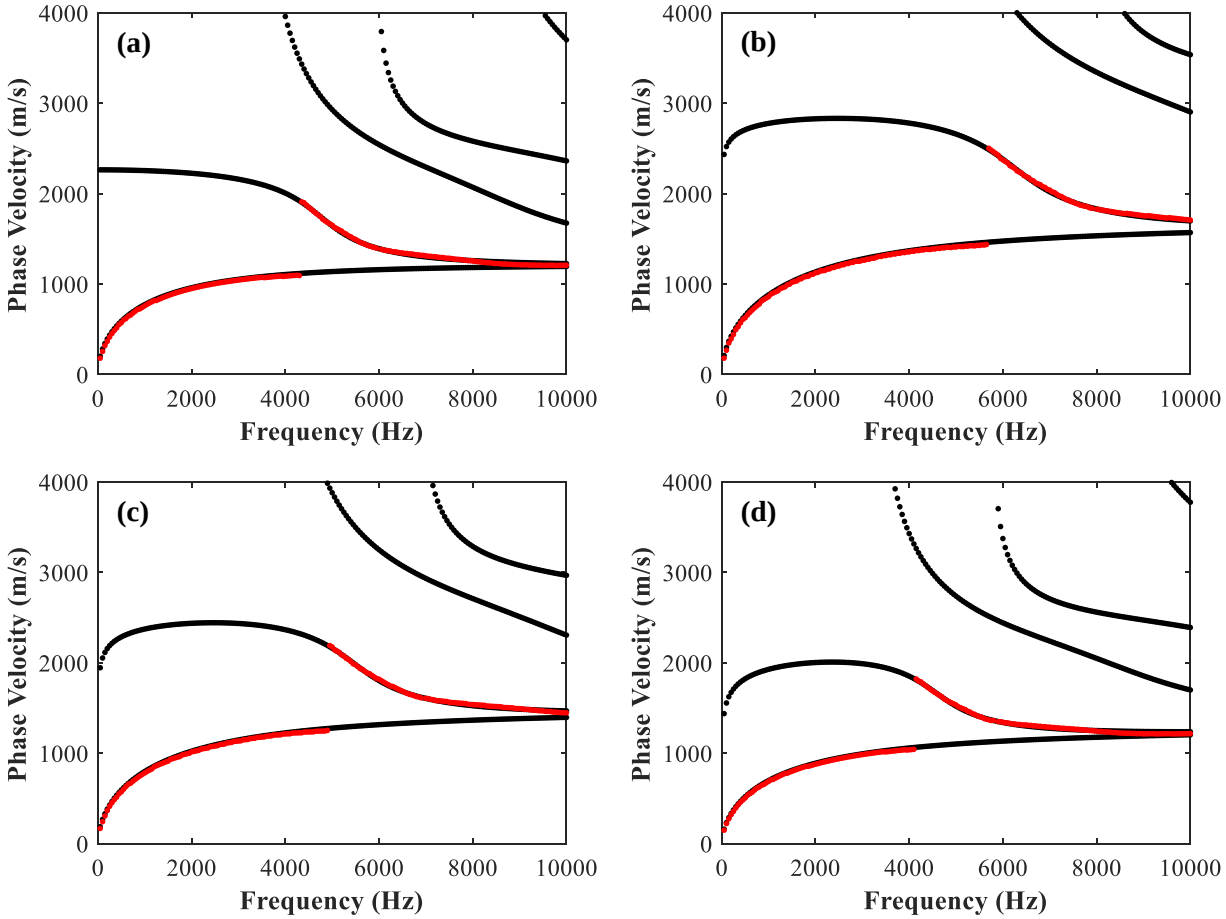

Figure E.4. Effect of viscosity of the asphalt layer; (a) Elastic asphalt layer (b) viscoelastic asphalt layer at 10°C, (c) viscoelastic asphalt layer at 20°C, and (d) viscoelastic asphalt layer at 30°C.

Appendix E References

Barnes, C.L. and Trottier, J.F. (2009). Evaluating High-Frequency Visco-Elastic Moduli in Asphalt Concrete. *Research in Nondestructive Evaluation*, *20*(2), 116-130.

Kausel, E. and Peek, R. (1982). Dynamic Loads in the Interior of a Layered Stratum: An Explicit Solution. *Bulletin of the Seismological Society of America*, 72(5), 1459-1481.

Rydèn, N. and Park, C.B. (2006). Fast Simulated Annealing Inversion of Surface Waves on Pavement Using Phase-Velocity Spectra. *Geophysics*, 71(4). R49-R58.

Vaziri, A.A. and Guddati, M.N. (2016). Improved Inversion Algorithms for Near-Surface Characterization. *Geophysical Journal International*, 206, 1410-1423.

This page is intentionally blank

APPENDIX F: SURFACE WAVE TESTING DATA

Different sensors were used during the testing as listed in Table F.1, but the data used in the analysis for this report were from the sensor code named "RegS". The legend of the plots follows the codenames mentioned in Table F.1. The other sensors were equivalent and did not show any differences in the portion of the dispersion curve used. In addition, since a four-channel data acquisition system was used in the experimental setup, whenever possible the response from up to three sensors were acquired. These sensors are named "S1", "S2", and "S3" in increasing distance from the first impact.

Table F.1. Sensor Legend

Sensor	Description	Code Name
PCB 352C33 (Uniaxial)	100 mV/g sensitivity	RegS
PCB 333B40 (Uniaxial)	500 mV/g sensitivity	HSen
PCB 356A45 (Triaxial with 100 mV/g sensitivity)	Parallel to the pavement surface along test line	TriX
	Perpendicular to pavement surface	TriY
	Parallel to pavement and perpendicular to the test line	TriZ

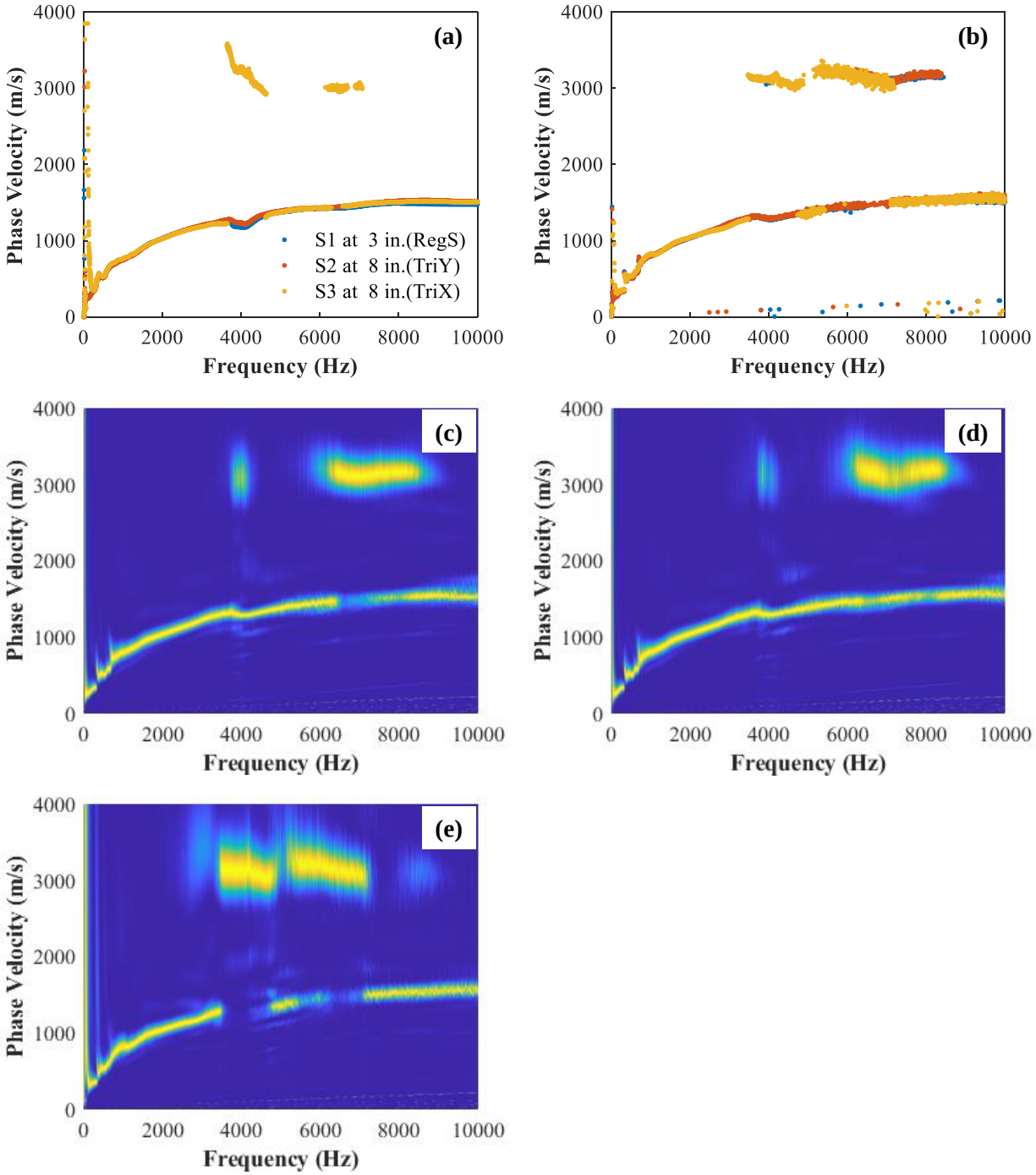

Figure F.1. CS1O at 6°C; (a) FK 64 offsets at 1 in. spacing, (b) FP peak from full array, (c) FP spectrum sensor 1, (d) FP spectrum sensor 2, and (e) FP spectrum sensor 3.

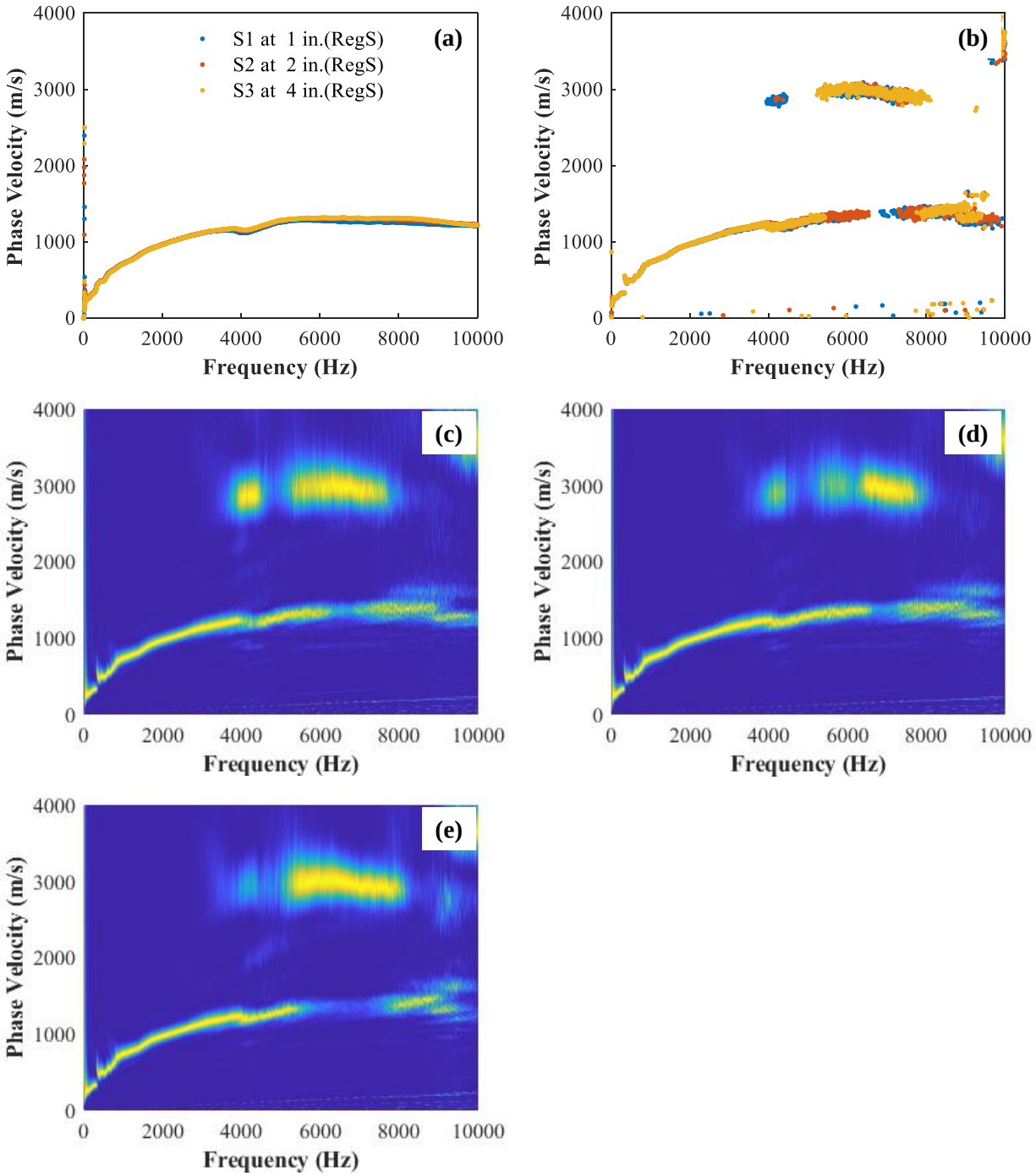

Figure F.2. CS1O at 23°C; (a) FK 64 offsets at 1 in. spacing, (b) FP peak from full array, (c) FP spectrum sensor 1, (d) FP spectrum sensor 2, and (e) FP spectrum sensor 3.

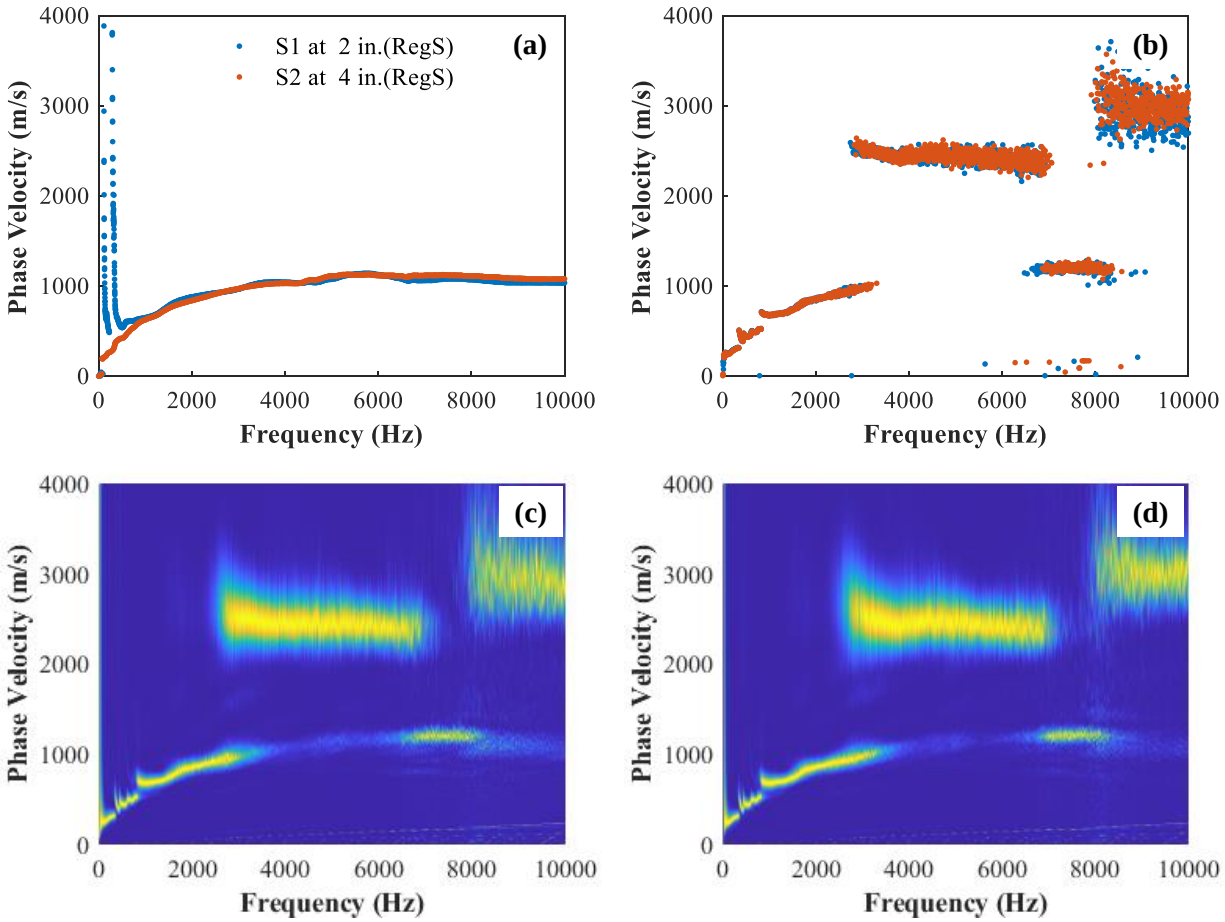

Figure F.3. CS1O at 32°C; (a) FK 64 offsets at 1 in. spacing, (b) FP peak from full array, (c) FP spectrum sensor 1, and (d) FP spectrum sensor 2.

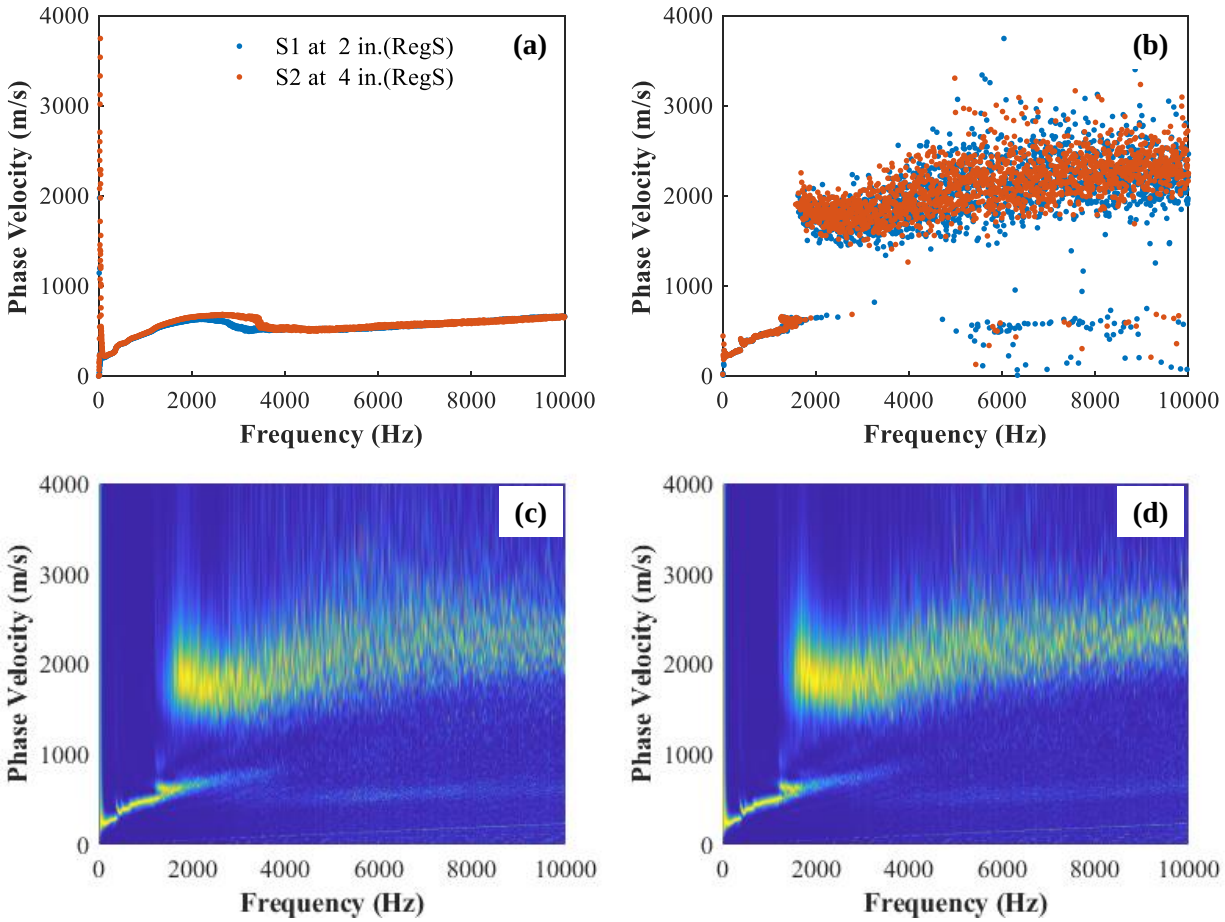

Figure F.4. CS1O at 51°C; (a) FK 64 offsets at 1 in. spacing, (b) FP peak from full array, (c) FP spectrum sensor 1, and (d) FP spectrum sensor 2.

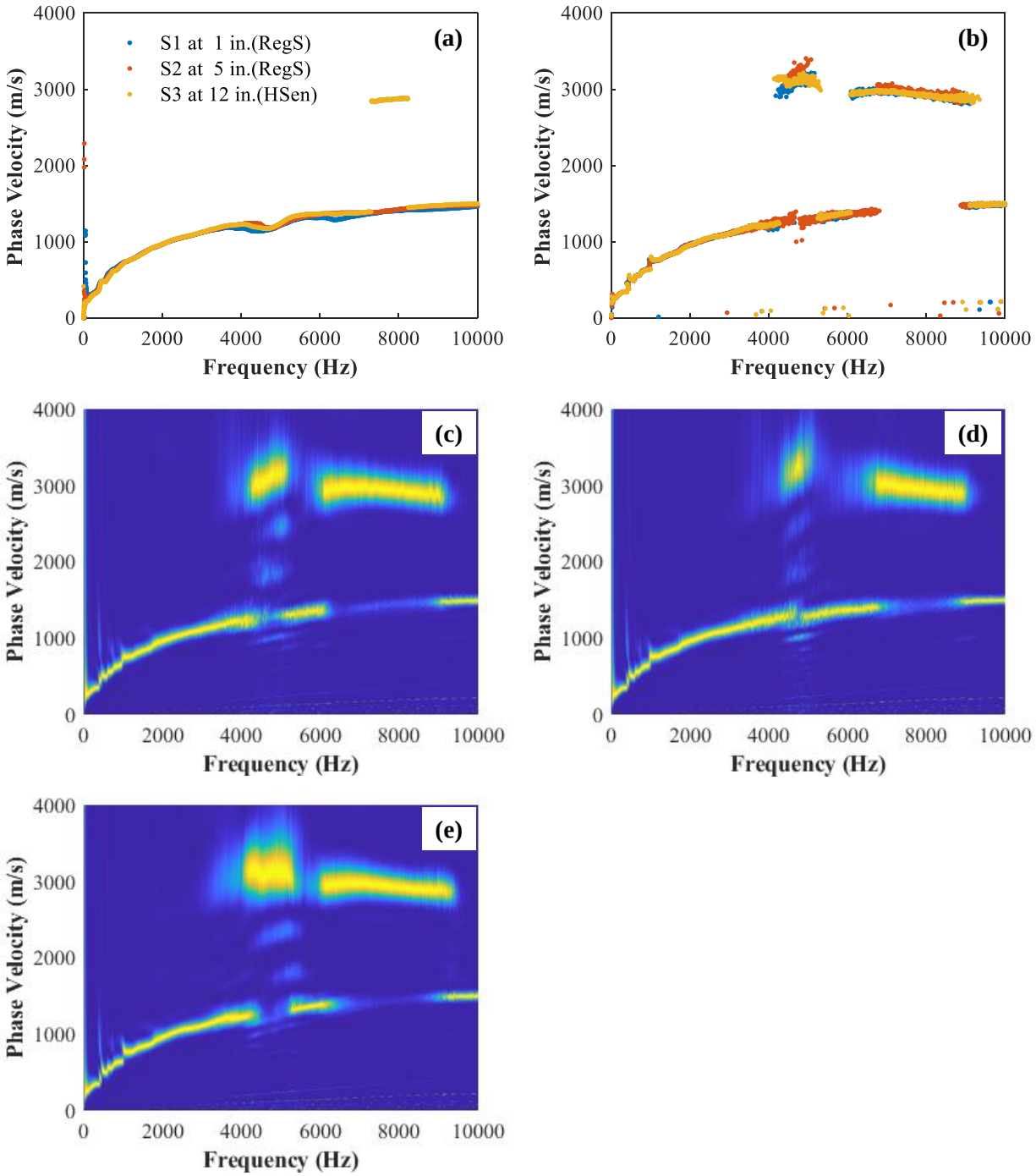

Figure F.5. CS1C at 6°C; (a) FK 64 offsets at 1 in. spacing, (b) FP peak from full array, (c) FP spectrum sensor 1, (d) FP spectrum sensor 2, and (e) FP spectrum sensor 3.

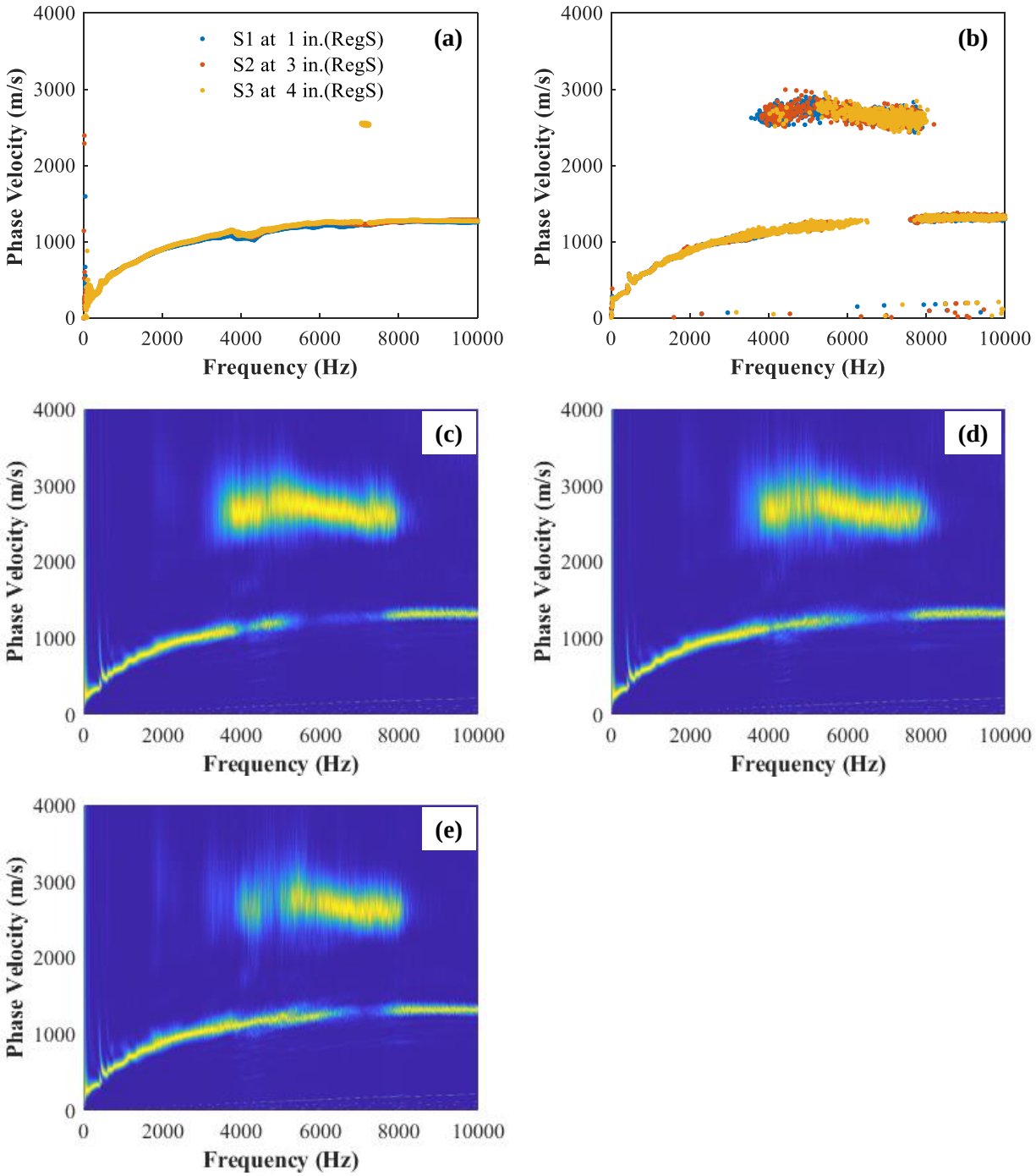

Figure F.6. CS1C at 22°C; (a) FK 64 offsets at 1 in. spacing, (b) FP peak from full array, (c) FP spectrum sensor 1, (d) FP spectrum sensor 2, and (e) FP spectrum sensor 3.

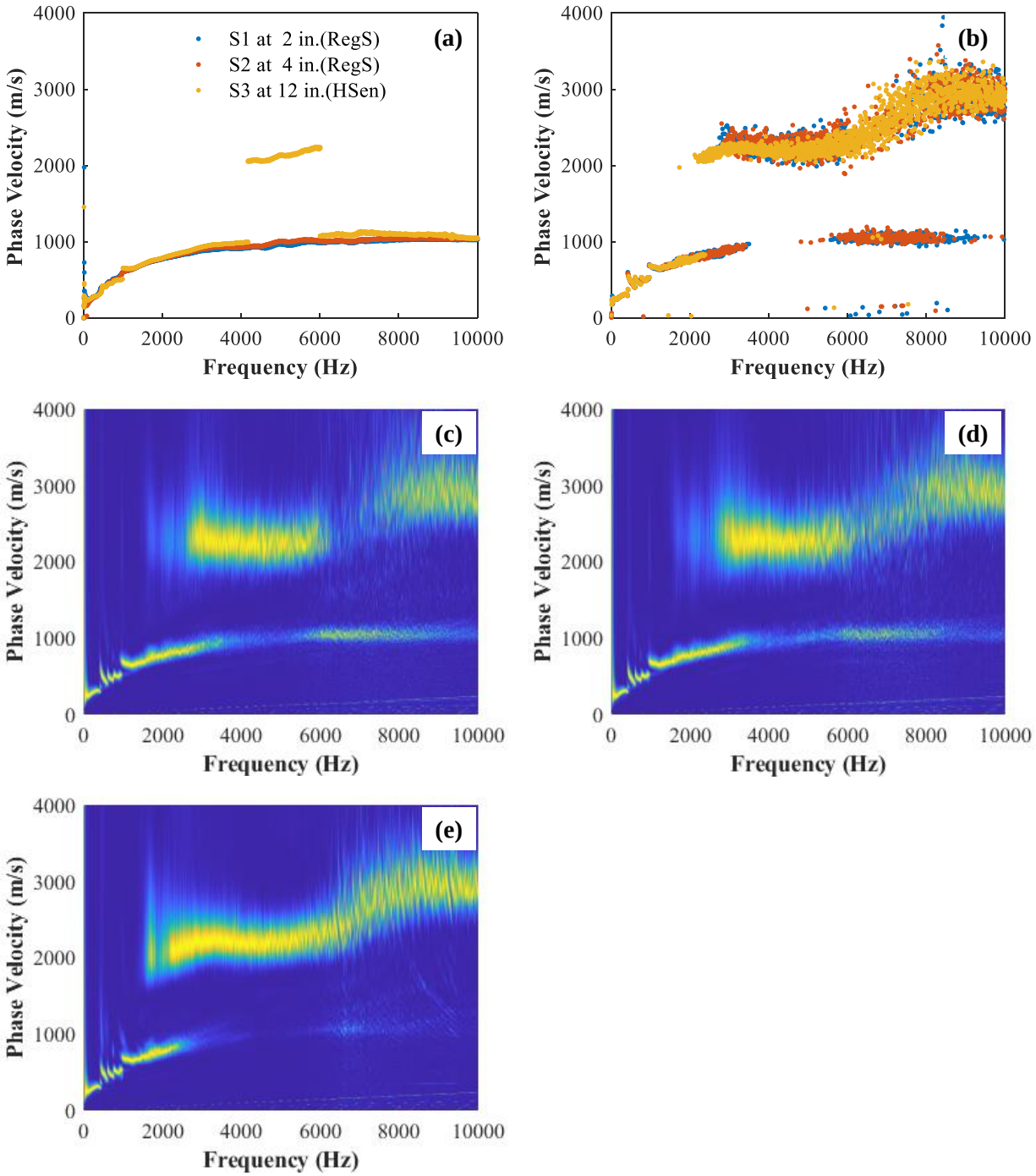

Figure F.7. CS1C at 29°C; (a) FK 64 offsets at 1 in. spacing, (b) FP peak from full array, (c) FP spectrum sensor 1, (d) FP spectrum sensor 2, and (e) FP spectrum sensor 3.

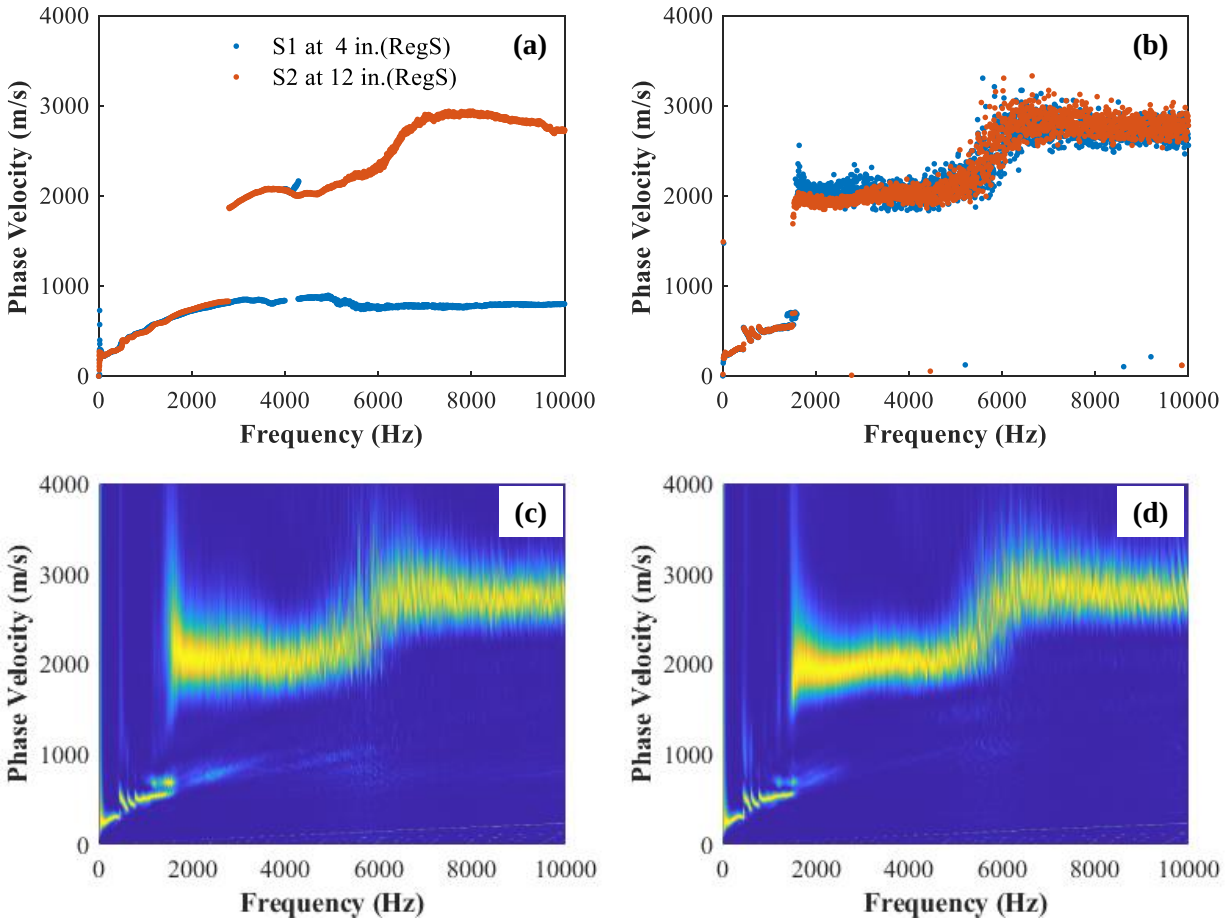

Figure F.8. CS1C at 41°C; (a) FK 64 offsets at 1 in. spacing, (b) FP peak from full array, (c) FP spectrum sensor 1, and (d) FP spectrum sensor 2.

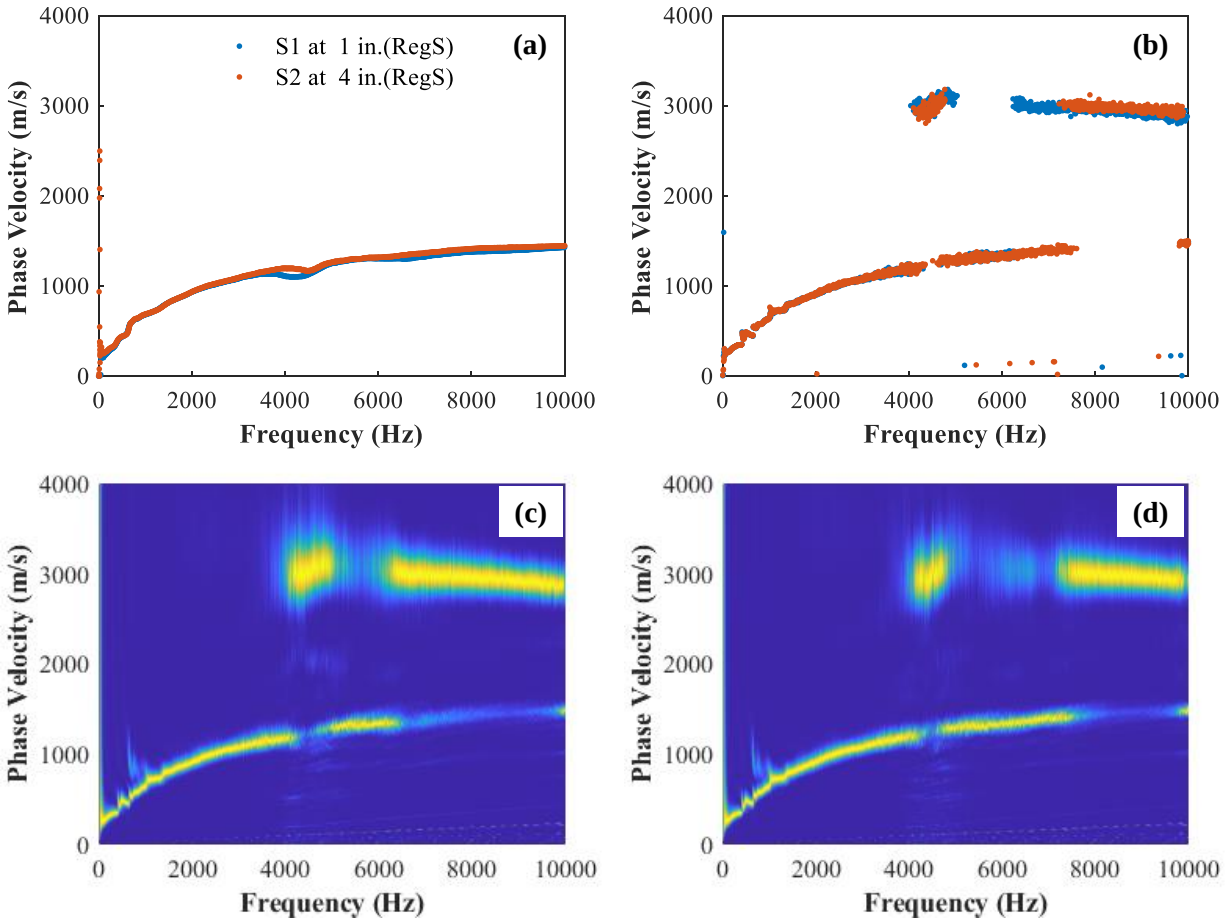

Figure F.9. CS1I at 7°C; (a) FK 64 offsets at 1 in. spacing, (b) FP peak from full array, (c) FP spectrum sensor 1, and (d) FP spectrum sensor 2.

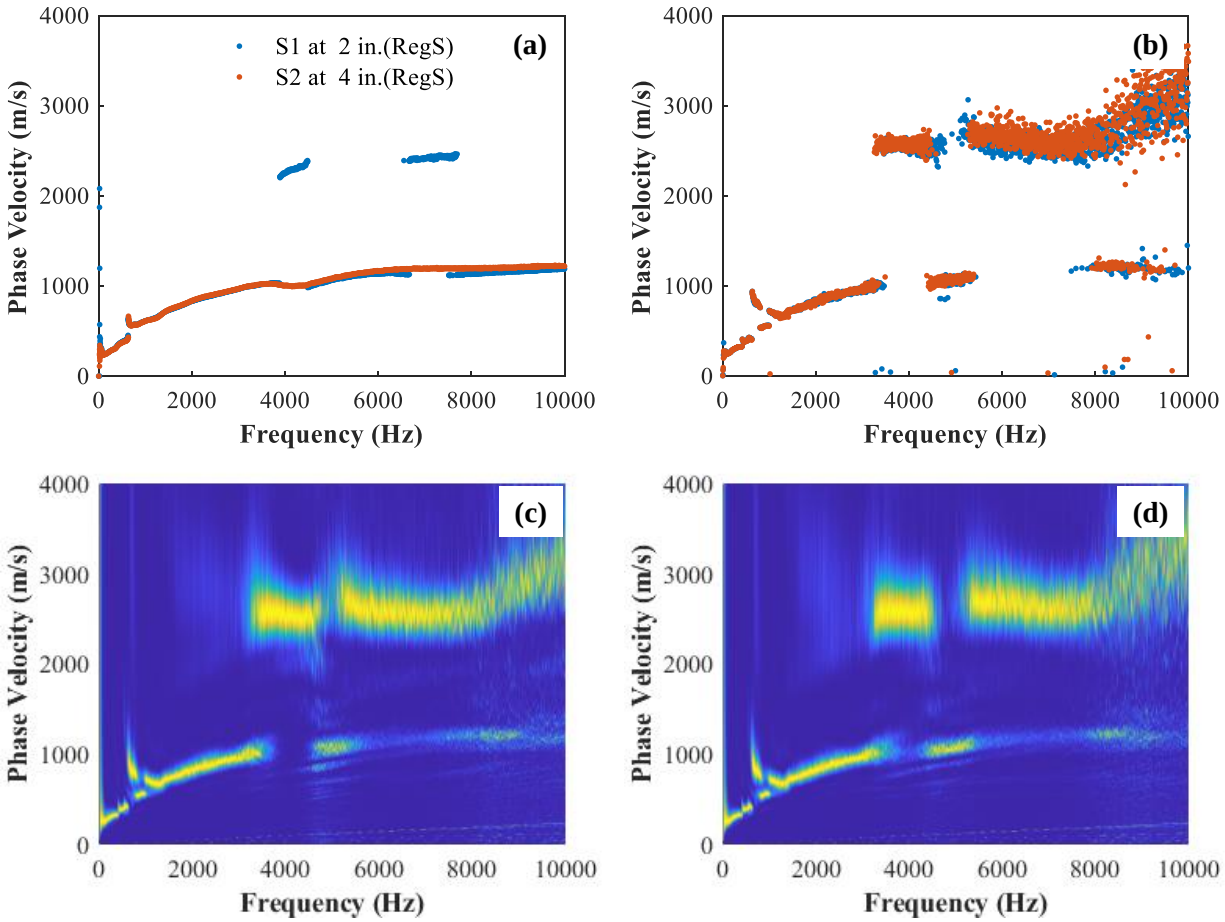

Figure F.10. CS1I at 25°C; (a) FK 64 offsets at 1 in. spacing, (b) FP peak from full array, (c) FP spectrum sensor 1, and (d) FP spectrum sensor 2.

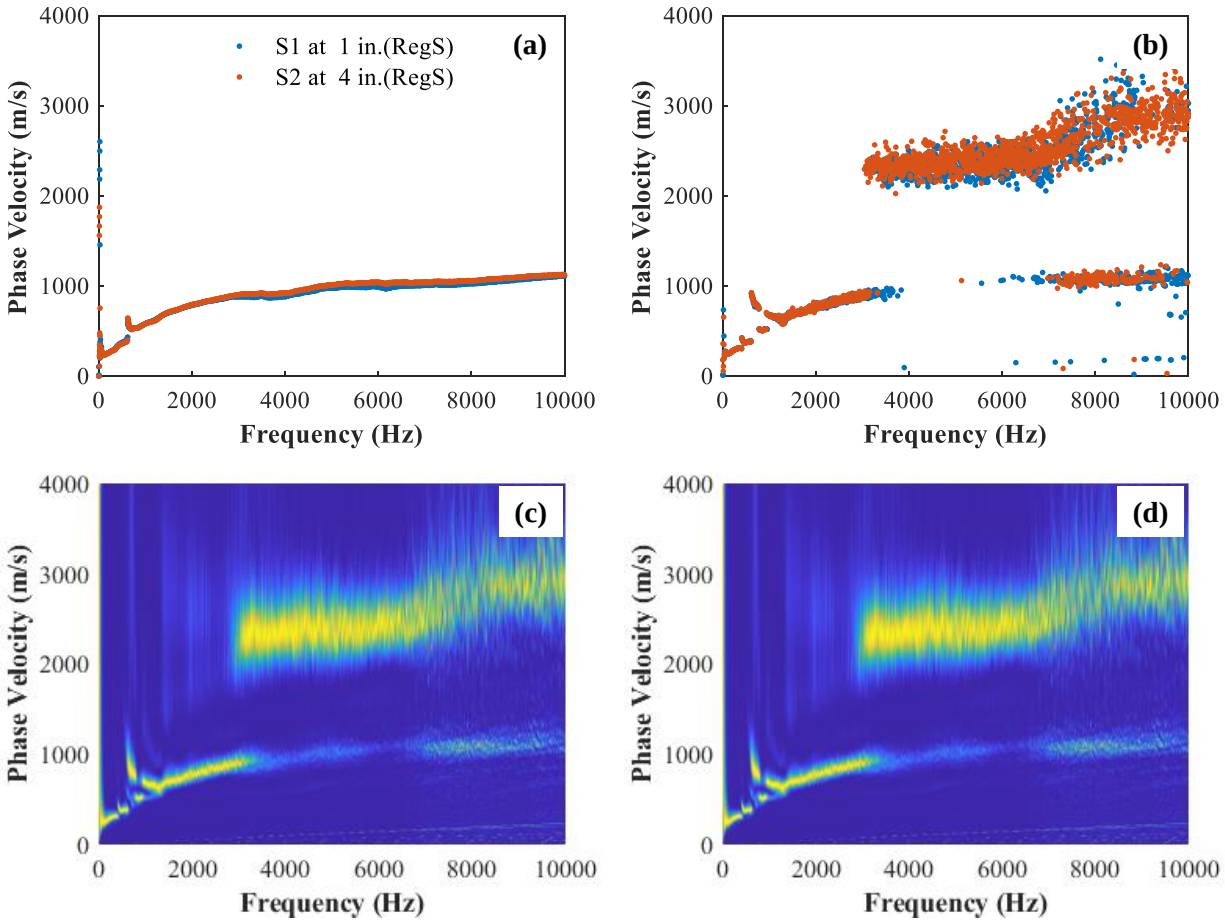

Figure F.11. CS1I at 27°C; (a) FK 64 offsets at 1 in. spacing, (b) FP peak from full array, (c) FP spectrum sensor 1, and (d) FP spectrum sensor 2.

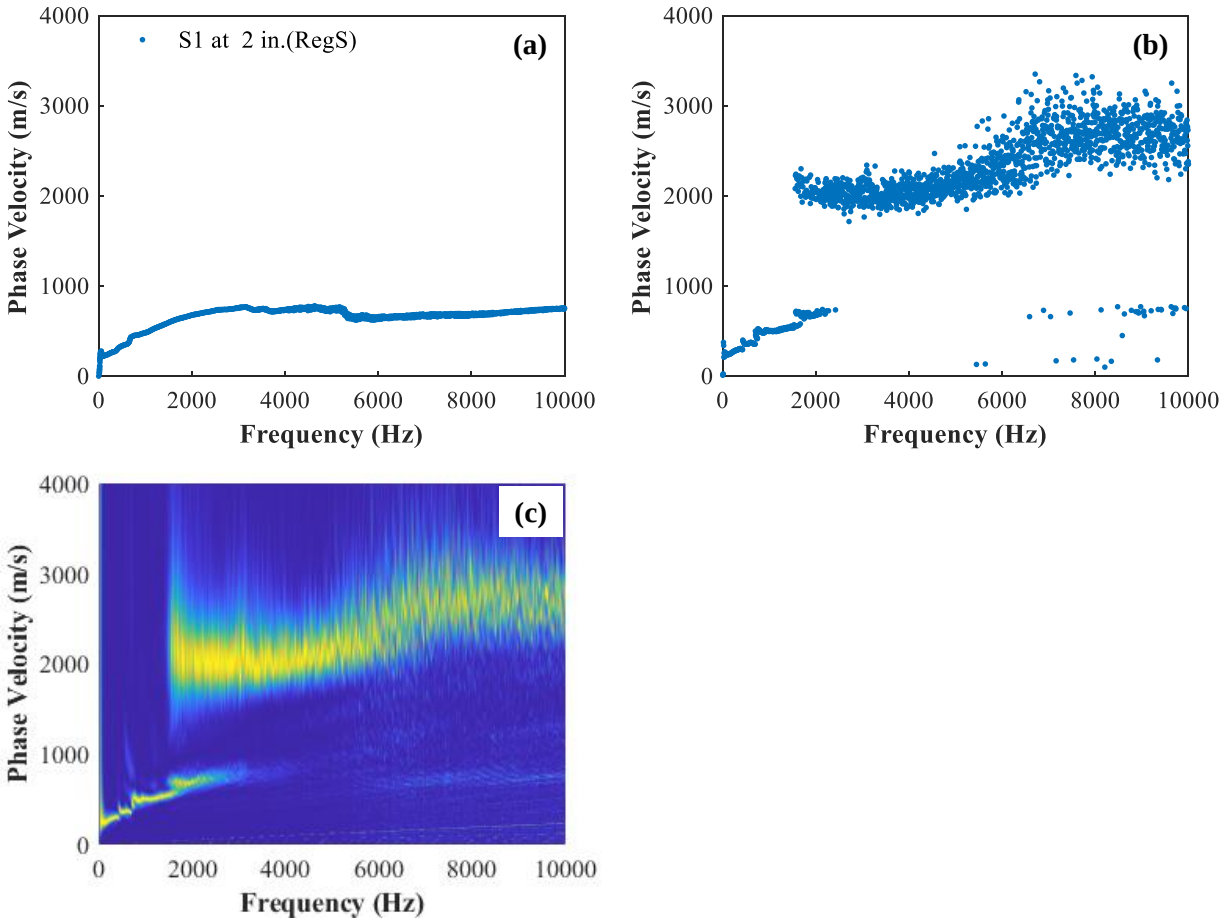

Figure F.12. CS1I at 40°C; (a) FK 64 offsets at 1 in. spacing, (b) FP peak from full array, and (c) FP spectrum sensor 1.

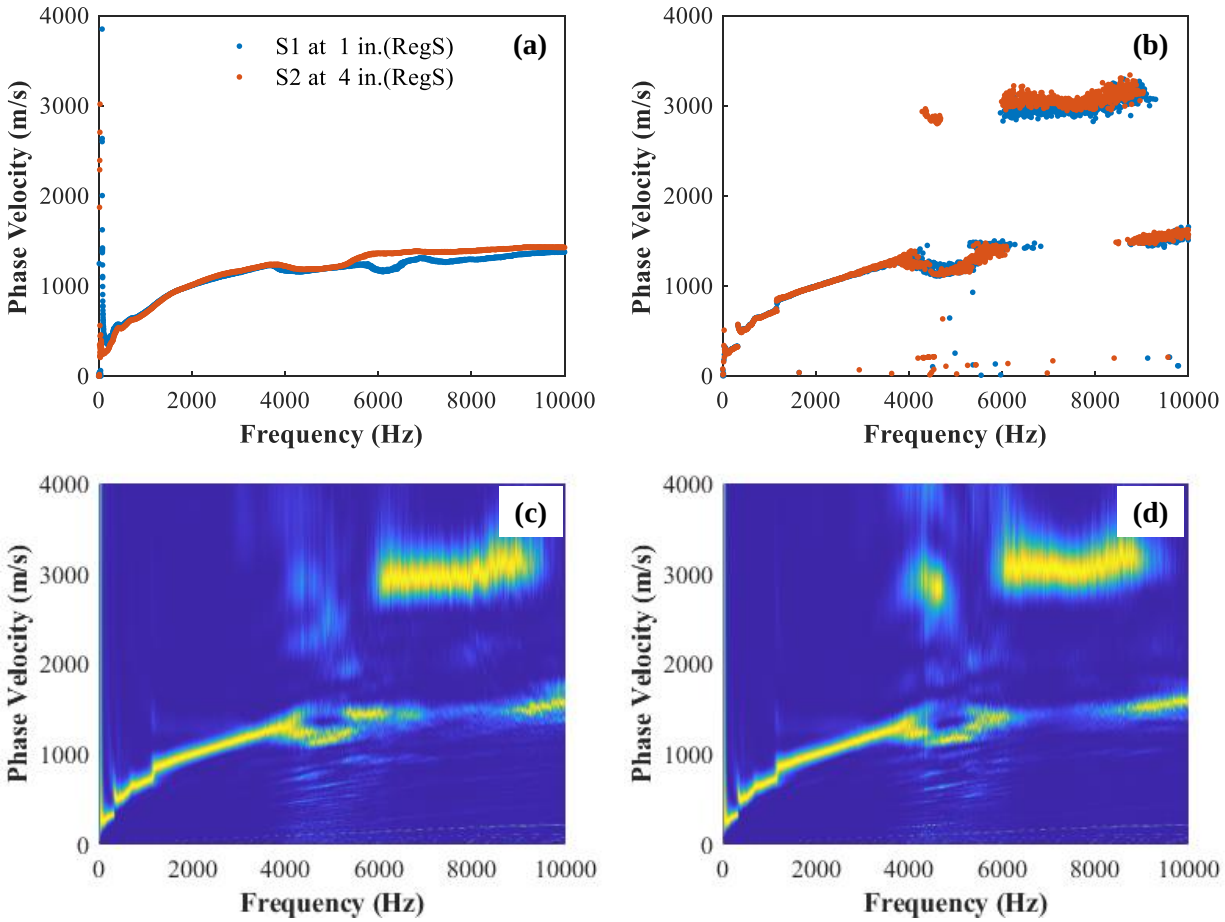

Figure F.13. CS2O at 13°C; (a) FK 64 offsets at 1 in. spacing, (b) FP peak from full array, (c) FP spectrum sensor 1, and (d) FP spectrum sensor 2.

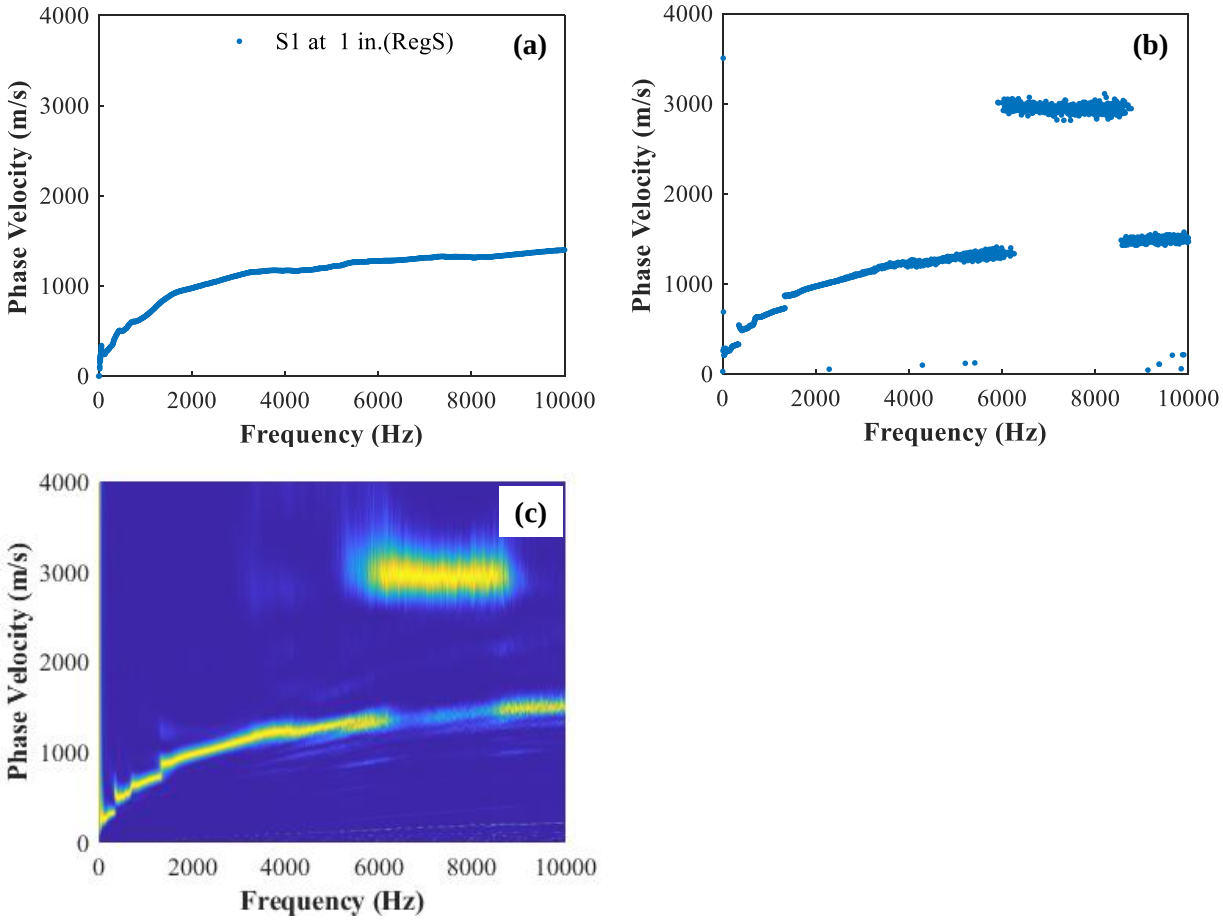

Figure F.14. CS2O at 17°C; (a) FK 64 offsets at 1 in. spacing, (b) FP peak from full array, and (c) FP spectrum sensor 1.

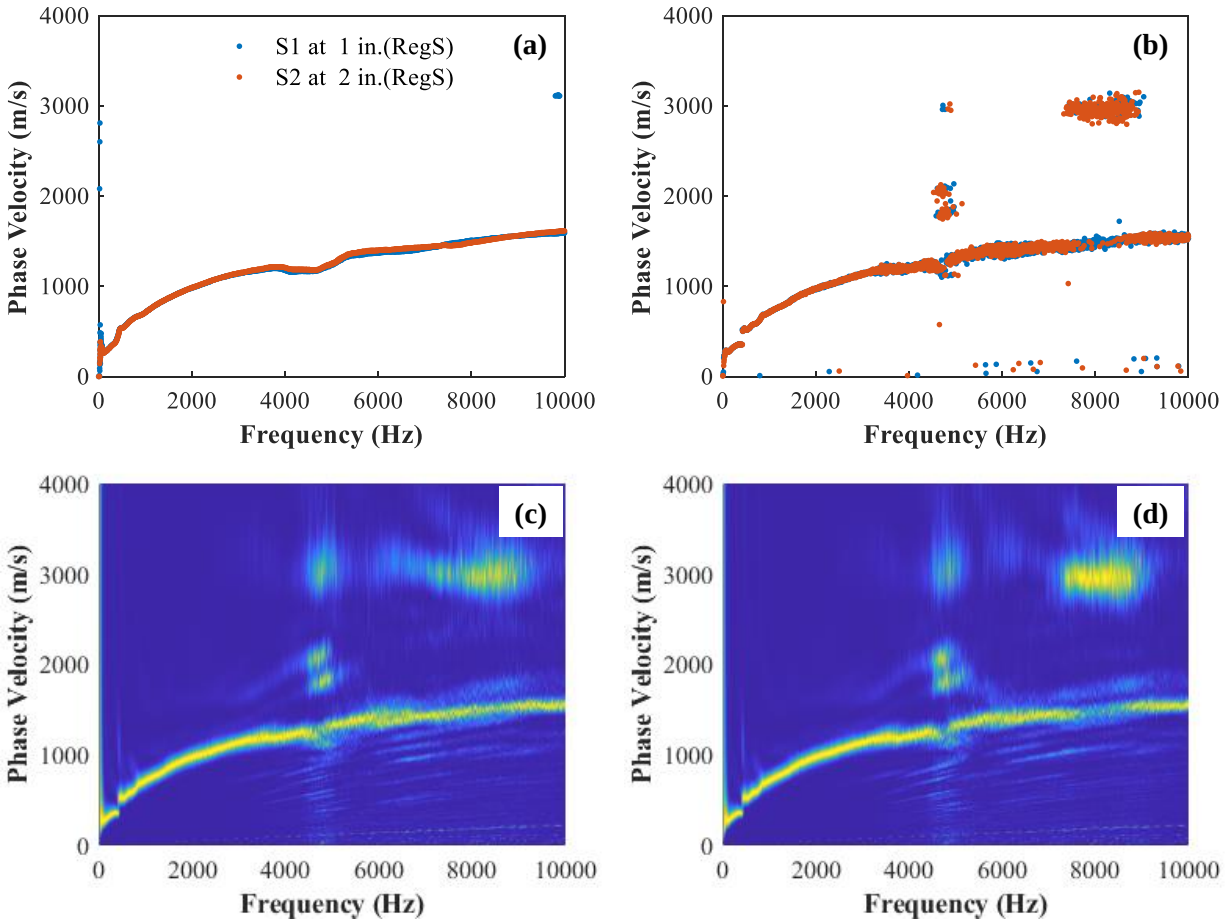

Figure F.15. CS2C at 16°C; (a) FK 64 offsets at 1 in. spacing, (b) FP peak from full array, (c) FP spectrum sensor 1, and (d) FP spectrum sensor 2.

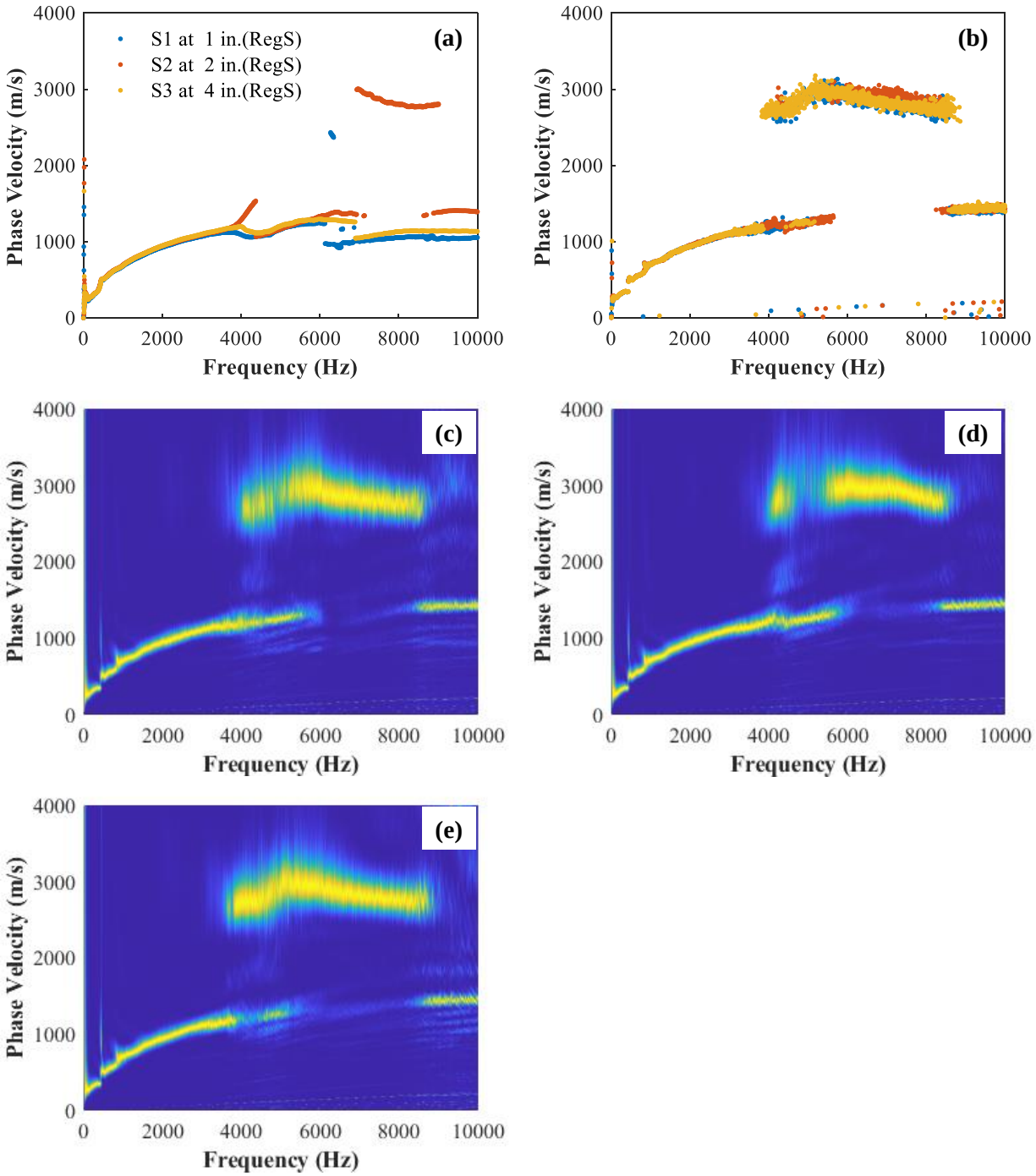

Figure F.16. CS2C at 19°C; (a) FK 64 offsets at 1 in. spacing, (b) FP peak from full array, (c) FP spectrum sensor 1, (d) FP spectrum sensor 2, and (e) FP spectrum sensor 3.

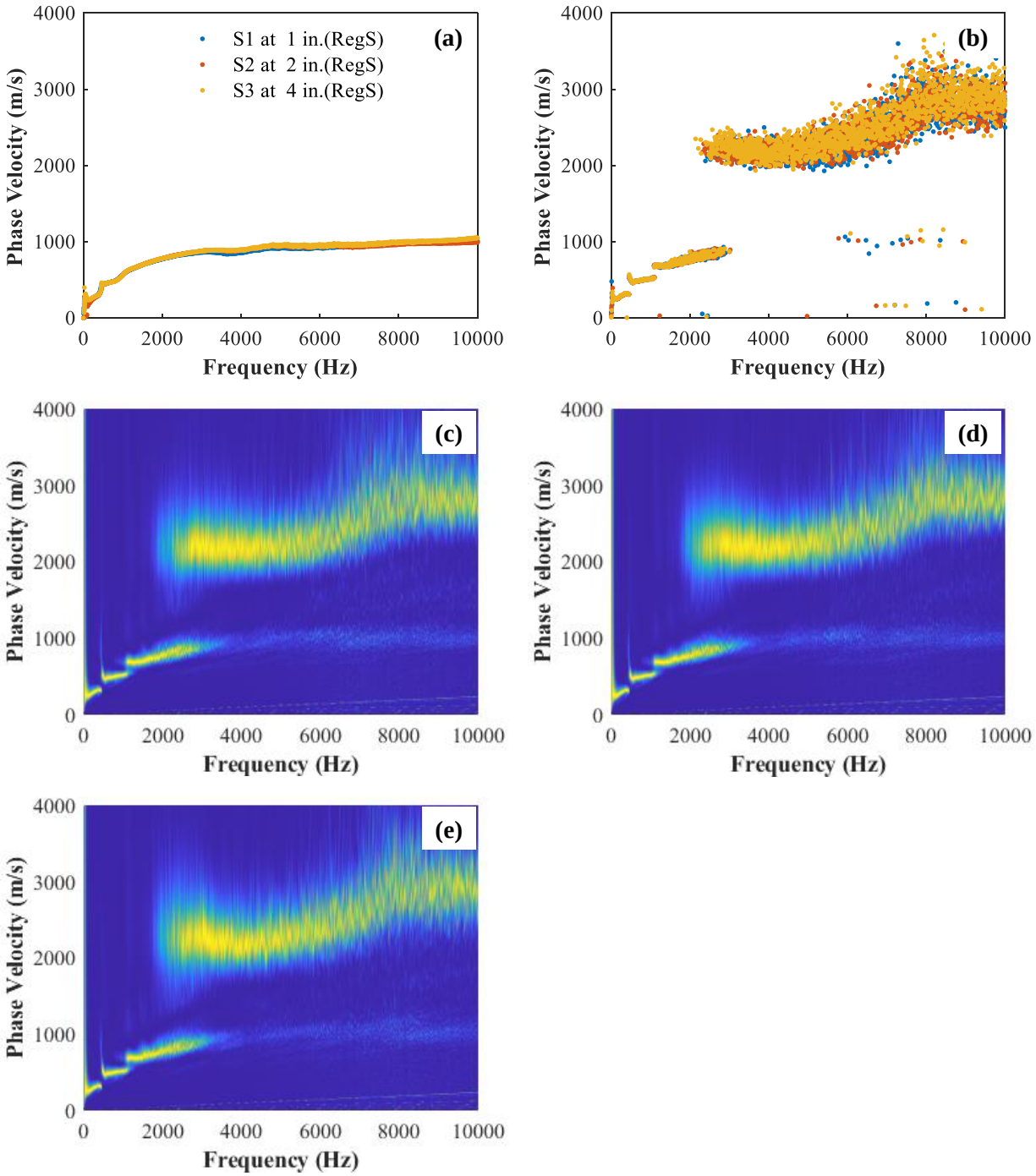

Figure F.17. CS2C at 37°C; (a) FK 64 offsets at 1 in. spacing, (b) FP peak from full array, (c) FP spectrum sensor 1, (d) FP spectrum sensor 2, and (e) FP spectrum sensor 3.

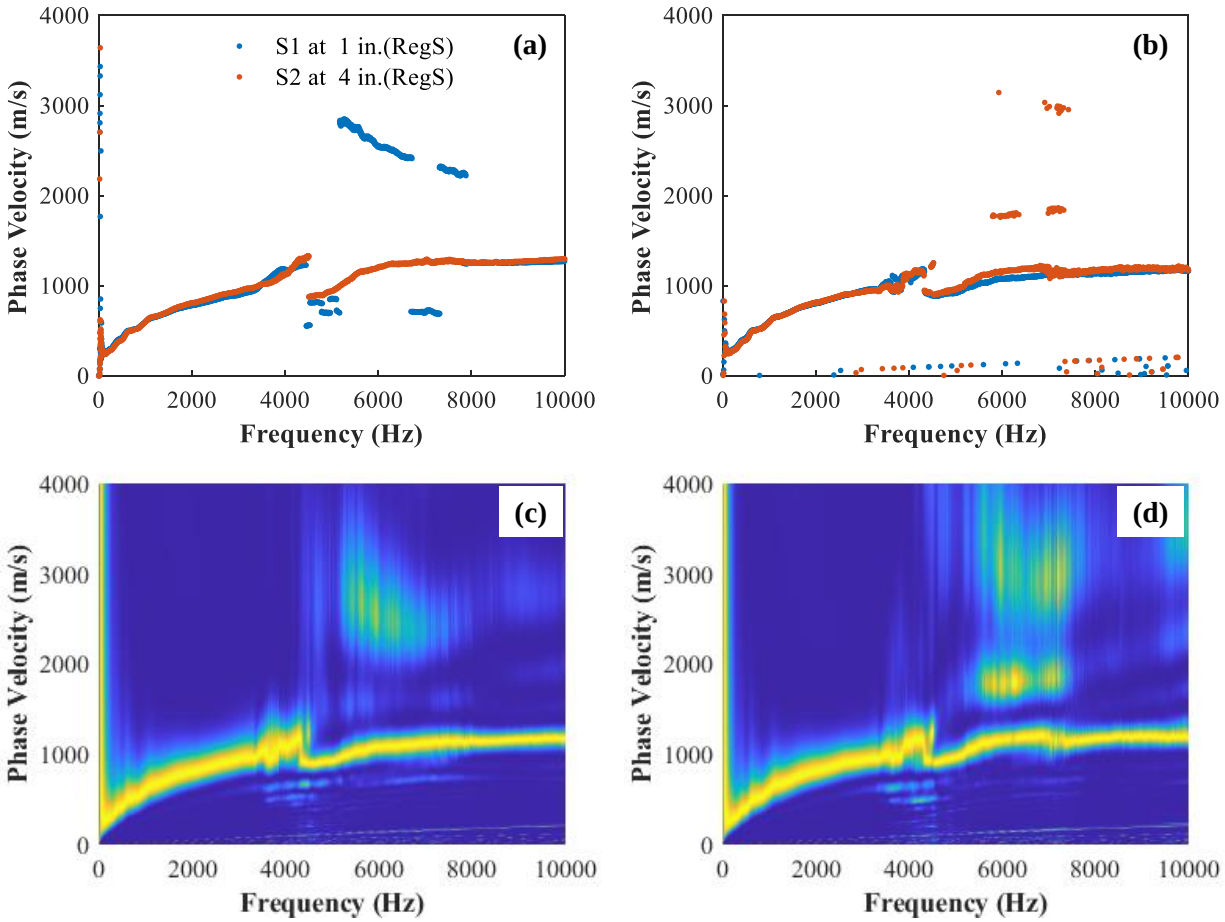

Figure F.18. CCS3C-CCS2C at 29°C; (a) FK 32 offsets at 1 in. spacing, (b) FP peak from 32 offsets, (c) FP spectrum sensor 1, and (d) FP spectrum sensor 2.

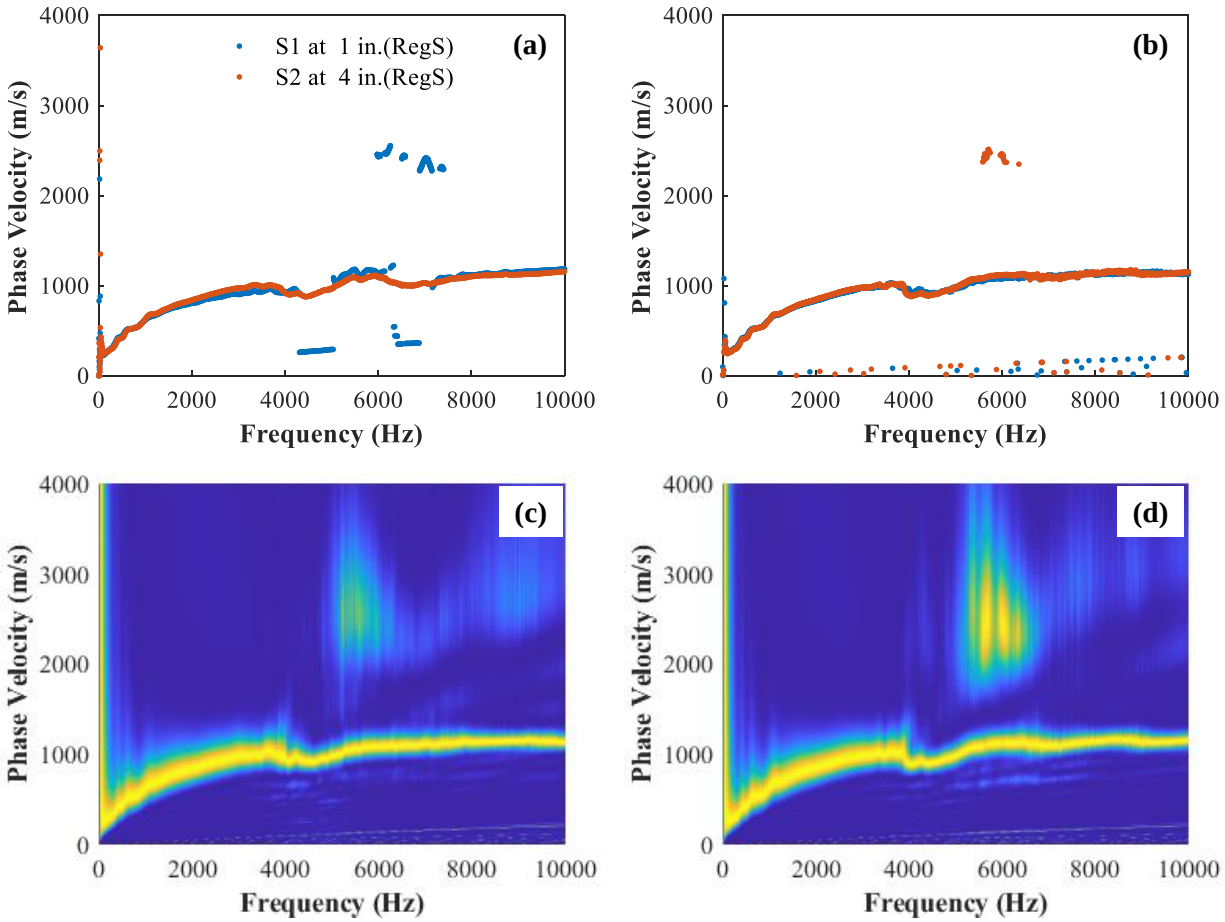

Figure F.19. CCS2C-CCS1C at 28°C; (a) FK 32 offsets at 1 in. spacing, (b) FP peak from 32 offsets, (c) FP spectrum sensor 1, and (d) FP spectrum sensor 2.

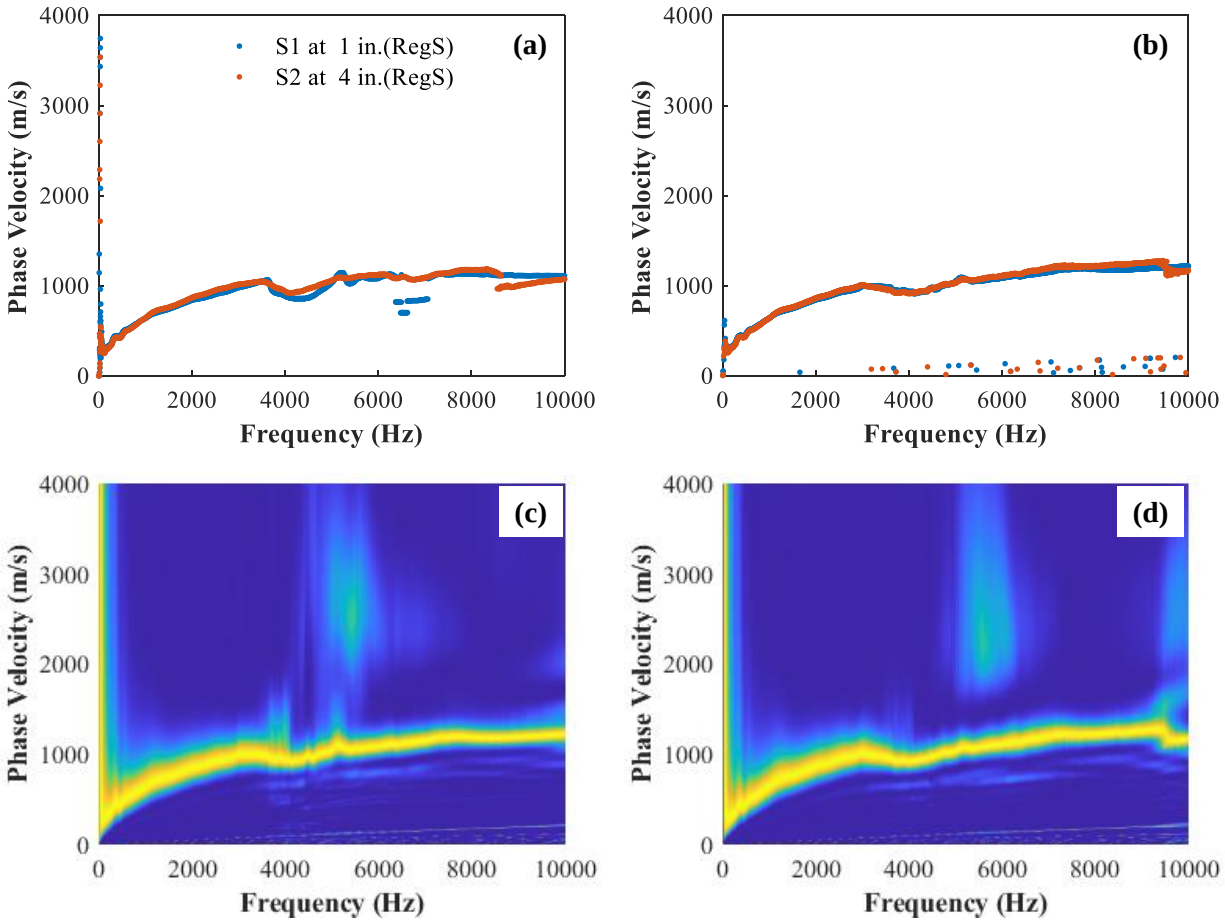

Figure F.20. CCS3O-CCS2O at 27°C; (a) FK 32 offsets at 1 in. spacing, (b) FP peak from 32 offsets, (c) FP spectrum sensor 1, and (d) FP spectrum sensor 2.

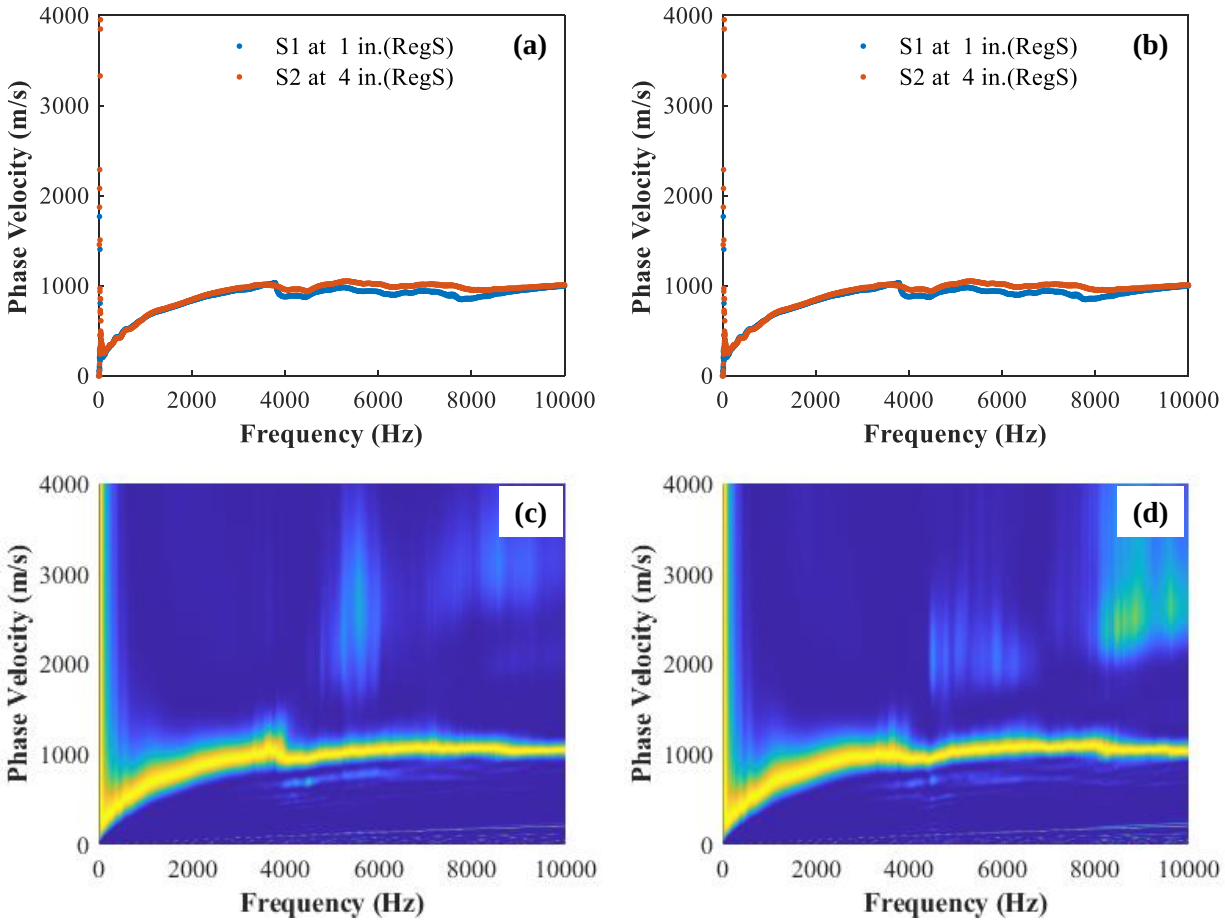

Figure F.21. CCS2O-CCS1O at 28°C; (a) FK 32 offsets at 1 in. spacing, (b) FP peak from 32 offsets, (c) FP spectrum sensor 1, and (d) FP spectrum sensor 2.

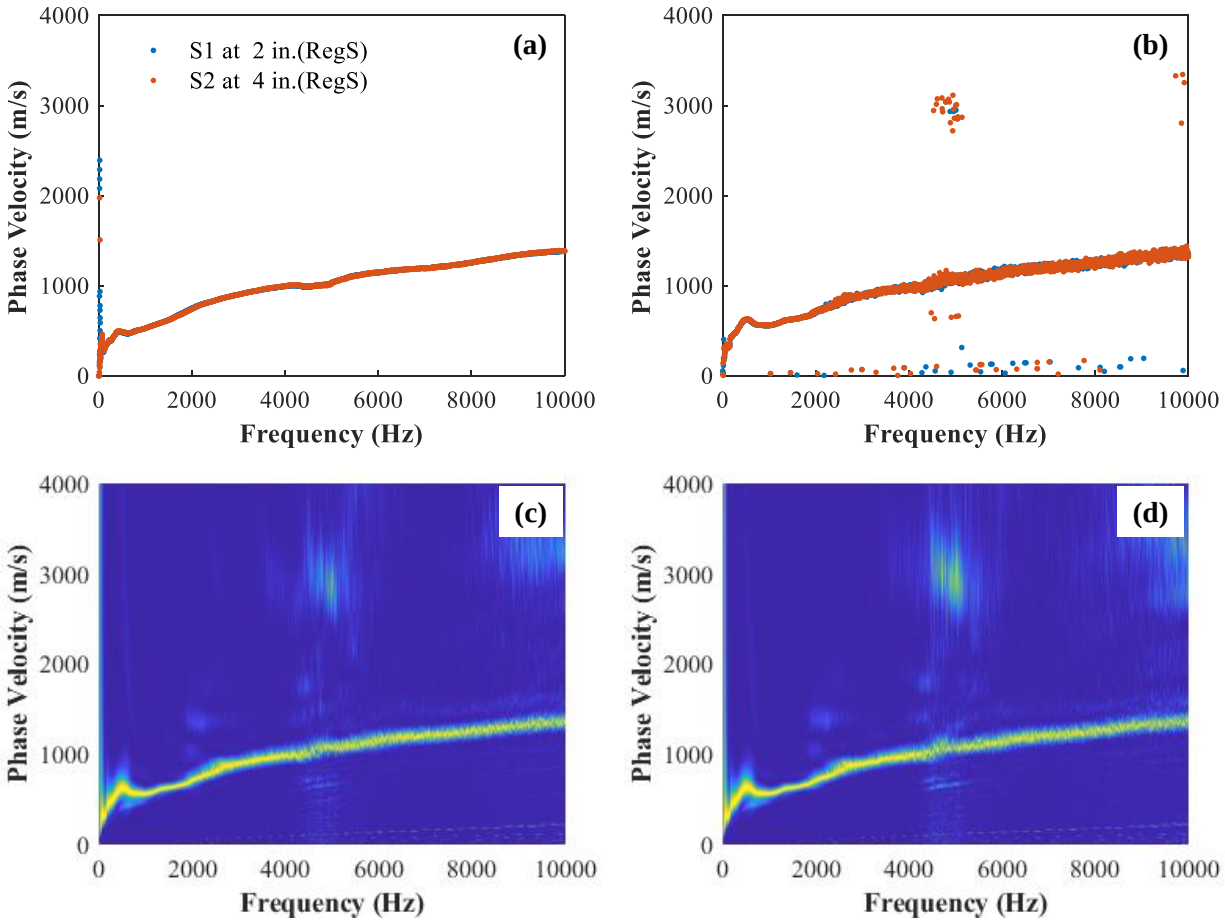

Figure F.22. IS1O at 13°C; (a) FK 64 offsets at 1 in. spacing, (b) FP peak from full array, (c) FP spectrum sensor 1, and (d) FP spectrum sensor 2.

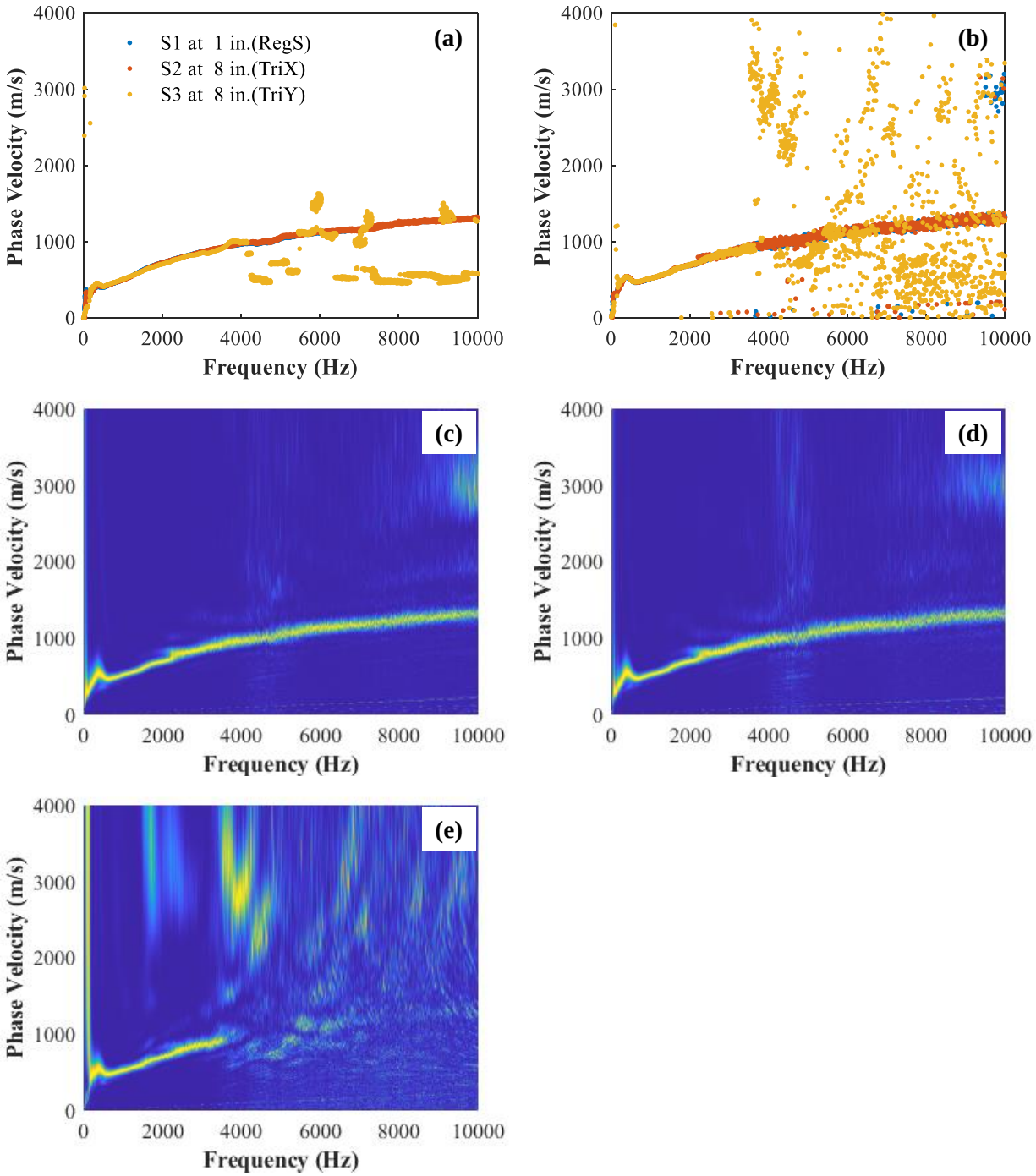

Figure F.23. IS1O at 19°C; (a) FK 64 offsets at 1 in. spacing, (b) FP peak from full array, (c) FP spectrum sensor 1, (d) FP spectrum sensor 2, and (e) FP spectrum sensor 3.

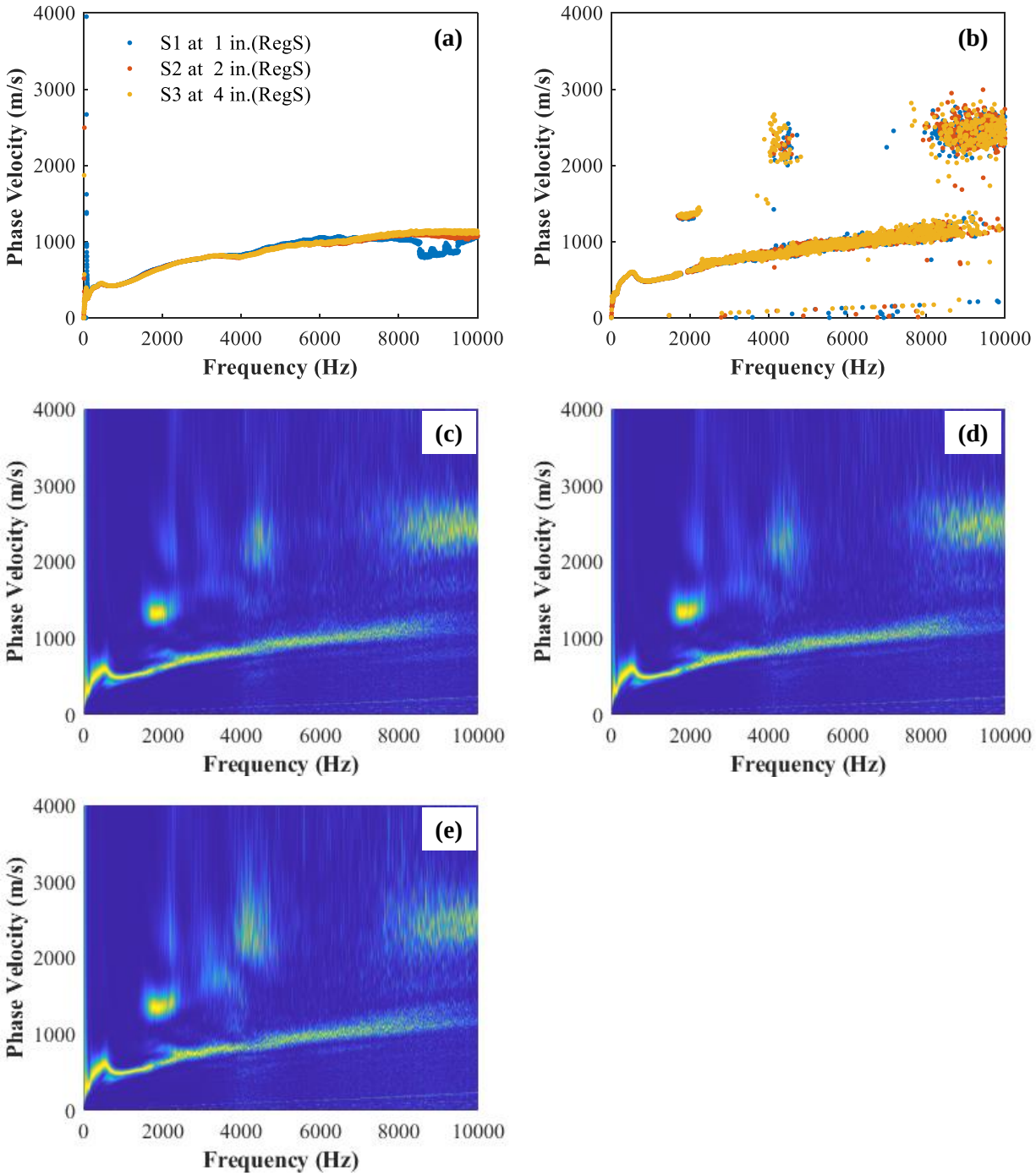

Figure F.24. IS1O at 30°C; (a) FK 64 offsets at 1 in. spacing, (b) FP peak from full array, (c) FP spectrum sensor 1, (d) FP spectrum sensor 2, and (e) FP spectrum sensor 3.

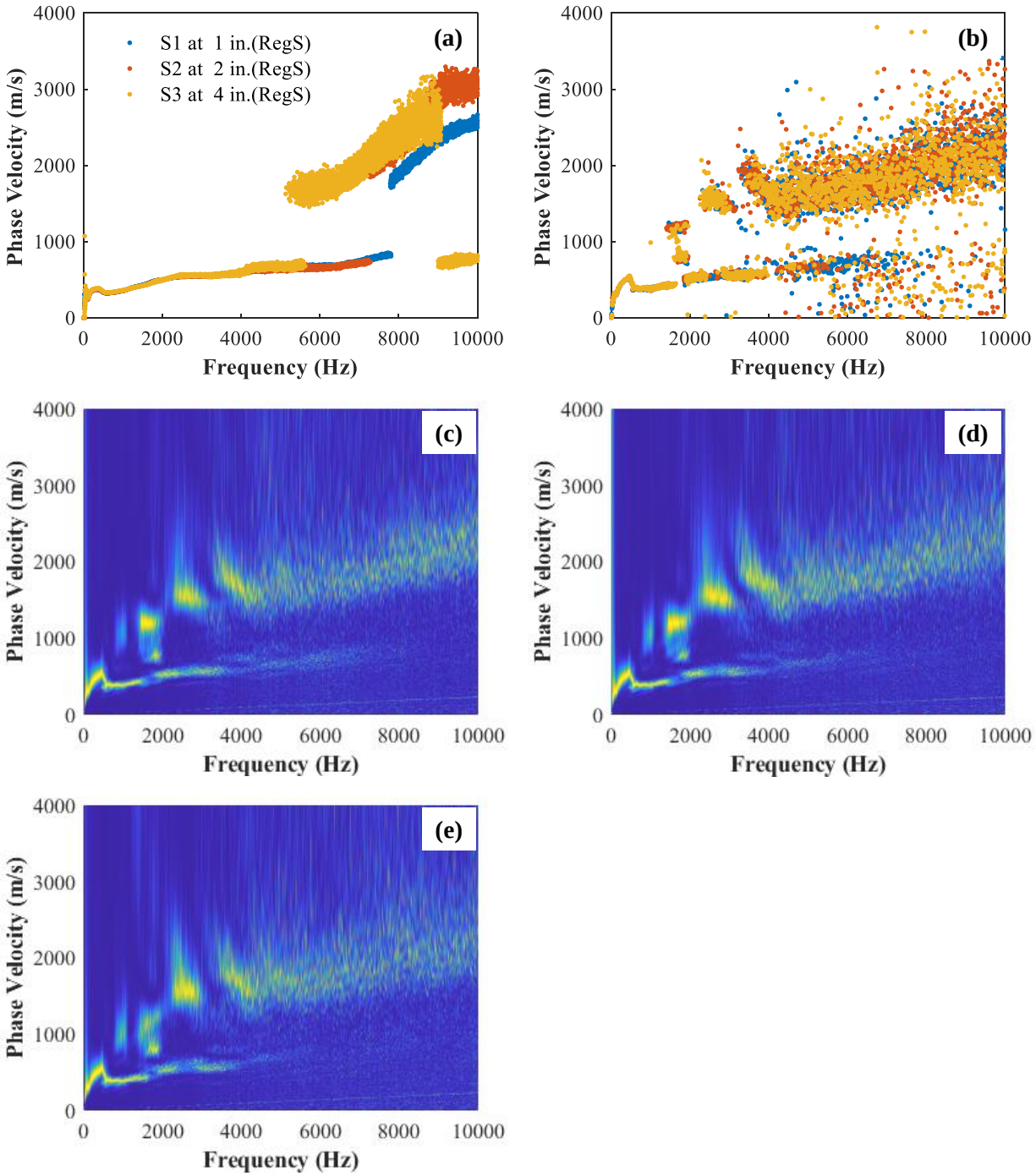

Figure F.25. IS1O at 51°C; (a) FK 64 offsets at 1 in. spacing, (b) FP peak from full array, (c) FP spectrum sensor 1, (d) FP spectrum sensor 2, and (e) FP spectrum sensor 3.

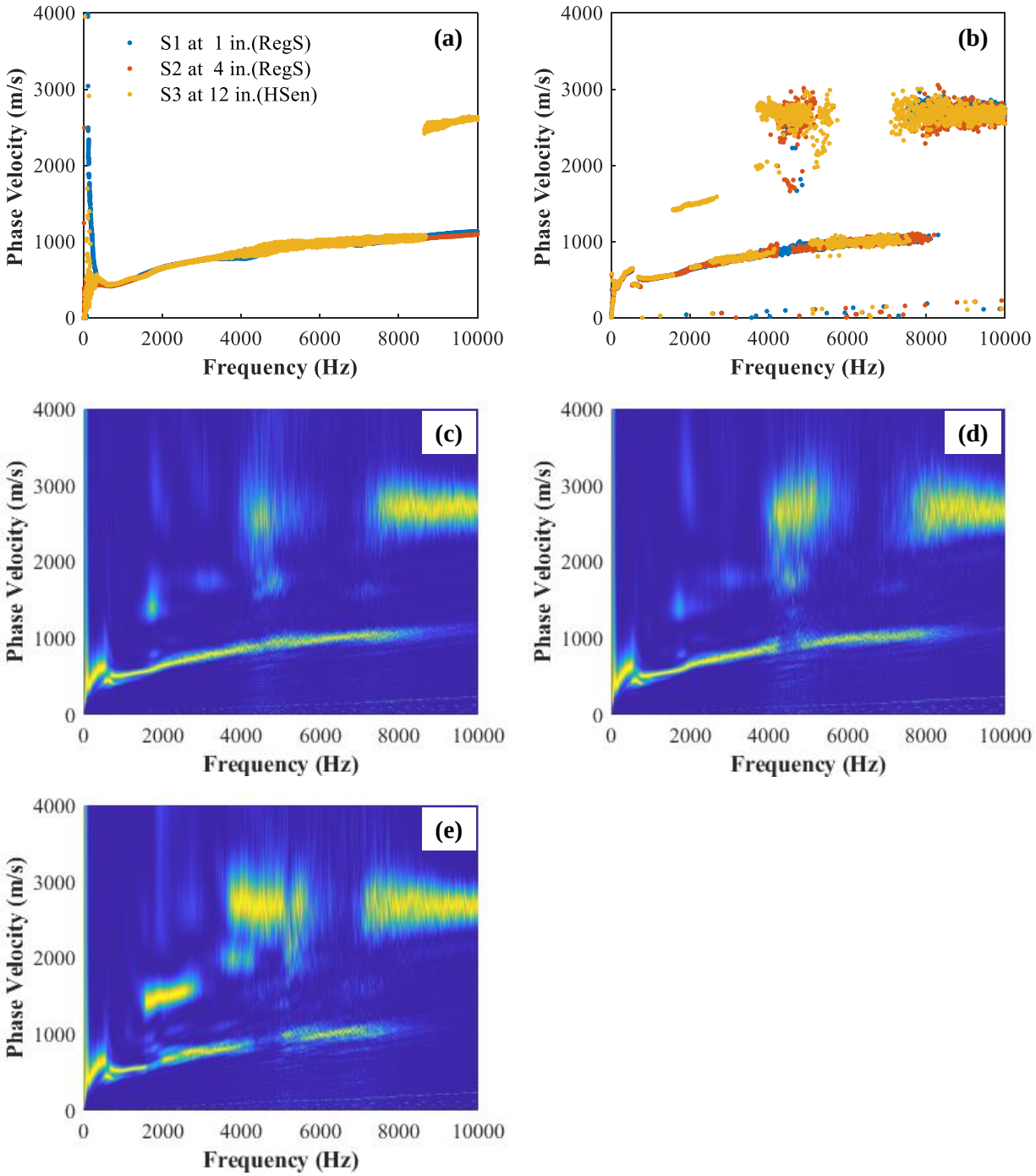

Figure F.26. IS1C at 14°C; (a) FK 64 offsets at 1 in. spacing, (b) FP peak from full array, (c) FP spectrum sensor 1, (d) FP spectrum sensor 2, and (e) FP spectrum sensor 3.

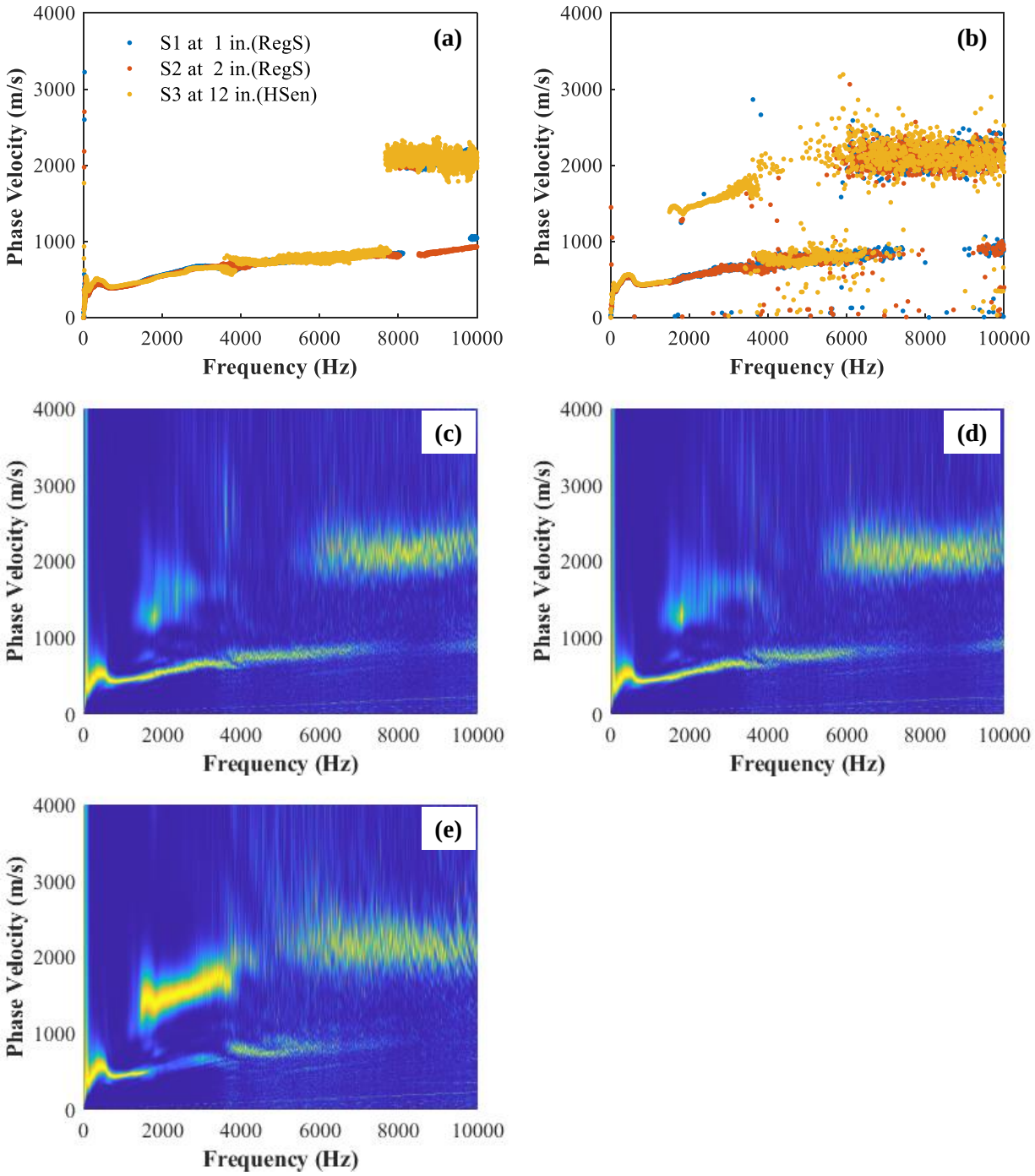

Figure F.27. IS1C at 28°C; (a) FK 64 offsets at 1 in. spacing, (b) FP peak from full array, (c) FP spectrum sensor 1, (d) FP spectrum sensor 2, and (e) FP spectrum sensor 3.

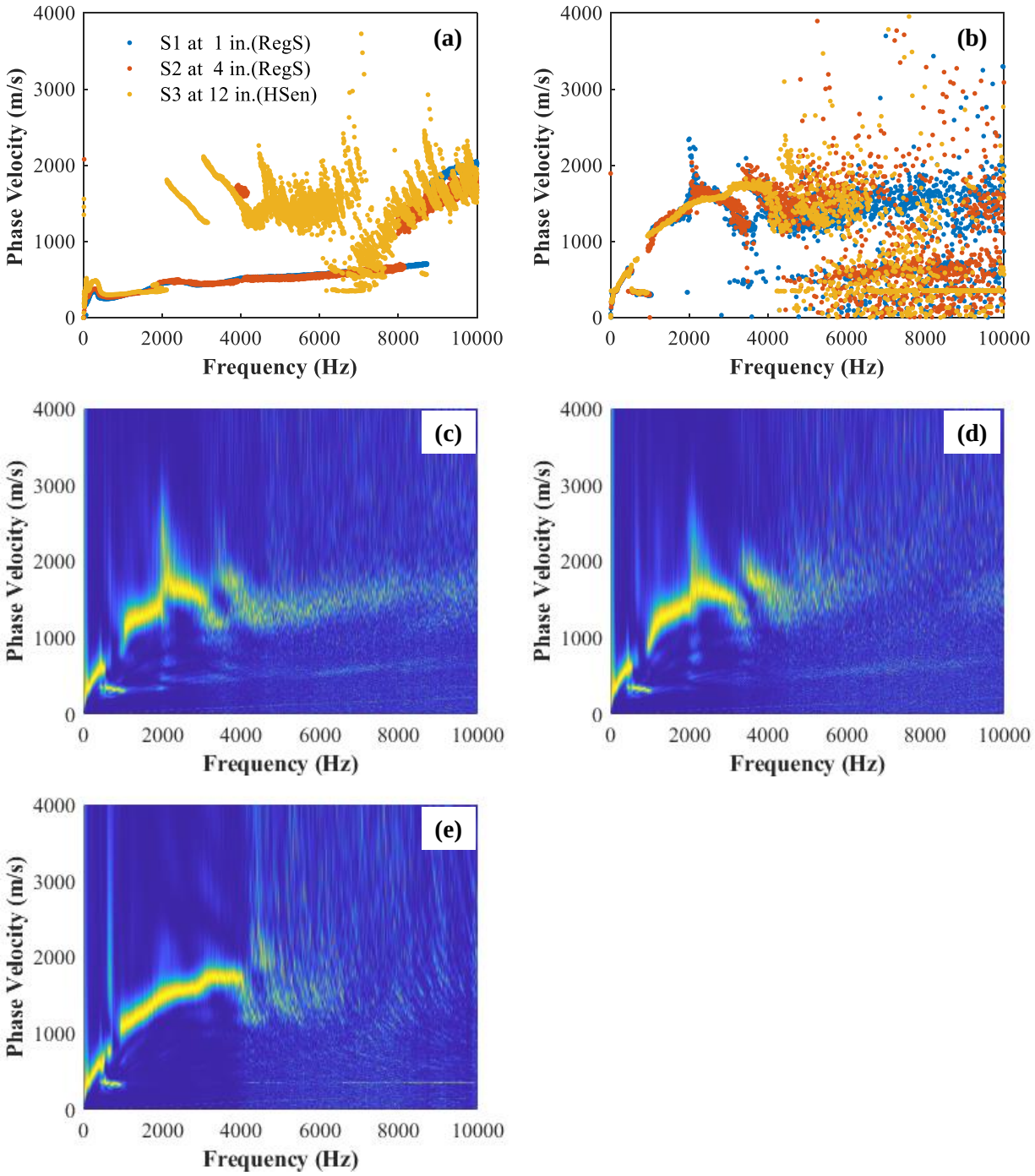

Figure F.28. IS1C at 53°C; (a) FK 64 offsets at 1 in. spacing, (b) FP peak from full array, (c) FP spectrum sensor 1, (d) FP spectrum sensor 2, and (e) FP spectrum sensor 3.

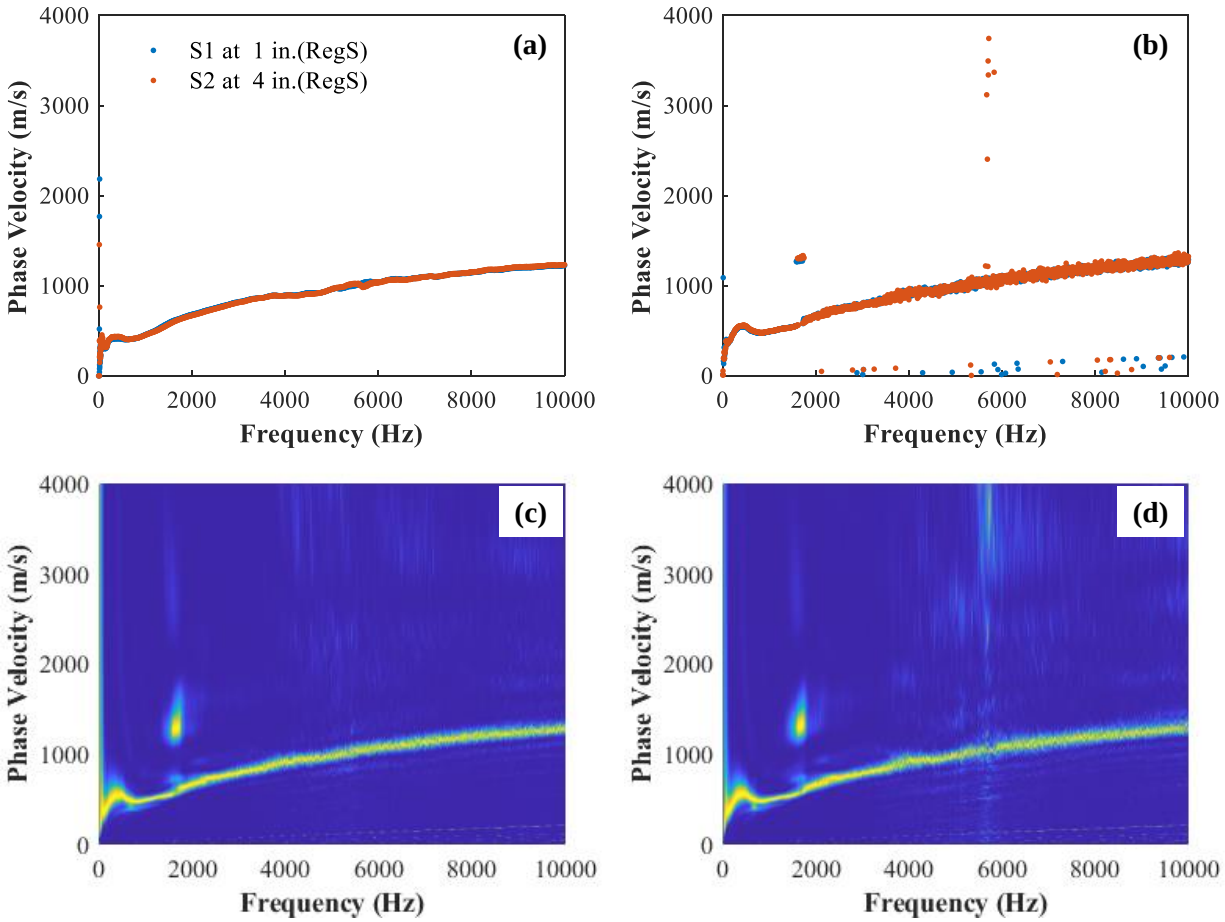

Figure F.29. IS1I at 17°C; (a) FK 64 offsets at 1 in. spacing, (b) FP peak from full array, (c) FP spectrum sensor 1, and (d) FP spectrum sensor 2.

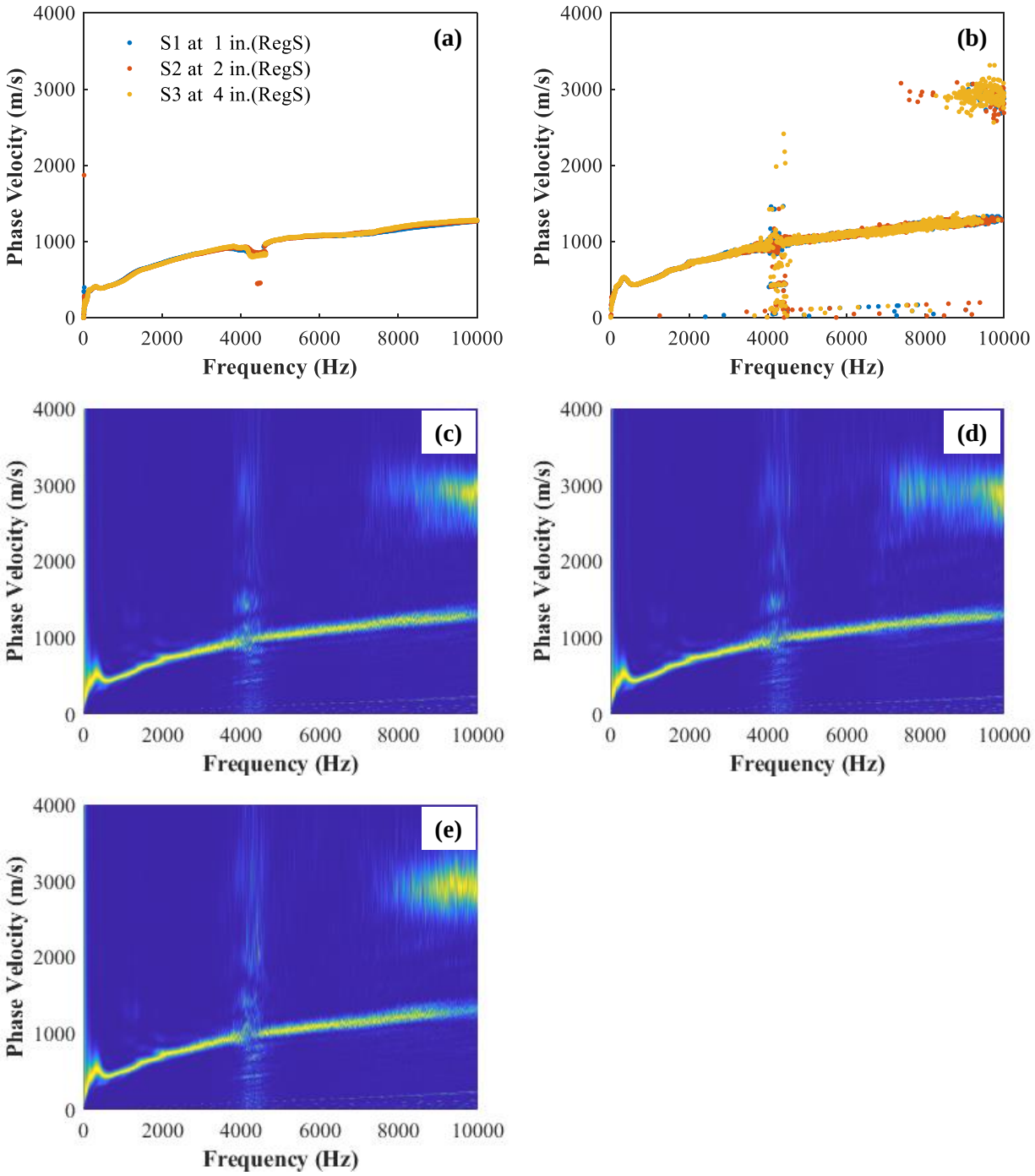

Figure F.30. IS2O at 10°C; (a) FK 64 offsets at 1 in. spacing, (b) FP peak from full array, (c) FP spectrum sensor 1, (d) FP spectrum sensor 2, and (e) FP spectrum sensor 3.

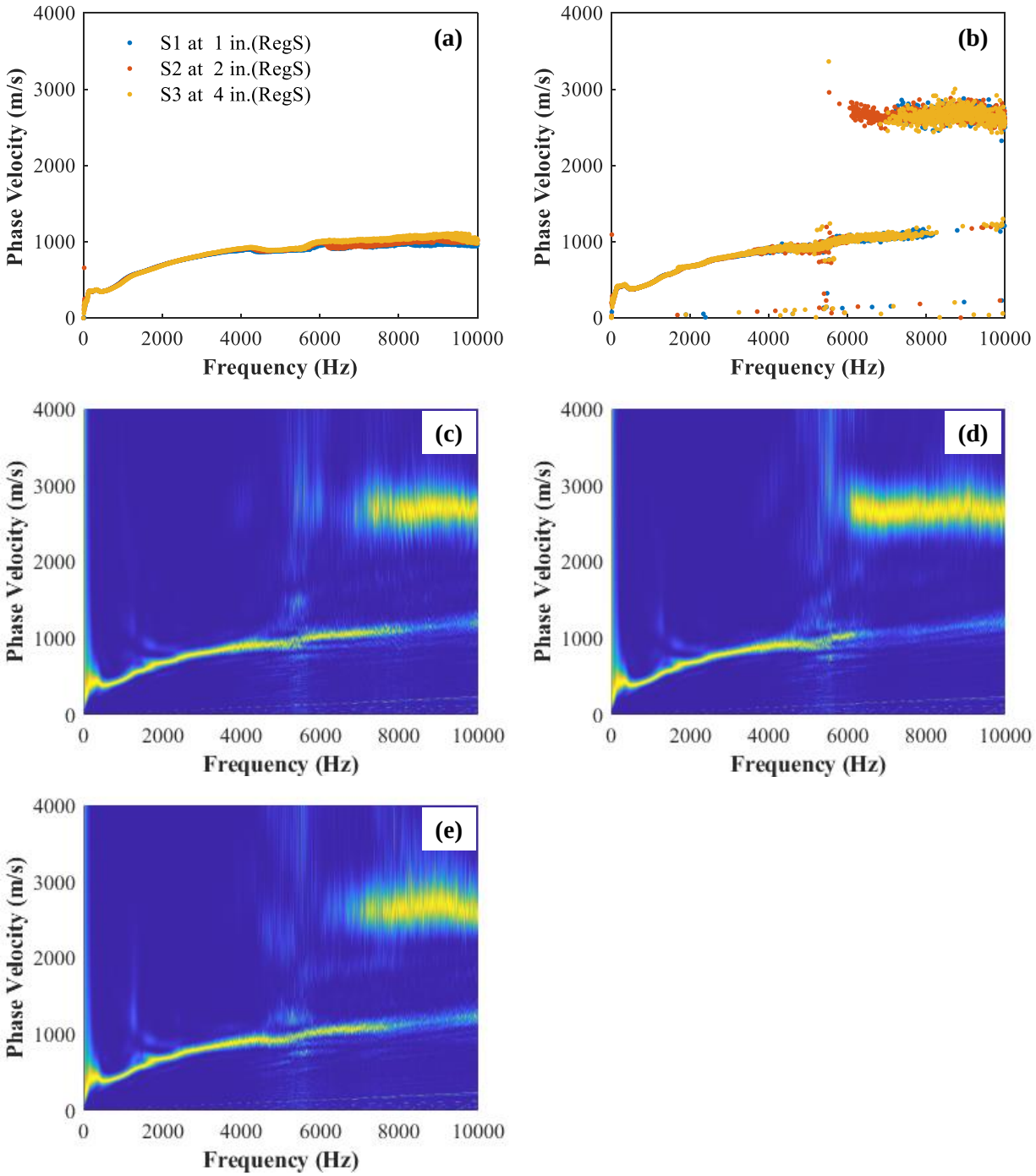

Figure F.31. IS2O at 18°C; (a) FK 64 offsets at 1 in. spacing, (b) FP peak from full array, (c) FP spectrum sensor 1, (d) FP spectrum sensor 2, and (e) FP spectrum sensor 3.

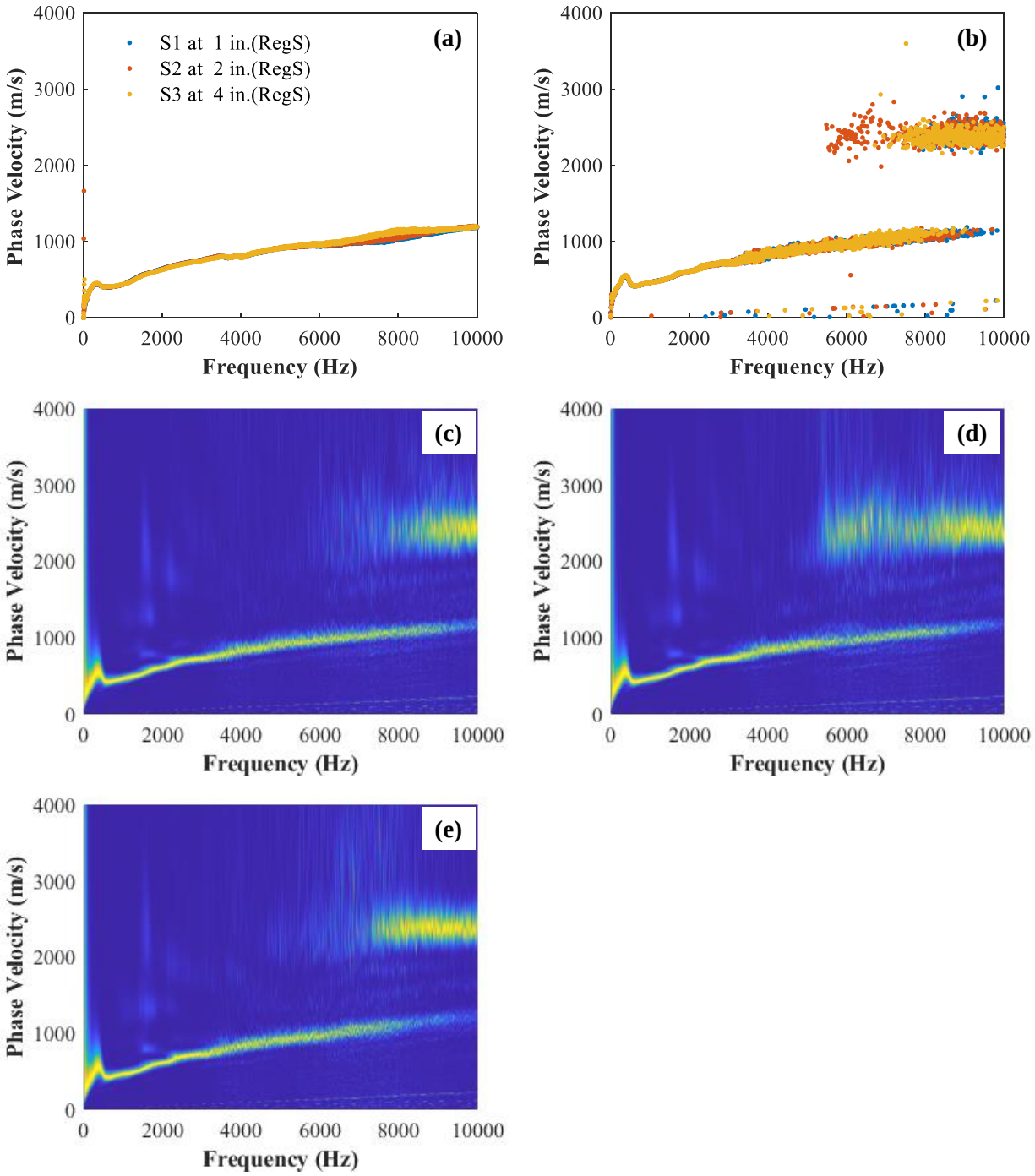

Figure F.32. IS2O at 27°C; (a) FK 64 offsets at 1 in. spacing, (b) FP peak from full array, (c) FP spectrum sensor 1, (d) FP spectrum sensor 2, and (e) FP spectrum sensor 3.

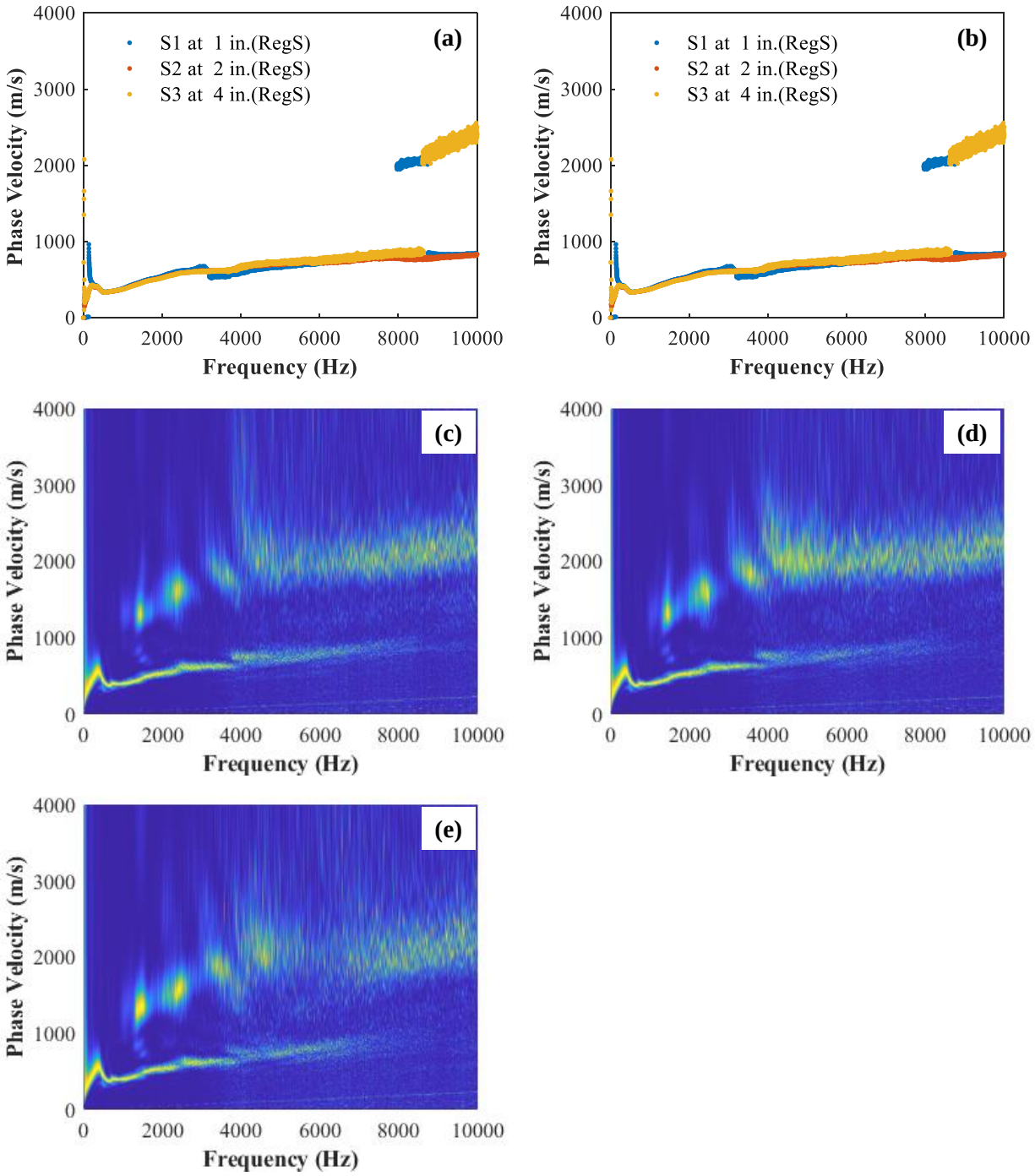

Figure F.33. IS2O at 44°C; (a) FK 64 offsets at 1 in. spacing, (b) FP peak from full array, (c) FP spectrum sensor 1, (d) FP spectrum sensor 2, and (e) FP spectrum sensor 3.

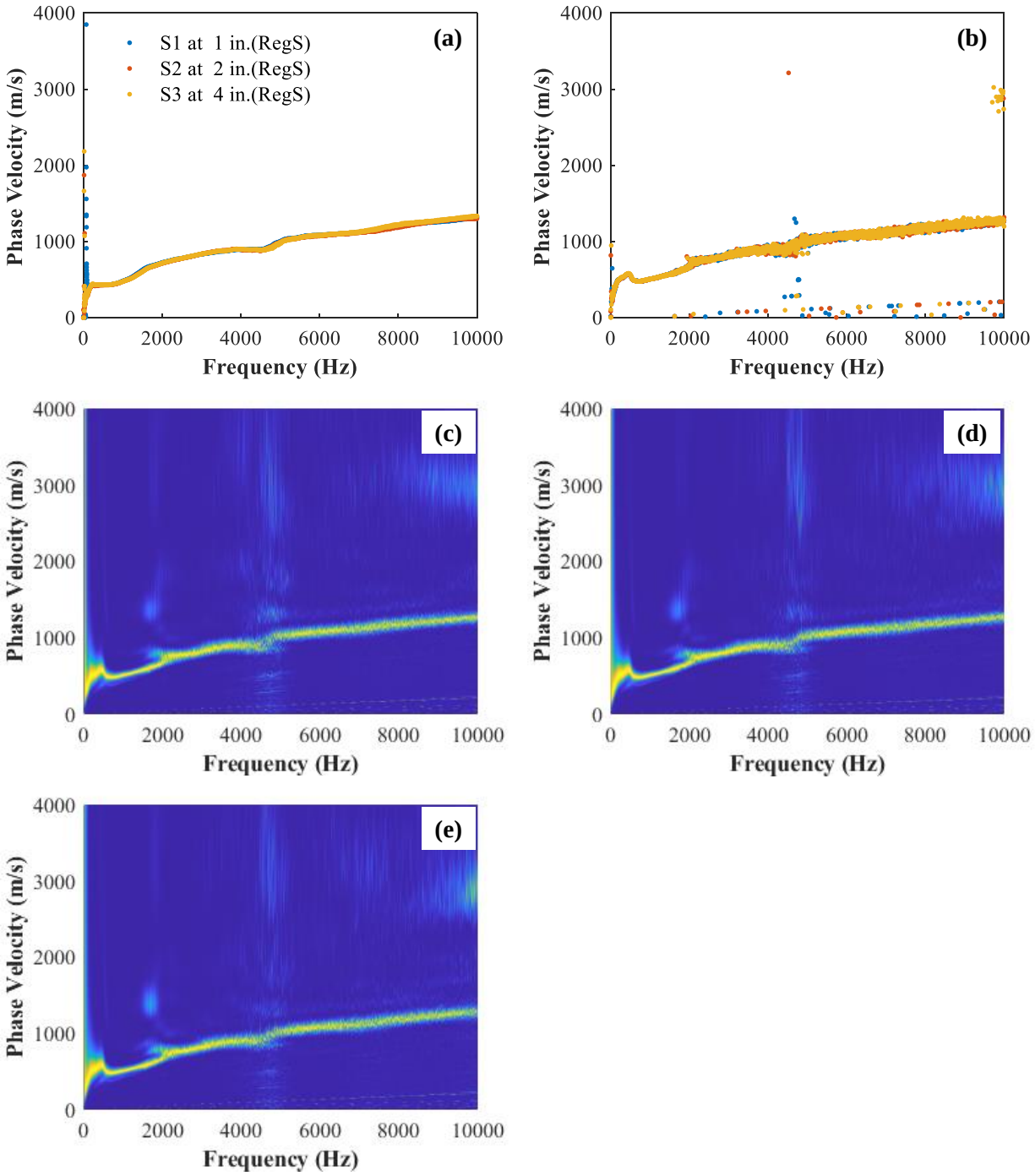

Figure F.34. IS2C at 10°C; (a) FK 64 offsets at 1 in. spacing, (b) FP peak from full array, (c) FP spectrum sensor 1, (d) FP spectrum sensor 2, and (e) FP spectrum sensor 3.

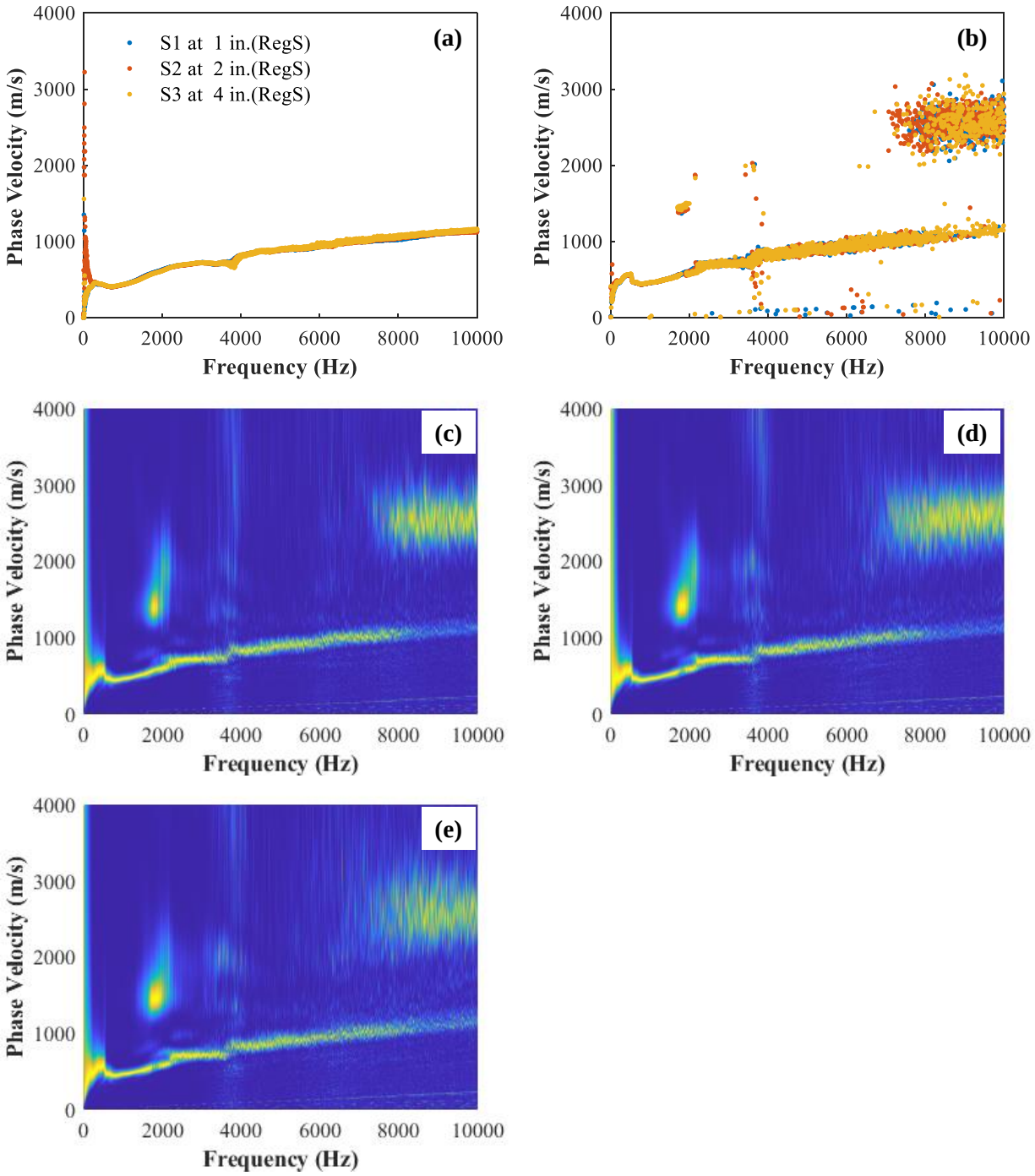

Figure F.35. IS2C at 25°C; (a) FK 64 offsets at 1 in. spacing, (b) FP peak from full array, (c) FP spectrum sensor 1, (d) FP spectrum sensor 2, and (e) FP spectrum sensor 3.

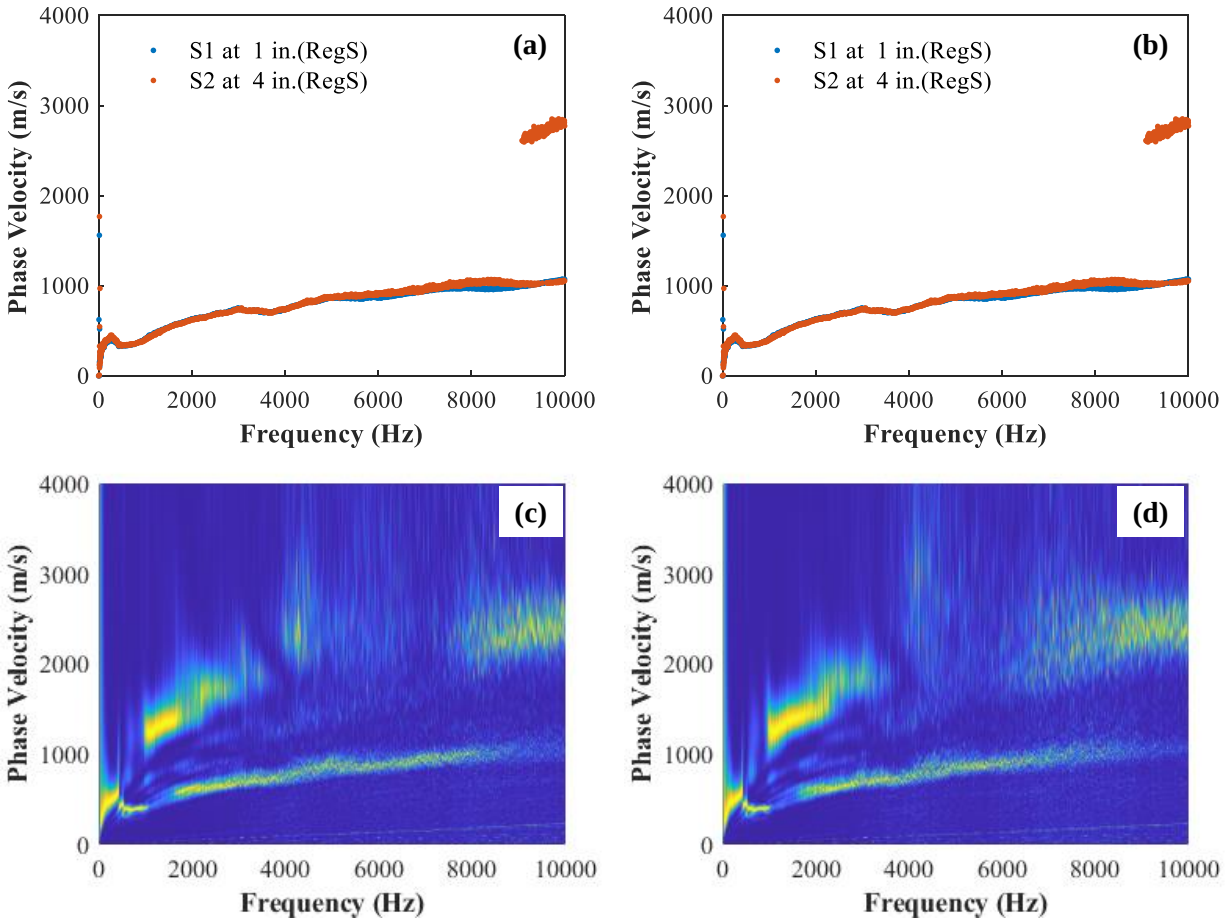

Figure F.36. IS2C at 30°C; (a) FK 64 offsets at 1 in. spacing, (b) FP peak from full array, (c) FP spectrum sensor 1, and (d) FP spectrum sensor 2.

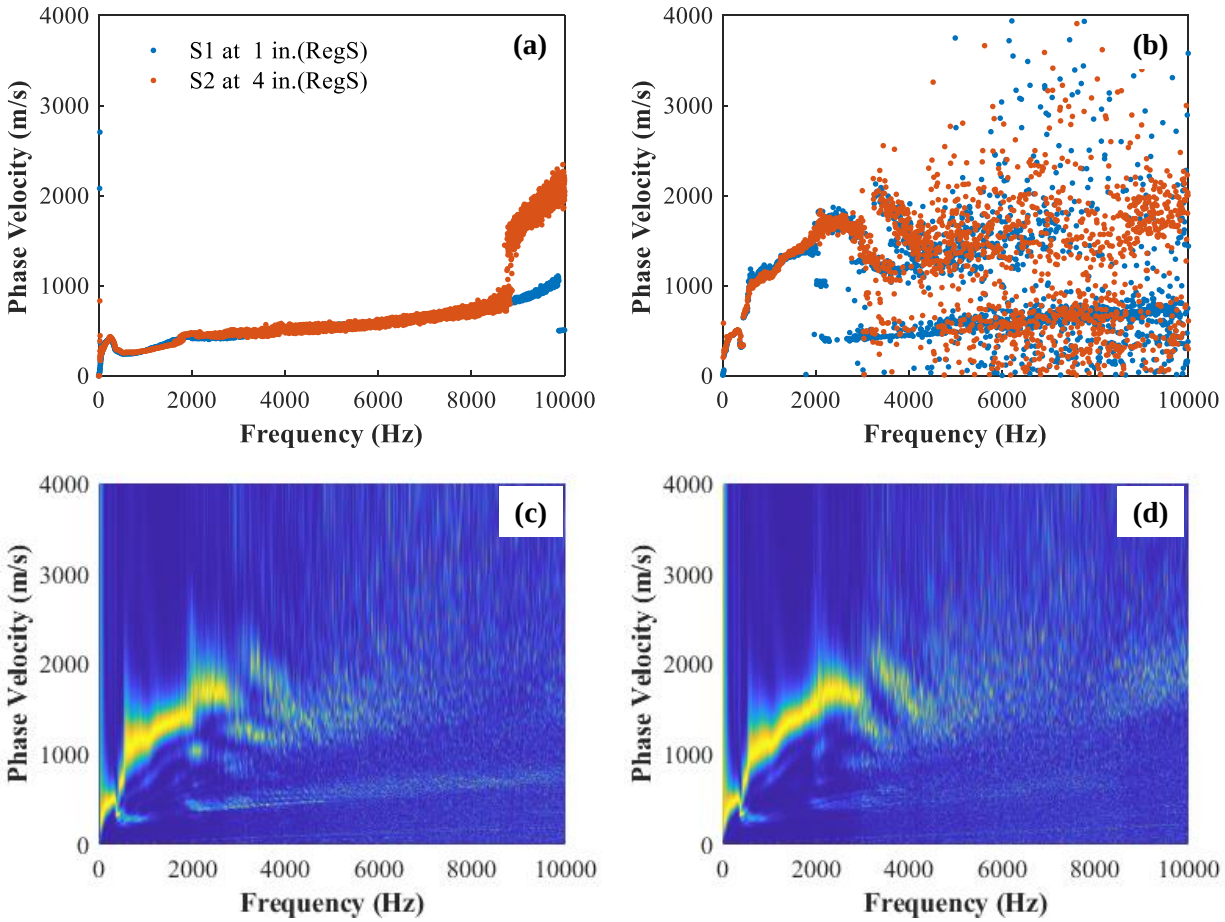

Figure F.37. IS2C at 57°C; (a) FK 64 offsets at 1 in. spacing, (b) FP peak from full array, (c) FP spectrum sensor 1, and (d) FP spectrum sensor 2.

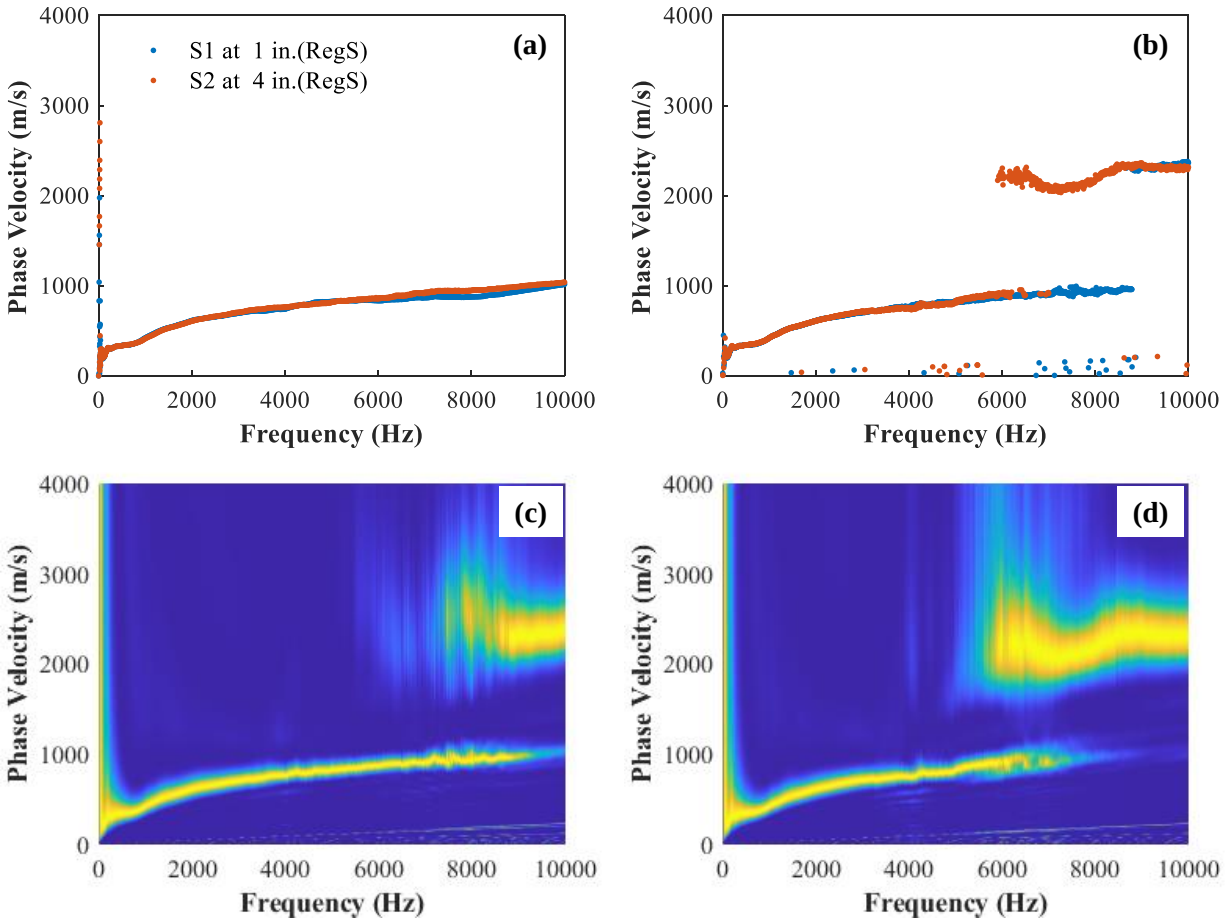

Figure F.38. ICS3C-ICS2C at 31°C; (a) FK 32 offsets at 1 in. spacing, (b) FP peak from 32 offsets, (c) FP spectrum sensor 1, and (d) FP spectrum sensor 2.

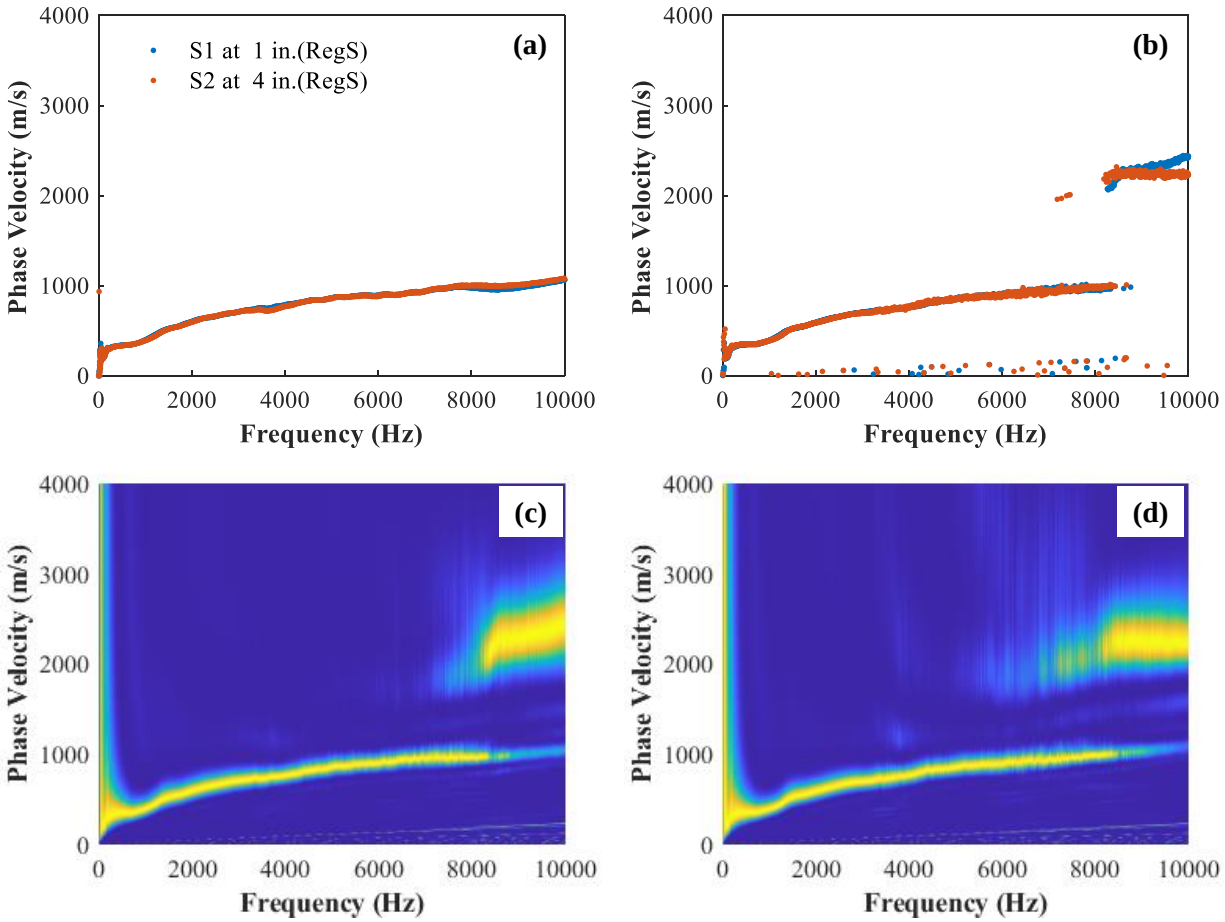

Figure F.39. ICS2C-ICS1C at 33°C; (a) FK 32 offsets at 1 in. spacing, (b) FP peak from 32 offsets, (c) FP spectrum sensor 1, and (d) FP spectrum sensor 2.

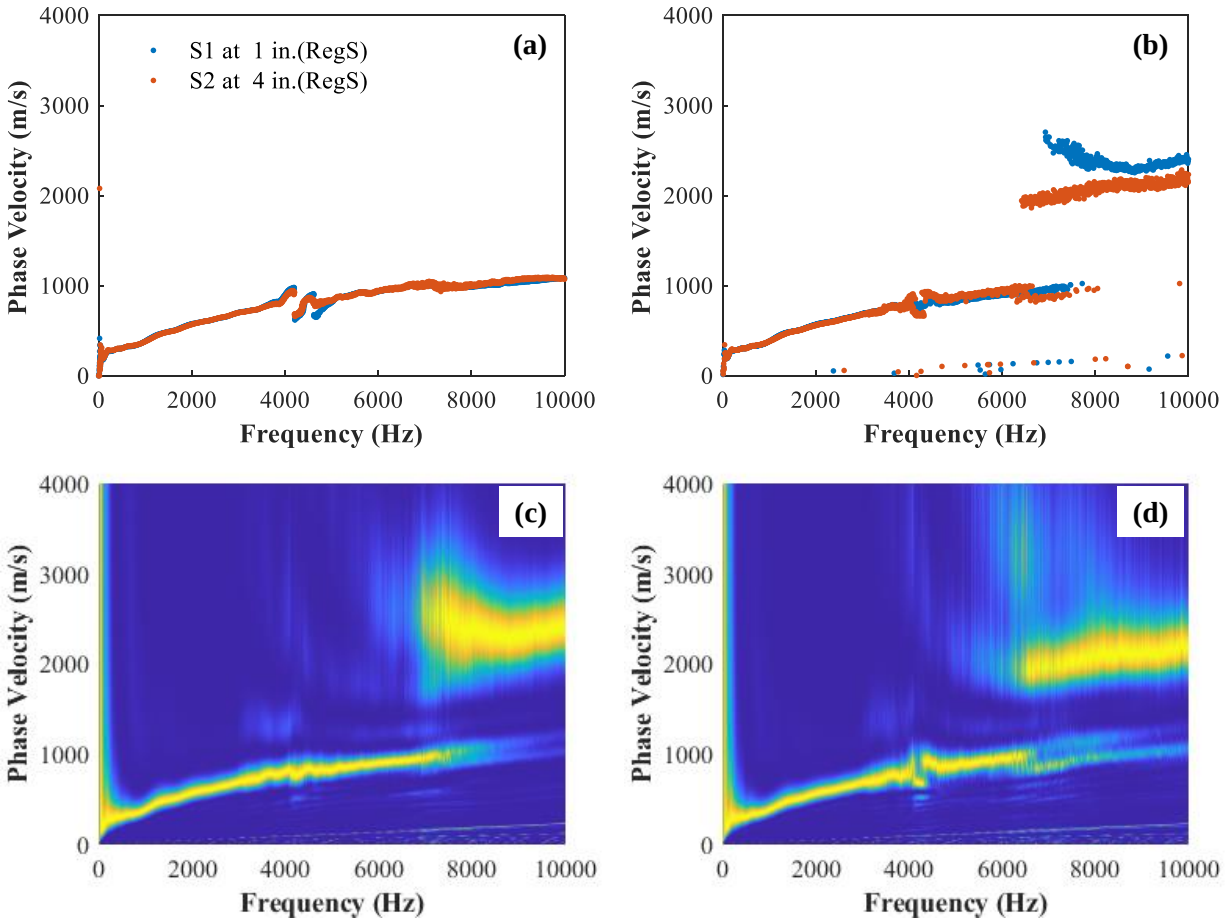

Figure F.40. ICS3O-ICS2O at 29°C; (a) FK 32 offsets at 1 in. spacing, (b) FP peak from 32 offsets, (c) FP spectrum sensor 1, and (d) FP spectrum sensor 2.

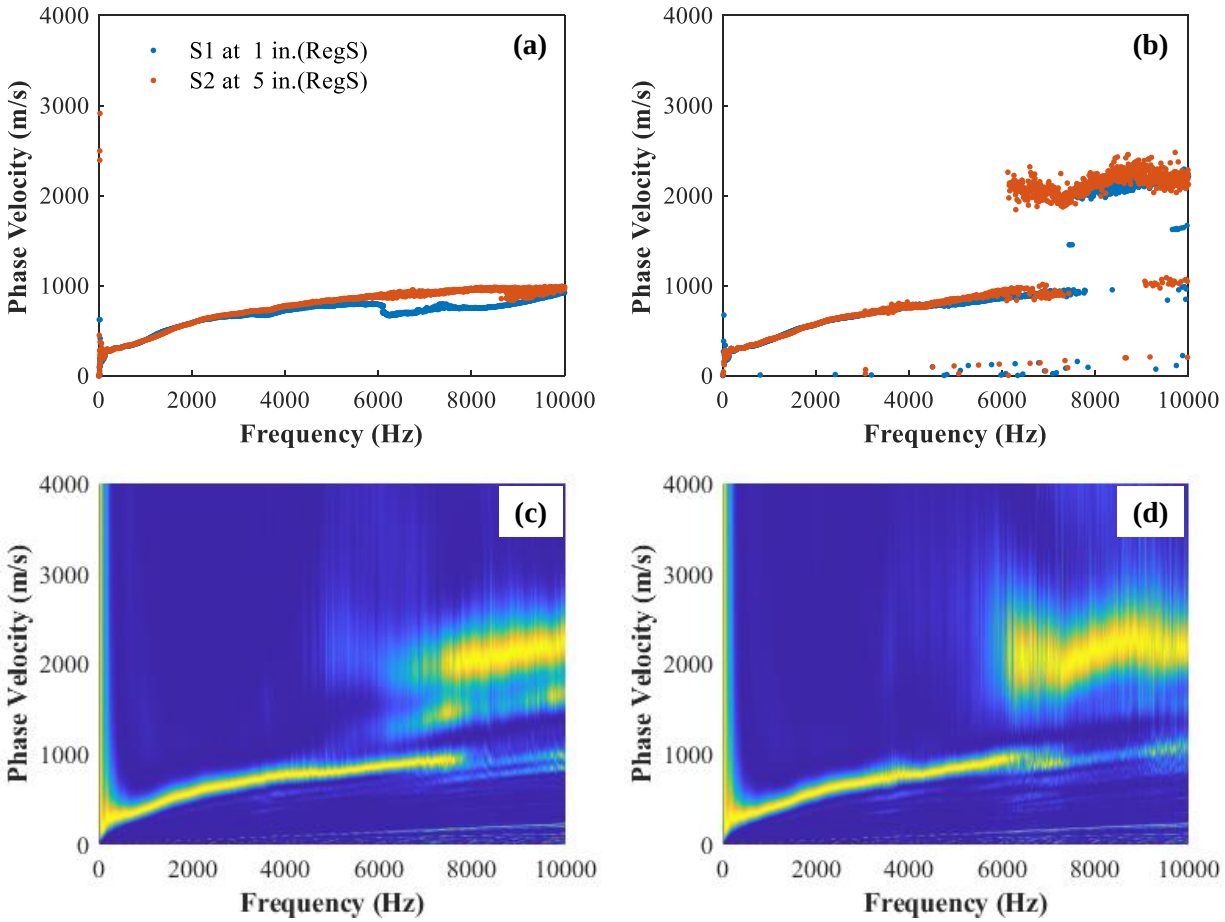

Figure F.41. ICS2O-ICS1O at 38°C; (a) FK 32 offsets at 1 in. spacing, (b) FP peak from 32 offsets, (c) FP spectrum sensor 1, and (d) FP spectrum sensor 2.